New insights into the current- and past hydrology of the north-western subtropical Pacific Ocean over the past 25 kyr, based on investigations of the Nd isotopic composition of seawater and deep-sea sediments from the northern South China Sea

Qiong Wu

UNIVERSITÉ PARIS-SUD

ÉCOLE DOCTORALE 534 :
MODÉLISATION ET INSTRUMENTATION EN PHYSIQUE, ÉNERGIES,
GÉOSCIENCES ET ENVIRONNEMENT

Laboratoire : Géosciences Paris Sud (GEOPS)

THÈSE DE DOCTORAT

SCIENCES DE L'UNIVERS

par

Qiong WU

New insights into the current- and past hydrology of the north-western subtropical Pacific Ocean over the past 25 kyr, based on investigations of the Nd isotopic composition of seawater and deep-sea sediments from the northern South China Sea

Date de soutenance : 08/09/2014

Composition du jury :

Directeur de thèse :	Christophe Colin	Professeur (Université Paris-Sud)
Rapporteurs :	Laure Meynadier	Professeur (Université Paris Diderot)
	Paolo Montagna	Chercheur (CNR-ISMAR)
Examinateurs :	Pinxian Wang	Professeur (Tongji University)
	Giuseppe Siani	Professeur (Université Paris-Sud)
	Zhifei Liu	Professeur (Tongji University)

Acknowledgements

This thesis represents a four-year journey full of amazing and pleasant memories. I have worked in excellent labs and have met many wonderful people in various fields who took me “under their wing” from the very beginning. I benefited immensely from their efforts and I wish to take this opportunity to express my sincere appreciation for their help.

First of all, I would like to sincerely thank my advisor, Prof. Christophe Colin, who offered me the opportunity to pursue this study in the Laboratoire de Geosciences Paris-Sud (GEOPS). Without his enthusiastic support, patient guidance, and invaluable advice in the process of this research, this work would not have been possible. His great interest in geochemistry and his passion for scientific research have inspired me in my pursuit of professional development.

I am particularly grateful to Prof. Zhifei Liu of Tongji University for his enthusiasm for this research project since the early stages, for his organizing of seawater sampling campaigns, and for my visits to Tongji University. Despite his busy schedules, he has always taken the time to share his thoughts regarding the progress of this work.

Particular thanks also go to Prof. Norbert Frank and Dr. Eric Douville for organizing my work in the geochemical lab at the Laboratoire des Sciences du Climat et de l'Environnement (LSCE) and for their constructive comments during the preparation of the manuscripts. Prof. Giuseppe Siani is much appreciated for sharing his expertise in foraminiferal identification and for fruitful discussions during the preparation of the texts.

Many people have helped me carry out essential laboratory work for this thesis. It has been a great pleasure to work with them. Special thanks go to François Thil and Quentin Dubois-Dauphin for their invaluable assistance with the Nd isotope analysis using the MC-ICP-MS instrument. I also thank Louise Bordier for her assistance in analyzing element concentration using the ICP-MS instrument whenever needed. Thanks also go to Eline Salle for her supervision of work carried out in the clean lab and for her assistance in solving each problem I encountered.

I would like to thank all of the members of the Paléoclimats et Dynamique Sédimentaire team at GEOPS and the members of the LSCE lab whom I cannot unfortunately name

individually here. My life would have been much less fun without the laughs and similes we shared. I enjoyed every small moment I spent with all of them.

I’m also grateful to the members of the jury for their willingness to review this thesis and for helping me to improve it.

The seawater sampling cruises were financially supported by the Natural Science Foundation of China projects (No. 91128206 and 40925008). I would like also thank the China Scholarship Council for the full scholarship support of my four-years stay in France.

Finally, I am eternally grateful to my very beloved family. Particular thanks to my loving parents for all their unconditional love and support for everything I do.

Contents

General introduction

Aims and scope of the study

In this section I outline the state of the art of Pacific Ocean hydrology, as well as the objectives of the present study. The main objective of this study is to reconstruct the hydrology of the western Pacific (Philippine Sea) during the last deglaciation and the Holocene using the εNd analysed on biogenic and authigenic phases of sediments from the northern South China Sea (SCS). To achieve this primary scientific objective, it was first necessary to constrain the Nd isotopic composition of water masses of the Philippine Sea and the northern SCS that up to now have remained poorly documented. In a second step, REE concentrations and Nd isotopic signatures of different species of foraminifera, cleaned using different procedures, as well as Nd extracted from authigenic Fe-Mn oxide fractions dispersed in sediment, have been investigated in order to test the ability of such archives to reconstruct past seawater Nd isotopic composition and to reconstruct past variability of ocean circulation in the northern SCS. In addition, the structure of this thesis and a summary of the contents of the constituent chapters are provided.

It is now widely recognized that large-scale thermohaline ocean circulation is one of the major factors driving the world's climate (Broecker and Denton, 1990; Rahmstorf, 2002; Clark et al., 2002). It affects climate through heat redistribution by surface current flow from the equator to sub-polar latitudes and it also affects regional temperature. Changes in the inter-basinal transfer of surface return flow also causes warm waters to exchange between ocean basins or to pool in the subtropics at shallow and intermediate depths, thereby affecting regional temperature and the evaporation/precipitation balance. In addition, changes in deep-water circulation and stratification have the potential to change the carbon storage capacity of the ocean (Stocker and Wright, 1996; Rahmstorf, 1995, 2003; Toggweiler and Russell, 2008; Marchitto et al., 2007; Bryan et al., 2010). Intermediate and deep-water masses of the global ocean constitute an important carbon reservoir that has the potential to release a huge amount of CO_2 to the atmosphere during reorganization of the ocean over time and at different time scales (Francois et al., 1997; Sigman et al., 2000; Spero and Lea, 2002; Broecker and Peng, 1987).

Records of past global climate preserve evidence of large-scale changes in temperature and ice volume at glacial-interglacial transitions. Although the timing of ice ages is broadly driven by Milankovich orbital cycles, the small insolation changes require amplifying mechanisms in order to produce the large glacial - interglacial climate changes. Variation in North Atlantic Deep Water (NADW) production is a potential amplifier and has been suggested as a trigger for the rapid global climate shifts that occurred during the last glacial period (e.g. Dansgaard/Oeschger (D/O) cycles and Heinrich events). Carbon dioxide (CO_2) is another possible amplifier, on glacial-interglacial time scales, because its atmospheric concentration is predominantly controlled by changes in deep-ocean storage (Francois et al., 1997; Broecker and Denton, 1990; Yu et al., 2010) and in the terrestrial carbon reservoir (e.g. Schimel et al, 1997; Shao et al., 2013). The North Atlantic Ocean is a strategic area in which to study deep convection, which mainly occurs in the Greenland, Iceland and Norwegian Seas, and to define the dynamic of thermohaline ocean circulation through time; because of this it has been intensively investigated during recent decades (Duplessy et al., 1988; Oppo and Lehman, 1993; Curry and Oppo, 2005). The Pacific Ocean has a major influence on global climate due to its large volume and its role as a potential carbon reservoir (Matsumoto et al., 2002; Yu et al., 2013). However, compared to the Atlantic Ocean, past hydrographical studies of the Pacific Ocean have been limited, particularly in the case of deep- and intermediate water masses.

Classic oceanographic proxies used to reconstruct past deep-water circulation, such as temperature and salinity, which are conservative in the ocean, as well as nutrient concentrations, such as phosphate, nitrate or silica, which are typical of certain water masses, are not preserved. Therefore, a number of proxies (tracers) have been developed to extract information from marine sediments regarding water mass distribution and flow in the past. The most commonly applied geochemical proxies for reconstructing past deep-water circulation have been stable carbon isotope composition ($\delta^{13}C$), Cd/Ca ratio, and ^{14}C (Keigwin, 1998; Marchitto et al., 2007; Boyle, 1988). Based on these proxies, it has been possible to establish the hydrological changes in the global ocean at different time scales. It is, however, difficult to make quantitative estimates of water mass mixing on the basis of the Cd/Ca or $\delta^{13}C$ proxies because these proxies can be greatly affected by changes in surface productivity over time. Recent investigations have focused on an alternative approach to evaluating the degree of global thermohaline circulation, at glacial-interglacial timescales, based on the $^{231}Pa/^{230}Th$ ratio adsorbed in marine sediment particles (McManus et al., 2004). However, the circulation signal inferred from these proxies can be affected by secondary effects such as regional thermodynamics (Charles et al., 1993; Lynch-Stieglitz et al., 1995), changes in biological productivity (Mackensen et al., 1993), dissolution of foraminiferal calcite (McCorkle et al., 1995), changes in bottom-water calcite saturation (Marchitto et al., 2000) and margin scavenging (Marchal et al., 2000). The history of global paleo-circulation is often the subject of intense debate because the different proxies used to trace paleo-water masses sometimes produce conflicting results.

The neodymium isotopic composition ($^{143}Nd/^{144}Nd$) of seawater has been shown to be a useful proxy for tracing water mass provenance within the ocean (Lacan and Jeandel, 2004a, 2004b and 2005; Von-Blanckenburg, 1999; Molinar-Kesscher et al., 2014; Amakawa et al., 2004, 2009, 2013; Jeandel et al., 1998 and 2013; Grass et al., 2012; Cater et al., 2012). Its advantage over several other proxies (e.g. $\delta^{13}C$ of dissolved inorganic carbon and Cd/Ca ratios as recorded by benthic foraminifera) lies in the fact that Nd isotopes are not known to be affected by biological processes and, thus, can serve as quasi-conservative water mass tracers (Frank, 2002; Goldstein and Hemming, 2003; Martin and Scher, 2004).

Nd isotopic composition is expressed as $\varepsilon Nd=[(^{143}Nd/^{144}Nd)_{Sample}/ (^{143}Nd/^{144}Nd)_{CHUR} - 1]$ x 10000, where CHUR stands for chondritic uniform reservoir and represents the present-day average earth value; $(^{143}Nd/^{144}Nd)_{CHUR} = 0.512638$ (Jacobsen and Wasserburg, 1980). The residence time of Nd, recently re-assessed to about 600–1000 yrs (Tachikawa et al., 1999 and

2003), is shorter than the global turnover time of the ocean (about 1000 yrs; Broecker and Peng, 1982). Consequently, as a result of continental lithogenic inputs of various ages, and boundary-exchange processes that occur at the continental margin (Lacan and Jeandel, 2005), intermediate- and deep-water masses acquire εNd from downwelling surface water (Goldstein and Hemming, 2003). In the ocean, the only way that the initial isotopic composition of a water mass can be changed is by the addition of Nd with a different isotopic composition through riverine or eolian inputs or by mixing with other water masses. However, away from the continental margins, and at short time scales (<500 years), εNd can be considered a quasi-conservative tracer. On the basis of these observations, εNd proxy has been widely used in order to track water mass mixing (Lacan and Jeandel, 2004a, 2004b, 2004c; Amakawa et al., 2004, 2009, 2013; Singh et al., 2012).

Although there are some limitations regarding the application of this proxy to track water mass provenance in certain areas of the ocean, numerous studies show that εNd can be reliably used in order to reconstruct past seawater evolution (Frank et al., 2006; Piotrowski et al., 2004, 2008; Pahnke et al., 2008; Basak et al., 2010; Martin and Scher., 2004). This proxy has already been used in paleo-oceanographic studies based on the dispersed authigenic ferromanganese oxide precipitates in sediments (Gutjahr et al., 2008; Pahnke et al., 2008; Piotrowski et al., 2004 and 2005; Rutberg et al., 2000), planktonic and benthic foraminifera (Burton and Vance, 2000; Roberts et al., 2010; Vance and Burton, 1999) as well as deep-sea coral skeletons (Colin et al. 2010; Copard et al., 2010, 2011, 2012; Robinson and van de Flierdt, 2009; van de Flierdt et al., 2006; Montero-Serrano et al., 2011) in order to track changes in water mass provenance and mixing at different time scales.

Throughout the last glacial-interglacial cycle, major reorganisation of water masses in the North Atlantic occurred. Several studies based on nutriment proxies ($\delta^{13}C$ and Cd/Ca) provide evidence that, during the last glacial period, production of the North Atlantic Deep Water (NADW) was shallower, significantly weaker and less exported to the south than is the case today (Oppo and Fairbank, 1987; Duplessy et al., 1988; Mix and Fairbanks, 1985; Curry and Oppo, 2005; Labeyrie et al., 1996).

Furthermore, based on the reconstruction of past seawater εNd, the deep water of the Atlantic Ocean and the Southern Ocean were characterized by more radiogenic εNd values during the LGM than is the case in the Holocene (Ruterg et al., 2000; Piotrowski et al., 2004,

2005, 2012; Robert et al., 2010; Robinson and van de Flierdt, 2009; Skinner et al., 2013). This implies a decreasing influence of NADW and a higher northward propagation of the SSW in the Atlantic Ocean and Indian Ocean during the glacial period. This pattern is clearly intensified during millennial-scale cold episodes in the high latitudes of the Northern Hemisphere (e.g. Heinrich stadials - HS). In addition, $^{231}Pa/^{230}Th$ records reveal that NADW formation during the last glacial period was slower than it is today and reached a minimum during Heinrich event (Lippold et al., 2012; McManus et al., 2004). All of these studies using complementary hydrological proxies indicate that, during the last glacial- and deglaciation periods, several episodes of iceberg and meltwater discharge from the Northern Hemisphere ice sheets (e.g. Heinrich events - HE and Younger Dryas - YD) were closely associated with the collapse of NADW formation, cooling in a large part of the Northern Hemisphere, and warming in the southern hemisphere (Rahmstorf, 1994 and 1995; Broecker, 1998; McManus et al., 2004). These cold episodes observed in the high latitudes of the Northern hemisphere are associated with relatively warm episodes in the high latitudes of the Southern Hemisphere and are probably triggered by sudden changes in North Atlantic and southern Ocean deep water formation rates. This climate system mechanism corresponds to the bipolar seesaw (Broecker, 1998; Shakun and Carlson, 2010; Pedro et al., 2011; Siani et al., 2013).

Several studies that focus on the Indian Ocean have revealed similar hydrological changes as those observed the Atlantic Ocean, with a higher northward propagation of the SSW during the last glacial period (Bryan et al., 2010; Piotrowski et al., 2009; Romahn et al., 2014). For example, past seawater εNd records obtained from sediments in the equatorial Indian Ocean suggest a pronounced northward intrusion of deep Southern Sourced Water (SSW) during the last glacial period and the HS1 (Piotrowski et al, 2009; Wilson et al., 2012). In addition, chemical tracers (e.g. $\Delta^{14}C$, $\delta^{13}C$,) also show northward propagation of the Antarctic Intermediate Water (AAIW) during Heinrich events (Jung et al., 2009; Byran et al., 2010; Romahn et al., 2014).

Compared to the Atlantic Ocean, paleohydrological studies of the North Pacific Ocean have been limited, particularly for deep and intermediate water masses. This is mainly due to the low sedimentation rate which is a feature of Pacific Ocean deep-sea sediments, poor preservation of bio-carbonate due to shallow carbonate compensation depth (CCD), and problems relating to the use of hydrological proxies (e.g. $\delta^{13}C$ of dissolved inorganic carbon and Cd/Ca ratios as recorded by benthic foraminifera) for determining the main water masses of

the Pacific Ocean that undergo considerable mixing in the North Pacific. Consequently, the variability of the northward propagation of the SSW in the North Pacific is, as yet, not well constrained. Today, deep convection of the NPIW and NPDW is very weak, or absent, due to the low salinity lid of the North Pacific Ocean and water vapour transport related to the Asian Monsoon. The evolution of these water masses of the North Pacific since the last glacial period is not well understood and is still a matter of debate.

Nevertheless, glacial ocean stratification of the South Pacific has been observed in many studies (e.g. Shackleton et al., 1988; Sikes et al., 2000; Matsumoto et al., 2002; Galbraith et al., 2007; Siani et al., 2013). Deep-water reservoir ages that are older than present day ages have been identified to the east of New Zealand during the glacial period, associated with the isolation of deep-water from atmosphere (Sikes et al., 2000). In the eastern South Pacific Ocean (off the southern Chilean coast), differences in foraminifera benthic - planktic ^{14}C and $\delta^{13}C$ also support the theory of the occurrence of less ventilated deep water in the glacial South Pacific Ocean and provide evidence for two major periods of enhanced upwelling in the southern Ocean during the last deglaciation. This could be an important mechanism responsible for the abrupt deglacial atmospheric CO_2 rise (Siani et al., 2013). This last study suggests synchronous changes in the Southern Ocean circulation and Antarctic climate during the last deglaciation. Recently, Basak et al. (2010) have reported on a study of εNd from core MV99-MC19/GC31/PC08, collected near southern Baja California, permitting the identification of variations in the relative proportions of NPIW and AAIW over the past 38 kyr. The variations observed support the concept of an increased contribution of AAIW at the beginning of the deglaciation (during the Heinrich Stadial 1 - HS1), suggesting that old carbon was transported from the deep southern abyss to the shallow tropics via the AAIW.

It has been suggested that increased $\delta^{13}C$ of benthic foraminifera in the subarctic Pacific Ocean are probably due to enhancing enhanced formation of the NPIW during the last glacial period (Rella et al., 2012). It was also recently suggested that the deep-water of the North Pacific was directly ventilated by dense waters formed in the subarctic Pacific during HS1. Recently, Okazaki et al. (2010) have compiled ^{14}C data from benthic and planktonic foraminifera from several cores in the North Pacific and have shown that ventilation age decreased drastically during the last HS1 event. In particular, they argue for a greater northward advection of salty subtropical waters to the subarctic gyre, overcoming the halocline (Emile-Geayet al., 2003), and forming “deep waters” during HS1. Indeed, there are many signs

of increased ventilation recorded in sediments deposited within the upper portion of the North Pacific water column during HS1 (Ahagon et al., 2003; Duplessy et al., 1989; Mix et al., 1999; Sagawa and Ikehara, 2008). However, a number of geochemical proxies, previously measured at multiple deep North Pacific core sites between 2710 and 3640 m, are inconsistent with local ventilation of the lower half of the ~5000 m deep water column at this time. Among these measurements, the high-resolution radiocarbon data of Lund et al. (2011) suggest that the waters at 2710 m were actually very poorly ventilated (i.e. ^{14}C-depleted) during the HS1, although these authors note the potential input of ^{14}C-derived carbon from geological reservoirs at this time. In addition, redox sensitive elements show that there was no deep-water formation in the North Pacific during the HS1 but support the idea that ventilation in the North Pacific during the HS1 was restricted to the NPIW above 1300 m (NPIW) (Jaccard and Galbraith, 2013). δ^{13}C values of benthic foraminifera investigated from several cores collected at different water depths indicate that strong ventilation only occurred at mid-depth in the North Pacific during the HS1 (Bostock et al., 2010; Max et al., 2014). Consequently, there is still debate regarding the possible formation of intermediate- deep-water masses (NPIW, NPDW) in the Pacific during deglacial North Hemisphere cold events when NADW formation had collapsed (HS1, YD) (Mix et al., 1999; Ohkushi et al., 2003; Okazaki et al., 2010; Rella et al., 2012; Herguera et al., 2012; Rae et al., 2014).

The objectives of this study

The South China Sea (SCS) is a semi-enclosed, marginal sea connected to the western subtropical North Pacific through the deep Luzon Straits. It receives deep-water masses from the Philippine Sea that result from the mixing of the Northern- (NPDW and NPIW) and Southern (SSW) Sourced Water masses. Consequently, the northern SCS constitute an ideal location in the western Pacific Ocean for reconstructing past hydrological changes in deep-water masses of the subtropical Pacific Ocean that, as yet, remain poorly documented. As εNd values of the NPDW/NPIW in the North Pacific are characterized by more radiogenic values (-4) than the UCDW in the South Pacific (-6 to -8) (Amakawa et al., 2004 and 2009; Piepergras and Wasserburg, 1980), εNd could be a useful proxy to constrain past changes in water mass provenance and mixing during the last deglaciation and the Holocene in the western subtropical North Pacific Ocean.

The aim of this study is to reconstruct the evolution of the hydrology of the western subtropical North Pacific Ocean by using εNd proxy analysed on foraminifera and dispersed authigenic ferromanganese oxide precipitates in sediments from deep-sea cores collected in the northern SCS. Over the last decade, several studies have reported distinct Nd isotopic compositions for the main deep-water masses of the Pacific Ocean (Amakwa et al., 2004, 2009, 2013; Piepergras and Wasserburg, 1980). However, the distribution of the Nd istotopic composition of seawater from the Philippine Sea and the SCS is not yet established. In addition, in marginal areas, seawater Nd isotopic composition can be affected by processes of "boundary exchange'' involving some combination of release, removal and exchange of Nd between seawater and ocean margin sediments (Lacan and Jeandel, 2001 and 2005; Grenier et al., 2013). This process, mostly observed in modern seawater studies, has the potential to modify the εNd composition along deep-water flow paths in some locations of the Ocean (e.g. Jeandel et al., 1998; Lacan and Jeandel, 2001 and 2005; Amakawa et al., 2009; Carter et al., 2012; Grasse et al., 2012). Consequently, before using the εNd proxy on deep-sea sediments of the SCS for the purpose of hydrological reconstruction, it is absolutely necessary to establish the spatial distribution of dissolved Nd isotopic composition of the main water masses of the Philippine Sea and the northern SCS. It is also necessary to establish the importance of "boundary exchange'' on the εNd values of the intermediate and deep-water masses of the SCS. Intermediate and deep-water masses that enter the SCS should not be strongly modified by sediments from the margin of the northern SCS that are characterized by unradiogenic Nd isotopic composition.

It is also necessary to carefully establish the reliability of Nd isotopic composition obtained from the Fe-Mn oxide fraction leached from sediments and foraminifera with εNd seawater. To test the viability of this climatic archive, we have investigated modern sediments (core-top samples) from several cores located in different part of the SCS. We have also finalised chemical protocols to extract the seawater Nd isotopic composition incorporated in the foraminifera and Fe-Mn oxide coatings of the SCS sediments. Finally, we have analysed the Nd isotopic composition of foraminifera and of dispersed authigenic ferromanganese oxide precipitates in sediments from one sediment core located in the northern SCS in order to reconstruct past variability of ocean circulation in the northern SCS during the last 25 kyr.

The results of all investigations undertaken as part of this thesis are organized in six chapters.

In **chapter 1**, I present the hydrological and geological settings of the Philippine Sea and the SCS, the Nd cycle in the ocean and the εNd proxy, the climatological setting around the SCS and a brief overview of hydrological changes and seawater εNd records available for the Pacific Ocean.

In **chapter 2**, I present the scientific strategy used to reply to the scientific questions addressed in this study. I present the material that we have selected in order to investigate modern and past hydrological changes of the Philippine Sea and the northern SCS, and I describe all procedures that have been used to analyse REE concentrations and Nd isotopic compositions of seawater samples, foraminifera and Fe-Mn oxide coatings.

In **chapter 3**, I present, for the first time, the vertical distribution of the Nd isotopic compositions of seawater samples collected from 16 stations located in the western Philippine Sea, in the Luzon Straits and in the northern SCS along the trajectory of the deep water which enters the SCS. These results allow me to (1) constrain the Nd isotopic composition of water masses along the west Pacific and the northern SCS that, up to now, has been documented; (2) track hydrological exchange through the Luzon Straits; and (3) establish if there is currently any impact from the process of "boundary exchange" in the SCS, between water masses entering the SCS and sediments from the margin, which are characterized by very contrasting εNd values (-4 and -12, respectively).

In **chapter 4,** I establish the analytical procedures permitting the extraction of present day seawater εNd values from different archives (authigenic Fe-Mn oxides and benthic - planktonic foraminifera). In this study, we have tested a number of different analytical cleaning procedures applied to foraminifera samples in order to remove Fe-Mn coatings. εNd values obtained on modern foraminifera for the SCS (core-top samples) have been compared to those of seawater obtained by means of the analyses presented in chapter 3. Results suggest that the Nd isotopic composition incorporated on foraminifera represent bottom water εNd regardless of the species (benthic and planktonic foraminifera). This allows us to determine the best chemical cleaning procedure in order to extract seawater εNd from SCS sediments. We have also demonstrated that εNd extracted from Fe-Mn oxide coatings can be readily affected by the dissolution of lithogenic particules.

In **chapter 5**, I present a seawater εNd record spanning the last 30 cal kyr BP obtained from the planktonic foraminifera. This is the first seawater εNd record obtained in the deep water masses of the SCS and it allows us to define new constraints on the hydrology of the western subtropical Pacific Ocean (Philippine Sea).

Chapter 6 presents a summary of this study and offers suggestions for future research.

Chapter 1: General background

Geological, hydrological and climatological settings

In this first chapter, I present important general background information that permits the reader to better understand the scientific problematic and the scientific strategy for this study. Firstly, I present the physiography of the study area and the hydrological setting of the Philippine Sea and the South China Sea (SCS). I outline the Nd cycle in the ocean and present the advantages and limitations of the use of Nd isotopic composition as a proxy for reconstructing ocean circulation. I go on to describe the geological setting and the εNd of river sediments and surface sediments of the study area because interactions between detrital particles and seawater have previously been shown to have an impact on seawater εNd. In the last sections, I describe the climatological setting of the SCS and provide a brief overview of hydrological changes and past seawater Nd records from the Pacific Ocean covering the past 35 kyr period. This allows me to introduce a past seawater Nd record that will be used later for comparison with our new εNd record.

1.1 Physiography of the study area

The main topographic features of the Pacific Ocean are shown in Figure 1.1. The Pacific Ocean is the largest of all the earth's oceans. It covers an area of 178.106 km^2 and represents 40% of the total surface area of the world's oceans. The inter-oceanic ridge system in the Pacific Ocean is located close to the eastern boundary, forming a large southeastern Pacific Ocean similar in size to the Indian Basin.

The central and the northern Pacific Ocean are subdivided, more by convention than topography, into the Northeast Pacific, Northwest Pacific, Central Pacific, and Southwest Pacific Basins. Another notable feature of the Pacific Ocean is that its ocean floor contains a large number of volcanic seamounts, particularly in the Northwest and Central Pacific Basins.

There are several marginal seas located along the western boundary of the Pacific Ocean. Marginal seas located in the western equatorial Pacific (Coral Sea, Sulu Sea, Celebes Sea, Philippine Sea and South China Sea) are of a great importance for global oceanic circulation because they permit connection of deep- and surface water masses between the Pacific Ocean and the Indian Ocean (Fig 1.1).

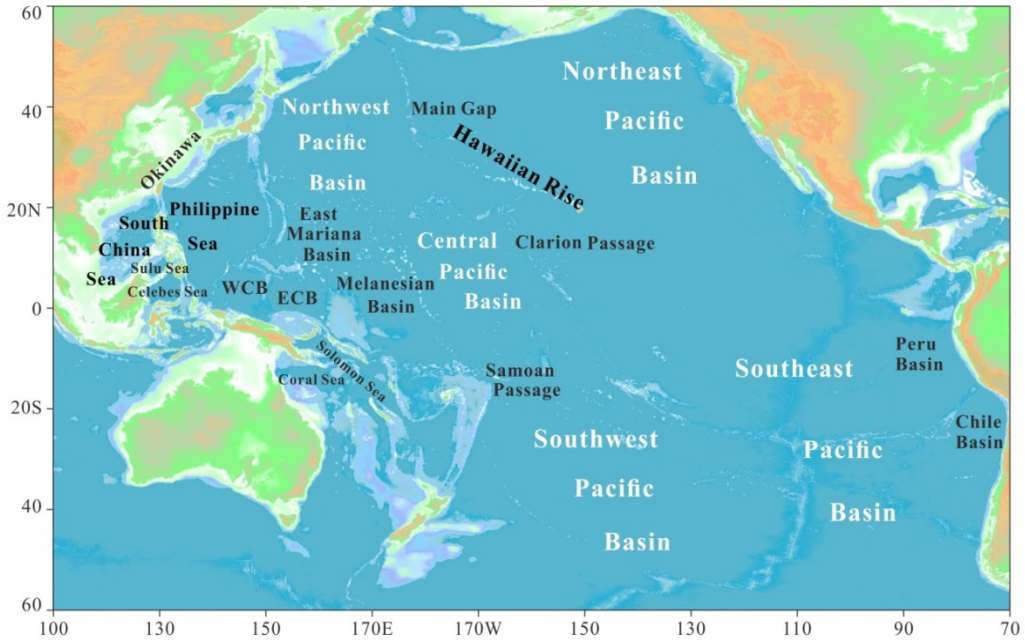

Fig. 1.1. Map of the main topographical features of the Pacific Ocean and its marginal seas. The acronyms WCB and ECB stand for the West Caroline Basin and East Caroline Basin, respectively.

The South China Sea (SCS) is the largest marginal sea in the western North Pacific. In the north it connects with the Philippine Sea and the East China Sea through the Luzon Strait (>2000 m) and the Taiwan Strait (<100 m) respectively (Fig 1.2). In the south, it connects with the Sulu and Javas Seas through the relatively shallow Mindoro (~200 m) and Karimata (<50 m) straits, respectively (Fig.1.2). On the west, the SCS is surrounded by a number of large rivers (e.g. Pearl River, Red River and Mekong River).

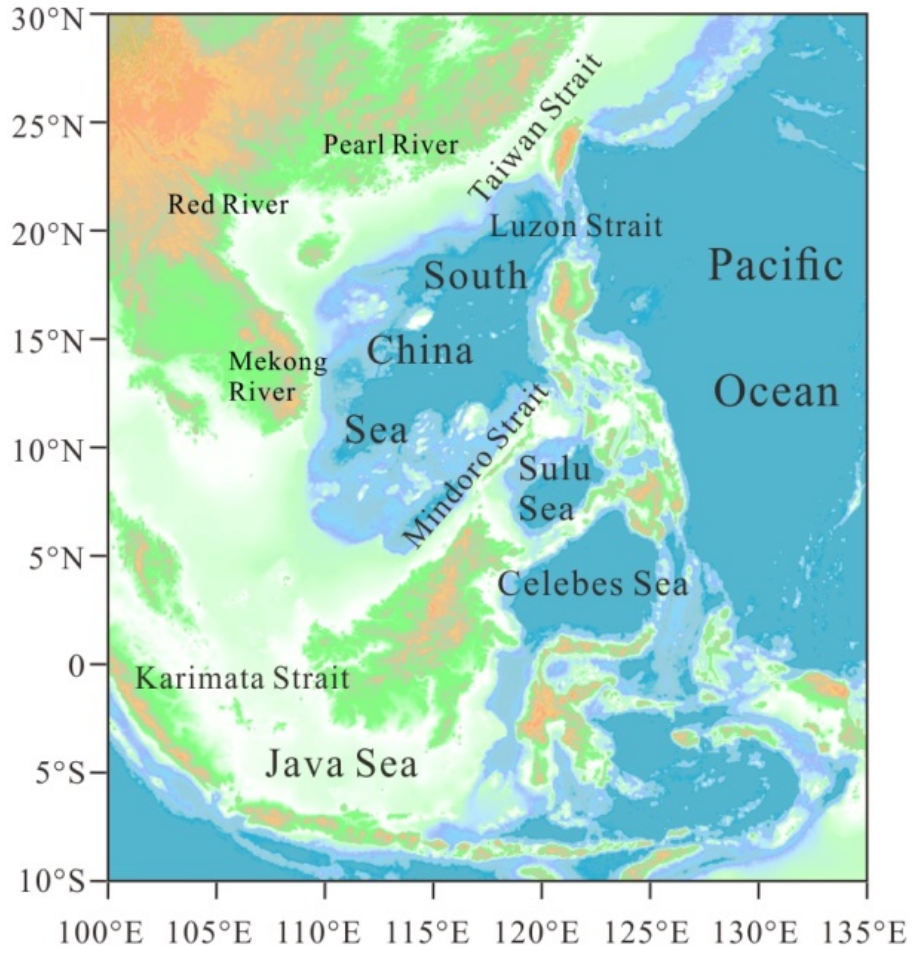

Fig. 1.2. Geographical map of the SCS. The main Asian rivers, as well as straits connecting the SCS with surrounding seas, are indicated.

1.2 Climatological and palaeoclimatological settings

The SCS and its surrounding continent are located in the low latitudes of the western Pacific. The tropical western Pacific is an important region in regulating global heat and

moisture transport (Trenberth et al., 1998; Qu et al., 2009). The regional climate is primarily affected by the East Asian Monsoon which is a sub-system of the Asian Monsoon (Wang et al., 2001 and 2004).

The Asian monsoon results from a contrast in land-sea sensitive heating (Webster, 1987) and is characterized by seasonal switches in wind direction, precipitation and runoff. It is a major determinant of land vegetation over SE Asia. During winter months, temperatures over the Asian continent, being lower than those over the Pacific Ocean, induce low surface pressure over the ocean and the development of a high pressure cell over northern Asia. This pressure gradient produces cold, dry winds that blow from Central Asia to the SCS. Conversely, during summer, the Asian continent heats up while the ocean stays cooler, inducing a low atmospheric pressure cell over central China, a reversal in wind direction and heavy monsoon rainfall over southern and eastern Asia (Webster, 1987). At the same time, this monsoon climate also has an influence on the SCS by generating a seasonal reversal of the oceanic circulation pattern (e.g. Wang and Wang, 1990).

Most of the paleoclimatic studies which permit the reconstruction of long-term East-Asian paleo-monsoon intensity variations, are based, primarily, on Chinese Loess Plateau deposits using several proxies such as grain size, magnetic susceptibility or clay minerals distribution (An et al., 2000; Porter and An, 1995; Xiao et al., 1995; Lu et al., 2000). Similar studies have been undertaken of deep-sea sediments from the Indian Ocean and the SCS. Such reconstructions have shown that, during glacial periods, summer East Asian monsoon intensity was weaker, whereas the winter one was stronger (Wang and Wang, 1990; Miao et al., 1994; Clemens et al., 1996; Pflaumann and Jian, 1999), when compared to the present conditions. These differences were marked by an increase in aridity over the northern Asian continent and significant eolian dust inputs, which originated from Chinese deserts, were deposited on the Central China Loess Plateau and in the northern Pacific Ocean. In contrast, interglacial periods are characterised by a stronger summer monsoon, coupled with strengthened southwestern winds and enhanced monsoon rainfall over the continent (Morley and Heusser, 1997; Lu et al., 1999).

In most of these studies, winter monsoon strength variations are characterized by strong cyclicities at ~100 and 41 kyr, with considerably less variance in the 23 kyr precession band, indicating a link between high-latitude climatic changes and monsoon variations (e.g. Ding et al., 1995; Xiao et al., 1995; Wang, 1999; Jian et al., 2001; Beaufort et al., 2003). Recent

studies have shown that the East Asian summer monsoon pattern could be independent from the winter monsoon intensity and be characterised by different orbital frequencies, which imply separate forcing controls. In terrigenous sediment records from the South China Sea, a strong 23 kyr precession cycle has been observed in East Asian summer monsoon intensity over the last glacial-interglacial cycles (Boulay et al., 2005), and during the period between 3.2 and 2.5 Ma (Wehaussen and Brumsack, 2002). Over low latitude areas, solar insolation, determined by the precession of the Earth orbit, has also been identified as the main factor controlling Indian summer monsoon intensity. It has already been widely studied in marine sediments from the Arabian Sea (e.g. Prell, 1984; Clemens et al., 1991; Clemens and Prell, 2003) and the Bay of Bengal (Colin et al., 1998 and 1999).

For the Holocene, several studies (stalagmite and SCS records) indicate a reduction in East Asian Monsoon precipitation well correlated with a southward shift of the ITCZ which, itself, is mainly driven by a reduction in summer solar insolation (Wang et al., 2005). At a shorter time scale, rapid changes in the East Asian Monsoon have been observed during the last climatic transition associated with a reduction in summer monsoon activity during the northern hemisphere cold event of the Younger Dryas (Wang et al., 2001). Such rapid climatic changes in the East Asian Monsoon have also been observed during the Holocene (Wang et al., 2005).

For the last glacial period, East Asian monsoon variations on Dansgaard–Oeschger time scales (1500 years) were reported from the SCS (Wang et al., 1999; Bühring et al., 2004; Higginson et al., 2003), the Sulu Sea (de Garidel-Thoron et al., 2001; Oppo et al., 2001), and the Sea of Japan (Tada et al., 1999). As an overriding feature these records reveal increased summer East Asian monsoons during interstadials, and increased winter East Asian monsoons during stadials. These marine-based results are consistent with the exceptionally well-dated monsoon records from Hulu cave (Wang et al., 2001) as well as with results from loess sections in China (Porter and An, 1995; An, 2000). In addition, opposite rainfall patterns have been observed in the northern and southern tropics during Heinrich cold events (H1) (Peterson et al., 2000; Wang et al., 2001; Placzek et al., 2006). However, the age models associated with these various archives are insufficient to assess either the fine details of phasing within the monsoon records themselves, or the details of monsoon phasing relative to high-latitude climate change, at the level necessary to determine which system initiates these abrupt transitions.

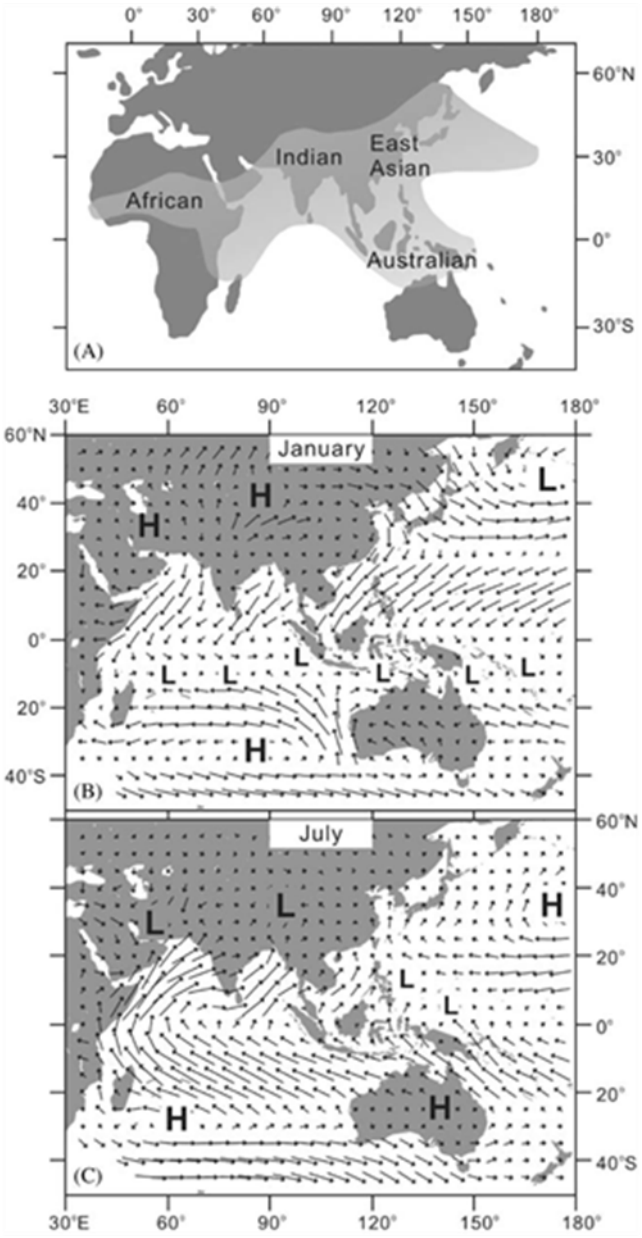

Figure 1.3. Modern Asian monsoon system: (A) distribution of modern monsoonal regions in Asia, Africa and Australia (Wang et al., 2005); (B) pressure and surface wind pattern in winter and (C) in summer.

1.3 Hydrological setting

1.3.1 Hydrology of the Pacific Ocean

Throughout the last two decades, numerous observational studies of deep circulation in

the Pacific Ocean have been carried out which have permitted us to greatly improve our understanding of the hydrology of the northern Pacific (Tsuchiya., 1991; Talley., 2007; Yasuda et al., 1997; Kaneko et al., 2001; Kawabe and Fujio, 2010). Salinity and water masses within different layers of two cross- sections in the North Pacific (24ºN) and the South Pacific (28ºS) are illustrated in Figure 1.4. This schematic map shows similar water mass structures in the North Pacific and South Pacific. Southern source waters from the South Pacific are observed in the North Pacific, but hardly any northern source water is observed in the South Pacific. This situation is essentially different from that of the Atlantic Ocean. To better understand what causes this particular characteristic, the hydrology of the Pacific Ocean is described in detail in the following section.

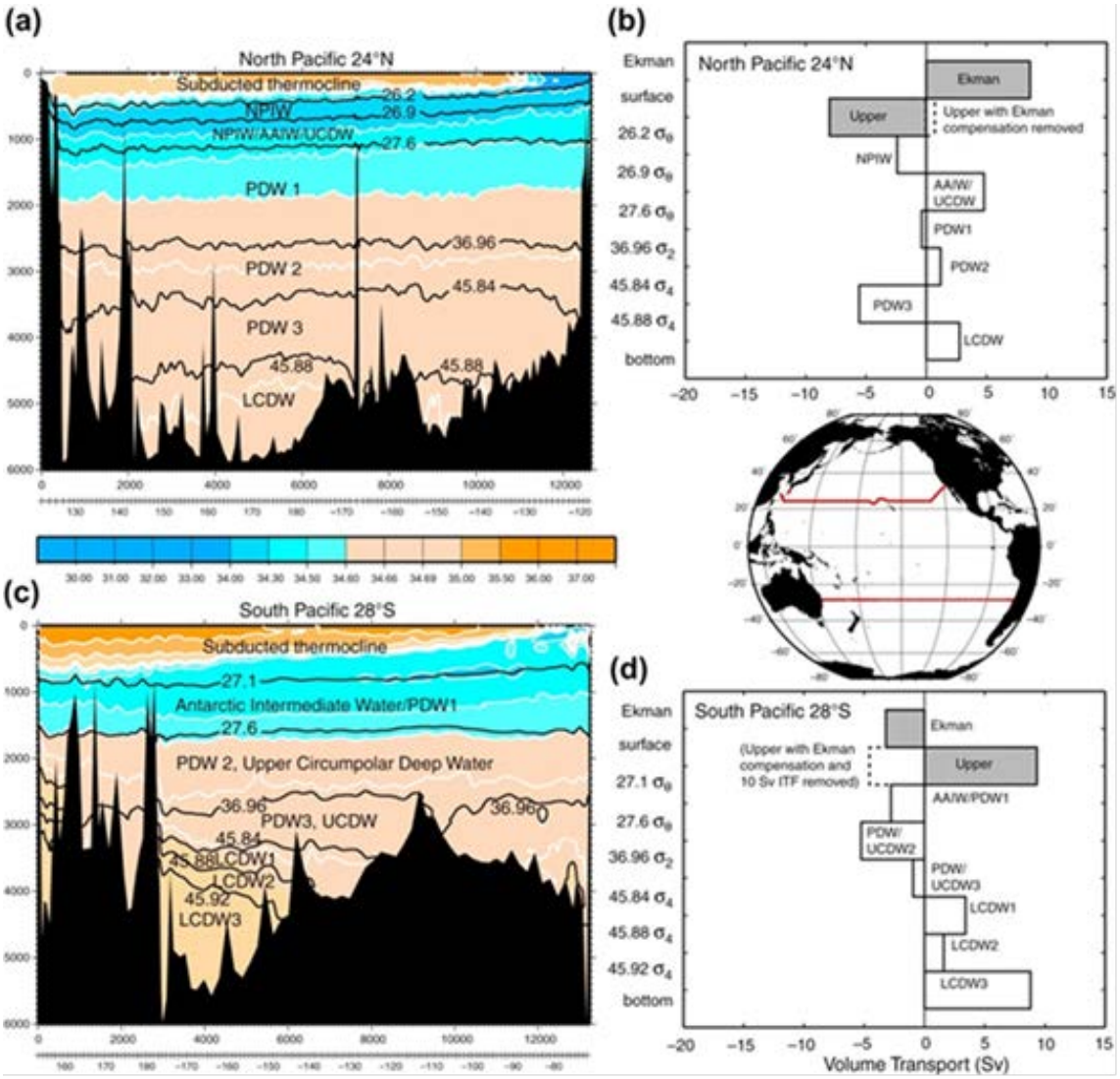

Figure 1.4. Spatial distribution of salinity and water mass components along cross sections centered at 24º N (a and b) and at 28º S (c and d) (Talley et al., Eds., 2011).

1.3.1.1 Surface water hydrology

The main surface currents of the Pacific Ocean are illustrated in the Figure 1.5.

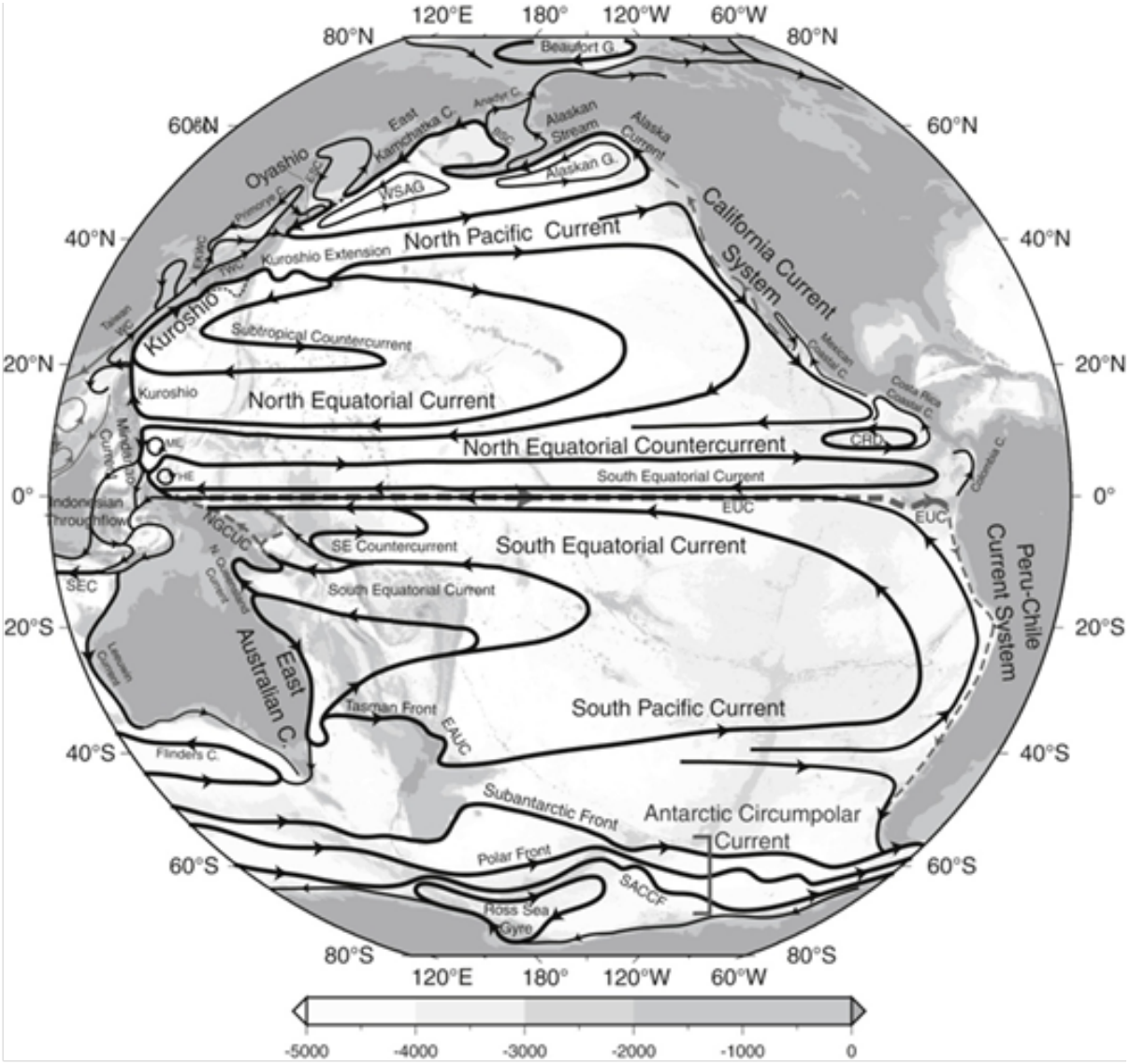

Fig. 1.5. Map showing the main surface currents in the Pacific Ocean (Talley et al., Eds., 2011).

In general, the surface layer, characterized by the highest salinity, originates in the region between latitudes 20ºN and 30ºN where evaporation dominates over precipitation (Suga et al., 2000). This extremely salty water is called North Pacific Tropic Water (NPTW) and occupies the layer above 200 m. The NPTW flows westward and is then advected in the North Equatorial Currents (NEC) (Suga et al., 2000; Lukas et al., 1996). On the western boundary of the North Pacific, the NPTW separates into two branches, the northward branch flows in the

Kuroshio Currents which contribute to the maximum salinity water component in the Philippine Sea. The southward branch of the NPTW, presumably carried by the Mindanao Currents, enters the Indian Ocean through the Indonesian Throughflow or is carried back to the North Pacific by the North Equatorial Countercurrent (NECC) (Fig 1.5) (Suga et al., 2000; Qiu and Lukas, 1996). Through salt exchanges with other water masses, the NPTW is the major source of salinity in the North Pacific and becomes gradually less saline along its westward pathway (Li and Wang, 2012).

1.3.1.2 Intermediate Water

At a greater water depth, there is a salinity minimum (34.0-34.4) clearly evident in the subtropical gyre of the North Pacific within a depth range of 300 to 900 m (You et al., 2000; Talley, 1993). This water mass corresponds to the North Pacific Intermediate Water (NPIW). It is believed that this NPIW is mainly formed in the eastern part of the Okhotsk Sea where the Kuroshio Extension mixes with the Oyashio currents (Talley., 1993; Yasuda et al., 1996; You et al., 2000) (Fig. 1.6). This water mass is formed by shallow convection in the Okhotsk Sea driven by wintertime brine rejection and is characterized by low salinity and high oxygen content. This relatively fresh water mass dominates most of the mid-depth layer (300-1000 m) in the North Pacific subtropical gyre. However, several recent studies have shown that the sources and process of formation of the NPIW, as well as the pathways of the NPIW in the North Pacific, are still not fully established (Miyao and Ishikawa, 2003; You et al., 2000; You., 2003; Nakano et al., 2007).

For the NPIW two pathways are currently debated in the literature (Fig 1.6). On the one hand, previous studies assumed that a considerable amount of the NPIW is transported into the subtropical gyre by the recirculation of the Kuroshio Extension in the North Pacific, which turns southwards around 160ºE and then back to the western part of the subtropical gyre (Talley., 1993; Yasuda et al., 1997; Masujima et al., 2003). A recent numerical study supports the existence of this short route for the NPIW (Fujii et al., 2013). On the other hand, other studies carried out by You (2003, 2010) have shown a long circulation pathway for the NPIW in the subtropical gyre, which implies that the NPIW spreads far further east of the 160ºE and enters the subtropical gyre at 140ºW.

The southern sourced intermediate water corresponds to the Antarctic Intermediate Water

(AAIW) and is also characterised by a salinity minimum (34.1-34.5) between 500 and 1500 m depth (Qu et al., 1998; Qu and Lindstrom, 2004; Lindstrom et al. 1990; Tsuchiya 1991) (Fig 1.6). AAIW generally originates from subduction of Antarctic Surface Water in the Antarctic convergence region and spreads to the west of South America (Reid, 1997; Talley, 1999). During winter, local winter convection induces a salinity minimum water. This water mass is injected into the AAIW. AAIW is carried to the Southeast Pacific through a wind-driven subtropical gyre. From there, it moves anticlockwise around the gyre and flows westward at low latitudes (~20ºS) as a tongue of low salinity and high oxygen (O_2) extending well into the Coral Sea (Fig 1.6). AAIW then spreads northward from the Coral Sea to the Solomon Sea and from the Solomon Sea to the Bismarck Sea. From there, AAIW is spread into the western North Pacific carried by the New Guinea Coastal Undercurrent (NGCUC) (Lindstrom et al. 1990; Tsuchiya 1991; Zenk et al., 2005).

After crossing the equator in the western Pacific, part of the AAIW flows eastward in the equatorial circulation, while the rest continues northward along the western boundary of the North Pacific (Reid 1965; Tsuchiya 1991). This northward AAIW is transported by the New Guinea Coastal Undercurrent (NGCUC) and the Mindanao Undercurrent, through which AAIW extends to about 15ºN along the Philippine coast (Qu et al. 1999; Qu and Lindstrom, 2004). The northern boundary between AAIW and NPIW is around 15ºN which prevents AAIW entering into the North Pacific subtropical gyre. The contribution of the AAIW becomes less pronounced as it flows northward via the western boundary currents into the North Pacific at 15ºN (Talley., 2007; Qu and Lindstrom, 2004).

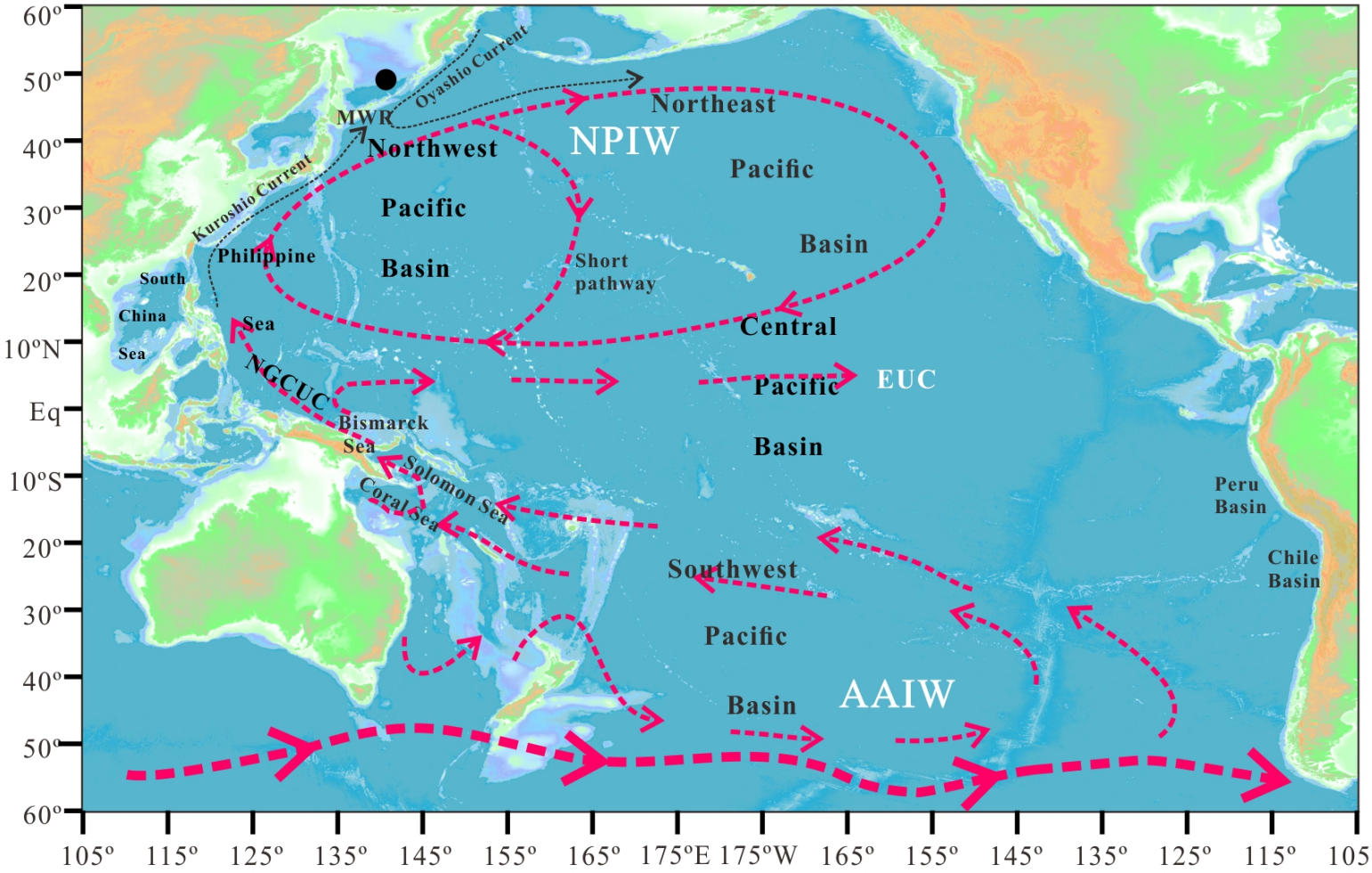

Fig. 1.6. Schematic map of mid-depth circulation in the Pacific Ocean. The round solid dot represents the main formation region of NPIW. The acronyms of MWR, EUC and NGCUC represent Mixed Water Region, Equatorial Under Current and New Guinea Coastal Undercurrent, respectively. The circulation mode is adapted from Zenk et al (2005), Kawabe and Fujo (2010) and You (2003).

1.3.1.3 Deep water masses

The deep water mass of the Pacific is characterized by two deep water masses, one originating from the Southern Ocean and one originating from the North Pacific (Fig. 1.7). Unlike the small amount of transport from the Pacific Ocean to the Atlantic Ocean through the Arctic Ocean, the water exchange between the Pacific Ocean and the Southern Ocean is estimated as being up to 100 Sv. The Southern Ocean circulation is dominated by the strong, deep, eastward-flowing current known as the Circumpolar Deep Water Current (CDW), which turns around Antarctica.

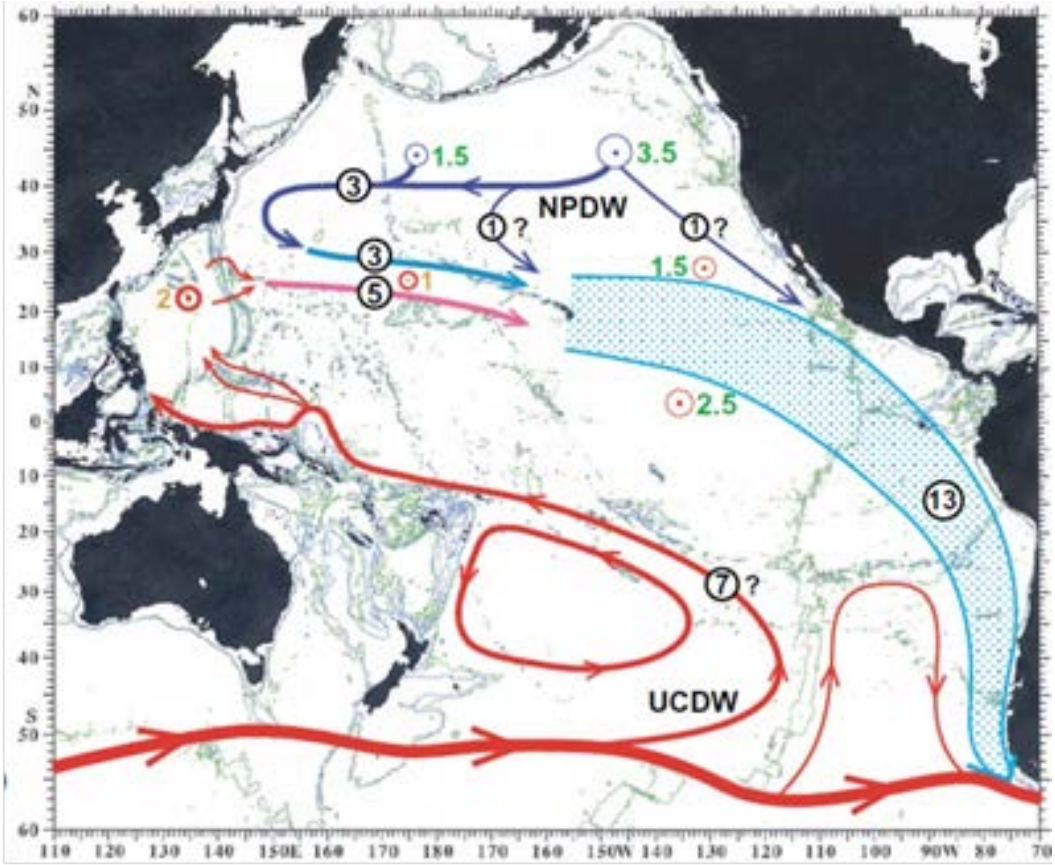

Fig.1.7. Schematic map of the upper deep-water circulation in the Pacific Ocean (after Kawabe and Fujio, 2010). Volumes of water masses transported by the main currents are indicated in Sv (10^6 m^3s^{-1}) within the dark circles.

The CDW is the very thick layer that extends from below the AAIW to above the dense bottom waters that are advected on the Antarctic shelves. The CDW contains a mixture of deep waters from each of the ocean basins: North Atlantic Deep Water (NADW), Pacific

Deep Water (PDW), and Indian Deep Water (IDW), as well as water formed locally within the Weddell Sea (Rodman and Gordon, 1982; Gordon et al., 2001; Oris et al., 1999; Rodehacke et al., 2007). It upwells south of the Antarctic Circumpolar Current (ACC) where a portion becomes the source of the bottom waters around Antarctica. Some of these dense Antarctic waters also modify the CDW which is usually divided into Upper CDW and Lower CDW (UCDW and LCDW) (Whitworth et al., 1999; Orsi et al., 1999; Rintoul et al., 2001).

UCDW originates from the Southern Ocean and is identified as an oxygen minimum layer created by the high contribution of low oxygen PDW and IDW and local deep water formed in the Antarctic area to the south of the Polar Front (PF). UCDW flows at a water depth of between 600 and 2000 m. In the South Pacific, UCDW lies below the AAIW and above the CDW. In the North Pacific, modified UCDW lies between NPIW and PDW (Fig 1.4).

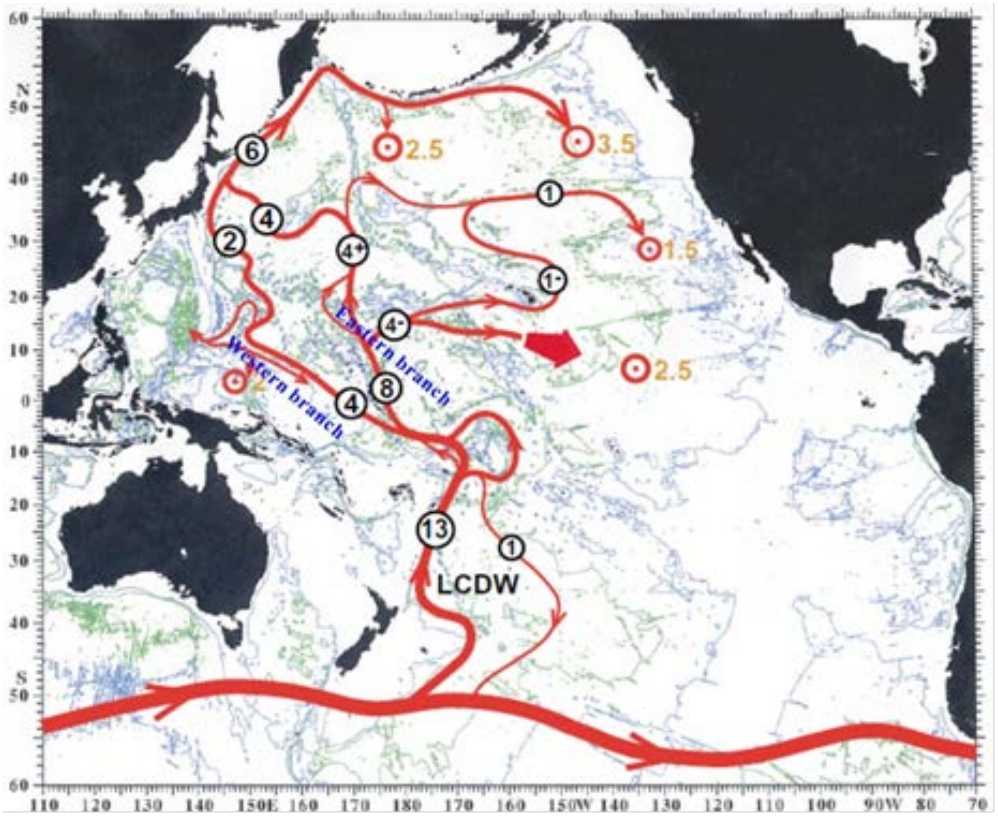

Fig.1.8. Schematic map of the lower deep-water circulation in the Pacific Ocean (after Kawabe and Fujio, 2010). Volumes of water masses transported by the main currents have been reported in Sv (10^6 m^3s^{-1}) within dark circles. The number x+ (x–) means a little more (less) than x Sv.

The LCDW is recognized in the Pacific by low temperatures and higher salinity than the overlying PDW. The LCDW enters the Pacific in the Deep Western Boundary Current (DWBC) in the southwest, east of New Zealand (Fig. 1.8). In the Central Pacific, the volcanic arc of the eastern Philippine Sea induced a separation of the LCDW into a western and an eastern branch. The western branch (about 4Sv) enters the Philippine Sea and flows northward to the Northwest Pacific Basin (Kawabe et al., 2003). The eastern branch (about 8 Sv) propagates eastward to the Northeast Pacific Basin through the western edge of the Central Pacific Basin (Kawabe et al., 2005 and 2009; Fujio et al., 2000). The Properties of the LCDW change while it propagates northward as a result of upwelling to the PDW in the North Pacific (Joyce et al., 1986; Johnson and Toole, 1993).

Pacific Deep Water (PDW) is observed everywhere in the North Pacific and is characterised by the absence of contact with the atmosphere. It is formed from internal mixing and upwelling of waters from the Southern Ocean (Talley, 2007). It is formed within the Pacific from upwelled bottom waters and modified UCDW/LCDW. In the North Pacific, north of 40ºN, the very oldest PDW is characterized by the lowest salinity of the North Pacific. The water acquires this property through downward diffusion of the upper-layer water mass that then forms “new” PDW corresponding to the North Pacific Deep Water (NPDW) (Talley & Joyce, 1992). PDW and UCDW occupy approximately the same density (and depth) range in the Pacific Ocean. The UCDW flows into the southeast Pacific whereas PDW flows to the west and then re-circulates to the South Pacific along the South American margin (Fig 1.7). The existence of this pathway of the PDW in the South Pacific is supported by silica concentration that indicates southward flow of PDW along the South American boundary (Kawabe and Fujio, 2010) (Fig 1.7).

1.3.2 Hydrology of the South China Sea

Regional hydrology investigations have been carried out in order to better understand the water masses in the SCS and its role in heat transportation in the region (Wyrtki, 1961; Qiu et al., 1984; Guo, 1985; Qu et al., 1997; Farris and Wimbush, 1996; Qu et al., 2000; Tian et al., 2006; Tozuka et al., 2007; Yuan et al., 2008). In general, the SCS is connected in the north to the Philippine Sea and the East China Sea through the Luzon Strait (>2000 m) and the Taiwan Strait (<100 m), respectively. In the south, it connects with the Sulu and Javas Seas through the relatively shallow Mindoro (~200 m) and Karimata (<50 m) straits, respectively (Fig.1.2).

The water exchange between the SCS and the surrounding seas involves a dominant inflow through the Luzon strait and a dominant outflow through the Karimata, Mindoro, and Taiwan straits. Recent studies have proposed a definition of this through flow as South China Sea Through Flow (SCSTF). These studies suggest that the SCSTF plays a key role in regulating the sea surface temperature pattern in the SCS and adjacent tropical Indian and Pacific Oceans (Qu et al., 2004, 2005, 2006, 2009; Tozuka et al., 2007 and 2009).

In addition, the surface circulation in the SCS is predominantly forced by the seasonal wind reversal during winter and summer monsoons. In general, during the winter, inflow of surface water into the SCS is predominant. On the contrary, during the summer an outflow of surface water predominates. (Fig. 1.9a and 1.9b). Within the water depth range of the thermocline, the intrusion of the Kuroshio Current into the SCS, during both summer and winter, has been observed in several studies (Farris and Wimbush, 1996; Caruso et al., 2006; Liang et al., 2008).

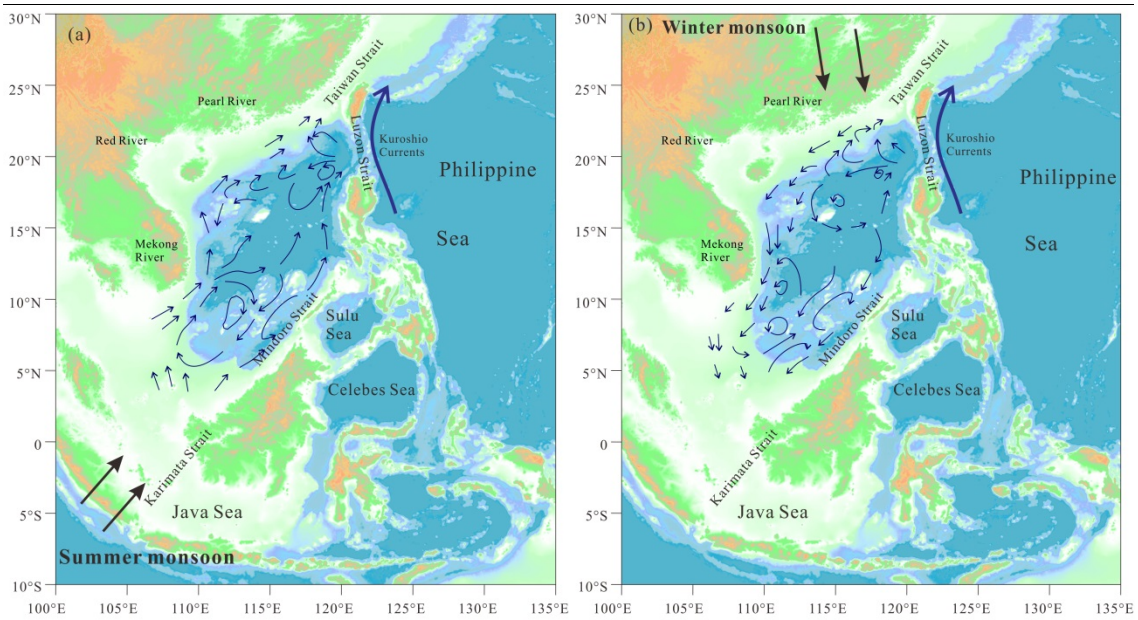

Fig. 1.9. Schematic map of the surface circulation in the SCS during the summer (a) and winter (b). (adapted from Fang et al., 1998).

The Luzon Strait is the deepest channel connecting the SCS with the Philippine Sea. It permits the intermediate and deep-water exchange between the SCS and the Philippine Sea. The hydrographic observations along a cross section roughly centred at 21ºN are illustrated in Figure 1.10. This figure shows a similar pattern of water T°C and salinity on both sides of the

Luzon Straits (Fig.1.10). However, slightly different potential temperature-salinity (θ-S) profiles between the SCS and the Philippine Sea indicate that modification of the water masses takes place in the SCS (Tian et al., 2009; Xie et al., 2011). As described below, the surface and upper layer of the Philippine Sea are dominated by NPTW. There is an intrusion of NPTW into the Northern part of SCS but the propagation of this water mass is restricted to the Northern part of the SCS due to the outflow of the South China Sea Tropical Water (SCSTW) to the Philippine Sea (Gong et al., 1992; Chen and Huang, 1996).

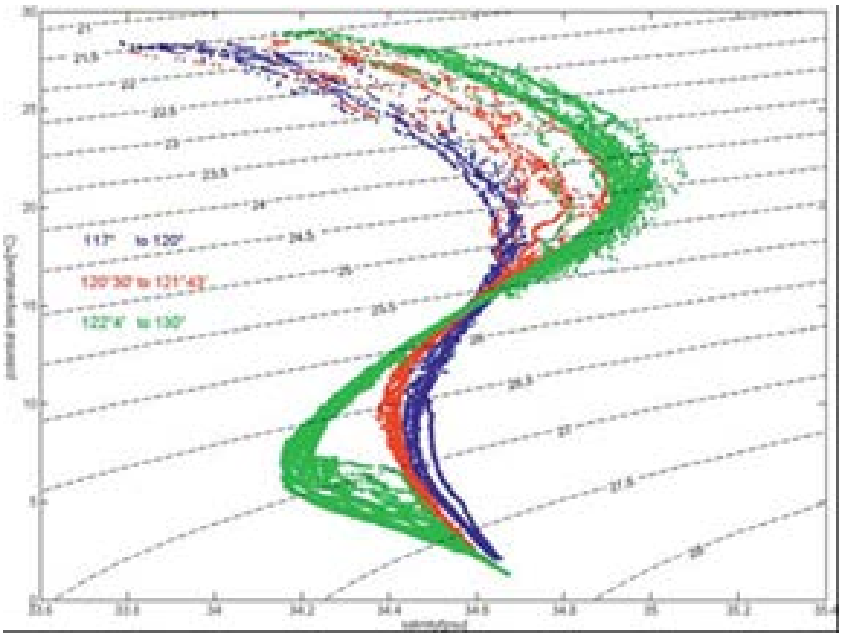

Fig. 1.10. Diagram of potential temperature versus salinity of water stations located along a cross section centered around a latitude of 21ºN (Tian et al., 2009).

Both hydrographic observations and numerical models indicate that, in order to compensate for the inflow of surface water (NPTW) into the SCS, there is an outflow of intermediate water from the SCS at depths between 500 m and 1500 m (Chao et al., 1996; Tian et al., 2006; Li and Qu, 2006; Yang et al., 2010). This water mass is called the South China Sea Intermediate Water (SCSIW) and is characterized by a weaker salinity minimum (>34.4) compared to NPIW (34-34.4) in the western Pacific Ocean. This weaker salinity minimum of the SCSIW results from the mixing of surface water with deep waters of the SCS (Chen et al., 2001; Liu and Liu, 1988). Nevertheless, the actual pathway of the intermediate layer through the Luzon Straits is not well understood (Tian et al., 2006; Yang et al., 2010; Xie et al., 2011).

Several studies show that the net transport of the intermediate layer is eastward and indicate a strong seasonal modification of the spatial distribution of the flow across the Luzon Strait. Field experiments conducted in July 2007 by Yang et al. (2010) indicate, at the intermediate layer, the existence of a westward flow in the northern part of the strait and an eastward flow in the southern part (Fig 1.11 a, b). Whereas earlier investigations, carried out in October 2005, in the same area demonstrated a reversed flow pattern across the strait, in which a westward flow and an eastward flow occur in the southern and the northern part of the strait, respectively. Consequently, the properties of intermediate water in the Luzon Straits vary seasonally (Qu et al., 2000).

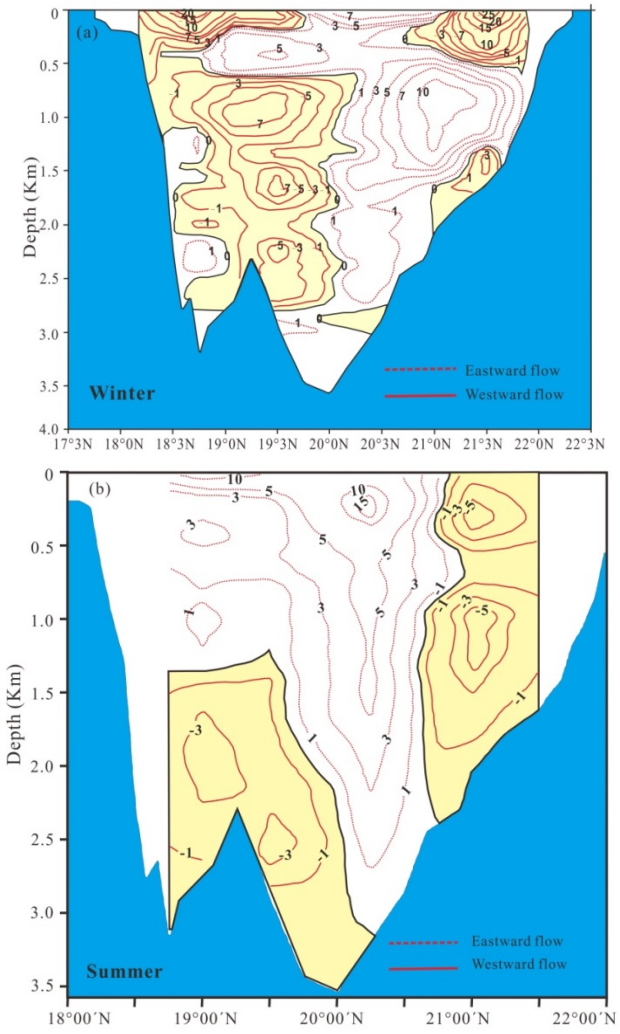

Fig.1.11. Flow velocity in the Luzon Strait, (a) and (b) show observation carried out in the October 2005 (winter) (Tian et al., 2006) and July 2007 (summer) (Yang et al., 2011), respectively. The dashed line indicates eastward flow whereas the solid line denotes westward flow. The area with westward flow is shaded in yellow.

Water masses below 2000 m in the SCS are characterized by relatively homogenous physical properties (T°C and S‰). They are similar to those of the western Pacific Ocean (Philippine Sea) at depths of around 2000 m (Li and Qu, 2006; Qu et al., 2006). PDW, characterised by low temperature (~2°C) and high salinity (>34.6), sinks in the deep SCS basin immediately after it crosses the Luzon Strait. It enhances vertical diffusion and upwelling and potentially contributes to upper layer circulation (Tian et al., 2009; Li and Qu, 2006; Qu et al., 2006). Both observations and models indicate that deep circulation in the SCS is strongly controlled by the complex bathymetry of the SCS (Li and Qu, 2006; Zhao et al., 2014; Wang et al., 2011; Zhang et al., 2014). It has been established that the PDW flows into the Luzon Straits mainly through the middle channel, then turns southward along the Luzon Trough, and finally enters the SCS (Fig. 1.12a). Forced by the Luzon overflow from the Pacific Ocean, basin-scale cyclonic circulation was found throughout the deep SCS. Embedded in the basin scale cyclonic circulation, a stronger sub-basin scale cyclonic circulation is seen around 116ºE in the central SCS where the current is probably influenced by a number of seamounts (Wang et al., 2011; Zhang et al., 2014) (Fig. 1.12b).

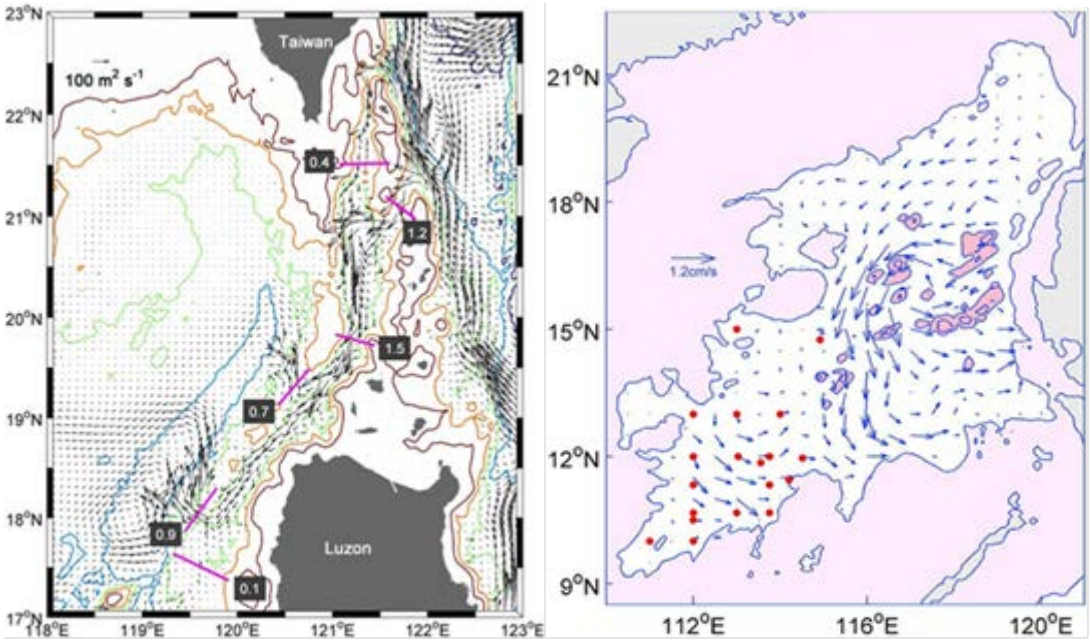

Fig. 1.12. (a) mean volume transport of the deep layer in the Luzon Straits from simulation (Zhao et al., 2014). (b) geostrophic current from 2400 m to the bottom, the light pink shading indicates water depths shallower than 2400 m. The dark pink shading indicates seamounts shallower than 3600 m (Wang et al., 2011).

The SCS is mainly affected by strong vertical mixing between deep and intermediate

water masses. As the intermediate water predominantly flows out of the SCS throughout the year, there is a strong inflow of deep water from the Pacific Ocean to compensate for this outflow. These processes induce the rapid turnover in the SCS deep water that has been recently estimated at around 30-50 years (Gong et al., 1992; Li and Qu, 2006., Wang et al., 2011). This suggests a very short residence time for deep-water in the SCS.

1.4 εNd as a proxy for reconstructing ocean circulation

Numerous recent studies have demonstrated the great potential of Nd isotopic composition ($^{143}Nd/^{144}Nd$) applied to seawater samples, as well as to authigenic phases or biogenic carbonates of marine sediments, to establish present and past hydrological changes of the ocean (Ling et al., 1997; Van de Flierdt et al., 2004; Rutberg et al., 2000; Piotrowski et al., 2005, 2008; Robert et al., 2010; Copard et al., 2010; Colin et al., 2010). This relatively new proxy is currently well developed and is widely used by the paleoceanography community. In this section, I present background information regarding the Sm/Nd geochemical system, the Nd cycle in the ocean, an overview of present day distributions of dissolved Nd isotopic composition of the SCS and the Pacific, and an overview of the different archives available for reconstructing past seawater εNd through time.

1.4.1 The Sm/Nd geochemical system

Neodymium (Nd) is a lanthanides series element (or Rare Earth Element - REE) that has seven isotopes: ^{142}Nd, ^{143}Nd, ^{144}Nd, ^{145}Nd, ^{146}Nd, ^{148}Nd, and ^{150}Nd. Of these, ^{143}Nd is a radiogenic daughter isotope produced by α-decay of ^{147}Sm, which has a long half-life of approximately 1.06×10^{-11} years (equations 1 and 2).

$$^{147}Sm \longrightarrow {}^{143}Nd + \alpha \qquad \text{(equation 1)}$$

$$(^{143}Nd)_t = (^{143}Nd)_i + (^{147}Sm)_t\,(e^{\lambda t} - 1) \qquad \text{(equation 2)}$$

Where the $(^{143}Nd)_t$ is the quantity of ^{143}Nd measured, $(^{143}Nd)_i$ is the quantity of initial ^{143}Nd, the $(^{147}Sm)_t$ is the quantity of ^{147}Sm measured, and the λ is the disintegration constant of ^{147}Sm ($\lambda = 6.54 \times 10^{-12}\ yr^{-1}$).

As is it very difficult to analyse the abundance of isotope ^{143}Nd, the ratio of radiogenic ^{143}Nd to stable ^{144}Nd has been used for geochemical investigations and equation 2 becomes:

$$\left(\frac{^{143}Nd}{^{144}Nd}\right)_t = \left(\frac{^{143}Nd}{^{144}Nd}\right)_i + \left(\frac{^{147}Sm}{^{144}Nd}\right)_i \left(e^{\lambda t}-1\right) \qquad \text{(equation 3)}$$

Where the $(^{143}Nd/^{144}Nd)_t$ is the Nd isotopic ratio measured, $(^{143}Nd/^{144}Nd)_i$ is the Nd initial isotopic ratio, and $(^{147}Sm/^{144}Nd)_t$ is the isotopic ratio measured.

The heterogeneity of the $^{143}Nd/^{144}Nd$ ratios of rocks depends mainly on the age differences and the fractionation of initial Sm/Nd ratios in the mantle and crust. Sm is selectively incorporated in mantle-derived oceanic basalts, whereas continental crust rocks are Nd-enriched. The Sm/Nd ratio of bulk earth can be assumed to be the same as that of chondritic meteorites. With increasing age, continental rocks display relatively lower $^{143}Nd/^{144}Nd$ ratios while oceanic basalts display higher ones (Fig. 1.13a). Due to the long half-life of ^{147}Sm, and the relatively comparable geochemical properties of the Sm and the Nd, the value range of the $^{143}Nd/^{144}Nd$ ratio analysed in rocks at the surface of the earth is very narrow. Nd isotopic compositions are, therefore, conventionally expressed using epsilon notation (εNd). This εNd is obtained by normalizing the $^{143}Nd/^{144}Nd$ measured in samples to the $^{143}Nd/^{144}Nd$ ratio of the Chondritic Uniform Reservoir (CHUR), which represents the present day average earth $^{143}Nd/^{144}Nd$ ratios (equation 4):

$$\varepsilon Nd = \left[\frac{\left(\frac{^{143}Nd}{^{144}Nd}\right)_{sample}}{\left(\frac{^{143}Nd}{^{144}Nd}\right)_{CHUR}} - 1\right] \times 10^4$$

Where the $(^{143}Nd/^{144}Nd)_{sample}$ and $(^{143}Nd/^{144}Nd)_{CHUR}$ represent the measured Nd isotope ratios in the sample and the CHUR, respectively. The $(^{143}Nd/^{144}Nd)_{CHUR}$ is 0.512638 (Jacobsen and Wasserburg, 1980).

For any rock, a negative or a positive εNd value implies that, on average over the history of the earth, the Sm/Nd ratio of that rock, or its precursors, has been lower/higher than the CHUR model. This in turn implies that the REE pattern of the rock, or its precursors, was light REE enriched/depleted (Fig. 1.13b). In general, crustal rocks are characterized by a wide range in εNd values, from 0 to -50, while mid-ocean ridge basalts (MORB) display positive εNd values of between 0 and + 12 (Piepgras and Wasserburg, 1980).

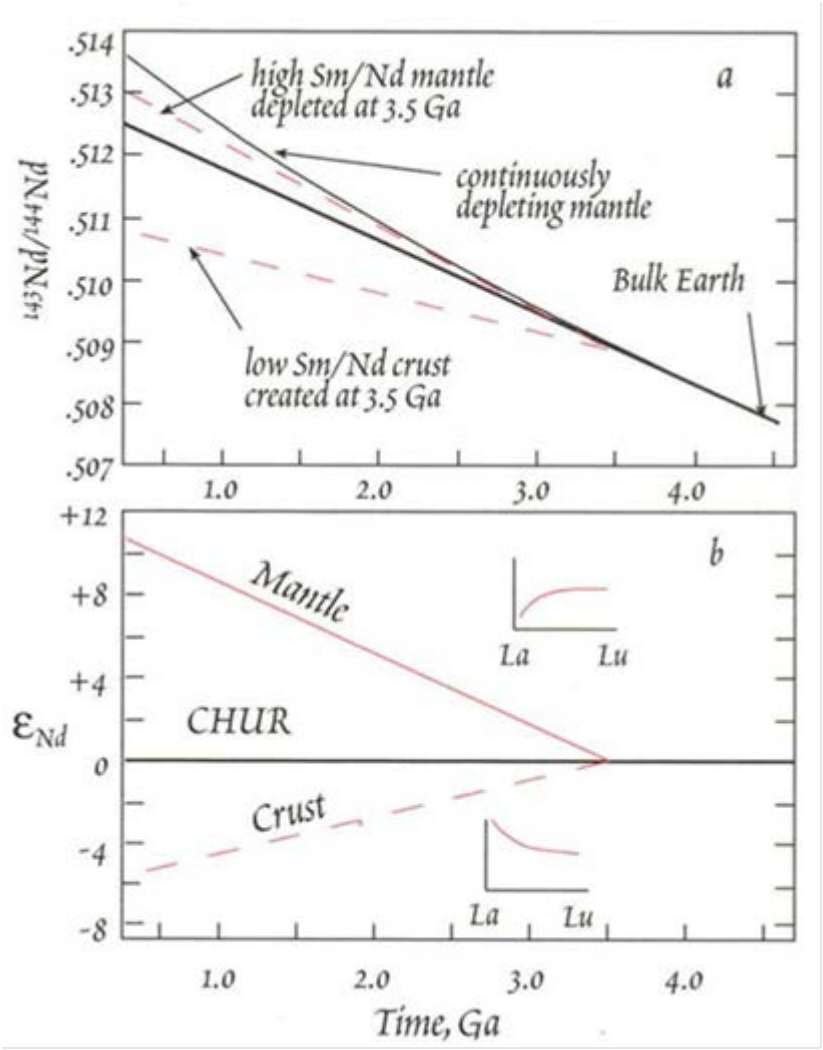

Fig. 1.13. (a) Evolution of the Nd isotopic composition in mantle and crust since 4.5 Ga. The bold line shows the evolution of the bulk earth or CHUR (chondritic uniform reservoir); also shown is the evolution of crust created at 3.5 Ga, the corresponding residual mantle, and the evolution of a continuously depleted mantle. (b) Evolution of bulk earth, crust, and mantle when $^{143}Nd/^{144}Nd$ is expressed by εNd (White, Ed., 2005).

1.4.2 Nd cycle in the ocean

Nd mainly exists in dissolved form in seawater (90 to 95 %), with a concentration of about 10^{-12} g/g which increases with water-depth (Jeandel., 1993; Amakawa et al., 2004; Singh et al., 2012). Its residence time, recently re-assessed to about 600 - 1000 yr (Tachikawa et al., 1999 and 2003), is shorter than the time for inter-ocean mixing. Consequently, through lithogenic inputs, water masses are characterised by different Nd isotopic compositions (Piepgras and Wasserburg, 1980; Jeandel, 1993; Jeandel et al., 1995; Lacan and Jeandel,

2004a; Lacan and Jeandel, 2004b; Lacan and Jeandel, 2004c; Lacan and Jeandel, 2005).

The provenances of the dissolved Nd in the ocean are outlined in the Figure 1.14. The dissolved Nd in the Ocean derives mainly from (1) the desorption of Nd from lithogenic particules originating mainly from eolian dust and riverine sediments; (2) dissolved Nd in rivers; (3) a process called “boundary exchange ”.

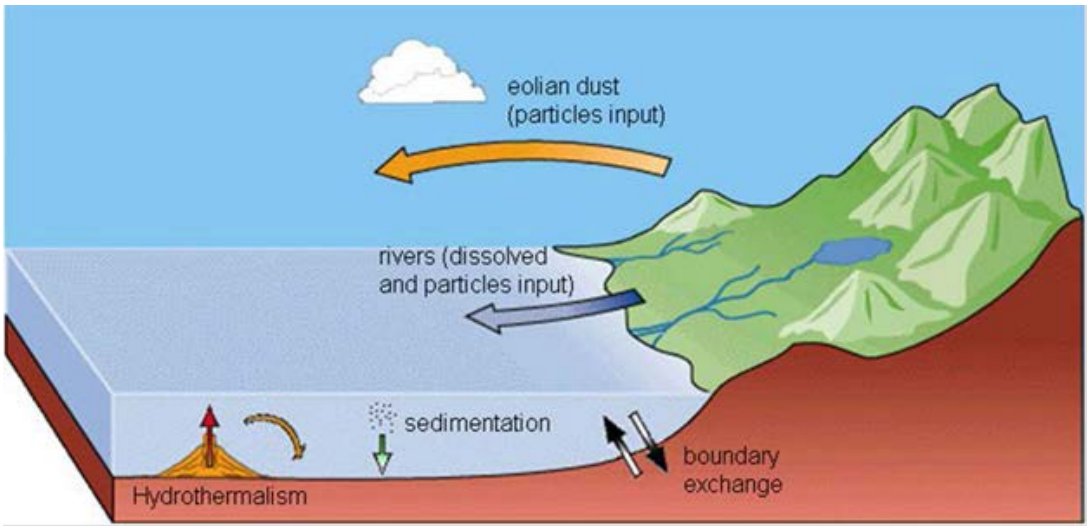

Fig. 1.14. Schematic diagram showing the main sources of dissolved Nd in the Ocean.

The contribution of each of these sources of Nd to the ocean, and the process involved in the global Nd oceanic cycle, are still poorly constrained. Over recent decades, great efforts have been made to better understand these issues (e.g. Arsouze et al., 2007; Rempfer et al., 2011; Lacan and Jeandel, 2005; Grenier et al., 2013; Grasse et al., 2012).

First of all, there is evidence that hydrothermal sources do not contribute significantly to the dissolved seawater Nd budget. It is generally admitted that the role of hydrothermal input is negligible because Nd, as well as all REEs, are scavenged quickly and very close to the hydrothermal sites (Michard et al., 1983; German et al., 1990; Halliday et al., 1992).

Riverine input, particularly in regimes of strong chemical weathering, is a very important source for the dissolved Nd budget of water masses, although most of the dissolved Nd load of rivers is precipitated in estuarine sediments (Frank, 2002; Elderfield et al., 1990; Ingri et al., 2000). Results from models also indicate that dissolved Nd input from rivers is an important component of the Nd cycle, particularly in the upper 500 m of the water column (Rempfer et

al., 2012).

Eolian dust can also influence the Nd isotopic signatures of surface waters by partial dissolution and desorption of dust particles. Tachikawa et al. (1997, 1999) suggested that up to 20% of the Nd contained in dust particles is released into seawater and, therefore, represents an important contributor to the dissolved Nd budget in the Atlantic Ocean. From REE patterns along an E-W transect across the Pacific Ocean, Greaves et al. (1999) showed that eolian inputs are important for the dissolved Nd budget of Pacific surface waters. In contrast, Jones et al. (1994) suggested that eolian sources of the Asian dust do not greatly modify the Nd isotopic composition of deep-waters in the NW Pacific. This is in agreement with recent simulations of the distribution of Nd in the ocean that indicate that Nd deriving from eolian dust inputs generally impacts only on the Nd isotopic composition of the upper layer of the ocean (Arsouze et al., 2007; Rempfer et al., 2012).

Earlier studies have indicated that continental margins play an important role in scavenging a number of elements in the ocean because of the efficient removal/deposition of the elements from the water column to sediments in areas affected by strong terrigenous fluxes (Anderson et al., 1990; Spencer et al., 1981). More recently, several studies have indicated an opposing interpretation of the role of the continent/ocean interface. These studies suggest an additional source of Nd to the Ocean induced by exchange of Nd between seawater and detrital particles delivered to the oceans from the continents by erosion (Lacan and Jeandel, 2001 and 2005; Grenier et al., 2013). Based on Nd isotopic composition analysis conducted on seawater located along four different oceanic margins (Fig. 1.15), Lacan and Jeandel (2005) showed, for the first time, that the Nd isotopic signatures of a water mass could be modified away from their original areas of production. They have demonstrated that the εNd of water masses flowing along an oceanic margin acquire the Nd isotopic composition of sediments from this margin. This modification of the Nd isotopic signature is caused by additional sources of Nd, whereas the Nd concentrations of the water masses show limited variations. This decoupling between Nd concentrations and Nd isotopic composition distributions in the ocean has been defined as the “Nd paradox”. A process called “boundary exchange” was proposed by Lacan and Jeandel (2005) to explain this “Nd paradox”. In this case, sediments on oceanic margins are not only the sink, but are also the source, of the Nd in the ocean. Indeed, “boundary exchange” corresponds to an exchange of elements (REEs) through the processes of absorption / desorption between water masses and sediments

deposited on the oceanic margin. Several studies have simulated Nd concentration and isotopic composition distributions in the Ocean (Arzouse et al., 2007, 2009; Grenier et al., 2011). Using different model configurations, Arzouse et al. (2007 and 2010) quantified the overall exchange rate of the “boundary exchange”. They found that the time needed for the oceanic margins to significantly imprint the Nd isotopic composition of the surrounding seawater ranges from 0.5 years for surface seawater to 10-50 years for deep water.

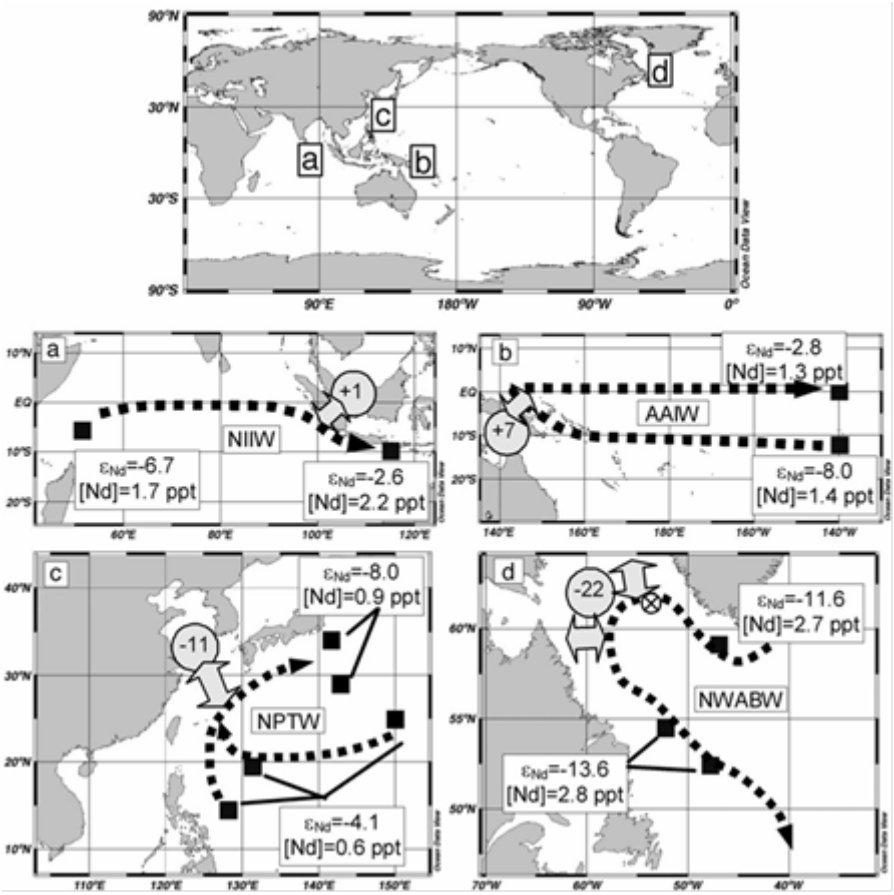

Fig. 1.15. Variations of the Nd isotopic compositions and Nd concentrations in different water masses flowing along 4 different oceanic margins (Lacan and Jeandel, 2005).

1.4.3 Nd isotopic composition of water masses in the western Pacific Ocean and the SCS

Compared with the large number of investigations carried out in the Atlantic Ocean, available data concerning Nd isotopic compositions in the western Pacific Ocean, and the surrounding continent, are scarce (Lacan et al., 2012, and reference therein).

Available full water column εNd data obtained from the Pacific Ocean are outlined in Fig.

1.16. Available surface seawater εNd values for the SCS, obtained by Amakawa et al., (2000), are listed in Fig. 1.17. Unfortunately, εNd values for intermediate and deep-water masses of the SCS and the Philippine Sea are not available. However, from all of these studies, it is possible to determine the Nd isotopic composition of the main intermediate and deep-water masses of the Pacific Ocean and Pacific sector of the Southern Ocean (Fig. 1.16).

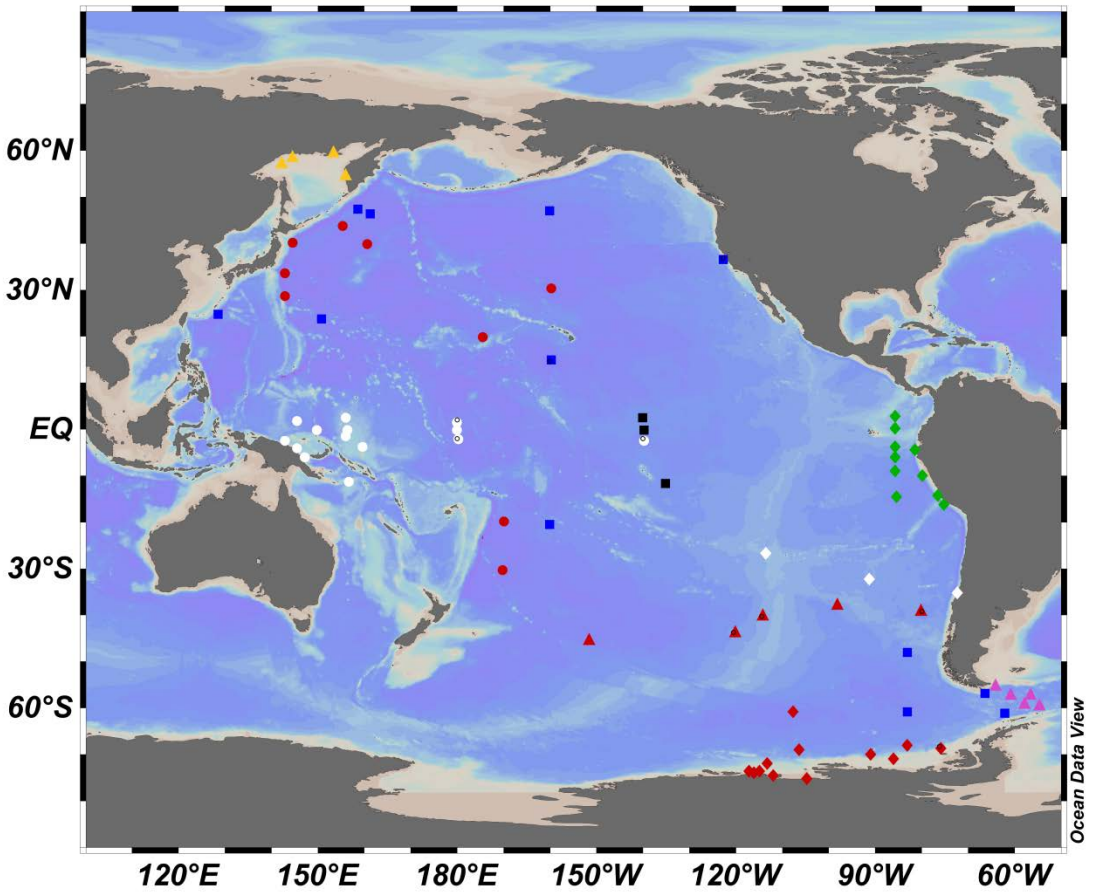

Fig. 1.16. Map of the positions of the water stations for which εNd are available for the full water column. Blue rectangles represent data from Piepgras and Wasserburg (1982), Piepgras et al. (1979), Piepgras and Jacobsen (1988). Black rectangles represent data from Lacan and Jeandel (2001). Red dots represent data from Amakawa et al. (2004, 2009, 2013). Green diamonds represent data from Grasse et al. (2012). Red diamonds represent data from Carter et al. (2012), Stichel et al. (2012). White dots represent data from Grenier et al. (2013). White diamonds represent data from Jeandel et al. (2013). Yellow triangles represent data from Haley et al. (2014). Red triangles represent data from Molina-Kescher et al. (2014).

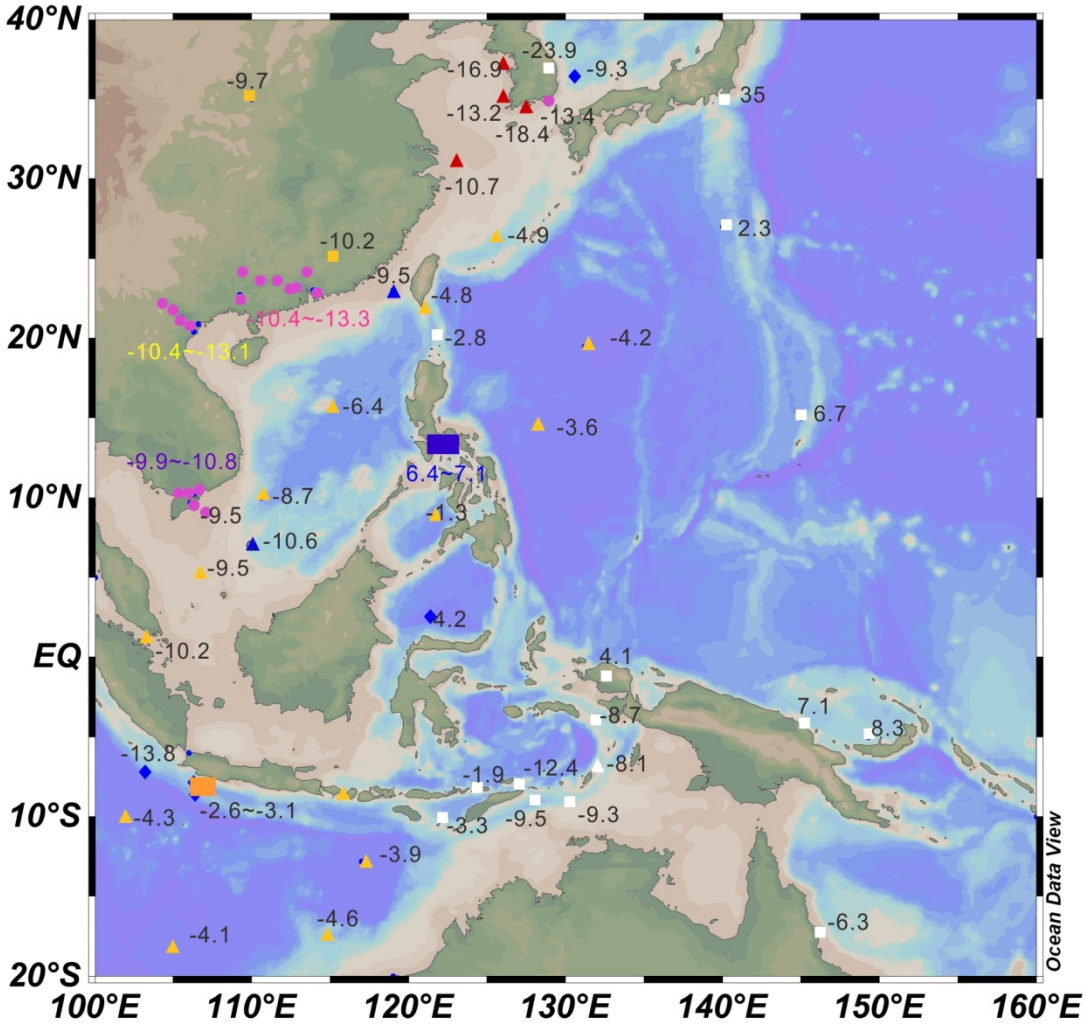

Fig 1.17. Map showing the distribution of sea surface water εNd values from the SCS and the surrounding marginal seas (orange triangle). εNd values of surface sediment and sediments from Asian rivers in the SCS and the surrounding marginal seas have also been included for comparison. Red triangles represent Korean and Yellow river sediments samples; blue diamonds represent core-top samples; yellow rectangles represent loess samples; white rectangles represent rocks samples; pink dots represent Pearl River/Mekong River/Red River sediments samples; blue triangles represent dust samples; blue rectangles represent Philippine river sediments samples. Data are from GEOROC database: http://georoc.mphmainz. gwdg.de/georoc/, Liu et al. (2007), Goldstein et al. (1984), Goldstein and Jacobsen (1988), Amakawa et al. (2000).

The εNd values of the water masses in the Southern Ocean range from -7 to -9. Such values are consistent with the mixing in the Southern Ocean of water masses from all the

oceans (Carter et al., 2012; Stichel et al., 2012) (Fig. 1.18a, b). In the North Pacific, the NPTW (<200 m) is characterised by a wide range of εNd values from 2 to -9 (Fig. 1.18 c, d, e). It is assumed that the eastern margins of the Pacific Ocean play an important role in the Nd isotopic composition of the NPTW in this region (Grasse et al., 2012). The NPTW carried by the NEC is transported westward and receives unradiogenic Nd from river particles, Asian dusts and/or exchange with the western Pacific margins (Amakwa et al., 2004).

The NPIW (300 m – 900 m) originates in the subarctic region and is characterised by a narrow range of εNd from -2 to -3.5 in the North Pacific. This is attributed to the volcanic nature of the margins of its zone of formation (Piepgras and Jacobsen, 1988; Haley et al., 2014; Amakawa et al., 2009) (Fig. 1.18 c). The εNd values for NPDW are around -4.5 and are slightly more negative compared to the εNd values of NPIW. This is because the NPDW is mainly fed by the southern sourced water mass (Fig. 1.18 a, b, f) characterized by unradiogenic Nd isotopic composition (Fig. 1.18 c). Vertical profiles of εNd values in the South Pacific show a negative trend from the surface (~-4) towards the bottom layer (~-9) and a positive shift with values ranging from ~-4 to -6 at depths of 2000 m. This implies that the water masses in the South Pacific are primarily transported from the south even though that the εNd of deep layers imprints the mixture with the NPDW (Jeandel et al., 2013).

Given that intermediate and deep-water masses of the Pacific are characterised by contrasting Nd isotopic signatures, εNd can be used to determine the provenance of the water masses and thus be used to constrain the circulation pattern in the Pacific Ocean. However, it is necessary to establish the Nd isotopic composition of water masses from the western Pacific Ocean (Philippine Sea) and the SCS where no εNd values for intermediate and deep-water masses are available.

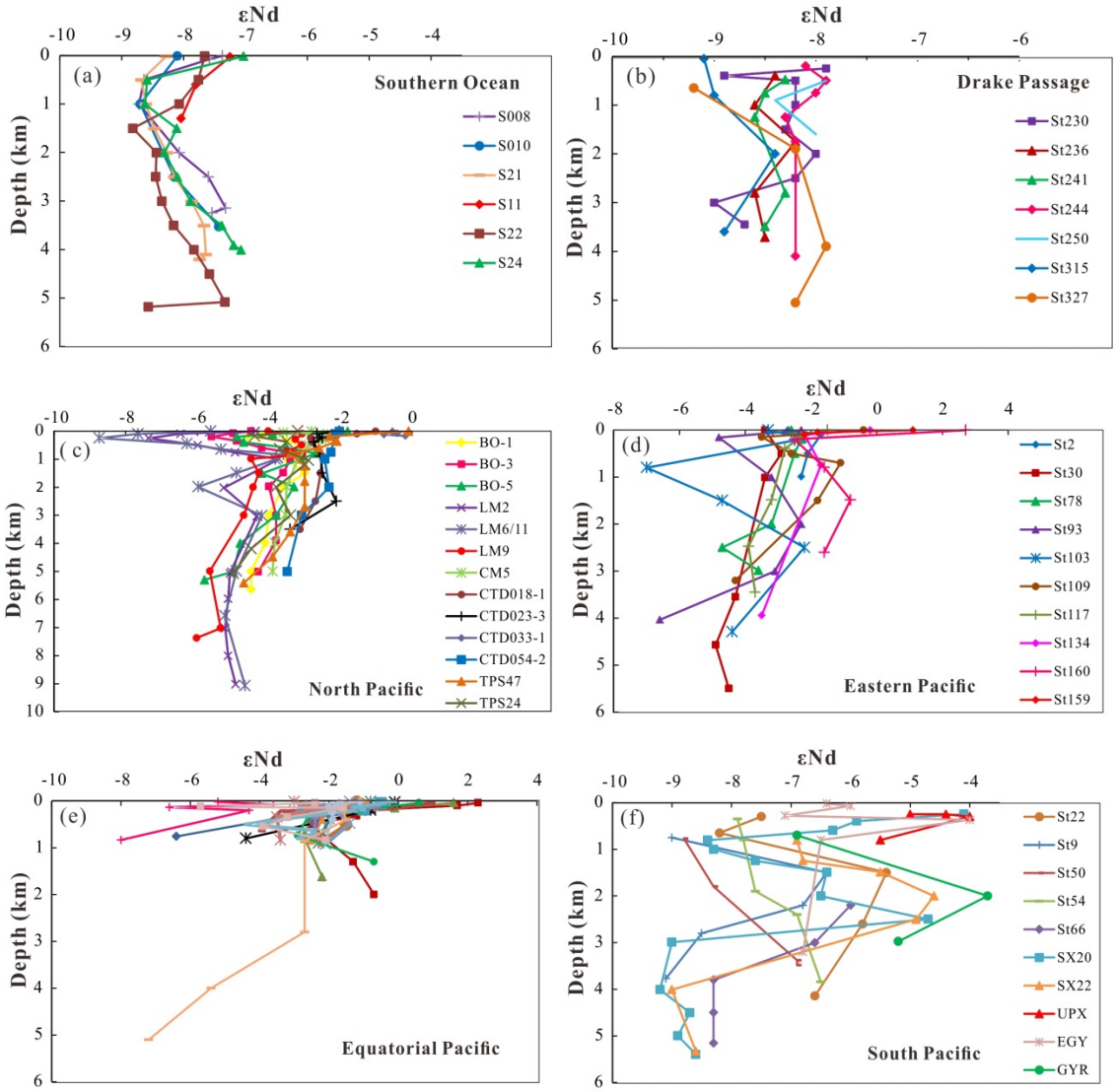

Fig. 1.18. seawater εNd versus depth of all water stations investigated in the Pacific Ocean and reported in the figure 1.16. Each diagram regroups seawater εNd data from a sector of the Pacific Ocean and the Southern Ocean. Data sources are indicated in the legend of figure 1.16.

1.4.4 Available archives for reconstructing past seawater εNd

Different archives have been used to reconstruct seawater εNd records, and to establish past ocean circulation patterns (Rutberg et al., 2000; Piotrowski et al., 2008, 2012; Bayon et al., 2004; Thomas., 2004; Martin and Haley, 2000; Martin and Scher, 2004; Meynadier et al., 2008; van de Flierdt et al., 2004; Ling et al., 1997; Gourlan et al., 2008; Colin et al., 2010; Copard et al., 2010). A reliable climatic archive needs to incorporate Nd from the seawater

and needs to maintain its integrity through burial and diagenesis. In addition, archives must be found throughout space and time, and must be datable.

During the last two decades, εNd has been investigated in numerous archives. These archives relate to biogenic carbonates (foraminifera and deep-sea corals), ferromanganese (Fe-Mn) oxide crusts and nodules, phosphates (particularly fossil fish teeth) and the Fe-Mn oxide coatings of sediments (e.g. Vance and Burton, 1999; Pomiès et al., 2002; O'Nions et al., 1998; Frank et al., 2006; Rutberg et al., 2000; Piotrowski et al., 2005; van de Flierdt et al., 2006; Copard et al., 2011).

Fe-Mn crusts and nodules record the Nd isotopic signature of the overlying seawater and thus the Nd isotopic signatures of the bottom water (Ling et al., 1997; O'Nions et al., 1998; van de Flierdt et al., 2004). Due to the relatively slow growth rate of ferromanganese (Fe-Mn) oxide crusts and nodules, they are commonly used to reconstruct oceanic circulation over long time scales (orbital to longer time scale) (Reynolds et al., 1999; Abouchami et al., 1997). More recently, the Fe-Mn oxide coating of particles and foraminifera has been proposed as a reliable archive from which to extract the Nd signature of bottom water (Rutberg et al., 2000; Piotrowski et al., 2004 and 2008; Gutjahr et al., 2008). It has been proposed that Fe–Mn oxides precipitate from the water column as coatings on biogenic carbonate and detrital particles. Consequently, Nd isotopic compositions analysed on the leachable Fe-Mn oxide components of sediments and foraminifera can be used to reconstruct past seawater εNd and ocean circulation at high-resolution time scales (centennial to millennial time scales) (Rutberg et al., 2000; Bayon et al., 2002; Burton and Vance, 2000). This proxy has been applied to South Atlantic sediments to track the northward propagation of the AABW when the formation of NADW had slowed down during the last glacial periods (Rutberg et al., 2000; Piotrowski et al., 2004, 2008; Pahnke et al., 2008). However, it has been demonstrated recently that this approach for extracting seawater εNd from the Fe-Mn coating of sediments is limited when it is applied in marginal regions. Indeed, river discharge can transport pre-formed authigenic Fe-Mn oxide from the land to the margin sediments (Bayon et al., 2004; Noble et al., 2012; Wilson et al., 2012). In this case, Fe-Mn oxides might record the Nd isotopic signature of water where pre-formed authigenic phase originated. Furthermore, the sequential leaching technique, involving different leaching times and/or different pre-treatments, could result in contamination through partial dissolution of Nd from the lithogenic fraction of sediments, particularly when mixed with volcanic ash. Consequently,

εNd, presumed to be from Fe-Mn oxide coatings, can be significantly influenced by Nd deriving from the detrital fraction due to the sequential leaching procedure used (Wilson et al., 2012 and 2013). Therefore, careful evaluation of Nd extraction from the Fe-Mn oxides is necessary and needs to be tested site by site before its application to a sedimentary core in order to establish the past seawater εNd record.

The fossil fish teeth/debris and the new deep-sea coral archive have been explored to reconstruct the Nd isotopic compositions of deep water and intermediate water (Thomas et al., 2003; Scher and Martin, 2004; Robinson and van de Flierdt, 2009; Colin et al., 2010; Copard et al., 2010, 2011, 2012). Fish teeth contain high concentrations of Nd mainly acquired during the early stage of diagenesis at the sediment - seawater interface (Staudigel et al., 1985). Thus fossil fish teeth record the Nd isotopic composition of the overlying bottom water (Martin and Haley, 2000; Thomas et al., 2004).

Nd incorporated in deep-sea corals was studied and showed similar εNd values to the seawater in which the corals grew (Copard et al., 2010; van de Flierdt et al., 2010). εNd were investigated in deep-sea coral in order to reconstruct past hydrological changes in intermediate and deep-water of the Atlantic and Southern Oceans at different time scales during the late Quaternary (Van de Flierdt et al., 2006 ; Robinson and van de Flierdt, 2009; Colin et al., 2010; van de Flierdt et al., 2010; Monterro-Serrano et al., 2013; Monterro-Serrano et al., 2011). Deep-sea corals have the potential to allow the reconstruction of past seawater εNd at unprecedented time resolutions (annual to decadal time scales) (Monterro-Serrano et al., 2013) and can be dated precicely using the U/Th method. Such dating allows coral-based records to be compared directly to continental records (ice cores). However, the lack of stratigraphic order in deep-sea coral sequences can also be a disadvantage because U/Th dating must to be performed on each and every coral individual to screen the age and/or growth rates of samples (Robinson et al., 2014).

Foraminifera are commonly used archives for paleoceanographic study. It is only in recent years that Nd isotopic composition has been applied to foraminifera in order to track past ocean circulation (Palmer., 1985; Palmer and Elderfield, 1985; Robert et al., 2012; Kraft et al., 2013; Tachikawa et al., 2013). While the analysis of Nd isotopic composition in foraminiferas has been widely used to reconstruct past changes in ocean circulation, the exact mechanism by which the Nd is incorporated in foraminifera is still a matter of ongoing

discussion. According to Palmer's assessment (1985), more than 90% of Nd is believed to be incorporated in the Fe-Mn oxide coatings of the foraminifera tested. This is in agreement with Pomiès et al. (2002) who have shown that Nd concentration in living planktonic foraminifera, collected in the water column of the Arabian Sea, is lower than that of cleaned planktonic foraminifera from the tops of sediment cores suggesting that cleaning procedures do not remove all Fe-Mn in foraminiferal coatings. In addition, Robert et al. (2012) present the same scenario based on analysis of foraminiferas from sediment traps, plankton and sediment cores. Recently, NanoSIMS ion probe- and electron probe microanalysis (EPMA), performed on uncleaned tests, together with scanning electron microscopy (SEM) imagery, have confirmed the significant role of Fe–Mn oxides as an Nd carrier in foraminiferas (Tachikawa et al., 2013). Kraft et al. (2013) also support this idea because the Nd extracted from different species of foraminiferas, using different cleaning methods, have produced similar εNd values that correspond to bottom water Nd isotopic signatures. However, there is some disagreement regarding the issue of whether the authigenic phase can be fully removed after sequential chemical cleaning (Vance and Burton, 1999; Kraft et al., 2013; Tachikawa et al., 2014; Pena et al., 2013). This is particularly important because Nd extracted from fully cleaned planktonic foraminiferas could be interpreted as representing seawater εNd from bottom water or surface water (Vance and Burton, 1999; Martínez-Botí et al., 2009; Pena et al., 2013). Due to the lack of large vertical gradient seawater εNd records at the study locations investigated to date, it is currently difficult to support the hypothesis that fully cleaned planktonic foraminiferas imprint the surface seawater Nd isotopic composition. Taking into account this argument, and the fact that Tachikawa et al. (2013) show clearly that Nd is mainly carried by Fe-Mn coating on the foraminifera test sample, it seems plausible that both cleaned and uncleaned planktonic foraminifera selectively record the εNd of the bottom water.

1.5 Geological and sedimentological settings and present day distributiosn of εNd in river- and in surface sediments of the SCS

Since the Nd isotopic composition of seawater can be modified by "Boundary exchange", I present in this section a brief overview of the geology of the study area as well as the Nd isotopic composition of the surface sediments of the SCS and of the river sediments feeding it.

1.5.1 Geological and sedimentological settings

The SCS is bounded by the South China (Yangzi) Block to the north, by the Indochina Block to the west, by the Philippine Sea Plate to the east, and to the south by the Island of Borneo and the Indonesian Archipelago (Fig. 1.19a). Heavy East Asian monsoon rainfall on the continent surrounding the SCS induces considerable runoff and chemical weathering on land. This is responsible for the supply and the deposit of approximately 700 million tons of sediment to the SCS, composed of about 80% terrigenous matter, delivered by numerous surrounding rivers, and 20% biogenic carbonates and silicates and volcanic ash (Huang., 2004).

The South China craton is mainly composed of Mesozoic-Cenozoic granite rocks and Paleozoic carbonates. Along the Pearl River drainage basin, Paleozoic-Mesozoic carbonate rocks, mainly Permian-Triassic limestone, dominate the western part; while in the eastern part of the basin, Mesozoic-Cenozoic granitic rocks and Paleozoic sedimentary rocks (limestone, shale, and sandstone) predominate.

In the Indochina Block, the Red and Mekong rivers originate in the Tibetan Plateau. Both of these rivers flow southeastward along the eastern Tibetan margin onto the Indochina plains before reaching the SCS. In the case of the Red River, Paleozoic-Mesozoic sedimentary rocks prevail in most parts of the upper and middle reaches, with minor outcrops of intrusive and extrusive igneous rocks exposed along the Red River fault zone. The Mekong River drainage basin is dominated by a major Paleozoic-Mesozoic sedimentary terrain (meta-sandstone, shale, slate, and phyllite): minor deposits of intrusive igneous rocks and Precambrian metamorphic rocks are found in its upper and middle reaches (Liu et al., 2004 and 2005). Mesozoic sedimentary rocks (mainly sandstone and mudstone) prevail in most parts of the lower Mekong River basin, in which several large Neogene basalt bodies outcrop.

The Philippine Sea Plate is accommodated across two major subduction zones, the east-dipping Manila Trench in the eastern SCS and the west-dipping East Luzon Trough in the western Pacific Ocean. Luzon is characterized by active volcanism, and a high degree of seismic activity. Cretaceous to Quaternary sedimentary and extrusive rocks and Cenozoic intermediate intrusive rocks abound throughout the island. The sedimentary rocks usually contain andesitic–basaltic pyroclastics and lavas. Plio-Quaternary volcanic deposits, mostly andesites and basalts with associated dacites and rhyodacites, mainly occur in southern Luzon.

In contrast, Cretaceous-Paleogene undifferentiated strata, commonly mapped as volcanics, are distributed in most of the mountainous regions of Luzon. Cenozoic intermediate-acid intrusive rocks, mainly as diorite, granodiorite, and quartz diorite, are associated with the undifferentiated Cretaceous-Paleogene volcanic rocks. Adakites and adakitic rocks have also been identified among the intrusive rocks (Bellon and Yumul, 2001). In addition, two blocks of Mesozoic ultrabasics, mainly peridotite, dunite and layered gabbro, are located at the eastern and southwestern margins of Luzon. A patch of Paleozoic metamorphic rocks also developed at the eastern margin. The largest river is the Cagayan River that flows through surrounding mountainous areas in northern Luzon, and then flows northward to the Luzon Strait. Cretaceous to Quaternary sedimentary and volcanic rocks and Cenozoic intermediate intrusive rocks occur in the drainage basin. A second large river, the Pampanga River, flows southward through southern Luzon into Manila Bay. Holocene to Miocene sedimentary rocks and Plio-Quaternary volcanic deposits are the major lithologies of this basin. The Vigan River in the NW and the Agno River in the SW drain through western Luzon and then flow into the South China Sea. A Mesozoic ultrabasic intrusive body developed in the Agno River drainage basin. In addition, there are more than 15 medium-sized rivers in western Luzon which drain into the South China Sea.

In the South, the bedrock of the Malay Peninsula consists mainly of Paleozoic–Mesozoic granite and granodiorite and Paleozoic sedimentary rocks. Minor Mesozoic (mainly Jurassic–Cretaceous) sedimentary rocks and occasional basic volcanic rocks developed in the central part of the Malay Peninsula. The sedimentary rocks mainly contain mudstone, sandstone, and limestone, interbedded with andesitic–rhyolitic volcanic rocks (Hutchison, 1989). Borneo is dominated by Tertiary sedimentary rocks, with a wide distribution of Paleozoic–Mesozoic sedimentary rocks in the central part and of Paleozoic–Mesozoic granite and granodiorite and Tertiary volcanic rocks in the south western part. The sedimentary rocks are generally sandy shale, partly interbedded with coal beds, sandstone, and carbonate rocks (Hutchison, 2004). Scattered Tertiary basic volcanic rocks and Mesozoic basic–ultrabasic intrusive rocks developed only in central tectonic belts, and late Tertiary acid volcanic rocks are scattered within Lower Tertiary sedimentary rocks. Sumatra is mainly covered by late Quaternary intermediate to basic volcanic rocks in the mountain ranges and slopes of the southwestern island and by late Tertiary sedimentary rocks on the plain of the north western island. There are also scattered occurrences of Paleozoic–Mesozoic volcanic, intrusive, and sedimentary rocks and Tertiary basalts.

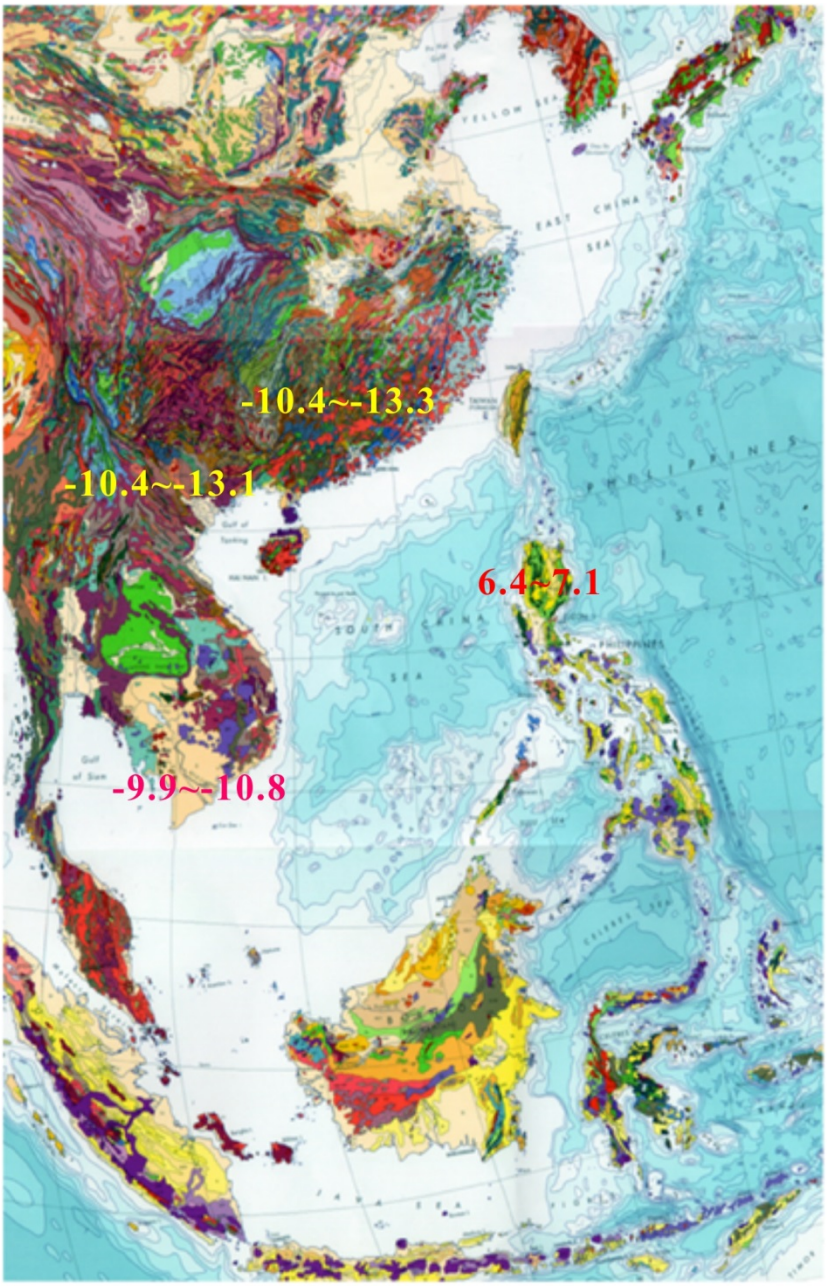

Fig. 1.19a. Geological map of SE Asia. εNd from the main Asian rivers delivering sediments to the SCS have been included (Liu et al., 2007; Goldstein et al., 1984, Goldstein and Jacobsen, 1988).

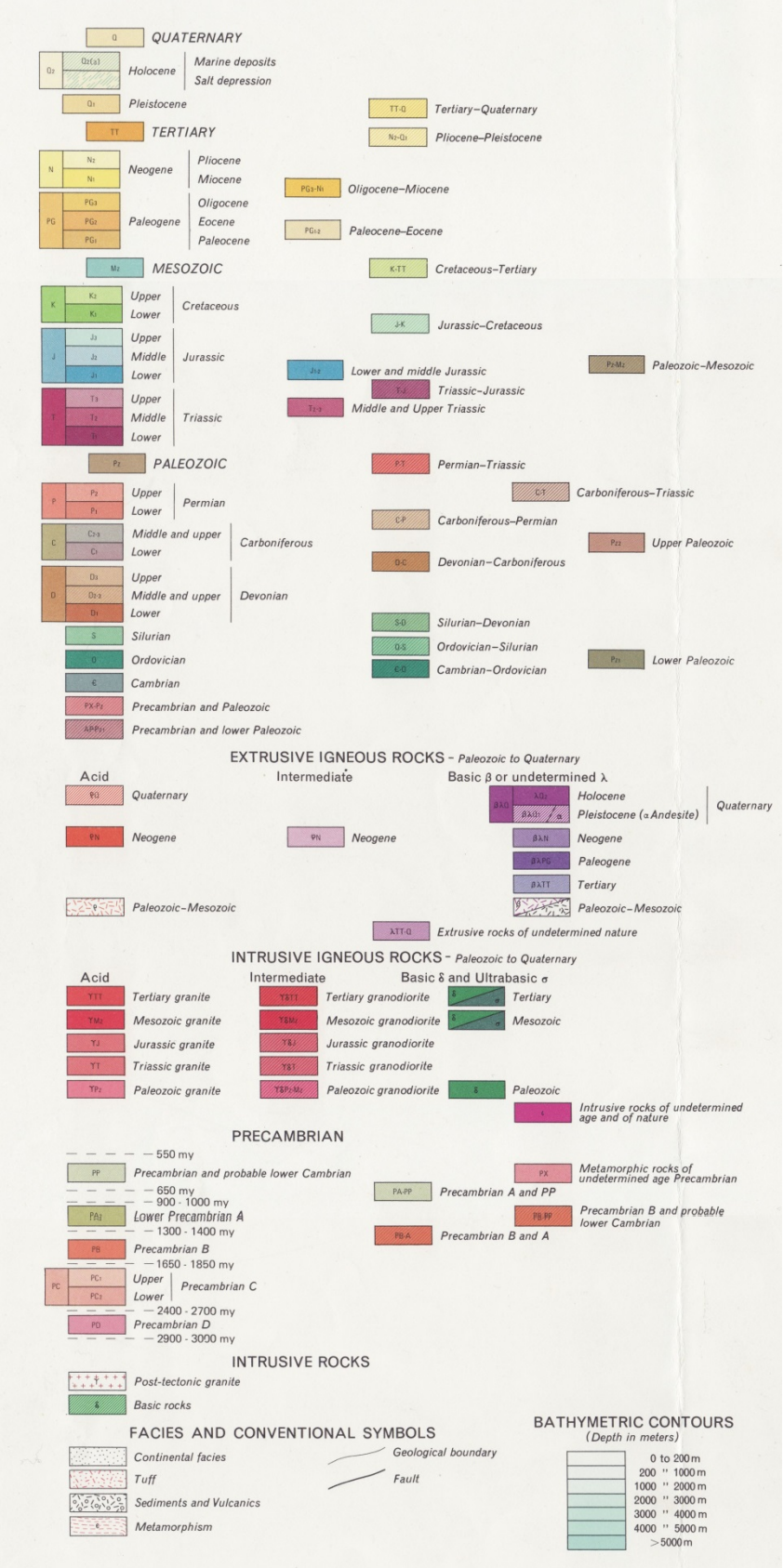

Fig. 1.19b. Legend for the geological map of SE Asia (Fig. 1.19a).

1.5.2 Present day distribution of εNd in river- and surface sediments of the SCS.

In general, εNd decreases over time, and therefore, as a consequence, continental rocks which tend to be old with low initial Sm/Nd ratios, yield relatively negative εNd values. In contrast, young rocks (basalts), derived from the mantle, are characterised by positive εNd values. Geochemical survey indicates that the εNd ranges from -56 in old granitic cratons to +12 in recent mid-oceanic ridge basalts (Goldstein and Hemming, 2003). Jeandel et al (2007) have compiled the available Nd isotopic composition data from the continent margins and have interpolated this data to produce a global map of Nd isotopic signatures for all of the ocean margins (Fig. 1.20). This interpolated map shows considerable spatial variability in the εNd and strong regional differences that are the potential source of dissolved Nd to local water masses. On this map, the margin Nd isotopic signatures vary from non-radiogenic values around the Atlantic Ocean to radiogenic values around the Pacific which are consistent with the trajectory of the "conveyor belt" global circulation, reinforcing the hypothesis that the exchange of Nd along the margins could play a significant role in driving the oceanic distribution of this tracer.

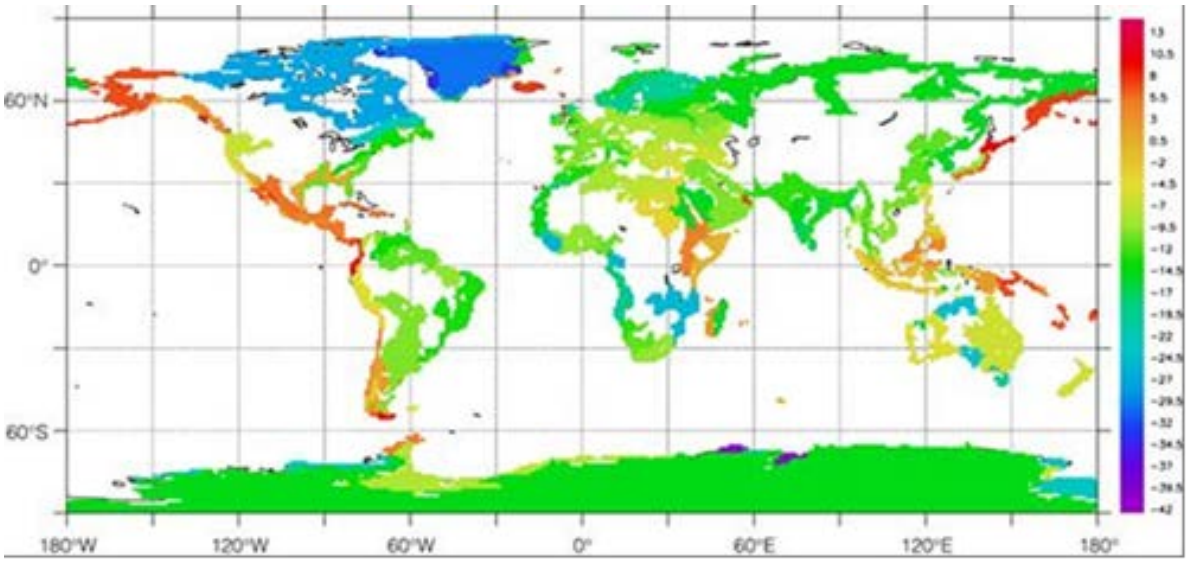

Fig. 1.20. Extrapolated map providing a picture of the Nd signatures of all ocean margins (Jeandel et al., 2007).

Around the SCS, the different geological formations are characterized by contrasting εNd values (Fig. 1.21). εNd values of rivers sediments surrounding the SCS are characterized by a large range of εNd from +7 to -13. The most positive εNd values (ranging from +6.4 to

+7.1) were observed in the Philippine Islands (Goldstein and Jacobsen, 1988). The εNd of the Pearl River drainage basin is characterised by negative values, around -13, which are similar to values obtained in the Red River basin (Liu et al., 2007). The εNd obtained from the Mekong River shows slightly higher values, of -10, compared to the Pearl River and the Red River (Liu et al., 2007).

A compilation of the Nd isotopic composition of surface sediments of the SCS is presented in Figure 1.21. In general, sedimentation in the SCS is mainly fed by river discharges from the surrounding rivers that are characterized by contrasting Nd isotopic compositions. The εNd of surface sediments from the SCS shows a zonal distribution dependent on sediment provenances (Wei et al., 2012). The most negative εNd values were obtained for sediments from offshore South China (-13.0 to -10.5), while those from offshore Indochina are slightly more positive (-10.7 to -9.4). The Nd isotopic compositions of sediments from offshore Borneo are even higher, with εNd values ranging from -8.8 to -7.0, and the sediments offshore from the southern Philippine Arc have the most positive εNd values of all, ranging from -3.7 to +5.3. This zonal distribution in εNd is in close agreement with the Nd isotopic compositions of the sediments supplied by river systems that drain into the corresponding regions (Wei et al., 2012; Li et al., 2003).

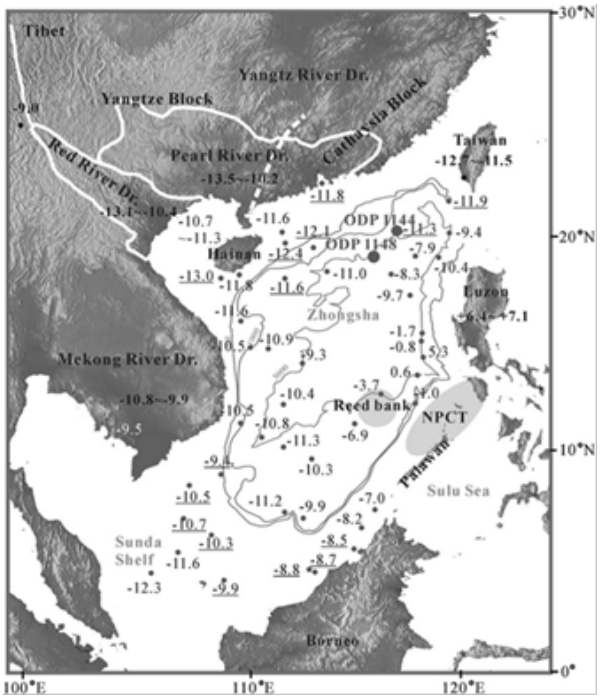

Fig 1.21. εNd values distribution in surface sediments from the SCS and from the surrounding rivers sediments (Wei et al., 2012).

1.6 State of the art of past seawater εNd records available in the Pacific Ocean: implications for past hydrological changes

Recently, Nd isotopic composition has been employed as a proxy to constrain past ocean circulation changes (Ruteger et al., 2000; Piotrowski et al., 2008, 2009, 2012; Robert et al., 2010; Basak et al., 2010). During the last glacial period, the formation of NADW was greatly reduced and water composition in the Southern Ocean was mainly dominated by locally-formed water around the Antartic and Pacific Deep Water (PDW). In addition, it has been shown that during North Hemisphere cold climate events, like the Henrich Stadial 1 (HS1) and the Younger Dryas, NADW production and its southward export to the Southern Ocean were reduced (Oppo and Fairbank, 1987; Labeyrie et al., 1996; Shemesh et al., 2002; McManus et al., 2004; Pahnke et al., 2008; Skinner et al., 2010). Ocean basins were replenished by the northward propagation of intermediate and deep water of Southern Ocean origin (Ninnemann and Charles, 1997; Rutberg et al., 2000; Piotrowski et al., 2009; Basak et al., 2010; van de Flierdt., 2006; Galbraith et al., 2007; Robert et al., 2010; Herguera et al., 2010).

Based on the reconstruction of paleo-seawater εNd, the Southern Ocean water masses display more radiogenic Nd isotopic composition during the LGM than the Holocene implying a decrease in the influence of NADW and an increase in southern water sources (Piotrowski et al., 2004 and 2008; Robinson and van de Flierdt., 2008; Skinner et al., 2013) (Fig. 1.22 a). Similar to the situation for the Southern Ocean, εNd of deep-water masses from the North Atlantic and the Indian Ocean also shift to positive values suggesting an intensification of southern water sources in different oceans (Robert et al., 2010; Pahnke et al., 2008; Piotrowski et al., 2009, 2012; Wilson et al., 2012) (Fig. 1.22 b, c). This suggests a northward intrusion of southern sourced water when the glacial NADW was unable to reach the Southern Ocean during the last glacial period.

In the Pacific Ocean, the εNd record presents a complex picture during the LGM: while the εNd of the Southern Ocean shifted to negative values, the εNd in the South Pacific Ocean, probably due the influence of the volcanic arc, shifted towards positive values during the LGM (Noble et al., 2013, Fig. 1.22.d). A negative excursion of the eastern Pacific Ocean εNd during cold intervals is revealed by the εNd at ODP Site 1240 (0º 1.31´ N, 86º 27.76´ W) and core MV99-MC19/GC31/PC08 (Baja California) (Fig. 1.22 d). This is more likely to reflect

changes in the amounts of southern sourced water rather than changes in the εNd of the Southern Ocean end-member (Basak et al., 2010; Pena et al., 2013).

During the HS1, εNd values in the Southern Ocean, revealed by Drake Passage deep-water corals, stand at -6.4 (Robinson and van de Flierdt, 2009). Such values are more radiogenic than those of modern Southern Ocean waters but are still more unradiogenic when compared to current NPDW εNd values (Piepgras and Wasserburg, 1982; Amakawa et al., 2009).

Several cores collected from the continental basin slope east of New Zealand show higher values of between -3 and -6 during the glacial period (Fig.1.22 d). This is probably due to the boundary exchange between volcanic sediments of the study area and seawater which modified overlying seawater εNd (Noble et al., 2013). In the equatorial and eastern Pacific Ocean, εNd negative excursions during rapid cold events (HS1, YD) indicate a higher proportion of southern source water in the study areas rather than changes in the εNd of the Southern Ocean end-member (Basak et al., 2010; Pena et al., 2013).

In the subarctic Pacific, where the enhanced glacial NPIW formation occurred, εNd values are nearly 2 epsilon units higher during the LGM than during the Holocene (Horikawa et al., 2010). In this study area, εNd of the sea surface water is strongly radiogenic due to particle exchange with sediments delivered by rivers from volcanic arcs. Therefore, this positive shift is interpreted primarily as being the result of vertical mixing with radiogenic εNd of sea surface water.

However, not all the studies agree on the same scenario. In the tropical Atlantic Ocean, reconstruction of paleo-seawater Nd isotopes indicates that the penetration of AAIW during HS1 did not increase but, rather, reduced instead (Xie et al., 2012; Huang et al., 2014).

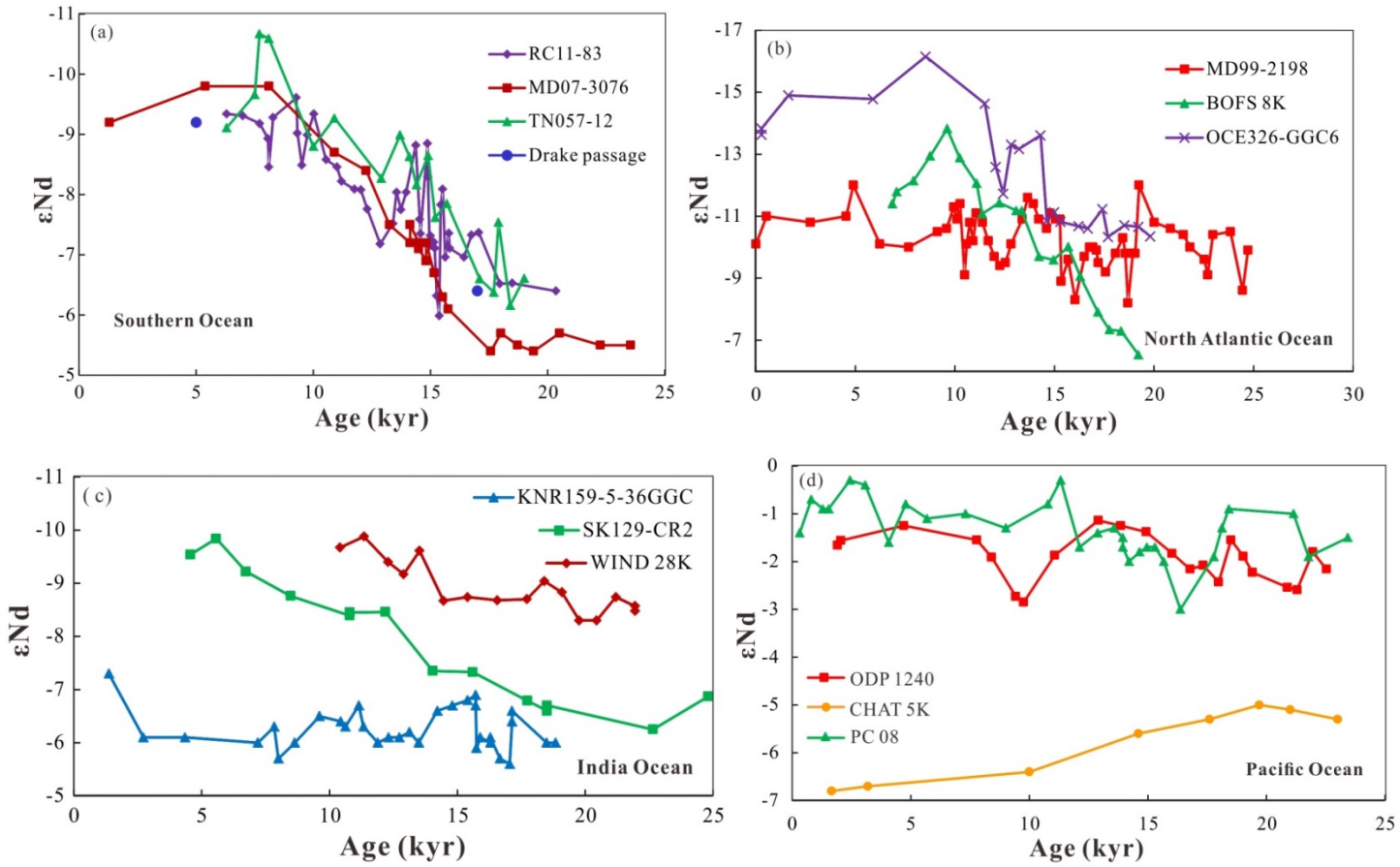

Fig. 1.22. Seawater-derived Nd records in the past ocean [(RC11-83, TN057-12, Piotrowski et al., 2004);(SK129-CR2, Piotrowski et al., 2009); (BOFS8K, Piotrowski et al., 2012); (Drake passage, Robinson and van de Flierdt, 2008); (KNR159-5-36GGC, MD99-2198, Pahnke et al., 2008); (PC08, Basak et al., 2010); (OCE326-GGC6, Robert et al., 2010); (WIND 28K, Wilson et al., 2012); (ODP1240, Pena et al., 2013); (MD07-3076, Skinner et al., 2013); (CHAT 5K, Noble et al., 2013)].

1.7 Summary of Chapter 1

Ocean circulation plays a key role in regulating the global climate. It transports huge amounts of heat from the tropical region to high northern and southern latitudes. Numerous paleo-climatological studies have dealt with the apparent links between ocean circulation changes and glacial/interglacial climate change (Broecker., 1998; Rutberg et al., 2000; Clement and Peterson, 2008; Baker et al., 2010; Skinner et al., 2010). The Pacific Ocean plays an important role in the global ocean circulation in terms of its volume, which, in turn, also has significant climatic implications. Compared to the Atlantic Ocean, the carrying out of hydrographical observation in the Pacific Ocean has been limited due to the complicated topography and the less distinguishable water characteristics, and little is known about the circulation below the 1000 m water depth. Nevertheless, it has received increasing attention over the last two decades (Talley et al., 1992; Talley and Yun, 2001; Reid., 1997; Zenk et al., 2005; Kawabe et al., 2003, 2006, 2009; Kawabe and Fujio, 2010).

The SCS constitutes the largest marginal sea in the western North Pacific. The deep-water below 2000 m in the northern part of the SCS is characterized by the PDW that enters the SCS from the Philippine Sea through the Luzon Strait. The deep-water masses of the SCS are characterized by a rapid turnover estimated at around 30 to 50 yrs.

Nd isotopic composition can be used to track the provenance of water masses and to reconstruct past changes in ocean hydrology, although the role of boundary exchange in affecting the seawater εNd is still open to question. The Pacific Ocean plays an important role by modulating global heat transportation and understanding the response of the ocean circulation to the climate changes. Nevertheless, the formation of NPDW, and the penetration of water originating from the Southern Ocean into the Pacific Ocean are, as yet, not well constrained. Using εNd records from various archives may constitute a promising way of constraining the paleo-hydrological changes in the region.

However, the Nd isotopic composition of the Philippine Sea and SCS water masses are not well established and require better constraint of the Nd isotopic composition of the different water masses of the studied area prior to the investigation of the Nd isotopic composition in marine climatic archives.

The relatively old geological formations along the western continent of the SCS are characterized by εNd values of between -10 and -13 (Goldstein et al., 1984; Liu et al., 2007). In contrast, the eastern margin of the SCS is surrounded by volcanic arcs characterized by εNd values ranging from +6.4 to +7.1 (Goldstein and Jacobsen, 1988). Consequently on the eastern margin of the SCS, river sediments from the Philippines display εNd values of between 6.4 and 7.1 (Goldstein and Jacobsen, 1988) (Fig.1.17). The SCS receives sedimentary input from the large Asian rivers (Mekong, Red River and Pearl River) which are characterised by higher unradiogenic Nd isotopic composition (-12) than those of North Pacific seawater (-4). In the context of the semi-closed SCS configuration, it is necessary to test the possible impact of boundary exchange on water masses entering into the SCS with sediments from the northeastern margin of the SCS that have the potential to modify the Nd isotopic compositions of the PDW, particularly in the northern part of the SCS which is characterized by a high sedimentation rate.

Chapter 2: Material and methods

In order to achieve the study aims outlined in the "General Introduction", analysis has been conducted of the Nd isotopic composition of seawater samples from several water stations in the Philippine Sea, the Luzon Straits and the northern SCS, as well as foraminifera and core-top sediments from the northern and southern SCS and a single gravity core from the north-western margin of the SCS.

In this chapter, a detailed introduction will be provided to the water stations and deep-sea cores which form the focus of the research and the reasons why these sites were selected will be outlined. In addition, details will be provided regarding the analytical methods adopted and the procedures used to develop the high temporal resolution age models for the marine cores investigated for the last 25 kyrs.

2.1 Material

The samples used in this study consist of seawater and sediments collected from core-top samples of gravity cores located in the northern and southern SCS. In addition, sediment samples from a single gravity core have been investigated at high temporal resolution for the last 25 kyr.

2.1.1 Seawater sample collection

112 seawater samples of 10-15 litres were collected from the northern SCS, Luzon Straits and the western Pacific during five oceanographic cruises which were carried out by R/V Kexue No.1, R/V Shiyan No.3 and R/V Dongfanghong No.2 during September 2009, May 2010, Novenber 2010, December 2010 and March 2013 (Table 2.1).

As indicated in chapter 1, up to now there have been no available εNd data for the Philippine Sea. As the Philippine Sea constitutes the main source of the deep-water masses (PDW) in the SCS, which enter via the Luzon Straits, it is absolutely necessary to constrain the Nd isotopic composition of the Philippine Sea water masses in order to understand the Nd isotopic composition distribution of the SCS. In addition, the Philippine Sea is a key area when reconstructing the hydrology of the Pacific because it constitutes an area where northern and southern origin water masses are mixing (Kawabe and Fujio, 2010; Qu and Lindstorm, 2004). Samples were collected from three stations (P1, P2, N18-05) in the Philippine Sea in order to determine, for the first time, εNd distribution in the water columns of this part of the western Pacific Ocean. This will allow the establishment of the εNd composition of the intermediate- and deep-water masses that enter the SCS (Table 2.1).

Seawater samples from 7 stations were collected from the northern SCS, along the speculated deep-water pathways, in order to trace deep water transportation from the western Pacific to the SCS. 3 stations in the northern SCS (C5, D3 and 10JJW-72) were sampled near, or above, significant drift sediment systems (Lüdmann et al., 2005). In addition, at stations C5 and D3, nepheloid layers were observed. For these two water stations, concentrations of particles in the water column have been analysed in order to identify nepheloid layers and seawater samples have been taken within the nepheloid layers in order to assess possible

exchange of Nd between particles and seawater.

In addition, several sea surface water samples were collected from both the northern and the central SCS. The SCS plays an important role in connecting the heat transport between the North Pacific and the Indian Ocean through surface circulation. It is known that there is a north - south gradient of εNd in the SCS (Amakawa et al., 2000). However, this result was obtained from unfiltered seawater. It is necessary to re-analyse the surface seawater in the north and the south SCS in order to confirm these results with filtered seawater samples.

Three stations (A3, C3a and A6) located at the Luzon Straits were sampled in order to constrain water exchange between the Philippine Sea and the SCS. Samples from station A3, in the northern part of the Luzon Straits, were collected during April 2013: the station is located in an area where inflow of intermediate water from the Philippine Sea to the SCS has been shown to be dominant during the summer monsoon season (Yang et al., 2010). Samples from station A6, which is located in the southern part of the Luzon Straits where outflow of intermediate water from the SCS to the Philippine Sea has been shown to be dominant, were collected in April 2013. Finally, samples were taken during November 2010 at a third station (C3a), located in the middle part of the Luzon Straits where outflow of intermediate water from the SCS to the Philippine Sea has been shown to be dominant (Tian et al., 2006). These three water stations were sampled in order to determine the εNd of intermediate- and deep-water masses that flow between the SCS and the Philippine Sea.

Seawater samples were collected with a Sea-Bird 911 *plus* conductivity-temperature-depth (CTD) equipped with a 12-L Teflon-coated Niskin bottles Rosette sampler that have been proven to be reliable for Nd and REE clean collection. Before the seawater collection, the Niskin bottles were rinsed with Suprapur HCl. All of the seawater samples were filtered through a 0.45 μm filter within 12 hours after collection or directly during collection on board. The filtered seawater was then acidified to pH= ~ 2 with 2 M Suprapur HCl. 500 ml of seawater was separated from the filtered water for REE concentration measurement.

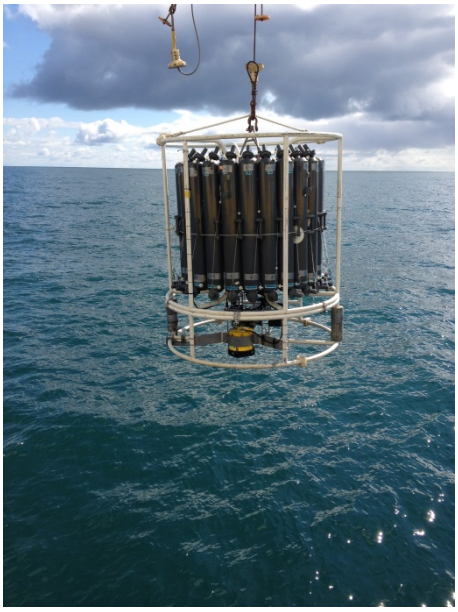

Fig.2.1. Picture of on board seawater sampling

Table 2.1: location of seawater stations and date of seawater sampling

Water station	Latitude	Longitude	Date of sampling	Cruise	Water depth (m)
P2	16°30′ N	130°00′ E	Dec-10	NSFC open cruise 2010	5
P2	16°30′ N	130°00′ E	Dec-10	NSFC open cruise 2010	500
P2	16°30′ N	130°00′ E	Dec-10	NSFC open cruise 2010	1400
P2	16°30′ N	130°00′ E	Dec-10	NSFC open cruise 2010	1600
P2	16°30′ N	130°00′ E	Dec-10	NSFC open cruise 2010	1800
P2	16°30′ N	130°00′ E	Dec-10	NSFC open cruise 2010	2000
P2	16°30′ N	130°00′ E	Dec-10	NSFC open cruise 2010	2200
P2	16°30′ N	130°00′ E	Dec-10	NSFC open cruise 2010	2400
P2	16°30′ N	130°00′ E	Dec-10	NSFC open cruise 2010	2600
P2	16°30′ N	130°00′ E	Dec-10	NSFC open cruise 2010	2800
P2	16°30′ N	130°00′ E	Dec-10	NSFC open cruise 2010	3000
P2	16°30′ N	130°00′ E	Dec-10	NSFC open cruise 2010	3500
P1	18°00′ N	130°00′ E	Dec-10	NSFC open cruise 2010	500
N18-05	18°00′ N	123°30′ E	Dec-10	NSFC open cruise 2010	500
N18-05	18°00′ N	123°30′ E	Dec-10	NSFC open cruise 2010	1400
N18-05	18°00′ N	123°30′ E	Dec-10	NSFC open cruise 2010	1600
N18-05	18°00′ N	123°30′ E	Dec-10	NSFC open cruise 2010	2000
N18-05	18°00′ N	123°30′ E	Dec-10	NSFC open cruise 2010	2400

N18-05	18°00′ N	123°30′ E	Dec-10	NSFC open cruise 2010	2600
N18-05	18°00′ N	123°30′ E	Dec-10	NSFC open cruise 2010	2800
N18-05	18°00′ N	123°30′ E	Dec-10	NSFC open cruise 2010	3000
N18-05	18°00′ N	123°30′ E	Dec-10	NSFC open cruise 2010	3500
A3	20º25.584′ N	120º274′ E	Apr-13	NSFC open cruise 2013	5
A3	20º25.584′ N	120º274′ E	Apr-13	NSFC open cruise 2013	300
C3a	20°01′ N	121°19′ E	Dec-10	NSFC open cruise 2010	5
C3a	20°01′ N	121°19′ E	Dec-10	NSFC open cruise 2010	500
C3a	20°01′ N	121°19′ E	Dec-10	NSFC open cruise 2010	1000
C3a	20°01′ N	121°19′ E	Dec-10	NSFC open cruise 2010	1400
C3a	20°01′ N	121°19′ E	Dec-10	NSFC open cruise 2010	1600
C3a	20°01′ N	121°19′ E	Dec-10	NSFC open cruise 2010	1800
C3a	20°01′ N	121°19′ E	Dec-10	NSFC open cruise 2010	2000
C3a	20°01′ N	121°19′ E	Dec-10	NSFC open cruise 2010	2200
C3a	20°01′ N	121°19′ E	Dec-10	NSFC open cruise 2010	2400
C3a	20°01′ N	121°19′ E	Dec-10	NSFC open cruise 2010	2500
C3a	20°01′ N	121°19′ E	Dec-10	NSFC open cruise 2010	2600
C3a	20°01′ N	121°19′ E	Dec-10	NSFC open cruise 2010	2800
C3a	20°01′ N	121°19′ E	Dec-10	NSFC open cruise 2010	3000
A6	19º0.048′ N	120º29.79′ E	Apr-13	NSFC open cruise 2013	5
A6	19º0.048′ N	120º29.79′ E	Apr-13	NSFC open cruise 2013	300
A6	19º0.048′ N	120º29.79′ E	Apr-13	NSFC open cruise 2013	600
A6	19º0.048′ N	120º29.79′ E	Apr-13	NSFC open cruise 2013	900
A6	19º0.048′ N	120º29.79′ E	Apr-13	NSFC open cruise 2013	1300
A6	19º0.048′ N	120º29.79′ E	Apr-13	NSFC open cruise 2013	1600
A6	19º0.048′ N	120º29.79′ E	Apr-13	NSFC open cruise 2013	1800
A6	19º0.048′ N	120º29.79′ E	Apr-13	NSFC open cruise 2013	2000
A6	19º0.048′ N	120º29.79′ E	Apr-13	NSFC open cruise 2013	2200
A6	19º0.048′ N	120º29.79′ E	Apr-13	NSFC open cruise 2013	2400
A6	19º0.048′ N	120º29.79′ E	Apr-13	NSFC open cruise 2013	2700*
A6	19º0.048′ N	120º29.79′ E	Apr-13	NSFC open cruise 2013	3012*
C5	20º25.812′ N	118º32.364′ E	Apr-13	NSFC open cruise 2013	10
C5	20º25.812′ N	118º32.364′ E	Apr-13	NSFC open cruise 2013	300
C5	20º25.812′ N	118º32.364′ E	Apr-13	NSFC open cruise 2013	600

C5	20º25.812´ N	118º32.364´ E	Apr-13	NSFC open cruise 2013	1000*
C5	20º25.812´ N	118º32.364´ E	Apr-13	NSFC open cruise 2013	1250*
C5	20º25.812´ N	118º32.364´ E	Apr-13	NSFC open cruise 2013	1400
C5	20º25.812´ N	118º32.364´ E	Apr-13	NSFC open cruise 2013	1600
C5	20º25.812´ N	118º32.364´ E	Apr-13	NSFC open cruise 2013	1800
C5	20º25.812´ N	118º32.364´ E	Apr-13	NSFC open cruise 2013	2000
C5	20º25.812´ N	118º32.364´ E	Apr-13	NSFC open cruise 2013	2200
C5	20º25.812´ N	118º32.364´ E	Apr-13	NSFC open cruise 2013	2500
C5	20º25.812´ N	118º32.364´ E	Apr-13	NSFC open cruise 2013	2800
D3	20º2.928´ N	117º25.098´ E	Apr-13	NSFC open cruise 2013	5
D3	20º2.928´ N	117º25.098´ E	Apr-13	NSFC open cruise 2013	200
D3	20º2.928´ N	117º25.098´ E	Apr-13	NSFC open cruise 2013	400
D3	20º2.928´ N	117º25.098´ E	Apr-13	NSFC open cruise 2013	700*
D3	20º2.928´ N	117º25.098´ E	Apr-13	NSFC open cruise 2013	900*
D3	20º2.928´ N	117º25.098´ E	Apr-13	NSFC open cruise 2013	1000
D3	20º2.928´ N	117º25.098´ E	Apr-13	NSFC open cruise 2013	1200
D3	20º2.928´ N	117º25.098´ E	Apr-13	NSFC open cruise 2013	1400
D3	20º2.928´ N	117º25.098´ E	Apr-13	NSFC open cruise 2013	1600
D3	20º2.928´ N	117º25.098´ E	Apr-13	NSFC open cruise 2013	1800
D3	20º2.928´ N	117º25.098´ E	Apr-13	NSFC open cruise 2013	2000
D3	20º2.928´ N	117º25.098´ E	Apr-13	NSFC open cruise 2013	2107
10-JJW-07	20º12´ N	118º17´ E	May-10	NSFC open cruise 2010	5
10-JJW-07	20º12´ N	118º17´ E	May-10	NSFC open cruise 2010	500
10-JJW-07	20º12´ N	118º17´ E	May-10	NSFC open cruise 2010	1000
10-JJW-07	20º12´ N	118º17´ E	May-10	NSFC open cruise 2010	1500
10-JJW-07	20º12´ N	118º17´ E	May-10	NSFC open cruise 2010	1750
10-JJW-07	20º12´ N	118º17´ E	May-10	NSFC open cruise 2010	2000
10-JJW-07	20º12´ N	118º17´ E	May-10	NSFC open cruise 2010	2250
E405	19º36' N	120º1' E	Sep-09	SCSIO open cruise 2009	1500
10-JJW-82	18º30´ N	114º15´ E	May-10	NSFC open cruise 2010	5
10-JJW-82	18º30´ N	114º15´ E	May-10	NSFC open cruise 2010	1000
10-JJW-82	18º30´ N	114º15´ E	May-10	NSFC open cruise 2010	1500
10-JJW-82	18º30´ N	114º15´ E	May-10	NSFC open cruise 2010	2000
10-JJW-82	18º30´ N	114º15´ E	May-10	NSFC open cruise 2010	2500

E418	18º00´ N	114º 30´ E	Sep-09	SCSIO open cruise 2009	2500
SEATS	17º59´ N	115º59´ E	Nov-11	NSFC open cruise 2010	5
SEATS	17º59´ N	115º59´ E	Nov-11	NSFC open cruise 2010	200
SEATS	17º59´ N	115º59´ E	Nov-11	NSFC open cruise 2010	400
SEATS	17º59´ N	115º59´ E	Nov-11	NSFC open cruise 2010	600
SEATS	17º59´ N	115º59´ E	Nov-11	NSFC open cruise 2010	800
SEATS	17º59´ N	115º59´ E	Nov-11	NSFC open cruise 2010	1000
SEATS	17º59´ N	115º59´ E	Nov-11	NSFC open cruise 2010	1200
SEATS	17º59´ N	115º59´ E	Nov-11	NSFC open cruise 2010	1400
SEATS	17º59´ N	115º59´ E	Nov-11	NSFC open cruise 2010	1600
SEATS	17º59´ N	115º59´ E	Nov-11	NSFC open cruise 2010	1800
SEATS	17º59´ N	115º59´ E	Nov-11	NSFC open cruise 2010	1900
SEATS	17º59´ N	115º59´ E	Nov-11	NSFC open cruise 2010	2000
SEATS	17º59´ N	115º59´ E	Nov-11	NSFC open cruise 2010	2100
SEATS	17º59´ N	115º59´ E	Nov-11	NSFC open cruise 2010	2200
SEATS	17º59´ N	115º59´ E	Nov-11	NSFC open cruise 2010	2300
SEATS	17º59´ N	115º59´ E	Nov-11	NSFC open cruise 2010	2400
SEATS	17º59´ N	115º59´ E	Nov-11	NSFC open cruise 2010	2500
SEATS	17º59´ N	115º59´ E	Nov-11	NSFC open cruise 2010	2600
SEATS	17º59´ N	115º59´ E	Nov-11	NSFC open cruise 2010	2700
SEATS	17º59´ N	115º59´ E	Nov-11	NSFC open cruise 2010	2800
SEATS	17º59´ N	115º59´ E	Nov-11	NSFC open cruise 2010	2900
SEATS	17º59´ N	115º59´ E	Nov-11	NSFC open cruise 2010	3300
E202	14º00´N	118º30´E	Sep-10	SCSIO open cruise 2010	5
10-JJW-46	11º00´N	111º00´E	May-10	NSFC open cruise 2010	5
10-JJW-55	14º31´N	111 º00´E	May-10	NSFC open cruise 2010	5

Samples marked with asterisks represent that they were collected at the depths where nephoild layers occurred.

2.1.2 Sediment samples

Core-top sediment samples were taken from cores MD05-2899 (13º47.66´N, 112º10.89´E, 2393 m), MD05-2901 (14º22.503´N, 110º44.6´E, 1454 m), MD05-2903 (19º27.31´N, 116º15.06´E, 2047 m) and MD05-2904 (19º27.32´ N, 116º15.15´ E, 2066 m) (Table 2.2). For this study, cores have been selected where the core-tops are well preserved and represent

modern time. In addition, these cores were selected close to the water stations investigated in this study in order to compare the reliability of the seawater-derived εNd record in planktonic/ benthic foraminifera and bulk sediment leachates with those of the seawater (Table 2.2 and Table 2.3). Core MD05-2904, which is characterized by a high sediment rate (between ~25 cm/kyr and ~70 cm/kyr), was also chosen in order to produce a high time resolution record of the past seawater εNd over the last 25 kyr (Table 2.4). All of the cores were retrieved by R/V Marine Dufrense during the MARCO POLO IMAGES XII voyage in 2005.

The age model of core MD05-2904 was established on the basis of the oxygen isotope curve and 8 accelerator mass spectrometry (AMS) C-14 dating analysed by Ge et al. (2010). Radiocarbon dates were performed on well preserved calcareous samples from planktonic foraminifera *Globigerinoides ruber (G.ruber)*. After subtracting 450 yr to account for the average surface regional reservoir effect (Butzin et al., 2005), the conventional radiocarbon ages were converted into calendar ages using the Calib 7 program (Stuiver and Reimer, 1993). The age model was established by linear interpolation between 8 calibrated dates for the first 10 m of the core. The MD05- 2904 core thus provides a continuous record spanning the last 25 cal kyr BP, with higher accumulation rates for the last glacial stages (around 70 cm/kyr) than for the Holocene (around 25 cm/kyr).

Table 2.2: Location of sediment cores and treatment of planktonic and benthic foraminifera (BF) samples

Core	**Latitude**	**Longtitude**	**Age (Cal. Kyr BP)**	**Sample ID**
MD05-2904	19.46º N	116.25º E	0.05	cleaned *G.ruber*
			0.05	cleaned BF
			0.05	cleaning solution of *G.ruber*
			0.05	cleaning solution of BF
MD05-2903	19.45º N	116.25º E	core-top	cleaned *G.ruber*
			core-top	cleaned BF
			core-top	cleaning solution of *G.ruber*
			core-top	cleaning solution of BF
MD05-2901	14.28º N	110.74º E	core-top	cleaned *G.ruber*
			core-top	cleaned BF
			core-top	cleaning solution of *G.ruber*
			core-top	cleaning solution of BF
MD05-2899	13.79º N	112.19º E	core-top	cleaned *G.ruber*
			core-top	cleaned BF
			core-top	cleaning solution of *G.ruber*
			core-top	cleaning solution of BF
MD05-2904	19.46º N	116.25º E	0.05	cleaned *G.ruber*

MD05-2904	19.46º N	116.25º E	0.05	cleaning solution of *G.ruber*
MD05-2904	19.46º N	116.25º E	0.05	cleaned BF
MD05-2904	19.46º N	116.25º E	0.05	cleaning solution of BF
MD05-2904	19.46º N	116.25º E	0.05	Cleaned foraminiferas of mixed species
MD05-2904	19.46º N	116.25º E	0.05	uncleaned *G.ruber*
MD05-2904	19.46º N	116.25º E	6.50	cleaned *G.ruber*
MD05-2904	19.46º N	116.25º E	6.50	cleaning solution of *G.ruber*
MD05-2904	19.46º N	116.25º E	6.50	cleaned BF
MD05-2904	19.46º N	116.25º E	6.50	uncleaned *G.ruber*
MD05-2904	19.46º N	116.25º E	11.24	cleaned *G.ruber*
MD05-2904	19.46º N	116.25º E	11.24	uncleaned *G.ruber*
MD05-2904	19.46º N	116.25º E	18.57	cleaned *G.ruber*
MD05-2904	19.46º N	116.25º E	18.57	cleaning solution of *G.ruber*
MD05-2904	19.46º N	116.25º E	18.57	Cleaned foraminiferas of mixed species
MD05-2904	19.46º N	116.25º E	20.04	cleaned *G.ruber*
MD05-2904	19.46º N	116.25º E	20.04	cleaning solution of *G.ruber*

Table 2.3: Leaching procedures for samples from MD05-2904

Weight (g)	**Leaching time (min)**	**Carbonate treatment**	**Age (Cal. Kyr BP)**
0.20	30	non-decarbonated	0.05
0.20	30	non-decarbonated	6.50
0.20	30	non-decarbonated	11.24
0.20	30	non-decarbonated	18.57
0.20	30	non-decarbonated	20.04
1.00	30	non-decarbonated	0.05
1.00	30	non-decarbonated	6.50
1.00	30	non-decarbonated	11.24
1.00	30	non-decarbonated	18.57
1.00	30	non-decarbonated	20.04
2.00	30	non-decarbonated	0.05
2.00	30	non-decarbonated	6.50
2.00	30	non-decarbonated	11.24
2.00	30	non-decarbonated	18.57
2.00	30	non-decarbonated	20.04
1.00	60	non-decarbonated	0.05
1.00	60	non-decarbonated	6.50
1.00	60	non-decarbonated	11.24
1.00	60	non-decarbonated	18.57
1.00	60	non-decarbonated	20.04
1.00	30	decarbonated	0.05
1.00	30	decarbonated	6.50
1.00	30	decarbonated	11.24
1.00	30	decarbonated	18.57

1.00	30	decarbonated	20.04
0.20	30	decarbonated	0.05
0.20	30	decarbonated	6.50
0.20	30	decarbonated	11.24
0.20	120	decarbonated	0.05
0.20	120	decarbonated	6.50
0.20	120	decarbonated	11.24
0.20	120	decarbonated	18.57
0.20	120	decarbonated	20.04
0.20	180	decarbonated	0.05
0.20	180	decarbonated	6.50
0.20	180	decarbonated	11.24
0.20	180	decarbonated	18.57
0.20	180	decarbonated	20.04

Table 2.4: Age information for planktonic foraminifera separated from sediment of core MD05-2904

Core depth (cm)	Age (Kyr BP)	Core depth (cm)	Age (Cal. Kyr BP)
1-2	0.05	327-328	11.24
15-16	0.82	383-384	12.57
35-36	1.63	423-424	13.52
59-60	2.57	475-476	14.76
83-84	3.52	535-536	15.73
91-92	3.83	600-601	16.73
111-112	4.62	675-767	17.85
158-159	6.50	727-728	18.57
171-172	6.97	771-772	19.27
191-192	7.55	800-801	20.04
227-228	8.56	835-836	21.02
259-260	9.45	880-881	22.22
295-296	10.45	915-916	23.20

2.2 Methods

2.2.1 Seawater pre-concentration and chemical procedures prior to instrumental measurement

The Nd IC of 10 to 15 L seawater samples was analysed following the analytical procedures described by Lacan and Jeandel (2001). Prior to the pre-concentration, the SEP-PAK Classic C18 cartridge used in this study was cleaned with 2 N HCl three times and

subsequently cleaned with Milli-Q water. Then, the cartridge was submerged in 1N HCl for 12-24 hours. Suprapure ammonia was added to the acidified seawater in order to adjust pH= 3.7±0.5. The seawater was allowed to settle for about 24 hours for equilibration to take place. After equilibration, seawater rare earth elements (REEs) were pre-concentrated using acid-cleaned SEP-PAK Classic C18 cartridges. Each cartridge, loaded with a HDEHP/H_2MEHP complexant (~300 mg), can be used for REE pre-concentration of up to 5 L of seawater. After the pre-concentration, unwanted elements were removed by pumping ~6 ml of 0.1 M suprapure hydrochloric acid into the cartridge. Subsequently, REEs were eluted using ~35 ml of 6 N suprapure HCl. The solution was collected using Teflon beakers and was dried on a hotplate for ion chromatographic purification, which is described in Table 2.5 and Table 2.7.

Fig. 2.2. Photos showing that REEs were pre-concentrated in the clean lab.

Following on-board filtering and acidification, 500 ml seawater samples were split from 10 L seawater for REE concentration measurements. A spike solution, enriched in ^{141}Pr and ^{169}Tm, was added to each sample. After a day of equilibration, the pH was increased to 8 by the addition of suprapure ammonia solution. 0.5 ml of purified iron solution (~100 mg per ml) was added to each 10 L sample which enabled the co-precipitation of REE by the iron oxide. After 1~2 days of co-precipitation, the supernatant was siphoned off and discarded while the precipitate was transferred into the centrifuge tube. The precipitate was rinsed to remove the

sodium. The precipitate was then dissolved in 6 M HCl and dried. The dried solution was eventually dissolved in 6 N HCl for the elution of REE using an anion exchange column packed with AG1W-X8 resin (Table 2.8).

2.2.2 Cleaning procedures for foraminifera

Wet sediments were sieved to separate bulk sediments of <63 μm in size from other size fractions. 8-30 mg monospecific samples of planktonic foraminifera G.ruber, mixed benthic foraminifera and mixed foraminifera with shells size larger than 150 μm were handpicked under a binocular microscope. All of the foraminifera were gently crushed between two glass plates to open all chambers. The calcite fragments were then sonicated in an ultrasonic bath for approximately 1 min before pipetting the suspended particles with water to separate the waste. This step was repeated until the water became clear and free of clay. All samples were checked under a binocular microscope to make sure that all possible contaminants from detrital fractions were removed.

The clay-free samples of foraminifera were transferred to centrifuge tubes in preparation for oxidative – reductive cleaning. Three samples were isolated and subjected to mechanical cleaning rather than chemical cleaning. The foraminiferal cleaning procedure followed Vance and Burton (1999), using 10 ml reductive solution (1 M hydrous hydrazine + 16 M NH_4OH +0.25 M citric acid in a ratio of 1:6:3) and 5 ml oxidative solution (0.2 M NaOH and 30% H_2O_2 in a 1:1 ratio) per sample to more efficiently remove the authigenic Fe-Mn coating. For the reductive step, samples were heated in a water bath at 80ºC for 30 min, and ultrasonicated for 10 s every 2.5 min. Before rinsing them thoroughly with deionized water, the reductive cleaning solution containing the Nd from reduced Fe-Mn coating was transferred to a centrifuge tube. This procedure was the same for the oxidative step; except that samples were ultrasonicated every 10 min for 30 s. All samples, including the non-reductively cleaned samples, underwent a weak acid leach for 5 min in 1ml 0.001 M HNO_3 with an ultrasonic bath. The samples were transferred to 1.5 ml tubes, 0.5 ml of deionized water was added to avoid vigorous reaction between the acid and the foraminiferal calcite, and then the foraminifera were allowed to completely dissolve in 100 μl aliquots

Finally, all of the dissolved foraminifera shell fraction, and reductive cleaning solution, were dried on a hotplate for Nd purification. Element concentration and REE pattern analysis

were performed on a 10% cut of both the dissolved foraminifera shells and the corresponding reductive cleaning solutions.

An efficient chromatographic extraction was applied to the purified Nd prior to the instrument analysis (Table 2.6 and 2.7).

2.2.3 Bulk sediment leaching procedures

In order to facilitate paleoceanographic reconstructions, a sequential chemical leaching procedure for bulk sediment has been developed by researchers involved in Nd isotope analysis (Chester and Hughes, 1969).

In order to remove sodium, ground bulk sediments were rinsed with deionized water. Non-decarbonated bulk sediments of 0.2, 1, 2 g were directly leached using 7 ml 0.02 M hydroxylamine hydrochloride in 25% (v/v) acetic acid (HH solution) for 30 min. After leaching, the samples were centrifuged and the supernatant collected. This then had to be evaporated for column chemistry. Non-decarbonated bulk sediments of 1 g were treated using the same leaching procedure but with a longer leaching time of 1 hour. 1 g of bulk sediments were de-carbonated using sodium acetate buffered acetic-acid solution after rinsing with Milli-Q water. The residue was rinsed with Milli-Q water three times and was centrifuged to eliminate the Milli-Q water. Subsequently, the decarbonated bulk sediments were leached with 7 ml 0.02 M HH solution for 30 min. Leachates were separated from sediments by centrifugation prior to evaporation. Similarly, 0.2 g de-carbonated samples were leached for 30 min, 2 hours and 3 hours with 7ml 0.02 M HH solution. Dried leachates were dissolved in 1 ml 1 N HNO_3 for column chemistry (Table 2.6 and Table 2.7).

2.2.4 Ion chromatographic purification

The cation exchange resin AG 50W-X8 was used to separate High Field Strength Elements (HFSEs) from REEs. It has a capacity of 1.7 meq/ml of resin. For reference, seawater has high ion contents with a concentration of about 605 meq/ liter (salinity 35). The processes of ion-exchange are as follow:

$$\underset{\text{resin}}{xRSO_3\text{-}H^+} + \underset{\text{solution}}{M^{x+}} \rightleftharpoons \underset{\text{resin}}{(RSO_3\text{-})_xM^{x+}} + \underset{\text{solution}}{xH^+}$$

Under different pH, different trace metals have different exchange coefficients with the resin. Therefore, it is possible to separate trace metals with the acid elution method. REEs have a higher affinity to the resin and need to be eluted using high concentration 2.5 N HNO_3. The major elements, including the Fe, Ba, were removed before collecting the REE section. Table 2.5 shows the detailed procedure used to separate REEs. After the separation of the REEs, the solution was dried and re-dissolved with o.5 N HNO_3 for Nd purification. Nd cuts were further separated using Ln-spec resin (Table 2.7).

Table 2.5: AG50W-X8 (200-400μm) column chemistry for seawater

Acid	**Volume**	**stage**
6 N HCl	15 ml	pre-clean
MillI-Q	10 ml	change pH
2 N HCl	5 ml	pre-condition
2 N HCl	1.5 ml	load sample
2 N HCl	50 ml	elute
2.5 N HNO3	27 ml	elute
2.5 N HNO3	35 ml	collect REE
6 N HCl	15 ml	clean
MillI-Q	10 ml	clean and store

For Nd purification of foraminiferas, we used a TRU-Spec and an Ln-Spec resin following the method described in detail by Pin and Santos Zaldegui (1997) that we adapted for our samples. In this method, samples were loaded using 2 ml of 1N HNO_3 on preconditioned TRU-Spec columns (83 mg portion of TRU-spec). The unwanted cations were eluted using 5 portions of 0.5 ml portion of 1N HNO_3. TRU-Spec columns were then placed over Ln-Spec columns. The LREEs were then eluted from the upper (TRU-Spec) column using seven portions of 0.1 ml of 0.05N HNO_3. After decoupling from the TRU-Spec columns, La, Ce and Pr were rinsed from the Ln-Spec columns with 3.25 ml of 0.25N HCl. Nd was then eluted with an additional 2.5 ml of 0.25N HCl. The Ln-Spec resin provides efficient separation of Nd from Sm, Ce and La. The details of TRU-Spec and Ln-Spec column chemistry used to separate Nd are shown in Table 2.6 and Table 2.7.

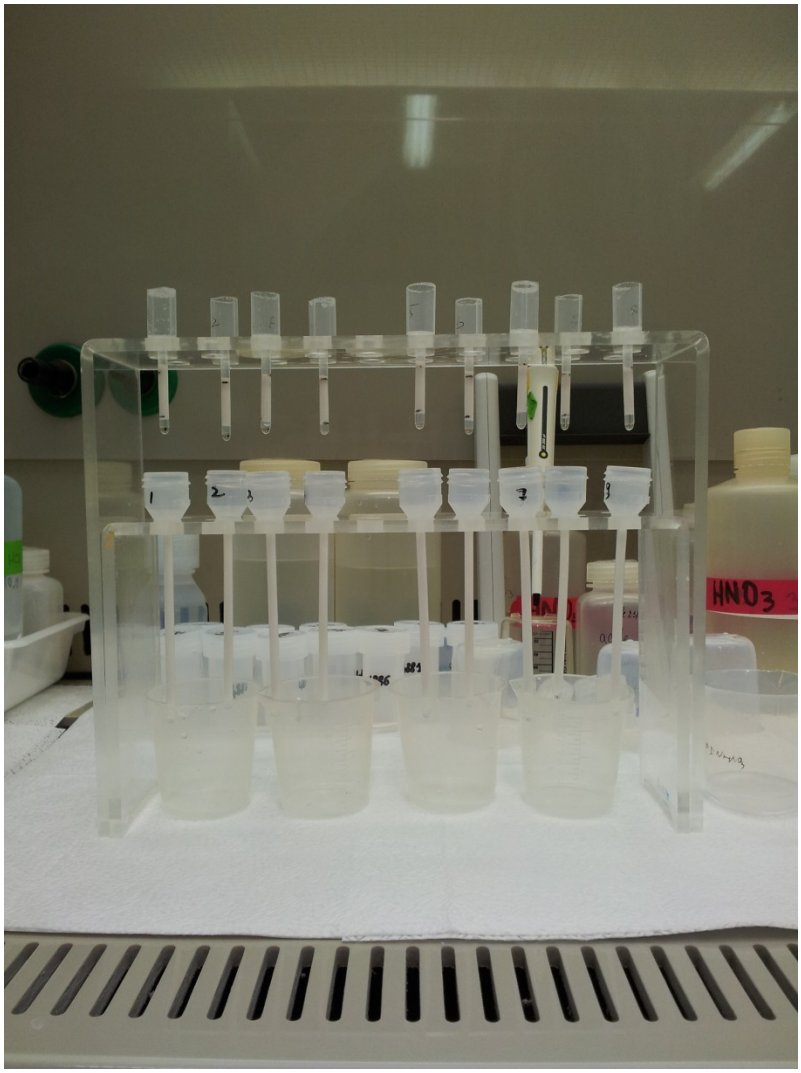

Fig. 2.3. Picture of TRU-Spec and Ln-Spec column used to purify Nd

Table 2.6: Eichrom®TUR-Spec (83 mg) column chemistry for REE separation for foraminiferas and leachates

Acid	Volume	stage
0.05 N HNO3	4 ml	pre-clean
1 N HNO3	2 ml	pre-condition
1 N HNO3	1 ml	load sample
1 N HNO3	2.5 ml	elute
0.05 N HNO3	0.25 ml	change pH
0.05 N HNO3	1 ml	collect REE

Table 2.7: Eichrom®LN-Spec (2ml, 50-100µm) column chemistry for Nd purification

Acid	Volume	stage
6 N HCL	10 ml	pre-clean
MillI-Q	10 ml	change pH
0.05 N HNO3	1 ml	pre-condition

0.05 N HNO3	0.7 ml	load sample
0.25 N HCl	3.25 ml	elute
0.25 HCl	2.75 ml	collect Nd
6 N HCl	10 ml	clean
MillI-Q	10 ml	clean and store

For the seawater REEs, AG1W-X8 resin was used to separate the REEs from the matrix co-precipitated within the iron oxides. The chemical procedure is described in Table 2.8:

Table 2.8: AG1W-X8 resin (2g, 200-400 mesh) column chemistry for seawater REE purification

Acid	Volume	stage
6 N HCl	10 ml	pre-clean
6 N HCl	5 ml	pre-condition
6 N HCl	1 ml	load sample
6 N HCl	1 ml	elute
6 N HCl	8 ml	collect REE

2.2.5 Analytical procedure for determining REE concentration in seawater samples

REE concentrations were analyzed using the inductively coupled plasma-mass spectrometer (quadrupole ICP-MS, X- Series Ⅱ) at the Laboratoire des Sciences du Climat et de l'Environnement (LSCE) in Gif sur Yvette. Seawater REE concentration was first pre-analyzed to calculate the dilution for the required sample concentration. During the analysis, purified REE standards, spanning three orders of magnitude in concentration, were used to generate a reliable calibration curve. BCR-2 and pure REE standards were used to monitor instrument drift. The ^{141}Pr and ^{169}Tm spikes, added before the pre-concentration, allowed the calculation of REE concentrations using isotopic dilution.

2.2.6 Analytical procedures for measuring REE concentration in foraminifera and Fe-Mn coatings

The calcium concentration of foraminiferas was measured before elemental analysis. All samples were diluted to a Ca concentration of 100 ppm. The isotopes ^{24}Mg, ^{43}Ca, ^{55}Mn, ^{88}Sr, ^{137}Ba and REE were measured with a inductively coupled plasma mass spectrometer (quadrupole ICP-MS, X- Series Ⅱ). A JCp-1standard, whose Ca concentration was adjusted to

match those found in foraminifera, was used to monitor instrument stability. The internal ^{115}In and ^{103}Rh standard were used to monitor instrument stability when analyzed REE concentrations of reductive cleaning solution and the bulk sediment leachates.

2.2.7 Nd isotopic composition analyses

All isotope measurements were performed at low mass resolution in static mode on a MC-ICP-MS ThermoScientific Neptune^{Plus} at the Laboratoire des Sciences du Climat et de l'Environnement (LSCE) in Gif sur Yvette. Gain calibration for the Faraday cup efficiency was carried out on a daily basis.

Samples were introduced into the mass spectrometer in 1N HNO_3. The concentrations of all purified samples were tested, and required sample amounts were calculated accordingly to get a similar beam for both the samples and the standards during the subsequent isotope measurement. Initially, the calculation subtracts the ^{144}Sm beam from the 144 beam (so ^{144}Nd beam is known). The ^{146}Nd/^{144}Nd ratio of 0.7219 was used to correct the mass fractionation. The reliability of this method critically depends on the amount of Sm present in the sample, since the ^{144}Sm beam is only roughly calculated from the ^{147}Sm beam without applying a mass fractionation rule. Therefore, to reduce the mass interference, it is important to carefully separate the Sm from the Nd during the purification procedure to meet these conditions.

During the analysis sessions, every two samples were bracketed with analyses of the La jolla and JNdi-1 standards at a concentration similar to those of the samples, and corrected to certified values of 0.511858 ± 0.000007 and 0.512115 ± 0.000007 (Tanaka et al., 2000), respectively. The external reproducibility (2σ) for time resolved measurement, deduced from repeated measurement of the La jolla and JNdi-1 standards at similar concentrations to the samples ranged from 0.2 to 0.5 εNd for different analytical sessions. The analytical error of each samples analysis is taken as the external reproducibility of the La jolla standard for each session. Blank values were <150 pg, and thus can be ignored as they represent less than 1.5% of the Nd from seawater samples analysed, taking into consideration the volume of the seawater sample (10 to 15 L) and the mean Nd concentration of seawater analysed.

Chapter 3

Introduction

The Philippine Sea and the northern South China Sea (SCS) are key areas for reconstructing hydrological variability in the western subtropical North Pacific. As the εNd of intermediate- and deep-water masses of the SCS and the Philippine Sea are not available, it is absolutely necessary to establish the present day distribution of seawater εNd prior to reconstructing past seawater Nd changes from northern SCS sediments. In this chapter, we attempt, firstly, to establish vertical profiles of seawater εNd collected from the Philippine Sea, the Luzon Straits and the SCS. Seawater εNd is used to track water mass exchange between the SCS and the Philippine Sea through the Luzon Straits. Secondly, the εNd values of seawater collected from drift sediment deposit systems and nepheloid layers are presented in order to constrain the potential influence on the seawater εNd of Nd exchange between the water masses which enter the SCS (PDW and NPIW) and the unradiogenic sediments of the northern SCS. Finally, a compilation of surface water εNd records from this study, and previous studies, is presented to assess the impacts of riverine input, and/or intrusion of the Indian Ocean surface water, on the Nd isotopic composition of the SCS surface seawater.

New insights into hydrological exchange between the South China Sea and the western Pacific Ocean based on the Nd isotopic composition of seawater

Qiong Wu[1, 2], Christophe Colin[1], Zhifei Liu[2], Eric Douville[3], Quentin Dubois-Dauphin[1], Norbert Frank[4]

1 Laboratoire de Geosciences Paris-Sud (GEOPS), UMR 8148, CNRS-Université de Paris-Sud, Bâtiment 504, 91405 Orsay Cedex, France.

2 State Key Laboratory of Marine Geology, Tongji University, Shanghai 200092, China.

3 Laboratoire des Sciences du Climat et de l'Environnement (LSCE/IPSL), UMR 8212 CNRS-CEA-UVSQ, Avenue de la Terrasse, 91198 Gif-sur-Yvette Cedex, France.

4 Universität Heidelberg, Im Neuenheimer Feld 229, 69120 Heidelberg, Germany.

* Corresponding author: E-mail: wuqiong06@gmail.com (Qiong Wu)

Abstract

Nd isotopic composition (εNd) of 16 seawater profiles collected in the northern South China Sea (SCS) and the Philippine Sea were investigated (1) to establish the distribution of the Nd isotopic composition of water masses along the tropical Western Pacific and the SCS that, until now have not been documented, (2) to constrain hydrological exchange between the SCS and the Philippine Sea through the Luzon Strait, and (3) to test, in the context of the semi-closed marginal sea (SCS), the possible impact of the process of exchange between deep and mid-depth water masses entering the SCS and sediments from the north-western margin of the SCS which are characterized by unradiogenic Nd isotopic compositions.

εNd values for mid- and deep-water masses of the Philippine Sea and the SCS range from -2.3 to -4.4 and generally increase slightly as water depth increases. In the Philippine Sea, εNd values for the North Pacific Intermediate Water (NPIW) reach -2.7±0.4 at mid-depths (500 to 1400 m). Below ~1800 m, the Pacific deep-water (PDW) is characterized by less radiogenic Nd (-4.1±0.5) indicating the intrusion of southern sourced water masses. For most of the stations in the Northern SCS, water masses below 1500 m (PDW) display homogenous εNd values (~ -4.1) similar to those of the PDW in the Philippine Sea. εNd values for the South China Sea Intermediate Water (SCSIW - 500-1500 m) vary from -3.0 to -3.9 as a result of the vertical

mixing of the NPIW with the PDW in the SCS. Seawater εNd values for the SCS (~5.3 to -7.0) display local modification in areas where the water lies above significant sediment drift deposit systems. This implies that ‘’boundary exchange’’ with unradiogenic sediments (around -11) probably only occur locally and temporarily and does not modify the Nd isotopic composition of the PDW in the Northern SCS. In addition, εNd values analyzed for the first time in seawater from nepheloid layers collected along the north-western margin of the SCS do not exhibit any significant modification of the seawater εNd which is confined to a narrow range between -3.7 and -4.3, similar to that of the PDW. A compilation of εNd from the sea surface water of the SCS indicates lower εNd values in the western and the central SCS (-3.3 to -9.5), induced by riverine input and/or penetration of surface water masses from the Indian Ocean which are characterized by unradiogenic εNd (-10). Finally, as significant variations are observed in seawater εNd at mid-depth between the SCS and the Philippine Sea, εNd values could be used in the future to track intermediate water mass exchange in the Luzon Straits, a process which, at present, remains poorly understood.

Keywords: Nd isotopic composition, seawater, South China Sea, Philippine Sea, hydrology, nepheloid layers.

3.1 Introduction

It is now widely recognized that the large-scale thermohaline ocean circulation plays a key role in regulating climate changes through heat redistribution and carbon cycling (Stocker and Wright., 1996; Rahmstorf., 1995, 2003; Toggweiler and Russell., 2008; Marchitto et al., 2007; Bryan et al., 2010). The Pacific Ocean plays an important role in global ocean circulation due to its volume and role as a potential carbon reservoir, which, in turn, also has significant climatic implications. Compared to the Atlantic Ocean, only limited hydrographical observation has been carried out in the Pacific Ocean due to its complicated topography and the less distinguishable water characteristics, and little is known about the circulation below a depth of 1000 m. Nevertheless, it has received increasing attention over the past two decades, but, as yet, the formation of NPDW and the penetration of water originating from the Southern Ocean into the Pacific Ocean remain poorly understood (Kawabe et al., 2003 and 2010; Talley, 2008).

In this context, the tropical western Pacific (Philippine Sea) and South China Sea (SCS)

are key areas for reconstructing hydrological variability in the western Pacific. The SCS is a semi-enclosed marginal sea connected to the western Pacific Ocean through the Luzon Straits. It receives Pacific intermediate and deep-water masses (NPIW and PDW) from the Philippine Sea through the Luzon Strait. As the Philippine Sea is fed by water masses from the North and the South of the Pacific, the tropical western Pacific (Philippine Sea) and the SCS are essential areas for reconstructing hydrological variability in the western Pacific (Johnson and Toole, 1993; Kawabe et al., 2003). In addition, as the SCS is characterized by high sedimentation deposit sequences it permits the reconstruction of past hydrological changes in the western Pacific at higher time resolutions.

Several studies have indicated that the neodymium (Nd) isotopic composition of ocean water masses can provide a proxy to track water mass provenance (e.g. Lacan and Jeandel, 2004c, 2005; Piepgras and Waserburg, 1988; Jeandel et al., 2013). Its advantage over numerous other proxies (e.g. $\delta^{13}C$ of dissolved inorganic carbon and Cd/Ca ratios as recorded by benthic foraminifers) lies in the fact that Nd isotope compositions are not known to be affected by biological processes, and thus they can serve as quasi-conservative water mass tracers (Frank, 2002; Goldstein and Hemming, 2003; Arsouze et al., 2007).

Nd isotopic composition is expressed as $\varepsilon Nd=[(^{143}Nd/^{144}Nd)Sample/ (^{143}Nd/^{144}Nd)_{CHUR} - 1] \times 10{,}000$, where $(^{143}Nd/^{144}Nd)_{CHUR}$ stands for chondritic uniform reservoir and represents the present-day average earth value $(^{143}Nd/^{144}Nd)_{CHUR}= 0.512638$; Jacobsen and Wasserburg, 1980). The residence time of Nd in the ocean, recently re-assessed to about 600–1000 yrs (Tachikawa et al., 1999 and 2003), is shorter than the global turnover time of the ocean (about 1000 yrs; Broecker and Peng, 1992). Consequently, through lithogenic inputs of material with various ages, and boundary-exchange processes that occur at the continental margin (Lacan and Jeandel, 2005; Jeandel et al., 2007), intermediate- and deep-water masses acquire Nd from downwelling surface water (Goldstein and Hemming, 2003). In the ocean, the only way that the initial isotopic composition of a water mass can be altered is through the addition of Nd with a different isotopic composition through riverine or eolian inputs or by mixing with other water masses. However, away from the continental margins, and on short time scales (<500 years), εNd can be considered as a quasi-conservative tracer in the ocean. This proxy has already been used in paleo-oceanographic studies using dispersed authigenic ferromanganese oxide precipitates in sediments (Gutjahr et al., 2008; Pahnke et al., 2008; Piotrowski et al., 2004 and 2005; Rutberg et al., 2000), planktonic foraminifera (Burton and

Vance, 2000; Roberts et al., 2010; Vance and Burton, 1999; Piotrowski et al., 2012) and deep-sea corals (Colin et al., 2010; Copard et al., 2010) to track changes in water mass provenance and mixing at different time scales (decadal to millennial time scales).

Compared to the wealth of data from the large number of investigations carried out in the Atlantic Ocean, available data concerning Nd isotopic compositions for the western Pacific Ocean, and the surrounding continent, are scarce (Amakawa et al., 2000, and reference therein). To date, seawater εNd values for the North Pacific have been established by Amakawa et al (2004 and 2009) and Piepgras and Jacobsen (1988). These results reveal stratified εNd values reflecting the water mass origins. εNd values of surface and the subsurface North Pacific Tropical Water (NPTW) vary spatially from 0 to -9 depending on the level of lithogenic input from surrounding margins. Mid-depths dominated by the NPIW have uniform εNd values of around -3, whereas deep layers of the North Pacific Deep Water (NPDW), penetrated by and/or transformed from the southern sourced water, produce lower radiogenic εNd values of between -4 and -10. Seawater εNd values are very scarce for the western Pacific Ocean and its marginal seas. Values for the deep-waters of the SCS and the western North Pacific off the Luzon strait, are currently not available and therefore do not permit us to construct a precise distribution of the Nd isotopic composition of water-masses that flow in and out of the SCS. In addition, the SCS receives unradiogenic Nd isotopic composition from northeast river systems (e.g. Pearl River or Mekong River with εNd values –between -13 and -10) and radiogenic Nd isotopic composition from southwest river systems (e.g. Philippine river system. εNd around +6) (Liu et al, 2007; Jones et al, 1994; Goldstein and Jacobsen, 1988). The Nd isotopic composition of seawater that enters the SCS can be modified significantly by boundary exchange while it is flowing along the northern margin of the SCS. Consequently, since seawater εNd values for the Pacific Ocean and the SCS are not well documented, it is currently difficult to investigate past seawater εNd from marine sediments in this area of major interest.

Here we describe for the first time the Nd isotopic composition of 16 seawater profiles from the northern South China Sea (SCS) and the Philippine Sea in order to (1) establish the Nd isotopic composition of water masses along the tropical western Pacific Ocean and the SCS which are still not well known, (2) to track hydrological exchange between the SCS and the Philippine Sea through the Luzon strait and (3) to test, in the context of the semi-closed marginal sea (SCS), the possible impact of the process of exchange between deep and

mid-depth water masses entering the SCS and sediments from the northwest margin of the northern SCS which are characterized by unradiogenic Nd isotopic compositions. In addition, several samples of seawater from nepheloid layers have been investigated for the first time in order to test the impact of re-suspended sediments, carried by strong deep-currents, on the Nd isotopic composition of seawater. In this study, we aim to demonstrate that the Nd isotopic composition of the PDW of the SCS is representative of that of the western tropical Pacific. This will allow the Nd isotopic composition of sediments archives in the SCS to be used to reconstruct, at centennial- to millennial time resolutions, the hydrological variability of the PDW of the tropical Pacific, which up to now has been poorly documented.

3.2. Hydrological setting

The deep-water hydrology of the Philippine Sea is controlled by a complex bathymetry which includes topographic barriers and numerous ocean basins (Fig.3.1). The deep-water of the western Pacific is characterized by the presence of the Circumpolar Deep Water (CDW) (Talley, 2008). Several studies have shown that the western branch (4 Sv) separates from the Lower Circumpolar Deep Water (LCDW) (> 3500 m) and flows northward to the Philippine Sea (Kawabe and Fujio, 2010; Johnson and Toole, 1993; Talley, 2007). Approximately 10 Sv of the Upper Circumpolar Deep Water (UCDW) reaches the equatorial western Pacific and flows into the Philippine Sea (Kawabe et al, 2003, 2005, 2009; Kawabe and Fujio, 2010). 5 Sv of the UCDW flows out of the Philippine Sea whereas the remaining UCDW (5 Sv) is vertically transformed into surface and intermediate-water masses within the Philippine Sea (Kawabe et al., 2009). UCDW and LCDW are transformed by vertical mixing in the North Pacific and form the North Pacific deep-water (NPDW) (Talley, 2008; Kawabe and Fujio, 2010). A branch of this very old NPDW spreads to the south and reaches the Philippine Sea as evidenced by high silica concentrations (World Ocean Atlas data 2009). At intermediate depth (around 500-800m), the presence of a salinity minimum indicates the core of the Antarctic Intermediate Water (AAIW) and the North Pacific Intermediate Water (NPIW) (Tsuchiya 1991; Zenk et al. 2005; You, 2003). The AAIW associated with the Antarctic Circumpolar Current crosses the equatorial Pacific and propagates to 15ºN in the Philippine Sea with no further northward extension along the western boundary (Qu and Lindstrom, 2004). The NPIW is mainly formed in the Sea of Okhotsk and is confined to the subtropical gyre of the North Pacific with a salinity of 34.0-34.3 (Talley, 1993; You, 2003; Talley et al, 1995). The core of the NPIW is centred at a depth of between 500 and 800 m in the Philippine Sea

(Kashino et al., 1999). Along the Philippine coast, most of the NPIW is re-circulated to the north via the Kuroshio and a small amount of this water mass flows into the SCS through the Luzon Straits (Qu et al., 2000). The North Pacific Tropical Water (NPTW) occupies the layer above a depth of 200 m and is characterized by the highest salinity (> 34.8). It originates in the region between latitudes 20ºN and 30ºN in the North Pacific where evaporation dominates over precipitation (Suga et al., 2000). NPTW is transported westward and is then advected in the North Equatorial Currents (NEC) and forms a subsurface salinity maximum. On the western boundary of the North Pacific, the NPTW is separated into two branches, the northward branch flows in the Kuroshio Currents which contribute to the salinity maximum water component in the Philippine Sea. The southward branch of the NPTW, carried by the Mindanao Currents, enters the Indian Ocean through the Indonesian Throughflow or flows back to the North Pacific via the North Equatorial Countercurrent (NECC) (Qu et al., 1999).

Numerous studies have been undertaken of deep-water circulation in the SCS (below 2000 m) in order to constrain the inflow and the pathway of the PDW into the SCS (Li and Qu, 2006; Qu et al., 2006, Wang et al., 2011; Tian et al., 2006; Zhao et al., 2014). The Luzon Strait is the only deep connection between the SCS and the North Pacific, with the deepest sill, at about 2400 m, located in the Bashi Channel. A vertical sandwich structure of water exchange between the SCS and the North Pacific has been observed recently in the Luzon Straits. During the winter an inflow of the western Pacific to the SCS occurs in the surface-and deep layers while an outflow from the SCS to the Philippine Sea can be observed in the intermediate layer to compensate for the inflow (Gong et al., 1992; Tian et al., 2006). Water masses below 2000 m in the SCS are characterized by relatively homogenous physical properties (2.1 ~ 2.3°C, 34.59 ~ 34.62) similar to those of the PDW observed in the Philippine Sea at around 2000m (Li and Qu, 2006; Qu et al., 2006, World Ocean Atlas data 2009). The PDW, characterised by a low temperature (1.6 °C) and high salinity (34.62), sinks in the deep SCS basins immediately after it crosses the Luzon Strait (Wyrtki, 1961). It enhances the vertical mixing (upwelling) and potentially contributes to the upper layer circulation (Tian et al., 2009; Li and Qu, 2006; Qu et al., 2006; Qu, 2002). These processes facilitate the rapid turnover of the SCS deep water that has been recently estimated at around 30 to 50 years (Gong et al., 1992; Li and Qu, 2006., Wang et al., 2011).

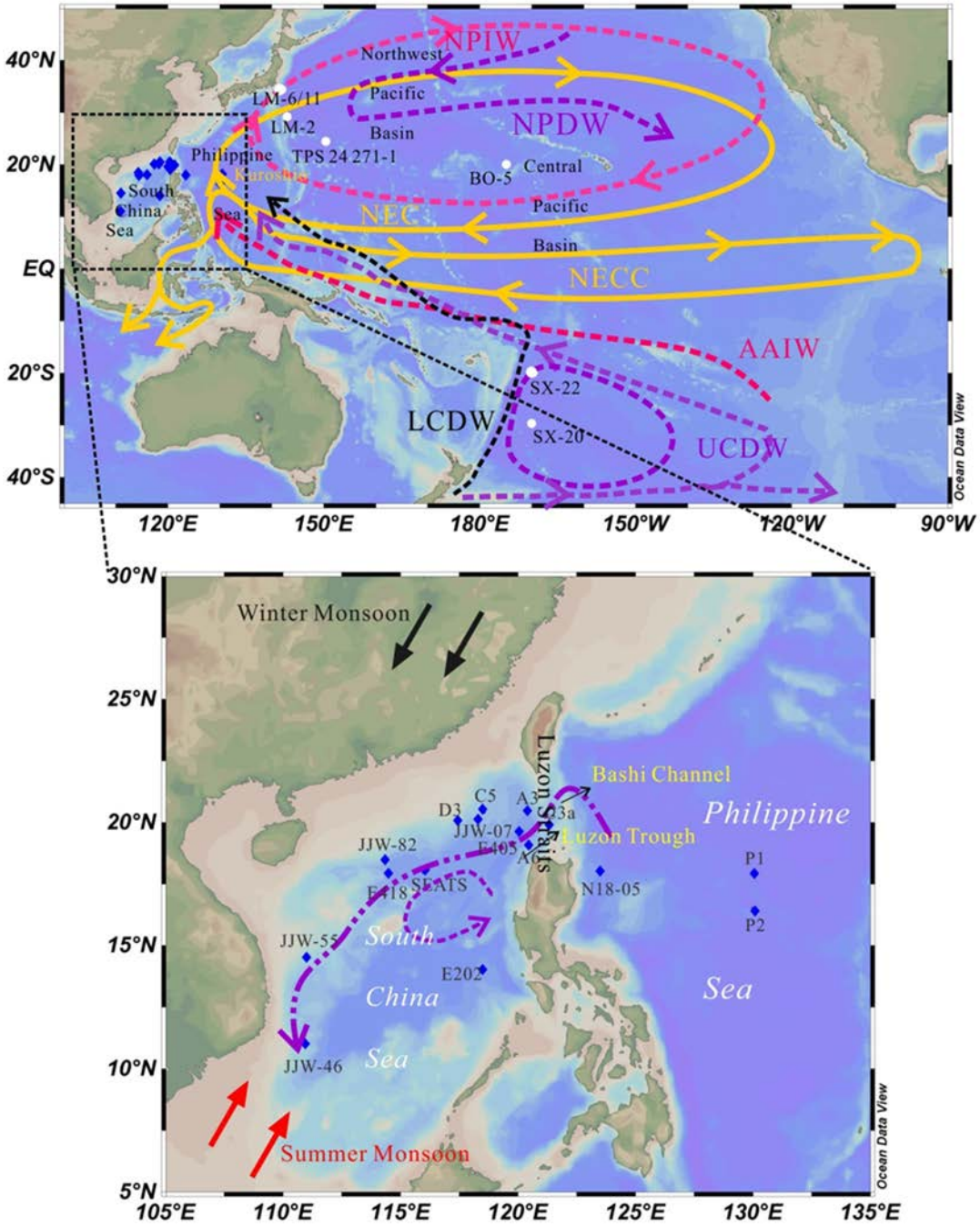

Figure 3.1. Sample location map. The sampling sites are marked with blue diamonds (this study) and the white dots (previous studies). The purple and pink arrows indicate the deep water currents and the intermediate currents, respectively. The orange arrows show the general circulation of the surface/subsurface water. The black and the red arrows indicate the seasonal winter monsoon and the summer monsoon. Pink circles stand for the upwelling water from lower layers to less than 3000 m. The circulations are based on Kawabe et al., (2009 and 2010), You (2003), Suga et al., (2000).

The basin-scale oxygen distribution suggests that deep water which enters the SCS is transported north-westward to the northern slope of the SCS and thereafter southward along the western margin of the sea (Qu et al, 2006; Li and Qu, 2006). Sub-basin scale cyclonic eddies are to be found in the deep basin (115°E ~ 118°E, 14.5°N ~ 16.5°N) (Wang et al, 2011). The South China Sea Intermediate Water (SCSIW) (350 ~ 1350 m) is characterized by higher salinity than the NPIW observed in the Philippine Sea. This is due to vertical mixing of the SCSIW with deep-water in the SCS (Chen, 2001; Xie et al., 2009; Tian et al., 2009). The intrusion of NPIW has been found to be greater in winter than in summer and is associated with leakage of the Kuroshio Current (Qu et al., 2000; Chen and Huang, 1996). Mid-depth water exchange in the Luzon Straits also displays seasonal variability. During the winter, there is an inflow of the NPIW into the SCS through the southern part of the Luzon Straits whereas the outflow of the SCSIW to the Philippine Sea is located in the northern part of the Luzon Straits. These waters masses flow in an opposite direction during the summer (Tian et al,, 2006; Yang et al., 2010; Xie et al., 2011).

Above a depth of 350 m, surface- and subsurface circulations in the SCS are primarily driven by the seasonal reversal of the winds induced by the East Asian monsoon. Cyclonic circulation occurs during the summer East Asian monsoon while anti-cyclonic circulation is a feature of the winter monsoon (Wyrtki, 1961). The high salinity NPTW (>34.8) enters the SCS through the Luzon Straits at a depth of ~150 m during the winter East Asian monsoon. The upward mixing of the lower layer also contributes significantly to the weaker salinity maximum (~ 34.6) of the surface layer which is termed South China Sea Tropic Water (SCSTW) (Xie et al., 2011).

3.3. Material and methods

112 seawater samples of 10-15 litres were collected at 16 stations in the Philippine Sea, the Luzon Straits and the SCS during five oceanographic cruises which were carried out by R/V Kexue No.1, R/V Shiyan No.3 and R/V Dongfanghong No.2 (Fig. 3.1, Table 3.1).

Samples were collected at Stations P1, P2 and N18-05 in the Philippine Sea in order to establish, for the first time, the vertical seawater εNd distribution of the Philippine Sea. 7 stations located along the speculated deep-water pathways in the northern SCS, were sampled in order to constrain deep-water transportation from the western Pacific to the SCS (Fig. 3.1).

Samples from three stations on the north-western margin of the SCS (SEATS, JJW-82 and E418), were analyzed in great detail in order to constrain the Nd isotopic composition of the different masses in the northern part of the SCS. Three further stations (D3, C5 and JJW-07), located above or near large sediment drift systems identified in a previous study (Lüdmann et al., 2005), were sampled in order to estimate the possible effect of Nd exchange between seawater and detrital particles. In addition, samples were collected at two stations (D3 and C5) in the north-western part of the SCS at a location where nepheloid layers have been observed. For these two water stations, the vertical distributions of particle concentrations were analyzed and several seawater samples were taken in the nepheloid layers in order to assess the possible exchange of Nd between lithogenic particles and seawater. Three stations (A3, C3a and A6) located at the Luzon Straits, were sampled in order to constrain water exchange between the Philippine Sea and the SCS. In addition, several sea-surface water samples, collected from both the northern and the central SCS, were investigated (Table 3.1).

Table 3.1. Locations, depths, hydrological Properties, Nd Concentrations, Nd ICs and εNd of the samples analyzed in this study

Depth (m)	Salinity	Pot.Temp (℃)	$^{143}Nd/^{144}Nd$	εNd	Nd (pmol/kg)
Central Philippine Sea station: P2 (16°30´N, 130°00´E; Dec 2010)					
5	34.374	29.496	0.512461±0.000024	-3.4±0.6	3.9
500	34.268	7.582	0.512497±0.000011	-2.8±0.3	12.7
1400	34.574	3.036	0.512464±0.000008	-3.4±0.3	--
1600	34.593	2.673	0.512474±0.000008	-3.2±0.3	33.5
1800	34.614	2.343	0.512428±0.000011	-4.1±0.5	28.6
2000	34.631	2.084	0.512436±0.000009	-3.9±0.3	26.8
2200	34.645	1.906	0.512455±0.000006	-3.6±0.4	29.2
2400	34.653	1.813	0.512432±0.000009	-4.0±0.3	31.1
2600	34.659	1.754	0.512438±0.000006	-3.9±0.4	32.5
2800	34.666	1.694	0.512438±0.000008	-3.9±0.3	--
3000	34.671	1.65	0.512421±0.000006	-4.2±0.4	32.4
3500	34.673	1.631	0.512414±0.000008	-4.4±0.3	36.3
Central Philippine Sea station: P1(18°00´N, 130°00´E; Dec 2010)					
500	34.197	8.325	0.512462±0.000012	-3.4±0.3	
Western Philippine Sea station: N18-05 (18°00´ N, 123°30´ E; Dec 2010)					
1400	34.582	2.758	0.512499±0.000018	-2.7±0.4	23.9
1600	34.49	2.5	0.512461±0.000008	-3.5±0.4	24.1
2000	34.634	2.1	0.512448±0.000011	-3.7±0.4	30.2
2400	34.655	1.802	0.512455±0.000010	-3.6±0.2	28.0

2600	34.662	1.722	0.512420±0.000008	-4.3±0.4	33.0
2800	34.663	1.665	0.512429±0.000008	-4.1±0.4	48.4
3000	34.671	1.611	0.512435±0.000011	-4.0±0.4	--
3500	34.679	1.554	0.512413±0.000005	-4.4±0.4	34.6

Northern Luzon Straits station: A3 (20º25.584´ N, 120º274´ E; Apr 2013)

0	33.895	26.975	0.512460±0.000010	-3.5±0.4	*10.5*
300	34.433	11.806	0.512464±0.000012	-3.4±0.4	*9.6*

Middle Luzon Straits station: C3a (20°01´ N, 121°19´E; Dec 2010)

0	34.409	24.872	0.512490±0.000022	-2.9±0.5	2.8
500	34.374	8.375	0.512429±0.000013	-4.1±0.3	15.9
1000	34.508	4.697	0.512454±0.000007	-3.6±0.3	25.9
1400	34.572	3.329	0.512447±0.000008	-3.7±0.3	29.8
1600	34.623	2.745	0.512438±0.000006	-3.9±0.3	34.6
1800	34.609	2.521	0.512416±0.000009	-4.3±0.3	30.8
2000	34.609	2.455	0.512415±0.000007	-4.3±0.3	43.1
2200	34.626	2.287	0.512425±0.000008	-4.2±0.3	--
2400	34.622	2.198	0.512433±0.000007	-4.0±0.3	30.4
2500	34.623	2.188	0.512427±0.000008	-4.1±0.3	29.1
2600	34.622	2.175	0.512454±0.000007	-3.6±0.3	29.7
2800	34.625	2.177	0.512421±0.000008	-4.2±0.3	30.7
3000	34.623	2.182	0.512449±0.000008	-3.7±0.3	32.6

Southern Luzon Straits station: A6 (19º0.048´ N, 120º29.79´ E; Apr 2013)

5	33.712	26.62	0.512548±0.000009	-1.9±0.4	*12.3*
300	34.479	12.489	0.512491±0.000019	-2.9±0.4	*11.3*
600	34.436	7.454	0.512497±0.000007	-2.7±0.4	*16.7*
900	34.516	4.588	0.512467±0.000008	-3.3±0.4	*19.1*
1300	34.567	3.35	0.512484±0.000005	-3.0±0.4	*26.3*
1600	34.598	2.679	0.512458±0.000005	-3.5±0.4	*27.7*
1800	34.605	2.527	0.512460±0.000005	-3.5±0.4	*27.0*
2000	34.612	2.347	0.512452±0.000005	-3.6±0.4	*27.3*
2200	34.615	2.252	0.512434±0.000004	-4.0±0.4	*31.6*
2400	34.618	2.166	0.512456±0.000005	-3.5±0.4	*29.8*
2700*	34.622	1.995	0.512445±0.000005	-3.8±0.4	*26.3*
3012*	34.625	1.944	0.512441±0.000005	-3.9±0.4	*27.7*

Northwest South China Sea station: C5 (20º25.812´ N, 118º32.364´ E; Apr 2013)

10	33.932	26.341	0.512409±0.000007	-4.5±0.4	*10.8*
300	34.433	11.961	0.512452±0.000006	-3.6±0.4	*11.1*
600	34.425	7.43	0.512456±0.000006	-3.6±0.4	*16.9*
1000*	34.52	4.412	0.512425±0.000006	-4.2±0.4	*28.0*
1250*	34.562	3.378	0.512419±0.000004	-4.3±0.4	*27.5*

1400	34.579	2.986	0.512419±0.000005	-4.3±0.4	*29.0*
1600	34.596	2.62	0.512414±0.000004	-4.4±0.4	*31.6*
1800	34.608	2.392	0.512419±0.000005	-4.3±0.4	*30.2*
2000	34.612	2.307	0.512409±0.000005	-4.5±0.4	*28.8*
2200	34.62	2.23	0.512421±0.000004	-4.2±0.4	*32.7*
2500	34.62	2.17	0.512416±0.000004	-4.3±0.4	*31.2*
2800	34.62	2.13	0.512428±0.000004	-4.1±0.4	*33.3*

Northwest South China Sea station: D3 (20º2.928´ N, 117º25.098´ E; Apr 2013)

5	33.998	26.724	0.512470±0.000007	-3.3±0.4	*10.3*
200	34.542	14.678	0.512443±0.0000011	-3.8±0.4	*8.8*
400	34.417	9.157	0.512449±0.000008	-3.7±0.4	*13.2*
700*	34.463	6.008	0.512439±0.000008	-3.9±0.4	*16.0*
900*	34.512	4.673	0.512450±0.000008	-3.7±0.4	*19.4*
1000	34.535	4.154	0.512426±0.000010	-4.2±0.4	*19.5*
1200	34.563	3.457	0.512459±0.000008	-3.5±0.4	*23.1*
1400	34.585	2.913	0.512434±0.000005	-4.0±0.4	*24.1*
1600	34.598	2.634	0.512436±0.000004	-3.9±0.4	*27.9*
1800	34.608	2.439	0.512426±0.000004	-4.2±0.4	*29.0*
2000	34.613	2.328	0.512421±0.000004	-4.2±0.4	*24.1*
2107	34.615	2.287	0.512430±0.000004	-4.1±0.4	*31.7*

Northwest South China Sea station: 10-JJW-07 (20º12´ N, 118º17´ E; May 2010)

5	34.295	26.113	0.512420±0.000007	-4.2±0.2	12.7
500	34.414	8.5	0.512434±0.000015	-4.0±0.3	17.2
1000	34.53	4.314	0.512472±0.000013	-3.2±0.3	21.7
1500	34.59	2.856	0.512433±0.000011	-4.0±0.2	28.2
1750	34.602	2.57	0.512391±0.000004	-4.8±0.4	35.5
2000	34.607	2.47	0.512365±0.000009	-5.3±0.2	37.8
2250	34.609	2.406	0.512280±0.000004	-7.0±0.4	55.3

Northwest South China Sea station: E405 (19º36' N, 120º1' E; Sep 2009)

1500	34.593	2.72	0.512412±0.000010	-4.4±0.4	32.52

Western South China Sea station: 10-JJW-82 (18º30´ N, 114º15´ E; May 2010)

5	34.112	29.581	0.512366±0.000006	-5.3±0.4	14.54
1000	34.558	3.596	0.512459±0.000007	-3.5±0.3	25.25
1500	34.599	2.71	0.512447±0.000006	-3.7±0.3	28.09
2000	34.613	2.45	0.512458±0.000008	-3.5±0.3	31.71
2500	34.618	2.338	0.512455±0.000011	-3.6±0.3	56.36

Western South China Sea station: E418 (18º00´ N, 114º 30´ E; Sep 2009)

2500	34.615	2.377	0.512425±0.000008	-4.2±0.3	32.9

Western South China Sea station: SEATS (17º59´ N, 115º59´ E; Nov 2011)					
0	33.596	26.29	0.512277 ±0.000011	-7.0±0.3	11.2
200	34.493	26.29	0.512466±0.000009	-3.4±0.3	13.1
400	34.406	9.564	0.512474±0.000008	-3.2±0.3	14.7
600	34.418	6.89	0.512483 ±0.000009	-3.0±0.3	18.2
800	34.468	5.255	0.512450±0.000005	-3.7±0.4	22.7
1000	34.517	4.131	0.512452±0.000008	-3.6±0.3	22.2
1200	34.552	3.395	0.512467±0.000007	-3.4±0.4	23.0
1400	34.571	2.947	0.512451±0.000005	-3.6±0.3	26.4
1600	34.582	2.713	0.512426±0.000009	-4.1±0.3	30.0
1800	34.59	2.555	0.512437±0.000005	-3.9±0.4	30.0
1900	34.592	2.51	0.512456±0.000006	-3.6±0.3	32.2
2000	34.594	2.461	0.512454±0.000009	-3.6±0.3	33.9
2100	34.596	2.427	0.512446±0.000006	-3.8±0.3	31.2
2200	34.597	2.397	0.512445±0.000008	-3.8±0.3	31.5
2300	34.598	2.383	0.512445±0.000004	-3.8±0.3	34.9
2400	34.599	2.371	0.512424±0.000007	-4.2±0.3	25.9
2500	34.599	2.358	0.512448±0.000009	-3.7±0.3	33.5
2600	34.6	2.351	0.512446±0.000004	-3.7±0.4	34.9
2700	34.6	2.349	0.512453±0.000007	-3.6±0.3	33.8
2800	34.601	2.347	0.512454 ±0.000009	-3.6±0.3	36.5
2900	34.601	2.348	0.512445±0.000004	-3.8±0.4	34.5
3300	34.602	2.369	0.512439±0.000004	-3.9±0.4	37.6
Central South China Sea station: E202(14º00´N, 118º30´E; Sep 2010)					
5	33.3297	29.351	0.512204±0.000009	-8.5±0.3	25.1
Southwest South China Sea station: 10-JJW-55(14º31´N, 111 º00´E; May 2010)					
5	33.2843	28.864	0.512204±0.000009	-8.5±0.3	24.1
Southwest South China Sea station: 10-JJW-46(11º00´N, 111º00´E; May 2010)					
5	33.248	30.389	0.512275±0.000008	-7.1±0.3	15.8

Seawater samples were collected using 12 litre, Teflon-lined, Niskin bottles which were mounted on a conductivity-, temperature-, and depth (CTD) profiler (Sea-Bird 911 plus, Sea-Bird Electronics Inc.) equipped with a transmissivity-sensor. All of the seawater samples were filtered on board using a 0.45 µm membrane (MilliPore Corp.) immediately after collection. The filtered seawater was then acidified to a pH lower than 2 with 2 N HCl suprapur acid.

Nd isotopic compositions of seawater were analysed on filtered samples following the

analytical procedures described in detail by Lacan and Jeandel (2001). In brief, the Nd was extracted from a seawater sample of about 10~15 L by ion exchange chromatography. Seawater REEs were preconcentrated using SEP-PAK Classic C18 cartridges loaded with a HDEHP/H_2MEHP complexing agent. REEs were then purified using a cationic resin (AG50W-X8). Nd was extracted and purified by using an Ln-Spec column following the method described in detail by Copard et al. (2010). In this method, samples were loaded using 0.7 ml of 0.05N HNO_3 on preconditioned LN-Spec columns. The unwanted cations were eluted using 3.25 ml of 0.25N HCl. Nd was then eluted with an additional 2.5 ml of 0.25N HCl.

The purified Nd fraction was analyzed using the ThermoFisher Neptune-Plus Multi-collector Inductively Coupled Plasma Mass Spectrometer (MC-ICP-MS) at the Laboratoire des Sciences du Climat et de l'Environnement (LSCE) in Gif-sur-Yvette. The Nd isotopic composition was analysed at a concentration of 10 ppb. $^{143}Nd/^{144}Nd$ ratios were corrected for mass fractionation relative to $^{146}Nd/^{144}Nd=0.7219$ and an exponential fractionation correction applied. During the analysis, every two samples were bracketed with analyses of Jndi-1 or La Jolla Nd isotopic standards at similar Nd concentrations to those of the samples. Replicate analyses of the La Jolla standard yielded a mean $^{143}Nd/^{144}Nd$ of 0.511835 ± 0.000020 (2SD, n=54) while the Jndi-1 standard yielded a mean value of 0.512100±0.000020 (2SD, n=16). The generally accepted εNd values of La Jolla and Jndi-1 are 0.511858±0.000020 and 0.512115±0.000007, respectively. We thus corrected all of the measurements affected by a machine bias when necessary. The external reproducibility of international La Jolla and Jndi-1 standards, at the same concentration as the seawater samples analyzed by MC-ICP-MS, is of 0.3 ε units. Despite high internal instrument precision, our reported data are inevitably affected by a relatively large external error bar as shown in Table 3.1. Blank values were <150 pg, and can be ingnored as they represent less than 1.5% of the Nd from seawater samples analysed, taking into consideration the volume of the seawater sample (10 to 15 L) and the mean Nd concentration of seawater analysed (Table 3.1).

Following on-board filtering and acidification, 500 ml seawater samples were split for REE concentration measurements. A spike solution, enriched in ^{141}Pr and ^{169}Tm, was added to each sample in order to determine the yield of the extraction chemistry. After an equilibration period of two days, the pH was increased to 8 by the addition of NH_4OH. A purified iron solution was then added to each sample which enabled the co-precipitation of REE by the iron

oxide. After centrifugation, the precipitate was dissolved in 6 M HCl and loaded on an anion exchange column packed with AG1W-X8 resin to elute the REEs. This solution was evaporated and REE concentrations were analysed using the Inductively Coupled Plasma-Quadrupole Mass Spectrometer (ICP-MS X SeriesII) at the LSCE. The added ^{141}Pr and ^{169}Tm spikes permitted the use of isotopic dilution to calculate REE concentrations. Internal REE standard and BCR-1 standard solutions were analysed to monitor and correct instrument drift. Due to isobaric interferences, Eu concentrations were corrected for the residual presence of Ba-generating oxides at masses 151 and 153, and Gd concentrations, taking into account the influence of Pr oxides (about 2%). Our measurements were characterized by analytical uncertainties ranging from 5% for the lightest REE, to 15 % for the heaviest, in accordance with previously published results (Bourdin et al., 2011). Based on Nd isotopes 145 and 146, the uncertainty associated with Nd concentrations was systematically better than 10% (2 σ).

3.4. Results

3.4.1. Hydrological parameters

Potential temperature and salinity results for all seawater samples investigated in this study are reported in Table 3.1. Graphs of potential temperature (θ) and salinity versus water depth, and of salinity versus potential temperature (Fig. 3.2), allow the identification of NPTW, NPIW and PDW in the Philippine Sea stations, and SCSTW, SCSIW and PDW in the SCS stations.

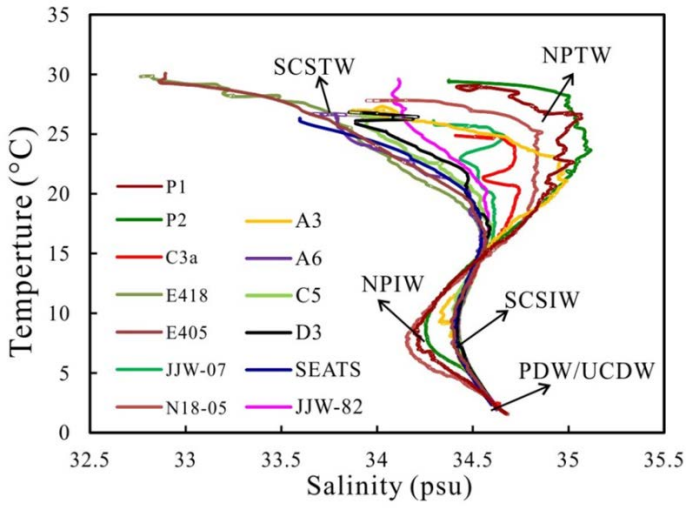

Figure 3.2. (a) Potential temperature (θ) –Salinity (S) plots for the stations investigated

in this study indicating the water masses discussed in the text.

At stations P1 and P2, the core of the NPTW (>34.8, Suga et al., 2000) is identifiable at a depth of approximately 160 m by a salinity maximum of 35.1 and a potential temperature of 23.6℃ (Fig. 3.3a and 3.3b). At a depth of around 425 m, the core of the NPIW (34.0~34.3, Talley, 1993) is characterized by a salinity minimum of ~34.25 and a temperature of ~9℃. At station N18-05, the NPTW occurs at a slightly lower water depth (~ 80 m) and is marked by similar salinity and temperature maxima (S = ~34.86, θ= ~25.15℃). The NPIW occurs at a depth of ~535 m and is characterized by lower salinity values (~34.15) compared to those at stations P1 and P2. Water masses below 2000 m are characterized in the three stations, P1, P2 and N18-05, by a similar downward decrease of potential temperature from 2.1°C to 1.5°C and an increase of salinity from 34.63 to 34.68. Such ranges of values confirm the presence in the Philippine Sea below 2000 m of the PDW, which mainly originates from the UCDW (θ of 1.6-2.1℃, salinity of 34.6 -34.7, Knauss, 1962; Amakawa et al., 2013).

Values for the seven stations in the Northern SCS (SEATS, 10-JJW-82, E405, E418, D3, C5 and 10-JJW-07) are outlined in Figures 3.3c, 3.3d, 3.3e and 3.3f. The intermediate and deep-water masses of all of these stations (Fig. 3.2) are identical which implies similar and homogenous water masses for the northern SCS. Above 80 m, the sea surface water exhibits a large range of potential salinity, from 32.8 to 34.6, mainly due to monsoon rainfall and freshwater input from Asian rivers around the SCS. At greater water depths, a salinity maximum of 34.6, associated with a temperature of ~16.5℃, occurs at a depth of approximately 120-200 m, while a salinity minimum of ~34.4, associated with a temperature of 7.7 ~ 9.2℃, is observed at a depth of around 470 m (Fig. 3.3c, 3.3d, 3.3e and 3.3f). Such variations in potential temperature and salinity of the Northern SCS have already been observed in several previous studies and permit the identification of the SCSTW above 350 m and the SCSIW between 350 m and 1500 m (Tian et al, 2006 and 2009; Gong et al, 1992, Chen et al, 2001; Xie et al, 2011). Below intermediate water (SCSIW), the 7 stations of the SCS are characterized by a narrow range of potential temperature (between 2.33 and 2.88℃) and salinity (between 34.58 and 34.62) which is attributed to the inflow of the PDW from the Philippine Sea to the SCS (~34.61).

The salinity versus potential temperature diagram (Fig. 3.2) indicates that surface and intermediate water masses of the SCS (SCSTW and SCSIW) and Philippine Sea (NPTW and

NPIW) are characterised by large differences in salinity and potential temperature. In general, the SCSTW is characterised by lower salinity than the NPTW whereas the salinity of the NPIW is lower than that of the SCSIW. The lower surface water salinity (SCSTW) and higher intermediate water salinity (SCSIW) of the SCS, relative to the Philippine Sea water masses (NPTW and NPIW), suggests modification of the original water mass properties of the Philippine Sea. In contrast, the deep-water masses of the SCS and the Philippine Sea display similar water mass properties.

Stations C3a, A3 and A6 (Fig. 3.3g and 3.3h), in the northern, middle and southern part of the Luzon Straits respectively, were revisited at different periods of the year (Fig. 3.1, Table 3.1). For these three stations, the salinity maximum observed at sub-surface (around 100 m depth) and the salinity minimum observed at mid-depth (around 400-800 m) display a degree of variation. In general, for the upper 1500 m, θ and the salinity profiles of stations A6 and C3a are more comparable to those of the SCS (Fig. 3.3e and 3.3f) whereas profiles at station A3 are similar to those of the Philippine Sea (Fig. 3.3a and 3.3b) implying variable directions in the flow of the sub-surface and mid-depth water masses in the Luzon Strait. This is dependent on the season in which seawater samples were collected and the location of the station within the Luzon Strait. The salinity profile of station A6, located in the northern Luzon Strait, is quite similar to those of the SCS with a less pronounced salinity maximum at a depth of 160 m (34.55) and a salinity minimum at 446 m (34.42), suggesting an eastward flow of the SCSTW and the SCSIW into the Philippine Sea. In contrast, for station A3, the salinity maximum at ~90 m and salinity minimum at 381 m reach 34.99 and 34.32, respectively. Such values are similar to those from stations P1 and P2 implying a westward flow of the NPTW and NPIW into the SCS. At station C3a, the salinity maximum of ~34.74 observed at a depth of about 100 m implies the intrusion of the NPTW into the SCS whereas at a depth of ~660 m, a salinity minimum of ~34.40 psu, associated with the temperature of ~7.2℃, implies the outflow of SCSIW into the Philippine Sea. The salinity of the deep layer below 1500 m for the three Luzon Strait stations decreases slightly from ~34.58 to ~34.62 at 3000 m, which indicates the inflow of the PDW from the Philippine Sea to the SCS.

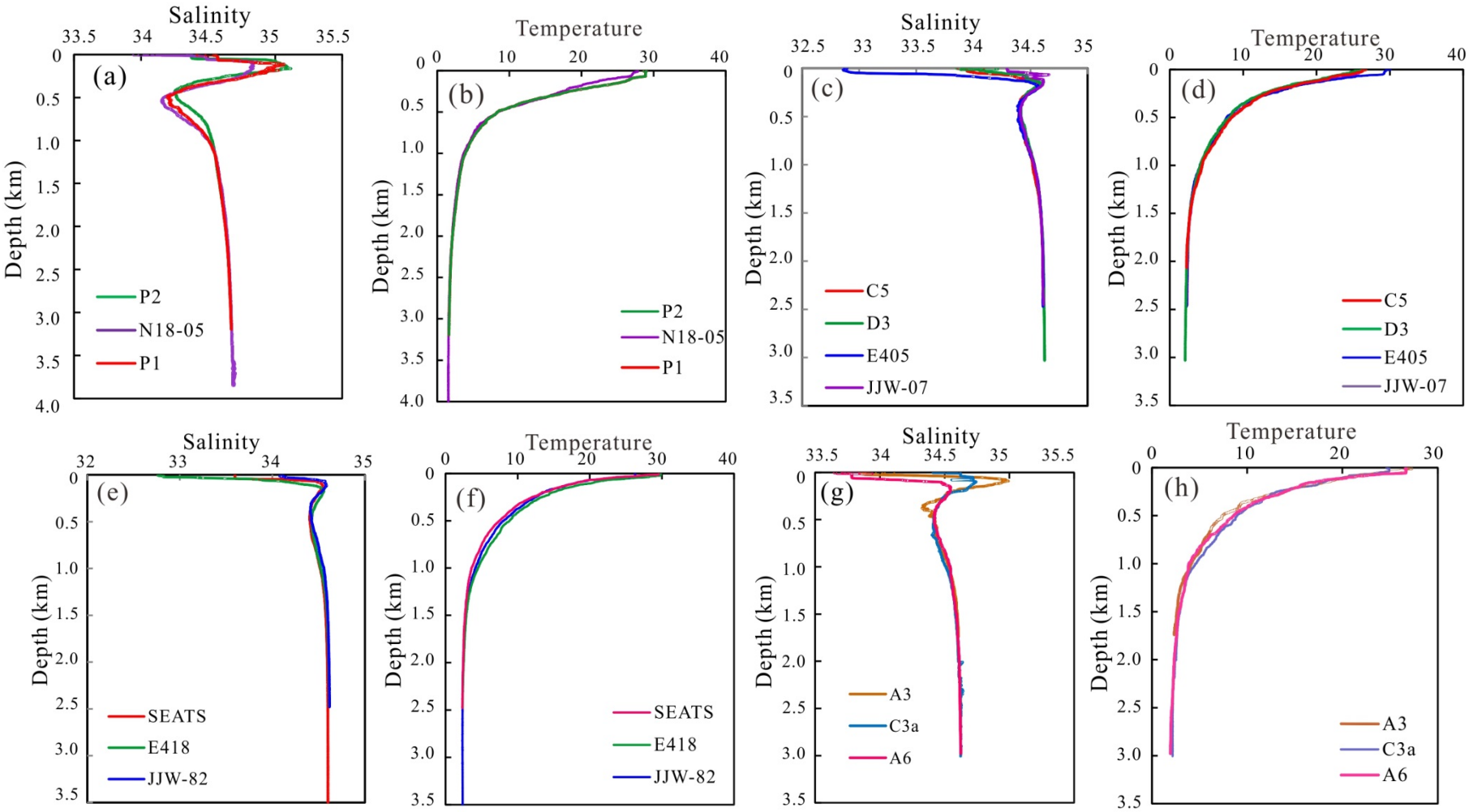

Figure 3.3. (a, b) Vertical salinity and temperature profiles of full water columns collected from the Philippine Sea. (c, d, e, f) The same as figure 3a and 3b, but for samples collected from the SCS. (g, h) As figures 3.3a and 3b, but for samples collected in the Luzon Straits.

3.4.2. Seawater REE concentrations

Nd concentrations from all of the water stations analysed range from 11 to 56 pmol/kg (Table 3.1). The range of Nd concentrations is comparable to the previously published values for the Philippine Sea (from 3 to 33 pmol/kg) and for the SCS (from 4 to 50 pmol/kg) (Alibo and Nozaki, 2000). All water stations analysed show a general increase of Nd concentrations from the surface downwards in agreement with previous results obtained in the study area (Alibo and Nozaki., 1999 and 2000) and in all other oceans (Piepgras et al., 1979; Amakawa et al., 2009; Stichel et al., 2012).

Post Archean Australian Sedimentary Rocks (PAAS) normalized REEs display similar patterns, typically characterised by a pronounced negative Ce anomaly together with enrichment of heavy REEs (Fig. 3.4). Such a pattern is consistent with oceanic REE behaviour, characterised by the poor solubility of Ce due to its specific redox properties and its oxidative state (IV) compared to the other trivalent REEs (Byrne and Sholkovitz, 1996; Jeandel et al., 2013). The relatively “flat” REE patterns of surface water collected from the Philippine Sea, with an almost complete absence of Ce anomaly, is typical of shallow open ocean REE patterns (Elderfield and Greaves, 1982; Piepgras and Jacobsen, 1992; Byrne and Sholkovitz, 1996; Wyndham et al., 2004; Jeandel et al., 2013). This is because the oxidation of Cerium is not complete: Ce III remains dissolved with the other trivalent REEs, and Ce IV is only partially affected by the process of REE scavenging by particles or Mn–oxides (Byrne and Sholkovitz, 1996). The strong influence of lithogenic input could also contribute to this weak negative Ce anomaly.

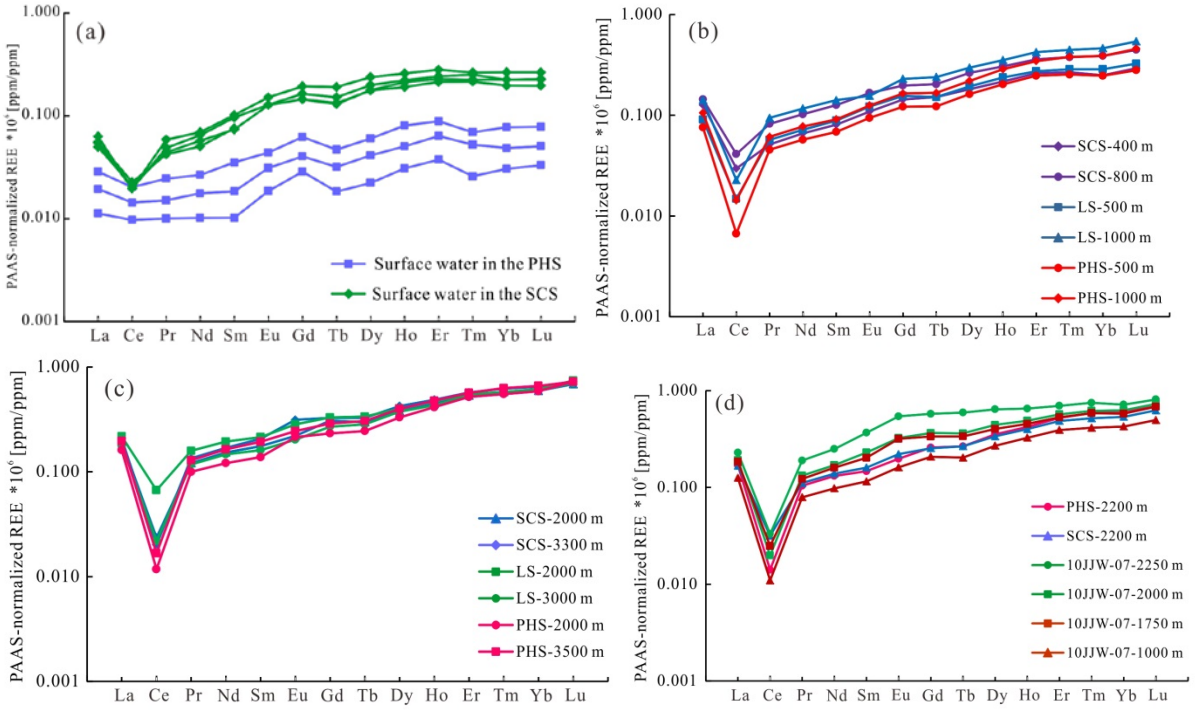

Figure 3.4. REE concentrations for various depths were normalized to PAAS REE values (Nance and Taylor, 1976). Except for the REE pattern for the shallow waters of the Philippine Sea (PHS), all REE patterns are similar and characterised by a Ce negative anomaly and a progressive increase of the REE from the lightest to the heaviest. Only a selection of the most representative patterns is included, corresponding to various depths and distinct water masses. Figures 3.4a, 3.4b and 3.4c show REE concentrations in surface-, intermediate- and deep layers, respectively. Figure 3.4d compares the REE patterns from the drift sediment deposit stations and from stations in the Philippines Sea and the SCS.

3.4.3. Seawater εNd

The Nd isotopic compositions of seawater samples are illustrated in Table 3.1. εNd values from stations P1, P2 and N18-05 in the Philippine Sea are outlined in Figure 3.5a. The vertical evolution of seawater εNd values obtained from the three stations in the Philippine Sea are consistent with each other and permit the establishment, for the first time, of the Nd distribution for water masses of the middle and western part of the Philippine Sea. εNd values decrease slightly from -2.7±0.4 for the upper layers to -4.4±0.3 at 3500 m depth (Fig. 3.5a). The most radiogenic εNd values (around -2.7±0.3) have been observed at depths of 500 m and 1400 m for stations P2 and N18-05, respectively. Below a water depth of 1500 m, seawater εNd displays more negative values, ranging between -3.6±0.4 and -4.4±0.3.

εNd values for samples from stations D3, C5, JJW-07 and E405 (collected in the northern part of the SCS during April, 2013) are displayed in Figure 3.5b. At station D3, εNd also exhibits a narrow range of values, from -3.3±0.4 to -4.2±0.4, between the surface and a depth of 2107 m, with no major significant changes. Only the surface seawater is characterised by a slightly more radiogenic Nd isotopic composition (εNd around -3.3±0.4). Station C5 presents a similar range of variations (between -3.6±0.4 and -4.5±0.4), as station D3, with significantly higher εNd values (-3.6±0.4) between depths of 300 and 1000 m.

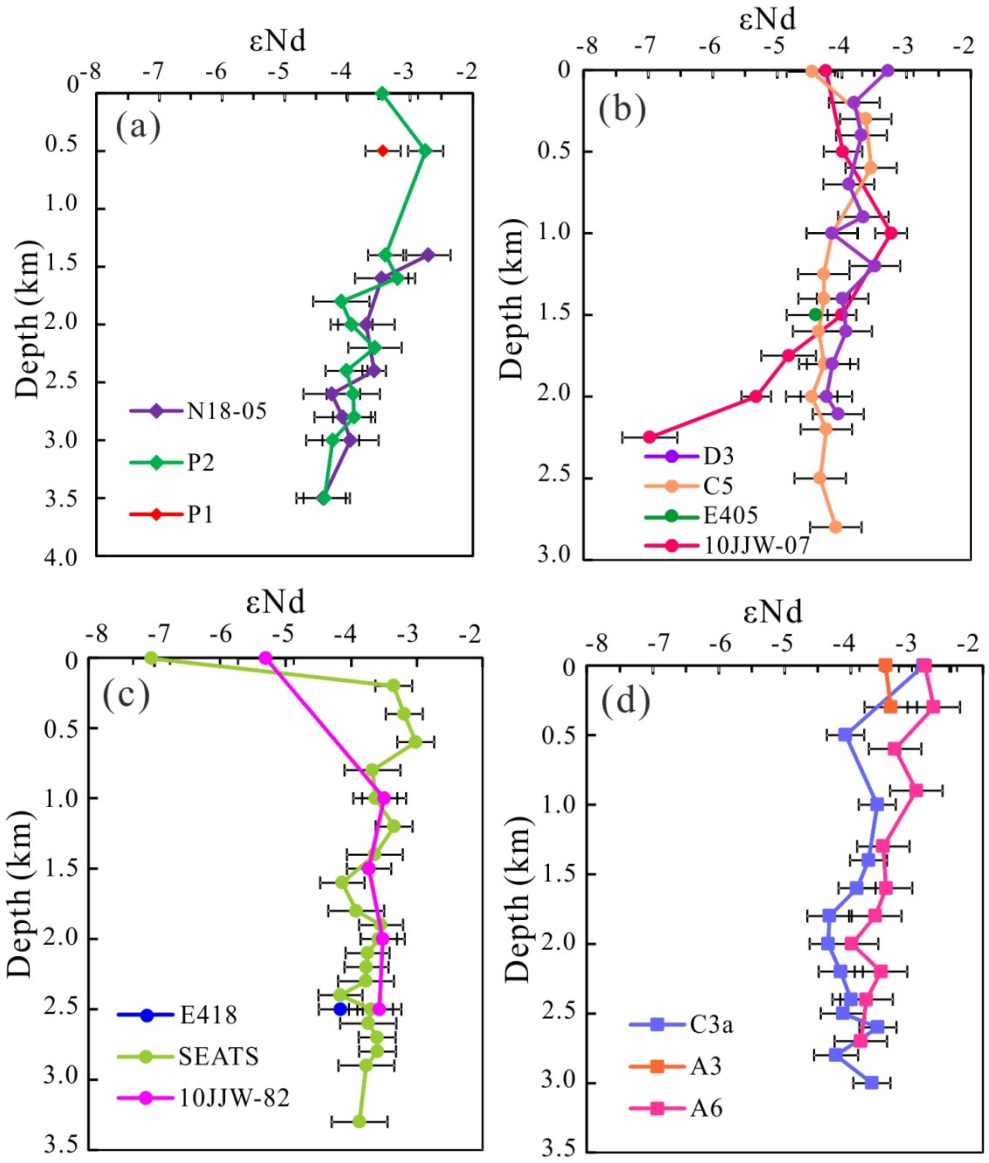

Figure 3.5. Vertical profiles of εNd values obtained in the course of this study. (a) εNd values profiles in the Philippine Sea. (b) εNd values profiles in the northwest SCS. (c) εNd values profiles in the western SCS. (d) εNd values profiles in the Luzon Straits.

For station JJW-07, εNd values exhibit large variations, ranging from -4.2±0.2 to -7.0±0.4, between surface- and bottom water. The sea surface water is characterised by a εNd value of -4.2±0.2 that decreases significantly with depth to reach -3.2±0.3 at a depth of 1000 m. As water depth increases the εNd values decrease continuously to reach -7.0 at the bottom of the water profile (2250 m).

εNd value profiles from stations SEATS, JJW-82 and E418, collected in a southern location along the northwest SCS margin (Fig. 3.1), are presented in Figure 3.5c. Samples from the SEATS station were analyzed at a very high vertical resolution in order to determine, in great detail and for the first time, the Nd isotopic composition of the water masses in the Northern part of the SCS. The εNd vertical profile obtained for station SEAT is similar to that of the nearby station JJW-82. Both stations, SEATS and JJW-82, present the most unradiogenic εNd values for surface seawater, reaching -7±0.3 and -5.3±0.4, respectively (Fig. 3.5c). Below a depth of 200-500 m, εNd values exhibit a narrow range of between -3±0.3 and -4.2±0.3 for both stations. In detail, for station SEAT, εNd values are slightly more radiogenic between 200 and 600 m depth (εNd from -3±0.3 to 3.4±0.3) than below 800 m depth (εNd from -3.6±0.3 to 4.2±0.3). εNd values obtained from station JJW-82 also display a narrow range of between -3.5±0.3 and -3.7±0.3, a pattern which closely matches the seawater εNd vertical profile obtained for the SEAT station below a depth of 1000 m. In addition, one seawater sample collected at 2500 m at station E405 also yields a similar value (-4.2±0.3) to those obtained for stations SEATS and JJW-82 at the same water depth (Fig. 3.5c).

For stations C3a and A6, located in the Luzon Strait (Fig. 3.5d), εNd values of deep water are relatively less radiogenic (-4.2±0.3) than the surface and intermediate waters (-1.9±0.4 to -3.3±0.4). In addition, εNd values at station C3a are also slightly less radiogenic than those of station A6 above 2000 m depth. For station C3a, εNd values decrease from -2.9±0.5 at the surface to -4.1±0.3 at 500 m and then increase to -3.6±0.3 at 1000 m before decreasing again towards -4.3±0.3 at 1800 m. Below a depth of 1800 m, εNd values are quite stable, displaying mean values of around -4.0. For station A6, εNd values are slightly more radiogenic above a depth of 1800m and range from -1.9±0.4 to -3.3±0.4. At greater depths, εNd values vary from -3.5±0.4 to -4.0±0.4 with the same range of variation as those of station C3a. In addition, at station A3, two seawater samples collected at 0 and 300 m depth exhibit a εNd value of around -3.5±0.4.

Despite the small variability of εNd values in mid- to deep-water masses at most of stations of the SCS, surface seawater displays large spatial variations in εNd values, from -2.9±0.5 to -8.5±0.3 (Table 3.1).

3.5. Discussion

3.5.1. Nd isotopic composition in the western Pacific Ocean

Stations N18-05 and P2, located in the Philippine Sea, are influenced by both northern and southern sourced water masses. Vertical variations of εNd values determined in both stations exhibit similar patterns (Fig. 3.5a) implying similar water mass sources. In general, intermediate water masses, corresponding to a salinity minimum at a depth of 400-800 m, are characterised by more radiogenic Nd isotopic composition (εNd ~ -2.8±0.3) compared to deep water (εNd ~ -4.4±0.3). A comparison of these results with those obtained previously in the Southwest and Southeast Pacific is illustrated in Figures 3.6a and 3.6b (Amakawa et al., 2013; Jeandel et al., 2013). εNd values for the AAIW, identified in the Southwest Pacific between depths of 1200 and 500 m at stations SX20 and SX22 (Fig. 3.1), range from -6±0.3 to -8.4±0.3 (Amakawa et al., 2013). This range of εNd values for the AAIW is also consistent with those obtained at stations EGY (31.90º S, 91.41º W) and GYR (26.07º S, 113.99º W) located in the Southeast Pacific (εNd from –4.0±0.5 to –7.1±0.2) (Fig. 3.6b) (Jeandel et al., 2013). Consequently, the range of εNd (from -2.7±0.4 to -3.5±0.4) observed at stations N18-05 and P2 for intermediate water masses between depths of 500 and 1600 m, differs from those determined for the AAIW in the Southwest and Southeast Pacific (Amakawa et al., 2013; Jeandel et al., 2013). In addition, εNd values of intermediate water masses from stations N18-05 and P2 are very different to seawater εNd values for the west equatorial Pacific Ocean close to the Papua New Guinea coast which are characterised by mean values of around -2 indicating the importance of boundary exchange with sediments characterised by radiogenic Nd isotopic composition deriving from surrounding volcanic margins (Grenier et al., 2013) (Fig. 3.6c). Furthermore, the intermediate water salinity for the studied stations in the Philippine Sea (~34.2) differs from that of the stations in the west equatorial Pacific Ocean (~34.6) investigated by Grenier et al. (2013). This suggests that stations N18-05 and P2 are unlikely to be affected by the same water masses as those of the west equatorial Pacific.

εNd vertical profiles for stations TP24 271-1, LM2, LM6/11 and BO5, located in the

subtropical gyre of the North Pacific, are illustrated for the purpose of comparison in Figure 3.6d (Amakawa et al., 2004 and 2009; Piepgras and Jacobsen, 1988). Between depths of 500 and 1500 m, εNd values at stations N18-05 and P2 are in agreement with those obtained from BO-5 (-2.7±0.3 to -4.2±0.6) and TPS24 271-1 (-2.9±0.3 to -3.8±0.3), for the same range of water depths and, to a lesser extent, with those of stations LM2 and LM6/11 (Fig. 3.6d) which are characterised by slightly negative values (-3.6±0.3 to 5.0±0.6). As intermediate water masses at the four stations (TP24 271-1, LM2, LM6/11 and BO5) are within the anti-cyclonic circulation of the NPIW, they permit the εNd values of the NPIW, which is mainly confined to the subtropical gyre of the North Pacific (Talley, 1993; You, 2003), to be constrained. Consequently, such results imply that intermediate water at stations N18-05 and P2 is strongly influenced by NPIW transported from the north rather than by AAIW from the south.

At greater water depths, εNd values in stations N18-05 and P2 decrease gradually from -3.2±0.3 to -4.4±0.3 between depth of 1600 and 3500 m indicating that water masses in the study area are well stratified. Previous studies exhibit spatial variability of deep-water εNd in the Pacific Ocean (Fig. 3.6). On the one hand, εNd values are more negative (εNd value of UCDW/LCDW ~ -8) at high southern latitudes of the South Pacific than in the western equatorial Pacific (~ -3) (Carter et al., 2012; Grenier et al., 2013). On the other hand, PDW εNd values for the North Pacific range from ~-4 to -6 (Carter et al., 2012; Molina-Kescher et al., 2014; Jeandel et al., 2013; Grasse et al., 2012; Grenier et al., 2013; Amakawa et al., 2004). At a latitude of around 30º South, the UCDW is characterised by εNd values ranging from -4 in the southeast Pacific Ocean, the result of mixing with old NPDW, to -6.5 in the southwest Pacific Ocean, whereas the LCDW is characterised by very negative εNd values of about -9 (Amakawa et al., 2013; Jeandel et al., 2013). Consequently, with the exception of the southeast Pacific Ocean station (Station GYR) where the presence of PDW has been identified, deep-water εNd values for both stations N18-05 and P2 are significantly higher than the range of UCDW/LCDW εNd observed in other South Pacific basins. On the contrary, εNd values obtained from stations N18-05 and P2 confirm that the NPDW is characterised by more radiogenic values in the Philippine Sea (-4.4) and North-western Pacific (-4) (Fig. 3.6d) than in the South Pacific (-8) (Fig. 3.6a). However, Philippine Sea deep-water exhibits εNd values which differ entirely from those of the equatorial Pacific close to the Papua New Guinea coast where deep-water masses are characterised by εNd values of between -0.5 and -2.5. Consequently, εNd values for southern source deep-water (UCDW) increase gradually along its northward trajectory. However, the strong modification that has been observed in the

equatorial Pacific Ocean (εNd values of -2 to -3 for UCDW; Grasse et al., 2012; Grenier et al., 2013) seems to be restricted to a localised area and does not impact strongly on the Nd isotopic signature of the PDW in the Philippine Sea (stations N18-05 and P2) and the Western North Pacific (Stations BO5 and TPS24).

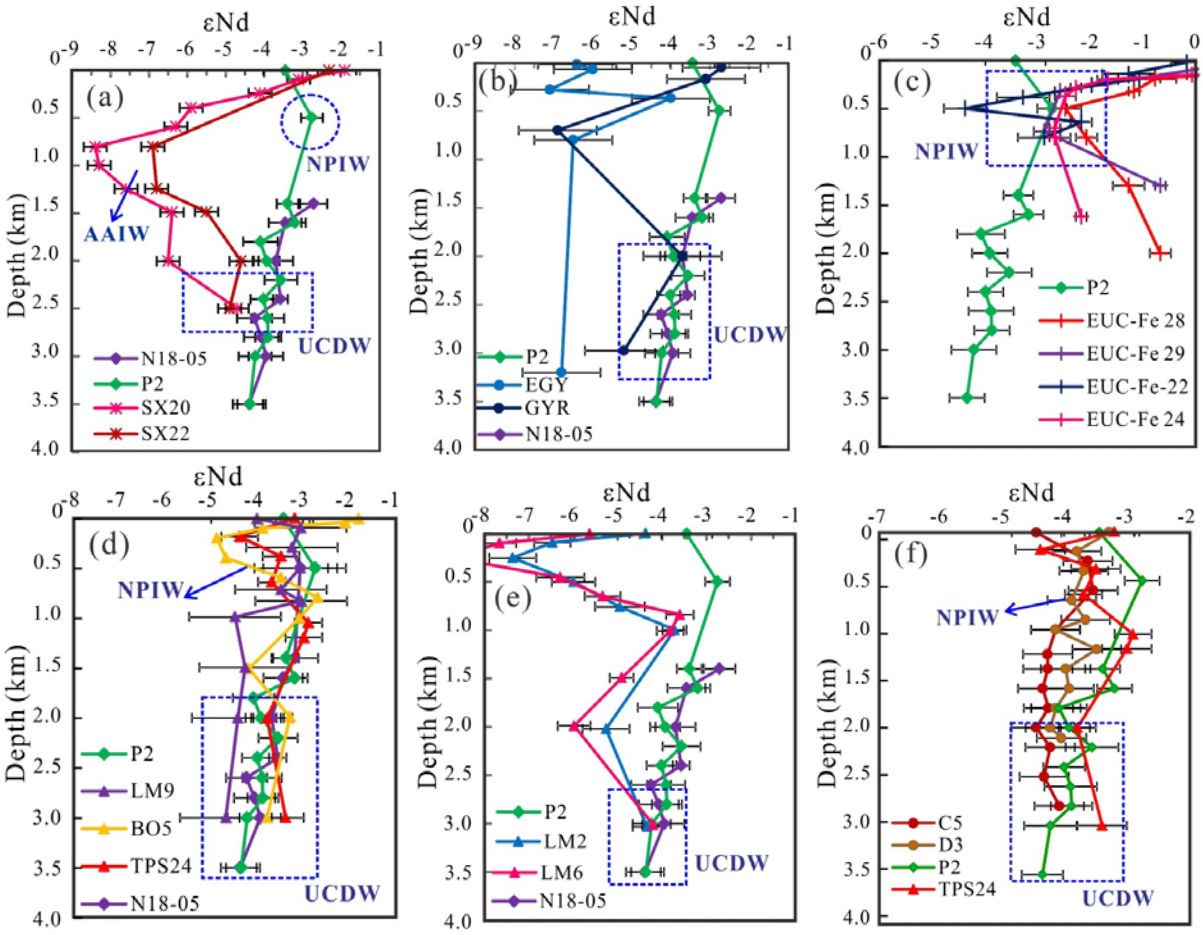

Figure 3.6. Comparison of εNd values from this study with previously published εNd data obtained in the Pacific Ocean. (a, b) Vertical profiles of εNd values in the western Pacific from this study, shown together with εNd data from the South Pacific investigated by Aamakawa et al. (2014) and Jeandel et al. (2013). (c) Reported εNd values for the equatorial Pacific (Grenier et al., 2013) and (d) for the North Pacific (Piepgras and Jacobsen, 1988; Amakawa et al., 2004 and 2009) were compared to εNd values at P2 and N18-05 in this study. (e) Comparison of Vertical Nd isotopic composition distribution in the western Pacific (this study) with εNd for the northwest Pacific. (f) εNd from the northern SCS were compared to εNd values for the North Pacific (Piepgras and Jacobsen, 1988).

In addition, seawater εNd values obtained in the Philippine Sea far from the oceanic

margin (station P2) are different from stations LM2 and LM6/11 located off the east of Japan where negative shifts of εNd values (-5 to -6) have been observed at a depth of around 2000 m (Fig. 3.6e). Such results confirm that stations LM2 and LM6/11 are affected by local boundary exchange with unradiogenic lithogenic material from adjacent marginal seas.

3.5.2. Hydrology of the South China Sea

Stations JJW-07, D3 and C5 in the northern part of the SCS are located on the presumed trajectories of deep- and intermediate water masses which enter the SCS through the southern part of the Luzon Strait and propagate towards the northwest SCS margin (Qu et al., 2006; Zhao et al., 2014).

Above a depth of 1500 m, SCIW εNd values in the northwest SCS (Stations JJW-07, D3 and C5) display slightly negative values (between -4.3±0.4 and -3.2±0.3) compared to NPIW εNd values (around -2.8±0.3) in the Philippine Sea. It is worth noting that, according to hydrographic observation and modelling results, SCIW was assumed to flow out of the SCS to the Philippine Sea (Tian et al., 2006; Gong et al., 1992; Qu et al., 2006). The SCIW is characterised by relatively higher salinity than the NPIW implying strong vertical mixing, in the SCS, of the intermediate water masses (NPIW) that enter the SCS with the PDW (Fig. 3.2). Consequently, the εNd value fingerprint of the SCSIW inevitably displays a slightly unradiogenic value due to vertical mixing with the PDW (-4.3±0.4).

Below 1500 m, the vertical profiles of εNd from stations D3 and C5 are similar, with a mean value of around -4.4, consistent with the deep water εNd values from stations P2 and N18-05 in the Philippine Sea (Fig. 3.6f), as well as reported εNd values from other stations in the North Pacific. In contrast, Nd isotopic composition of deep water obtained at station JJW-07 exhibits a shift to unusual negative εNd values (-7.0±0.4) (Fig. 3.5b) associated with a significant increase in Nd concentrations at the bottom (56 pmol/kg). Such negative values have not been observed in the other bottom stations of the Northern SCS which present a narrow range of εNd, between -3.9±0.4 and 4.2±0.4, similar to those of the PDW. As the UCDW is not characterised by such unradiogenic εNd in the North Pacific, these negative εNd values can only be caused by the local effects of boundary exchange (Amakawa et al., 2009). Station JJW-07 was sampled near a series of large sediment drifts (Lüdmann et al., 2005) where surface sediments are characterised by negative εNd values of around -11 (Li et

al., 2003; Wei et al., 2012). Considering this fact, we suggest that the extremely negative εNd value for the deep water is primarily the result of the particle-seawater exchange process.

Stations 10JJW-07, D3 and C5 were also sampled close to an area where large sediment drifts are deposited (Lüdmann et al., 2005). Transmissivity data were generated for stations D3 and C5 on the northern part of the SCS allowing us to test the possible impact of re-suspended sediments on water masses. Nepheloid layers were identified between 500 and 1000 m at station D3 and between 1000 and 1500 m at station C5.

At station D3, two seawater samples analyzed in the nepheloid layers at depths of 700 m and 900 m display εNd values of -3.7±0.4 and -3.9±0.4, values which are comparable to seawater samples collected above (-3.7±0.4) and below (-4.2±0.7) this nephloid layer. At station C5, two seawater samples analyzed from the nepheloid layers, at depths of 1000 m and 1250 m, display εNd values of around -4.2±0.4 which are similar to values for adjacent samples collected outside these layers. In addition, seawater samples collected in nearby station JJW-07, at 500 m and 1000 m, yield εNd values of -4.0±0.30 and -3.2±0.25, respectively. Taking into consideration the εNd values of surface sediment in this part of the SCS (around -11) (Wei et al., 2012), we can hypothesise that sediments transported in these nepheloid layers are around 7 epsilon units lower than the values of the PDW which enters the SCS and flows through these stations. Consequently, stations D3 and C5, located near active drift sediment systems and currently active nepheloid layers, do not exhibit any significant changes in Nd isotopic signatures as a result of exchange between seawater and re-suspended sediments characterised by unradiogenic Nd isotopic composition. This implies that the exchange of Nd between lithogenic particles and seawater, observed at station JJW-07, might be of a localised and temporary nature and does not have the potential to greatly modify the Nd isotopic composition of the PDW in the northern part of the SCS. Further investigations need to be undertaken in the future in order to establish the spatial distribution of this unradiogenic seawater εNd above and near this large drift sediment system.

Three additional stations (SEATS, JJW-82 and E418) located at around 16º N in the northwest SCS have been investigated (Fig. 3.5c). Among these, the εNd vertical profile for station SEATS, obtained by high resolution sampling, parallels those obtained at stations D3 and C5, despite the absolute εNd value at SEATS being slightly higher than those from stations D3/C5. At stations E418 and JJW-82, the εNd distribution is consistent with that from

station SEATS. The εNd result at station SEATS reveals a minor decreasing trend from mid-depth water to deep water. Above 800 m, the εNd values fall into a narrow range from -3.0 to -3.4. The salinity minimum depth at around 400 m is marked by a εNd value of -3.2±0.3. Since seawater samples from station SEATS were collected during November 2010, the mid-depth εNd values reflect the fact that the Nd isotope signature of intermediate water at SEATS is more influenced by the intrusion of the NPIW (around -3) than by vertical mixing from deep water. This is probably due to the greater intrusion of Kuroshio Currents into the SCS, which could transport NPIW to the SCS during strong winter monsoon periods (Nan et al., 2011; Gan et al., 2006; Yuan et al., 2009). At greater depths (below 1500 m), mean εNd value is around -4, which is in agreement with values obtained at stations in the northern SCS and the Philippine Sea, suggesting the presence of the PDW.

3.5.3. εNd in the Luzon Strait and its implications for the hydrology

Vertical profiles of εNd at stations A6 and C3a are similar and exhibit decreasing εNd values as depth increases (Fig. 3.5d). As indicated by salinity profiles (Fig. 3.3g), mid-depth water masses of the C3a station are characterised by similar salinity vertical distribution as station A6, which is characterised by a weaker salinity minimum between 300 and 800 m compared to those of the SCS. In contrast, station A3 presents lower salinity at mid-depths and exhibits similar water properties to the Philippine Sea. Although several studies have shown that intermediate water from the SCS (SCIW) is assumed to flow into the western Pacific (Cheng and Huang, 1996; Qu., 2000; Qu et al., 2006), recent studies indicate that intermediate water exchange through the Luzon Strait is more complex than expected (Tian et al., 2006; Yang et al., 2010; Xie et al., 2011). These studies have indicated strong seasonal variability of intermediate water transportation.

Above 2000 m, and particularly around 800 m depth, εNd values at station A6 (from -2.9±.4 to -3.3±0.4), located in the southern part of the Luzon Straits, are significantly higher than those from station C3a (from -3.6±0.3 to -4.0±0.3), which is located in the middle of the Luzon Strait (Fig. 3.5d). Such differences observed at mid-depth in station A6 are also visible in the εNd profile of the NPIW of the Philippine Sea (stations P2 and N18-05) and in previous results from the western Pacific (Amakawa et al., 2004, 2009; Piepgras and Jacobsen, 1988). Consequently, the difference in the εNd observed at mid-depth in both stations located in the Luzon Strait can be taken to indicate the presence of a relatively higher proportion of NPIW

in station A6 than in station C3a. As station A6 samples were collected at the end of the winter monsoon, and C3a samples during the winter monsoon, we can deduce that the mid-depth of the southern part of the Luzon Strait is influenced by the intrusion of NPIW into the SCS, as evidenced by the εNd values obtained from both stations. However, we cannot exclude the possibility of an exchange of Nd between seawater and sediments deriving from the volcanic Luzon Island, which is characterized by positive εNd (Goldstein and Jacobsen, 1988).

Below a depth of 2000 m stations C3a and A6 display similar εNd values (from -3.6±0.3 to -4.3±0.3) indicating the presence of the PDW which flows from the Philippine Sea to the SCS. We can also note that no clear shift of εNd values or Nd concentrations occurred at the bottom of the water column at station A6 where re-suspended sediments are observed (Fig. 3.6f)

3.5.4. Surface circulation in the SCS and the western Pacific Ocean

A compilation of the Nd isotopic compositions of the surface water obtained in the present study, and previously by Amakawa et al, (2000), are reported in Figure 3.7. In the Pacific Ocean, a surface εNd value of -3.6 is generally consistent with previous studies which have produced values of around -3.6 to -4.2 (Amakawa et al, 2000). For the seawater collected in the northern part of the SCS, the εNd value (-4) is roughly consistent with that of the western Pacific Ocean, implying inflow from the western Pacific Ocean to the SCS. Surface samples collected in the Luzon Strait, characterised by εNd -1.9, are likely to be influenced by volcanic particles transported from surrounding volcanic margins. On the other hand, a gradually decreasing trend occurs between the southern shelf of the SCS and the middle of the SCS. This spatial distribution of εNd could be attributed to 1) sediment inputs from large rivers, mainly located on the western margin of the SCS, which deliver large volumes of sediment characterised by unradiogenic Nd isotopic composition (εNd=~-10 in the Mekong River, ~-10.4 in Red River, and ~-13 in Pearl River (Liu et al, 2007; Goldstein et al., 1984); 2) the intrusion of surface water from the Indian Ocean. Today, sea surface circulation in the southern SCS varies seasonally in response to the relative intensity of summer and winter East Asian monsoons. In the present study, samples from the middle and the southern part of the SCS were collected in May, 2010. During this period of the year, the summer monsoon is active and induces inflow of surface seawater from the Indian Ocean

(εNd between -9.5~ -10) to the SCS. However, for the samples collected in the north, the negative εNd values are potentially controlled by riverine input since the εNd values display an increasing trend from the southern part of the SCS to the middle SCS.

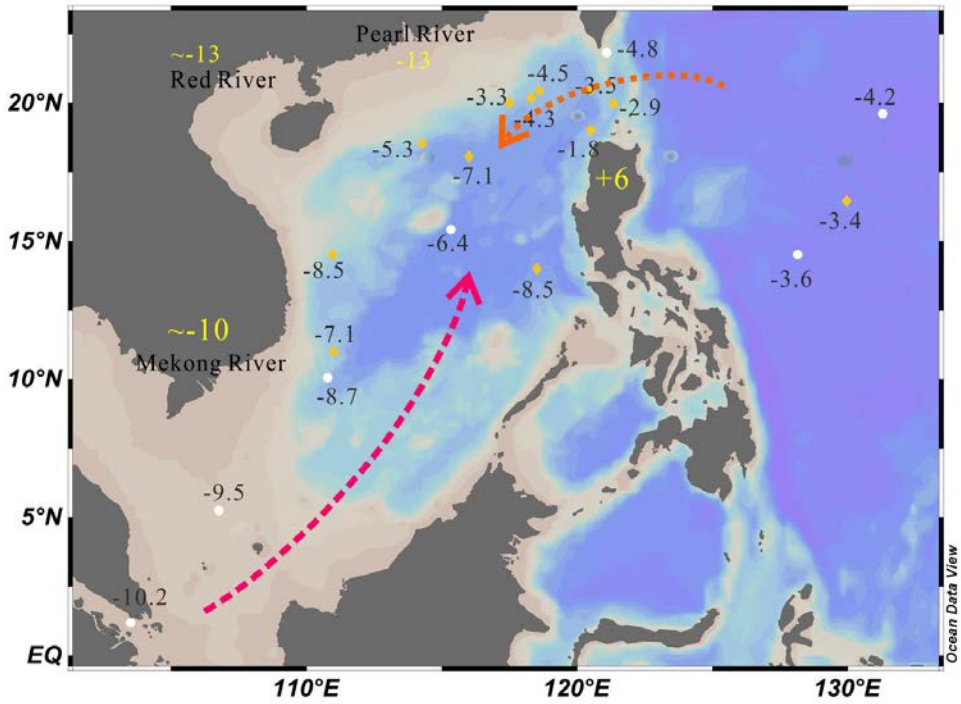

Figure 3.7. Nd isotopic composition of surface seawater in this study (yellow diamonds) and previous studies (white dots, Amakawa et al, 2000). The gradient between the northern SCS and the southern SCS suggests surface water variability.

3.6. Conclusions

For the first time, Nd isotopic composition of seawater collected from 16 stations in the SCS and the Philippine Sea has been investigated in order to determine εNd distribution in the Philippine Sea and the South China Sea. Up to now this distribution has been poorly documented even though this location constitutes a key area for understanding the palaeohydrology of the tropical Pacific. Our results reveal that vertical Nd isotopic composition in the Philippine Sea is associated with stratified water masses. εNd values of surface NPTW are typically in the order of -3.4±04; mid-depth water, associated with NPIW, has relatively higher εNd values reaching -3.0±0.3; PDW, with εNd values of around -4.4±0.3, and is influenced by the contribution of southern sourced UCDW water. For the SCS, the εNd value of deep water is homogenous and is consistent with those measured in the Philippine Sea thus indicating the inflow of PDW into the SCS. Due to vertical mixing in the SCS, the

εNd value of the SCIW is slightly lower than that of the NPIW observed in the Philippine Sea.

The Nd isotopic composition of deep water samples, obtained above or near a series of significant sediment drifts characterised by negative εNd values of around -11, shifts to negative εNd values ranging from -5 to -8.5. This shift is associated with a significant increase in the Nd concentration at the bottom implying that particle exchange plays an important local and temporary role in altering the seawater εNd. However, seawater samples investigated from several nepheloid layers in the same area do not display any impact of the local/regional Nd isotopic composition on the Nd isotopic composition of the PDW that flows on the North-western margin of the SCS. This suggests that exchange between seawater and re-suspended sediments above drift deposit systems may occur locally at certain times but does not have the potential to greatly modify the Nd isotopic composition of the PDW in the Northern Part of the SCS. The north-western margin of the SCS constitutes an ideal area for further investigation in order to reconstruct past changes in the PDW during the late Quaternary.

Finally, εNd values of surface water are controlled by riverine inputs and/or by Indian Ocean surface water flowing into the SCS through straits in the southern part of the sea. Stations investigated in the southern- and middle parts of the Luzon Strait are characterised by similar intermediate water εNd values as those of the SCS implying an outflow of the SCSIW to the Philippine Sea. The fact that the SCIW and the NPIW display slightly different εNd values permits the use of this new tracer to track water mass exchange between the western Pacific and the SCS through the Luzon Strait in the future.

Acknowledgements

We are grateful to Ziding He, Jiawang Wu and Hao Wang for the excellent quality of their sampling campaign undertaken during 2010. Thanks also to Yanli Li, Quan Chen and Shiwen Zhou for their help during the 2013 sampling campaign. We also thank the captain, crew and scientific team of R/V Dongfang Hong, Kexue No.1 and Shiyan No.3 for their collaboration in sampling. Special thanks are addressed to Louise Bordier and François Thil for their kind assistance in REE element concentration and Nd isotopic composition measurement. This work was supported by the Natural Science Foundation of China projects (No. 91128206 and 40925008) and the Labex L-IPSL. The study is a part of the French-Chinese collaborative project LIA MONOCL.

Chapter 4

Introduction

εNd values constitute a quasi-conservative proxy of water mass provenance in the ocean that has already been applied to different marine archives (e.g. fossil fish teeth; Fe-Mn crust; planktonic and benthic foraminifera; deep-sea corals and bulk sediment authigenic phases) (Ling et al., 1997; Frank, 2002; Vance et al., 2004; Martin and Scher, 2004; Colin et al., 2010; Piotrowski, 2012). Over the past decade, this new εNd proxy has been increasingly used in investigations based on planktonic foraminifera and bulk sediment authigenic phases because these sources are widely spread in the world ocean and provide the possibility of relatively high-resolution investigation. However, controversial issues have been raised regarding the reliability of εNd extraction from these two archives (Vance and Burton, 1999; Kraft et al., 2013; Elmore et al., 2011; Piotrowski et al., 2012; Wilson et al., 2013). Studies have suggested that authigenic phases precipitated on planktonic foraminifera at the sediment-seawater interfaces, overwrites the REE incorporated into living planktonic foraminifera calcite (Pomiès et al., 2002; Robert et al., 2012; Tachikawa et al., 2013). These studies suggest that εNd in the planktonic foraminifera reflect the bottom water Nd signature regardless of the cleaning procedures used. In contrast, some recent studies have used cleaned planktonic foraminifera to reconstruct εNd of surface seawater (Vance and Burton, 1999; Martínez-Botíet al., 2009). In addition, the reliability of εNd from bulk sediment authigenic phases has also been challenged on the basis of εNd contamination from the detrital fraction induced by the leaching process (Wilson et al., 2013; Kraft et al., 2013). It is therefore necessary to assess the εNd extracted from these archives and to compare them with the surrounding bottom water εNd. In this chapter, we present different methods of εNd extraction from foraminifera and bulk sediments retrieved from the northern SCS: a vertical profile of the SCS seawater εNd has been presented in the Chapter 3. Then, we also established the first εNd record from the planktonic foraminifera and bulk sediment authigenic phases over the last 25 cal kyr BP. The time resolution achieved was low but was based on different analytical procedures to extract seawater εNd, which should provide a guide for higher time-resolution investigations in the future. This εNd record permits an initial discussion of the past hydrological changes of the western subtropical Pacific since the last glacial maximum.

Neodymium isotopic composition in foraminifera and authigenic phases of South China Sea sediments: implications for the hydrology of the North Pacific Ocean over the past 25 kyr

Wu Qiong[1,2], Christophe Colin[1], Zhifei Liu[2], Francois Thil[3], Quentin Dubois-Dauphin[1], Norbert Frank[4], Eric Douville[3]

1 Laboratoire de Geosciences Paris-Sud (GEOPS), UMR 8148, CNRS-Université de Paris-Sud, Bâtiment 504, 91405 Orsay Cedex, France.

2 State Key Laboratory of Marine Geology, Tongji University, Shanghai 200092, China

3 Laboratoire des Sciences du Climat et de l'Environnement (LSCE/IPSL), UMR 8212 CNRS-CEA-UVSQ, Avenue de la Terrasse, 91198 Gif-sur-Yvette Cedex, France.

4 Universität Heidelberg, Im Neuenheimer Feld 229, 69120 Heidelberg, Germany.

* Corresponding author: E-mail: wuqiong06@gmail.com (Wu Qiong)

Abstract

The Northern South China Sea (SCS) is a key area for reconstructing past hydrological changes in the western subtropical Pacific. It receives deep-water sourced from northern and southern high latitudes of the Pacific but remains poorly documented. In this study, the Neodymium isotopic compositions (εNd) of benthic and planktonic foraminifera and Fe-Mn coatings precipitated on sediments have been analysed for the first time for the SCS. These are compared to modern seawater εNd to assess the reliability of the extraction of past seawater εNd from such an archive for a period spanning the last 25 kyr. Reductively cleaned mono-specific planktonic foraminifera (*Globigerinoides ruber*) and mixed benthic foraminifera in core-top sediments display indistinguishable εNd values, similar to those of the PDW (-4). Furthermore, the εNd of the reductive cleaning solutions shows similar values to εNd values obtained on cleaned foraminifera. Combined with PAAS-normalized REE patterns, these results confirm that the oxidative and reductive cleaning procedure applied to foraminifera is not effective in removing all of the Fe-Mn coating and that εNd values yielded by cleaned planktonic foraminifera retain the εNd imprint of the bottom water and/or sediment pore water. εNd values obtained from a leaching procedure carried out on the bulk non-decarbonated sediments are comparable to seawater εNd, whereas a similar leaching procedure applied to the carbonate free fraction of sediments reveals a bias due to

contamination with Nd deriving from lithogenic particles. In core MD05-2904, seawater εNd, reconstructed from planktonic foraminifera, indicates that the last glacial maximum (LGM) period is characterised, on average, by more unradiogenic seawater εNd (-5±0.2 to -5.9±0.2) than the late Holocene (- 4.1±0.2). These variations imply significant variations in the relative proportions of Southern Source Water (UCDW) and Northern Source Water (NPDW) in the deep-water of the western subtropical Pacific Ocean. The εNd values of foraminifera from core MD05-2904 reveal evidence of significant re-organization of the deep-water masses of the Pacific, which needs further investigation, at a higher time resolution, for the late Quaternary.

Keywords: Neodymium isotopic composition; foraminifera; authigenic phases, hydrology; subtropical Pacific Ocean, South China Sea.

4.1. Introduction

The importance of global ocean circulation for climate variability is now widely recognized (Broecker, 1990; Rahmstorf, 2002). The Pacific Ocean plays a key role in global ocean circulation in terms of heat redistribution through surface current flow from the warm pool to sub-polar latitudes, which in turn changes the carbon storage capacity of the ocean by deep-water ventilation or stratification, resulting in significant climatic implications (Matsumoto et al., 2002; Herguera et al., 2010). In particular, the oceanic histories of the Southern and Pacific Oceans during the last glacial period and Holocene are largely unknown, because sedimentation rates were typically low and calcium carbonate preservation poor precluding high resolutions studies. Even though, it has received increasing attention over recent decades (Talley et al., 1992; Talley and Yun, 2001; Reid., 1997; Zenk et al., 2005; Siedler et al., 2004; Kawabe et al., 2003, 2006, 2006, 2009; Kawabe and Fujio, 2010), the evolution through time of North Pacific Deep and Intermediate Waters (NPDW and NPIW), as well as the penetration of Southern Sources Water (SSW) into the North Pacific Ocean, are as yet not well constrained. The SCS is connected to the Northern subtropical Pacific through the deep Luzon Straits. It receives deep-water masses from the Philippine Sea that result from the mixing of the Northern- (NPDW and NPIW) and Southern Sourced Water (SSW) masses (Johnson and Toole, 1993; Kawabe et al., 2003). Consequently, sediments from the northern SCS constitute an ideal archive in the western Pacific Ocean to reconstruct past hydrological

changes of deep-water masses in the subtropical Pacific Ocean.

The neodymium isotopic composition ($^{143}Nd/^{144}Nd$) of seawater has been shown to be a proxy for tracing water mass provenance (Von-Blanckenburg, 1999; Lacan and Jeandel, 2004a, 2004b, 2005). The residence time of Nd, recently re-assessed to about 500-1000 yrs (Tachikawa et al., 1999 and 2003), is shorter than the global turnover time of the ocean (about 1000 yrs; Broecker, 1982). Consequently, through lithogenic inputs of material with various ages, and boundary-exchange processes that occur at the continental margin (Lacan and Jeandel, 2005), intermediate- and deep-water masses acquire Nd from downwelling surface water (Goldstein and Hemming, 2003). In the ocean, the only way to alter the initial isotopic composition of a water mass is to add Nd with a different isotopic composition through riverine or eolian inputs or by mixing with other water masses. The Nd isotopic composition ($^{143}Nd/^{144}Nd$) is expressed as εNd, which is the deviation of the $^{143}Nd/^{144}Nd$ ratio from its average value in the ''bulk Earth'' $^{143}Nd/^{144}Nd$ ratio of 0.512638 in parts per 10^4 (Jacobsen and Wasserburg, 1980), expressed as: $\varepsilon Nd = [(^{143}Nd/^{144}Nd)sample/0.512638]-1)\times 10000$.

Unlike nutrient proxies, such as $\delta^{13}C$ or Cd/Ca, Nd isotopes are not known to be affected by biological processes, and thus they can serve as a quasi-conservative water mass tracer (Frank, 2002; Goldstein and Hemming, 2003; Vance et al., 2004; Martin and Scher, 2004). The Nd isotopic composition of seawater is currently recognised as an effective tracer of water mass provenance and mixing (e.g. Lacan and Jeandel, 2004, 2005b, Piepgras and Wasserburg, 1983, Spivack and Wasserburg, 1988). In addition, it has been shown that sedimentary archives such as foraminifera, fossil fish teeth, dispersed authigenic Fe-Mn sediment coatings, ferromanganese crusts and deep sea corals allow us to trace past ocean circulation changes at various time scales (Ling et al., 1997; Martin et al., 2006; Martin and Scher, 2004; Scher and Martin, 2004; Thomas, 2004; Piotrowski, 2008; Vance and Burton, 1999; Burton and Vance, 2000; Colin et al., 2010; Copard et al., 2010).

The spatial distributions of seawater εNd have been recently established for the Philippine Sea and for the northern and middle part of the SCS thereby allowing us to characterise the Nd isotopic composition of the main water masses of these seas and to investigate past seawater εNd records from deep-sea sediments. Seawater εNd of deep-water masses in the Philippine Sea results from the vertical mixing of the SSW, corresponding to the Upper and Lower Circumpolar Deep Water (UCDW and LCDW) characterised by an εNd value of around -8

(Jeandel et al., 1993; Carter et al., 2012; Piepgras and Wasserburg, 1982; Jeandel et al., 2013; Amakawa et al., 2013), and the Northern Sourced Water (NSW), corresponding to the North Pacific Deep-Water (NPDW) characterised by an εNd value of -4 (Piepgras and Wasserburg, 1988; Amakawa et al., 2004 and 2009). Several stations sampled in the northern SCS have shown that εNd composition of the deep-water masses of the SCS is homogenous (~-4.1±0.3) and similar to that of the western subtropical Pacific (-3.9±0.4 ~ -4.4±0.4). In addition, it has been demonstrated that the Nd isotopic composition of the deep-water masses of the SCS is only modified locally and temporarily above significant sediment drift deposits through the process of particle / seawater exchange. Such lithogenic influences do not modify the εNd values of the PDW which enters the Northern SCS (Wu et al., in prep.a). Consequently, εNd obtained from marine cores from the north-western margin of the SCS can be used to reconstruct past changes in the deep-water masses of the western subtropical Pacific where SSW and NSW, characterised by contrasting εNd values, are mixing vertically.

Given that εNd is a useful proxy for investigating past hydrological change in the subtropical Western Pacific, it is important to establish a reliable method for εNd extraction from SCS marine cores. Recent studies have debated about how to extract seawater εNd from foraminifera and dispersed authigenic Fe-Mn coatings of deep-sea sediments (Piotrowski et al., 2012; Bayon et al., 2002; Vance et al., 2004; Kraft et al., 2013).

While the Nd isotopic composition obtained from benthic foraminifera can undoubtedly be used to reconstruct bottom εNd seawater records, the significance of εNd values obtained from reductively and non-reductively cleaned planktonic foraminifera is still under debate. Investigation of REEs in various phases of foraminifera suggests that approximately 90% of the REEs reside in the coating fraction, and the remaining 10% is contained in the foraminifera calcite lattice (Palmer, 1985). Thus, it has been proposed that εNd values obtained from the diagenetic Fe-Mn coatings precipitated on the foraminifera shells, primarily correspond to bottom seawater and/or pore water εNd values. Nevertheless, Vance and Burton (1999) suggest that the reductive cleaning procedure can efficiently remove the Fe-Mn coatings precipitated on the foraminifera and can be used to establish εNd of surface seawater. This is further supported by several recent studies (Burton and Vance, 2000; Vance et al., 2004; Martínez-Botí et al., 2009; Pena et al., 2013).

The εNd seawater record for the late quaternary has been successfully reconstructed from

εNd analysed on the Fe-Mn oxide fraction leached from sediments collected in certain areas of the ocean (Rutberg et al., 2000; Piotrowski et al., 2004; Gutjahr et al., 2008; Martin et al., 2010). In some other locations, however, especially close to continental margins under the influence of strong river discharges, εNd values of sediment leachates do not match the seawater εNd but appear to be biased by pre-formed Fe-Mn coatings delivered from rivers (Bayon et al, 2002; Gutjar et al., 2007). In addition, the analytical procedures permitting the correct extraction of seawater εNd from the authigenic phase in bulk sediment are controversial (Bayon et al., 2002; Kraft et al., 2013; Piotrowski et al., 2012). Recently, Wilson et al. (2013) have re-assessed the reliability of different approaches to extract Nd isotopes preserved in Fe-Mn coatings. These authors suggest that short leaching times and high sediment/solution ratios allow the correct extraction of seawater εNd from sediment and could be considered as a reliable proxy for reconstructing past seawater εNd. In any case, the analytical procedure used to extract the Nd isotopic signal from the leaching of the Fe-Mn oxide of the sediments needs to be evaluated for each indivdual site rather than being used as a simple method that can be uniformly applied.

Consequently, in order to reconstruct past seawater εNd of the SCS, it is necessary to carefully verify that Nd isotopic compositions obtained from the Fe-Mn oxide fraction leached from sediments and foraminifera are reliable and reflect seawater εNd signature. Here, we have investigated several core-top samples from different parts of the SCS where a vertical gradient of the seawater εNd has been observed in order to evaluate the reliability of different procedures for the extraction of seawater εNd from foraminifera and Fe-Mn coatings of detrital particles. Nd values obtained from cleaned and uncleaned foraminifera are compared to seawater εNd recently established by Wu et al. (in prep.a). Additionally, we briefly present and discuss the Nd isotopic composition of foraminifera collected from a number of samples taken from a single core located in the Northwestern margin of the SCS in order to establish past hydrological changes in deep water masses in the western subtropical Pacific.

4.2. Hydrological setting

The SCS is connected in the south with the Sulu and Java Seas through the shallow Mindoro (~200 m) and Karimata Straits (<50 m) and in the north with the East China Sea and Pacific Ocean through the Taiwan Straits (<100 m) and the deep channel of the Luzon Straits (>2400 m), respectively (Qu et al., 2009) (Fig. 4.1). The sea surface circulation of the SCS is mainly controlled by the seasonal reversals of the wind direction during the summer and winter

monsoons. This induces a cyclonic surface circulation in winter and an anti-cyclonic one in summer (Shaw and Chao, 1994; Fang et al., 1998). North Pacific Tropical Water (NPTW), characterised by high salinity, enters the SCS and is diluted by freshwater discharged by the large Asian rivers, thereby inducing the relatively fresher South China Sea Tropical Water (SCSTW) (Xie et al., 2011). In contrast, due to vertical mixing with deep water, the intermediate water in the SCS (SCIW) shows relatively higher salinity (~-34.4) compared with the North Pacific Intermediate Water (NPIW) (~-34.0) (Tian et al., 2009; Xie et al., 2011). Compared with surface- and intermediate water studies, few investigations have been carried out of deep-water circulation in the SCS. It has been established that the deep-basins of the SCS, below a depth of 2000 m, are occupied bya water mass characterized by homogenous physical properties, similar to those of the subtropical western Pacific, and corresponding to the Pacific Deep Water (PDW) (Qu et al., 2006; Tian et al., 2006).

More recently, Wu et al. (in prep.a) have shown that εNd values of deep-water masses of the Philippine Sea and the Northwestern margin of the SCS present a narrow range between -4.0±0.3 and -4.5±0.4, corresponding to the presence of the Pacific Deep-Water (PDW). In the Philippine Sea, above a depth of around 1000 m, the North Pacific Intermediate Water (NPIW) is characterised by εNd values that reach -2.7±0.4 and which are similar to those obtained from the subtropical North Pacific. εNd of the South China Sea Intermediate Water (SCIW) is slightly lower (between -3.6±0.3 and 3.9±0.3) than that of the NPIW due to vertical mixing with the PDW in the SCS. Finally, compared to the Philippine Sea, Nd isotopic composition of surface water in the SCS is less radiogenic and displays a strong north – south gradient with higher unradioganic values in the southern SCS (εNd = ~-9; Wu et al., in prep.a).

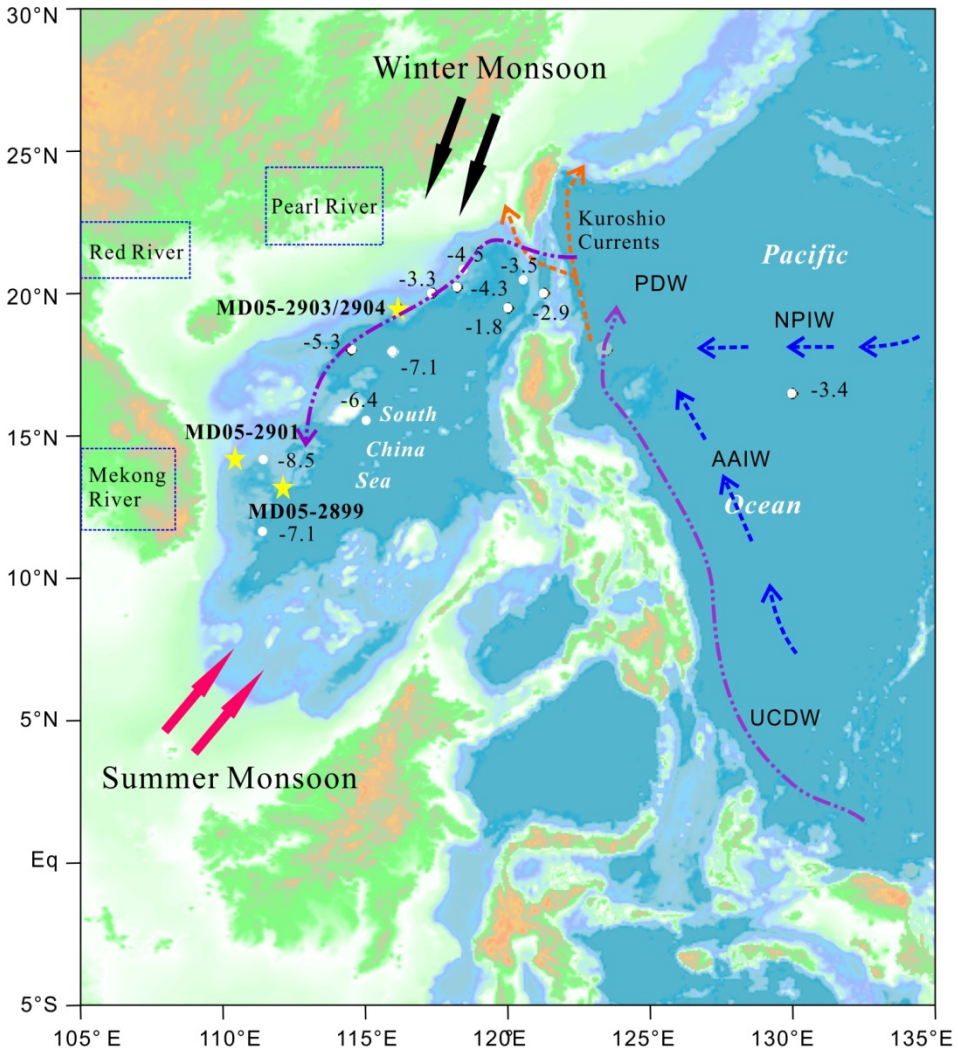

Figure 4.1. Sample location map showing locations of the sites discussed in the text. Also shown on the map are surface seawater εNd values from previous studies, marked by white dots (Wu et al., in prep.a). Red stars represent the stations with a water column εNd profile. Yellow stars show the locations of gravity cores. The black arrows indicate the direction of the winter monsoon. The pink arrows indicate the direction of the summer monsoon. Kuroshio Currents are indicated by orange dashed lines. The possible flow pattern of northern sourced North Pacific Intermediate Water (NPIW) and southern sourced Antarctic Intermediate Water (AAIW) are indicated by blue arrows. The possible pathways of Upper Circumpolar Deep Water (UCDW) and Pacific Deep Water (PDW) are shown by purple dashed lines.

4.3. Material and methods

4.3.1 Material

The Calypso cores MD05-2899 (13º47.66´N, 112º10.89´E, 2393 m), MD05-2901 (14º22.503´N, 110º44.6´E, 1454 m), MD05-2903 (19º27.31´N, 116º15.06´E, 2047 m) and MD05-2904 (19º27.32´ N, 116º15.15´ E, 2066 m) were retrieved on the north-western margin of the SCS during the R/V Marion Dufresne MARCO POLO IMAGES XII Cruise in 2005 (Fig. 4.1, Table 4.1). Four core-top sediment samples were taken from each core investigated and these represent modern time. In addition, four additional downcore sediment samples were collected in the upper 10 m of core MD05-2904. The age model of core MD05-2904 has been established by Ge et al. (2010). It is based on eight C-14 AMS dates obtained from planktonic foraminifera *G. ruber*. On the basis of this age model, the four downcore sediment samples span the last 25 kyr (Table 4.1).

Table 4.1. Nd isotopic composition of reductively cleaned foraminiferas and cleaning solutions together with corresponding Mn/Ca ratios and Nd/Ca ratios

Core	Latitude	Longtitude	Age (Cal. Kyr BP)	Sample ID	εNd	2σ	Mn/Ca (µmol/mol)	Nd/Ca (nmol/mol)
MD05-2903	19.45º N	116.25º E	core-top	cleaned *G..ruber*	-4.68	0.19	_	_
			core-top	cleaned BF	-3.68	0.35	_	_
			core-top	cleaning solution of *G..ruber*	-4.28	0.35	_	_
			core-top	cleaning solution of BF	-4.66	0.35	_	_
MD05-2901	14.28º N	110.74º E	core-top	cleaned *G..ruber*	-6.33	0.25	_	_
			core-top	cleaned BF	-6.91	0.19	_	_
			core-top	cleaning solution of *G..ruber*	-7.20	0.19	_	_
			core-top	cleaning solution of BF	-6.94	0.35	_	_
MD05-2899	13.79º N	112.19º E	core-top	cleaned *G..ruber*	-6.61	0.19	_	_
			core-top	cleaned BF	-5.85	0.25	_	_
			core-top	cleaning solution of *G..ruber*	-6.20	0.35	_	_
			core-top	cleaning solution of BF	-5.95	0.35	_	_
MD05-2904	19.46º N	116.25º E	0.05	cleaned *G..ruber*	-4.07	0.23	215.91	1155.39
			0.05	cleaning solution of *G..ruber*	-4.10	0.28	_	_
			0.05	cleaned BF	-4.08	0.36	294.52	1981.43
			0.05	cleaning solution of BF	-4.79	0.44	_	_
			0.05	Cleaned foraminiferas of mixed species	-4.23	0.32	127.92	616.68
			0.05	uncleaned *G..ruber*	-4.22	0.23	612.51	1742.87
			6.50	cleaned *G..ruber*	-4.66	0.23	298.20	1365.16
			6.50	cleaning solution of *G..ruber*	-4.98	0.28	_	_
			6.50	cleaned BF	-4.22	0.46	337.59	1379.82
			6.50	uncleaned *G..ruber*	-4.75	0.23	858.82	1783.30
			11.24	cleaned *G..ruber*	-5.05	0.23	421.38	1156.46
			11.24	uncleaned *G..ruber*	-5.21	0.23	836.59	1736.02
			18.57	cleaned *G..ruber*	-5.89	0.23	301.00	1490.41
			18.57	cleaning solution of *G..ruber*	-5.55	0.28	_	_

18.57	Cleaned foraminiferas of mixed species	-5.92	0.32	190.47	1600.60
20.04	cleaned *G..ruber*	-5.55	0.23	375.19	1723.47
20.04	cleaning solution of *G..ruber*	-5.18	0.28	_	_

4.3.2 Analytical procedures

30 mg of mono-specific planktonic foraminifera *G.ruber*, mixed planktonic foraminifera, and around 8 mg mixed benthic foraminifera, with shells sizes larger than 150 µm, were handpicked under a binocular microscope. All of the foraminifera were gently crushed between two glass plates to open all chambers. The calcite fragments were then sonicated in an ultrasonic bath for approximately 1 min before pipetting the suspended particles with water to separate the waste. This step was repeated until the water became clear and free of clay. All samples were checked under a binocular microscope to ensure that all particles had been removed. Physically cleaned samples were transferred to centrifuge tubes for the oxidative – reductive cleaning step (foraminifera which underwent this process are hereafter referred to as "cleaned foraminifera"). For the purpose of comparison, three samples were subjected to mechanical cleaning only (hereafter referred to "uncleaned foraminifera"). The oxidative – reductive foraminiferal cleaning procedure used in this study followed that described by Vance and Burton (1999), using 10 ml reductive solution (1 M hydrous hydrazine, 16 M NH_4OH, 0.25 M citric acid + 16 M NH_4OH in a ratio of 1:6:3) and 5 ml oxidative solution (0.2 M NaOH and 30% H_2O_2 in a 1:1 ratio) per sample to more efficiently remove authigenic the Fe-Mn coatings. For the reductive step, samples were heated in a water bath at 80ºC for 30 min, and were ultrasonicated every 2.5 min for 10 s. After transferring the reductive cleaning solution to a centrifuge tube, the cleaned foraminifera were rinsed thoroughly with deionized water. The analytical procedure for the oxidative step was similar except that samples were ultrasonicated every 10 min for a period of 30 s. All samples, including non-reductively cleaned samples, underwent a weak acid leach for 5 min in 1ml 0.001 M HNO_3 with ultrasonication. After the cleaning step, samples were then transferred into a 1.5 ml tube. 0.5 ml of deionized water was first added to the tube, and then the foraminifera were dissolved using stepwise 100 µl weak nitric acid (0.5 N HNO_3) until the dissolution reaction stopped. The dissolved samples were centrifuged and the supernatant was immediately transferred to Teflon beakers to prevent the leaching of any possible remaining phases. All of the dissolved foraminifera shell fraction and authigenic fraction contained in the reductive cleaning solution were dried on a hotplate for Nd purification. Element concentrations and REE pattern analysis were performed on a 10% cut of both the dissolved foraminifera shells and the corresponding reductive cleaning solutions

collected from core MD05-2904.

Several studies have been carried out to test the reliability of seawater derived Nd extraction from bulk sediment involving different leaching procedures (Bayon et al., 2002; Gutjahr et al., 2007; Wilson et al., 2013). Firstly, it is recommended not to remove the carbonate fraction of the bulk sediments; secondly, the leaching time should not be too long; and thirdly, the sample size/ leachate ratios need to be large (Wilson et al., 2013). In this study, in order to better understand the reliability of using bulk sediment leachates to reconstruct past seawater Nd, an evaluation was conducted on 5 samples covering the Holocene and the Last Glacial Maximum (LGM). First, sequential analysis was performed on ground samples of 0.2, 1 and 2 g which were simply rinsed with deionized water and then directly leached with 7 ml 0.02 M hydroxylamine hydrochloride in 25% (v/v) acetic acid (HH solution) for 30 min. Then, 5 additional samples of 1 g were treated using the same leaching procedure but with a longer leaching time of 1 hour. Parallel samples of 1 g were de-carbonated using a sodium acetate buffered acetic-acid solution, and subjected to 30 min of leaching with 7 ml 0.02 M HH solution in order to assess the possible influence of the de-carbonation process. De-carbonated samples of 0.2 g were leached for 30 min, 2 hours and 3 hours with 0.02 M HH solution in order to test the influence of leaching times.

Nd was purified from all samples following the analytical procedure described in detail by Copard et al. (2010). In brief, we used TRU-Spec and Ln-Spec resins following the method described in detail by Pin and Santos Zaldegui (1997). In this method, samples were loaded using 2 mL of 1N HNO_3 on preconditioned TRU-Spec columns (83 mg portion of TRU-spec). The unwanted cations were eluted using 5 portions of 0.5 mL of 1N HNO_3. The TRU-Spec columns were then placed over the Ln-Spec columns. The LREEs were then eluted from the upper (TRU-Spec) column using seven portions of 0.1 mL of 0.05N HNO_3. After decoupling from the TRU-Spec columns, La, Ce and most of the Pr were rinsed from the Ln-Spec columns using 3.25 ml of 0.25N HCl. Nd was then eluted with an additional 2.5 mL of 0.25N HCl.

4.3.3. Ca, Mn and REE concentrations and $^{143}Nd/^{144}Nd$ analyses

Ca, Mn and REE concentrations were analyzed using the Inductively Coupled Plasma-Quadrupole Mass Spectrometer (ICP-QMS X Series$^{II\ Thermo\ Fisher}$) at the LSCE by measuringtheir isotopes, ^{46}Ca, ^{55}Mn and ^{146}Nd, and by using appropriate carbonate standards

(JCp-1 coral). Samples and standard solutions were systematically adjusted at 100 ppm Ca through dilution, without further chemistry. This is because (1) dominant Ca signals need to be avoided as high concentrations can increase salt deposition on cones affecting ICP-MS stability and (2) adjusted Ca concentration levels introduced into ICP-QMS at 100 µL/min provide a way to control matrix effects due to the presence of Ca. Instrumental calibration, based on the standard addition method, was achieved using a mono-elementary standard solution for each element (Harding et al., 2006) and by routinely measuring carbonate standards (JCp-1, Okai et al., 2004). To compensate for the signal deviation of a few percentage values during a day, a standard (JCp-1) was run for every nine samples. When analysing the REE of the reductive cleaning solution from foraminifera and leachates from bulk sediments, a high purity REE solution was measured every 9 samples and additional internal standards (^{115}In and ^{103}Rh) were added to samples in order to monitor instrument stability. Our measurements were characterized by analytical uncertainties ranging from 5% for the lightest REE to 15 % for the heaviest as published previously (Bourdin et al., 2011). The reproducibility of measurements for two repeated samples varied according to the different element to calcium ratios (2σ: 10% for Mn/Ca, 5% for Nd/Ca). The concentrations of Nd in blanks are less than 100 ppt, which is negligible compared to the average concentration of 15 ppb ± 5 % measured in samples.

The Nd isotopic composition was analysed using a NEPTUNE Plus Plasma multi-collector induced coupled plasma mass spectrometer (MC-ICPMS) at Laboratoire des Sciences du Climat et de l'Environnement (Gif-sur-Yvette, France). The mass-fractionation correction was made by normalizing ^{146}Nd/^{144}Nd to 0.7219 and applying an exponential-fractionation correction. During the analysis sessions, every two sample were bracketed with analyses of the JNdi-1 and La Jolla standards at a concentration similar to those of samples, and corrected to certified values of 0.512115 ± 0.000006 and 0.511858 ± 0.000007 (Tanaka et al., 2000), respectively. The external reproducibility (2σ) for time resolved measurement, deduced from repeated measurement of the La Jolla standard and JNdi-1 at similar concentrations to the samples, ranged from 0.2 to 0.4 Epsilon units for different analytical sessions. The analytical error of each sample analysis is taken as the external reproducibility of the La Jolla standard for each session.

4.4. Results

4.4.1. Element/Ca ratios and REE concentration

Ca, Mn and REE concentrations were measured on dissolved cleaned foraminifera and reductive cleaning solutions in order to evaluate the efficiency of the cleaning procedures. Mn/Ca ratios vary between 128 µmol/mol and 421 µmol/mol for cleaned foraminifera and between 612 µmol/mol and 858 µmol/mol for uncleaned foraminifera (Fig. 4.2 and Table 4.1). Unlike Mn/Ca ratios, Nd/Ca ratios in cleaned foraminifera are randomly distributed from 1155 nmol/mol to 1723 nmol/mol, with one exception with very low ratios (617 nmol/mol). Nd/Ca ratios obtained from uncleaned foraminifera are around 1736 to 1783 nmol/mol. Although the uncleaned foraminifera are characterised by higher Mn/Ca ratios, Nd/Ca ratios in cleaned and uncleaned foraminifera display similar ranges of variations and are not correlated with Mn/Ca ratios (r^2 = 0.29) (Fig. 4.2).

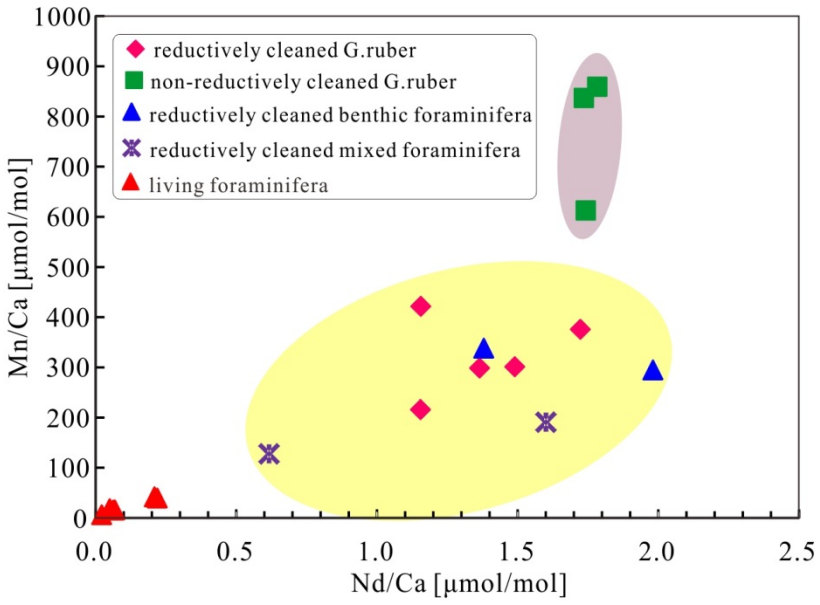

Figure 4.2. Mn/Ca ratios versus Nd/Ca ratios measured in foraminifera calcite samples from downcore samples. Non-reductively cleaned foraminifera show higher Mn/Ca ratios compared to reductively cleaned foraminiferas. Comparison of Nd/Ca ratios between reductively cleaned foraminiferas and non-reductively cleaned foraminiferas show no correlation with cleaning methods. Data for living foraminifera are from Pomiès et al. (2002).

REE concentrations obtained from planktonic and benthic foraminifera and reductive cleaning solutions were normalized to Post-Archean Average Australian Sedimentary rock

(PAAS, Nance and Taylor, 1976). All of the PAAS-normalized REE patterns are quite similar and present negative Ce-anomalies as well as MREE enrichment (Fig. 4.3a). This pattern of negative Ce-anomalies is similar to other published seawater REE patterns in the SCS (Alibo and Nozaki, 2000). PAAS-normalized REE from the fraction of reductive cleaning solution shows a similar negative Ce-anomaly pattern and MREE enrichment, with the exception of two benthic foraminifera samples that are characterised by a positive Eu-anomalie (Fig.4. 3b).

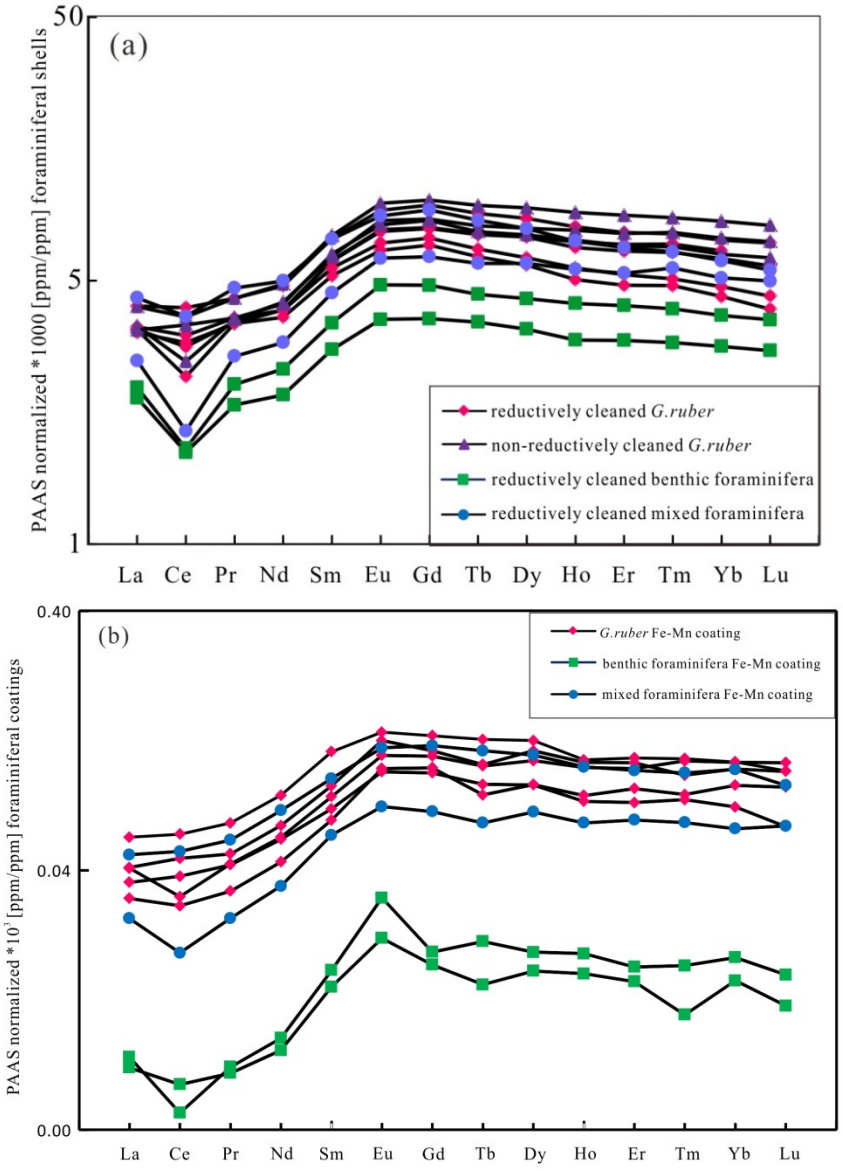

Figure 4.3. (a) PAAS - normalized REE patterns obtained from foraminifera shells from downcore samples show similar overall patterns marked by pronounced Ce-anomalies and MREE enrichment. (b) PAAS – normalized REE patterns obtained from reductive cleaning solutions show similar patterns except for two samples extracted from benthic foraminifera.

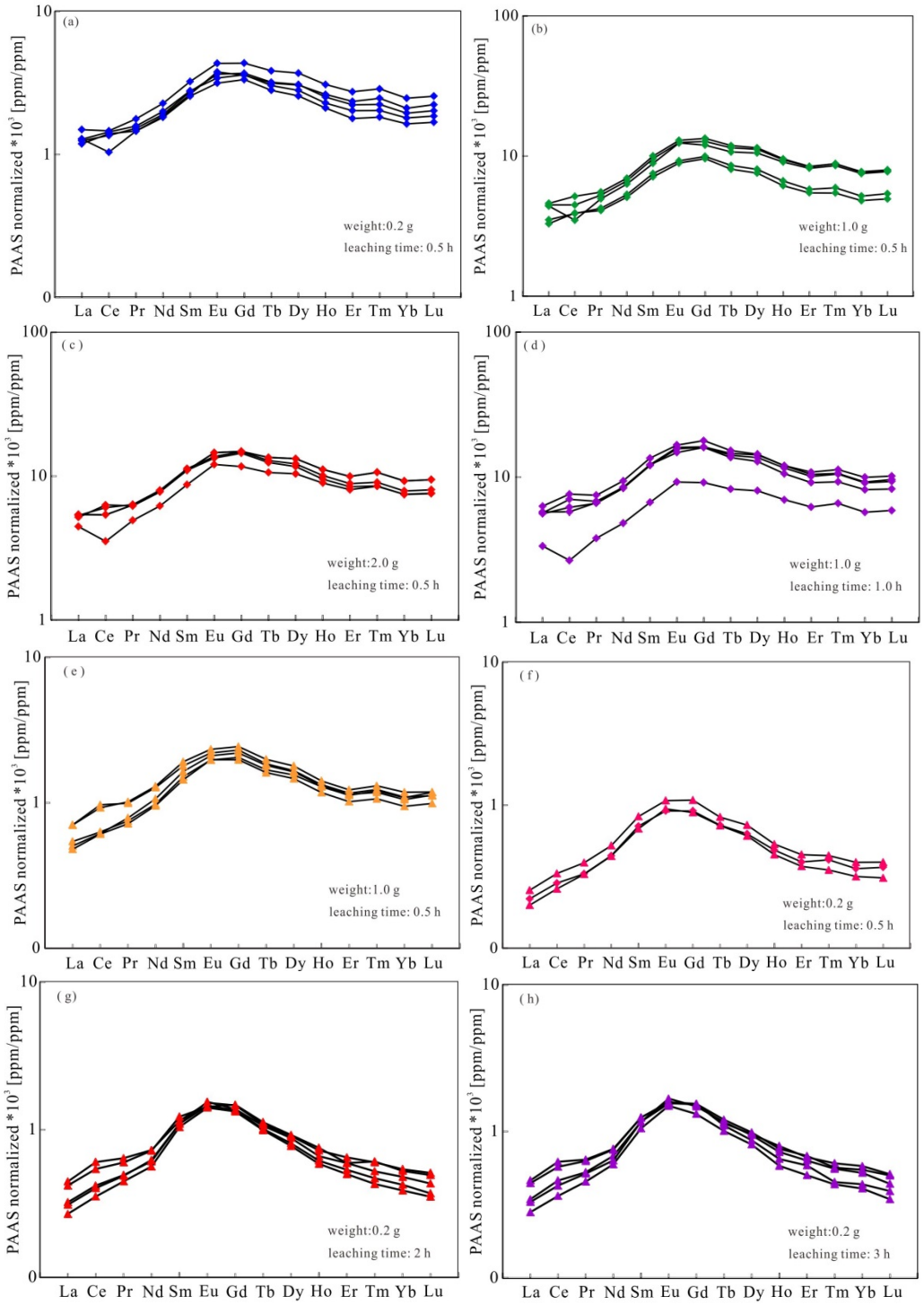

Figure 4.4. PAAS – normalized REE patterns obtained from bulk sediment leachates. (a) (b) (c) (d) represent those bulk sediments where carbonate was not removed; (e) (f) (g) (h) represent bulk sediments which were de-carbonated.

REE concentrations were also measured in the bulk sediment- and de-carbonated sample

leaching solutions. The PAAS-normalized REE patterns display an MREE enrichment that is independent of the leaching procedures (Fig. 4.4). For bulk samples, the PAAS-normalized REE patterns of leachates extracted from core-top sediments show negative Ce-anomalies regardless of the sample sizes and leaching time. The other samples, collected at a greater depth in core MD05-2904, do not present negative Ce-anomalies. PAAS-normalized REE patterns of the leaching solution of all the de-carbonated samples exhibit MREE enrichment with no negative Ce-anomalies.

4.4.2. εNd in foraminifera and bulk sediment leachates

εNd values of planktonic and benthic foraminifera from core-top samples and reductive cleaning solution fractions are reported in the Table 4.1. These values vary between -3.7±0.4 and -6.9±0.4. εNd values obtained on monospecific samples of planktonic foraminifera G.ruber, mixed planktonic foraminifera and mixed benthic foraminifera lie in a narrow range from -3.7±0.4 to - 4.7±0.3 for the core-top sample from MD05-2903 and from - 4.1±0.3 to - 4.8±0.4 for the core-top sample from MD05-2904 (Table 4.1). It is worth noting that εNd values obtained on foraminifera cleaning solutions are slightly different, and often more unradiogenic, than those obtained on samples of foraminifera. εNd values for all foraminifera samples, and reductive cleaning solutions from core-top samples of cores of MD05-2899 and MD05-2901 (obtained from a more southern position of the SCS), ranged from -5.9 ± 0.3 to -6.6 ± 0.2, and from -6.3 ± 0.3 to -7.2 ± 0.2, respectively. Consequently, εNd values obtained on the same sediment sample from a monospecific sample of planktonic foraminifera G.ruber, mixed planktonic foraminifera, mixed benthic foraminifera and reductive cleaning solution are more or less similar each other (Table 4.1).

In core MD05-2904, εNd values were analysed on samples of foraminifera from the Holocene and the Last Glacial Maximum (LGM) in order to examine the reliability of Nd extraction from downcore post-mortem foraminifera. εNd values of all samples of foraminifera investigated from core MD05-2904 exhibited a wide range from -5.9±0.2 to -4.1±0.2 (Table 4.1 and Fig. 4.5). The LGM period is characterised, on average, by higher unradiogenic εNd (-5 to -5.9±0.2) than the late Holocene (-4.1±0.2). In general, εNd values obtained for each monospecific sample of planktonic foraminifera *G.ruber*, mixed planktonic foraminifera, mixed benthic foraminifera and from the reductive cleaning solution are quite similar. Again it is worth noting that εNd values obtained from foraminifera cleaning solutions are generally slightly more unradiogenic than those obtained from cleaned planktonic and benthic

foraminifera.

For core MD05-2904, εNd obtained from acid-reductive HH leachates of bulk decarbonated and non-decarbonated sediments are outlined in Figure 4.6 and Table 4.2. εNd obtained from acid-reductive HH leachates of bulk non-decarbonated sediments vary from ~ -6.0±0.3 for LGM sediments to ~-4.2±0.3 for core-top samples. On the other hand, εNd obtained from acid-reductive HH leachates of bulk decarbonated sediments range from -6.9±0.2 for LGM sediments to ~-5.3±0.3 for core-top samples and they systematically display lower values of around 1.0 Epsilon unitcompared to non-decarbonated sediments. For both non-decarbonated and decarbonated sediments, εNdvalues are slightly affected by the leaching procedure used in this study. In general, a reduction of the leaching time (from 3 h to 0.5 h), and an increase in sample weight (from 0.2 g to 1 g) , induce a significant decrease of the εNd values (Fig. 4.6 and Table 4.2).

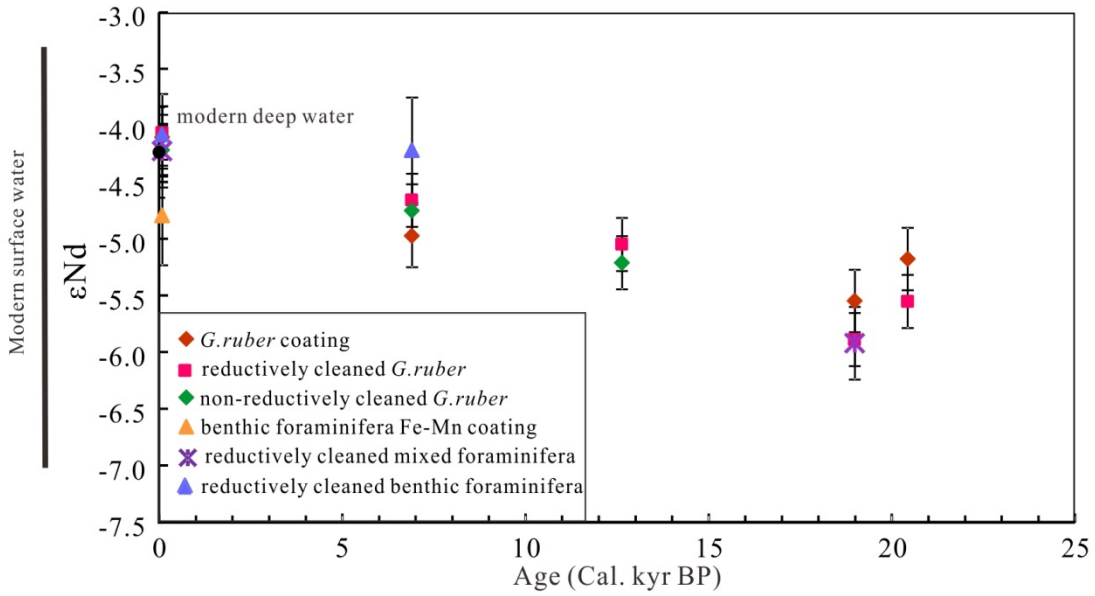

Figure 4.5. Comparison of εNd values obtained from reductively cleaned G.ruber, non-reductively cleaned G.ruber, reductively cleaned mixed foraminifera, reductively cleaned benthic foraminifera and associated authigenic phase of downcore samples over the past 25 kyr. The Nd isotopic compositions in various phases from samples taken at the same depth are indistinguishable.The black bar represent εNd values of modern surface water. εNd values show a clear shift from LGM samples to Holocene samples.

4.5. Discussion

4.5.1. Elemental ratios and REE patterns in foraminifera

The Mn/Ca ratio in foraminifera has been identified as an indicator for early diagenetic Fe-Mn oxides, or Mn-rich carbonates, which precipitate on the foraminiferal carbonate (Boyle, 1983; Pomiès et al., 2002). The ratio is usually used to monitor the efficiency of reductive cleaning (Boyle, 1983; Pena et al., 2005). Mn/Ca ratios range from 128 µmol/mol to 421 µmol/mol for reductively cleaned foraminifera, and from 612 µmol/mol to 858 µmol/mol for non-reductively cleaned foraminifera. Consequently, Mn/Ca ratios in the reductively cleaned foraminifera shells are around three times lower than those of the non-reductively cleaned foraminifera samples. However, such values are 10 to 30 times higher than Mn/Ca ratios obtained from living and non-fossil planktonic foraminifera collected in plankton tows and sediment traps (0.25 to 15 µmol/mol) (Martínez-Botí et al., 2009; Pomiès et al., 2002; Robert et al., 2012). Similarly, Nd/Ca ratios from cleaned foraminifera range from 1155 nmol/mol to 1723 nmol/mol, and are much higher than Nd/Ca ratios obtained previously from planktonic foraminifera collected in sediment traps (8 to 700 nmol/mol) (Martínez-Botí et al., 2009; Pomiès et al., 2002) (Fig. 4.2).

Table 4.2: Nd isotopic composition of bulk sediment leachates of gravity core MD05-2904.

Weight (g)	Leaching time (min)	Carbonate treatment	Age (Cal. Kyr BP)	εNd	2σ
0.20	30	non-decarbonated	0.05	-4.50	0.31
0.20	30	non-decarbonated	6.50	-4.95	0.31
0.20	30	non-decarbonated	11.24	-5.27	0.31
0.20	30	non-decarbonated	18.57	-6.16	0.31
0.20	30	non-decarbonated	20.04	-5.85	0.31
1.00	30	non-decarbonated	0.05	-4.21	0.31
1.00	30	non-decarbonated	6.50	-4.44	0.31
1.00	30	non-decarbonated	11.24	-4.81	0.31
1.00	30	non-decarbonated	18.57	-5.96	0.31
1.00	30	non-decarbonated	20.04	-5.62	0.31
2.00	30	non-decarbonated	0.05	-4.48	0.31
2.00	30	non-decarbonated	6.50	-4.90	0.31
2.00	30	non-decarbonated	11.24	-5.21	0.31
2.00	30	non-decarbonated	18.57	-6.22	0.31
2.00	30	non-decarbonated	20.04	-5.70	0.31
1.00	60	non-decarbonated	0.05	-4.32	0.31
1.00	60	non-decarbonated	6.50	-4.60	0.31
1.00	60	non-decarbonated	11.24	-5.31	0.31
1.00	60	non-decarbonated	18.57	-6.07	0.31
1.00	60	non-decarbonated	20.04	-6.38	0.31
1.00	30	decarbonated	0.05	-5.25	0.31
1.00	30	decarbonated	6.50	-6.07	0.31
1.00	30	decarbonated	11.24	-6.11	0.31

1.00	30	decarbonated	18.57	-6.73	0.31
1.00	30	decarbonated	20.04	-6.43	0.31
0.20	30	decarbonated	0.05	-5.90	0.31
0.20	30	decarbonated	6.50	-6.19	0.31
0.20	30	decarbonated	11.24	-6.91	0.31
0.20	120	decarbonated	0.05	-5.94	0.23
0.20	120	decarbonated	6.50	-6.50	0.23
0.20	120	decarbonated	11.24	-6.85	0.23
0.20	120	decarbonated	18.57	-6.90	0.23
0.20	120	decarbonated	20.04	-6.92	0.23
0.20	180	decarbonated	0.05	-5.96	0.23
0.20	180	decarbonated	6.50	-6.75	0.23
0.20	180	decarbonated	11.24	-7.11	0.23
0.20	180	decarbonated	18.57	-7.01	0.23
0.20	180	decarbonated	20.04	-6.83	0.23

Whereas Nd/Ca ratios in both uncleaned and cleaned foraminifera exhibit different features, no linearly decreasing trend from uncleaned samples to cleaned samples was observed (Fig. 4.2). Cleaned benthic foraminifera show systematically higher Nd/Ca ratios than cleaned planktonic foraminifera. Such results are consistent with previous investigations (Klevenz et al., 2008). Palmer (1985) has suggested that around 90% of REEs were incorporated into authigenic phases in foraminifera shells. This is supported by several previous studies indicating that Fe-Mn coatings mainly carry pore water REEs (Haley et al., 2004; Elderfield and Sholkovitz, 1987). In addition, the distribution of planktonic foraminifera Nd investigated recently at micrometer-scale has revealed that Nd concentration in Fe-Mn riched parts was much higher than in foraminiferal calcite, where Nd distribution was randomly heterogeneous (Tachikawa et al., 2013). Thus, despite the absence of correlation between Mn/Ca ratios and Nd/Ca ratios (r^2 =0.29), we can conclude that Nd in authigenic phases was not completely removed.

Reductively cleaned and non-reductively cleaned foraminifera exhibit similar PAAS-normalized REE patterns despite the large range of concentrations obtained (Fig. 4.3). PAAS-normalized REE patterns reveal negative Ce-anomalies and middle REE enrichment similar to those identified in dissolved foraminifera and fossil fish teeth (Gutjahr et al., 2007; Martin et al., 2010; Kraft et al., 2013). REE patterns in both the surface and deep water in the SCS (Wu et al., submitted), and in other ocean basins, merely display pronounced negative Ce-anomaly patterns but no MREE enrichment (Fig.4. 4) (Alibo and Nozaki, 2000; Bayon et al., 2011; Jeandel et al., 2013). Several hypotheses have been put forward to explain this puzzling feature in the ocean (Elderfield et al., 1990; Hannigan and Sholkovitz, 2001; Haley et al., 2005; Palmer, 1985). In general, these authors hypothesise that the MREE enrichment in various

dissolved phases is related to fractionated REEs incorporated in foraminifera and/or an overprinted pore water signature during early diagenetic processes. Authigenic phases in the ocean were suggested to be an important carrier of REEs as they contain higher concentrations of REE than seawater (Haley et al., 2004; Robert et al., 2012; Piotrowski et al., 2012; Tachikawa et al., 2013). REE patterns characterised by MREE enrichment have been observed in both pore water and Fe-Mn hydroxide phases (Haley et al., 2004). Here, PAAS-normalized REE patterns obtained from cleaned foraminifera and reductive cleaning solutions are similar (Fig. 4.3). Thus, we suggest that MREE enrichment in foraminifera is associated with REEs incorporated in authigenic components precipitated on the foraminifera. For the reductive cleaning solution, PAAS-normalized REE patterns are essentially similar to those of foraminiferal shells apart from solutions extracted from two benthic foraminifera samples which were characterized by positive Eu-anomalies (Fig. 4.3). Since the positive Eu anomalies were observed in residues after sequential leaching of ferromanganese deposits (Surya Prakash et al., 2012), the positive Eu anomalies in the reductive cleaning solution are probably due to the influence of lithogenic particles trapped in foraminifera pores which may not have been completely removed during the physical cleaning procedure (Elmore et al., 2011). εNd obtained from these two samples is characterised by slightly negative values compared to those of cleaned foraminifera, thus confirming the influence of a small contribution of lithogenic material (εNd = -12).

In this study, we also observed that the chemical cleaning process could not fully remove the Nd released from authigenic phases. Therefore, εNd values obtained in both reductively cleaned and non-reductively cleaned foraminifera are more likely to be associated with bottom and/or pore water εNd values rather than surface seawater values.

4.5.2. REE patterns in bulk sediment leachate

REEs in bulk non-decarbonated and decarbonated sediment leachates were extracted by using different leaching procedures (Fig. 4.4). PAAS-normalized REE patterns obtained on bulk non- decarbonated sediment leachates display MREE enrichment regardless of leaching procedures indicating that REEs in leachates are associated with Fe-Mn hydroxides (Palmer, 1985; Haley et al., 2005; Bau and Koschinsky, 2009). Negative Ce-anomalies were identified only on core-top samples of non-decarbonated sediments. For the other samples, Ce-anomalies were either not identified or some samples yielded positive Ce-anomalies. Previous studies

have shown that a long leaching time could introduce REE contamination from lithogenic fraction thereby leading to unusual Ce-anomalies (Bayon et al., 2002; Gutjahr et al., 2007). In this study, using identical leaching times, no Ce-anomalies were observed in samples collected deep within the core whereas core-top samples display unambiguous negative Ce-anomalies (Fig. 4.4). Furthermore, in leachates extracted from decarbonated sediments, the same quantity of core-top samples (1 g), subjected to the same leaching time (0.5 h), did not display negative Ce-anomalies similar to those of non-decarbonated sediments. Thus, it seems that the leaching time might not be an important factor influencing the Ce distribution in these sediment leachates. REE mobilization has been reported during the early state of diagenesis associated with redox cycling of Fe-Mn oxyhydroxides within surface sediment leading to preferential Ce enrichment in pore water (Elderfield and Sholkovitz, 1987). Several studies show positive Ce-anomalies associated with Fe-Mn oxide after leaching of the easily exchangeable fraction of ferromanganese deposits (Ohta and Kawabe, 2001; Bau and Koschinsky, 2009). The results indicate that Fe-Mn oxides can scavenge Ce from ambient seawater and that the oxidation of Ce mainly takes place after its sorption on the metal oxide surface. Hence, we suggest that the positive Ce-anomalies in those samples that did not undergo carbonate removal, might be due to REE remobilization during the early part of the diagenitic process, and that the presence of carbonate could reduce REE extraction from detrital fraction thus avoiding contamination by the residue.

4.5.3. εNd in the foraminifera and reductive cleaning solutions of core-top samples

εNd values determined from cleaned monospecific samples of planktonic foraminifera (*G. ruber*), cleaned mixed foraminifera, non-reductively cleaned planktonic foraminifera, mixed benthic foraminifera and associated authigenic phases, all taken from core-top samples from the same site, are characterized by a narrow range (Table 4.1; Fig. 4.5). In general, Nd isotopic compositions obtained from benthic foraminifera leachates are significantly more negative than εNd values obtained from cleaned planktonic foraminifera and their associated authigenic phase.

Furthermore, εNd values obtained from core-top samples exhibit variations of at least 2 epsilon units between the northern- and the southern SCS. For cores MD05-2904 and MD05-2903, located in the northern SCS, εNd values varied from -4.1 ± 0.3 to -4.8 ± 0.4 and from -3.7 ± 0.4 to -4.7 ± 0.3, respectively. For the purposes of comparison, seawater εNd values

at the surface and at depth of both cores obtained from neighbouring water stations are reported in Figure 4.1. Benthic and planktonic foraminifera and their associated authigenic phases are similar to those of the bottom water (εNd = ~ -4.2) and are significantly different from surface seawater samples (~ -7.1 to -2.9) in the Northern SCS. For cores MD05-2899 and MD05-2901 in the western SCS, εNd values varied from -5.9±0.3 to -6.6±0.2 and from -6.0±0.4 to -7.2±0.2, respectively. Although εNd values from deep water are not available for the southern SCS, the reported proximal surface water εNd are more negative (~-8.5 to -7.1) compared with the εNd values observed in foraminifera and incorporated authigenic phases (Amakwa et al., 2000; Wu et al., in prep.a) (Fig. 4.1). These results confirm that εNd obtained from planktonic foraminifera do not exhibit the imprint of the seawater εNd of the surface of the ocean. Taking into consideration that planktonic and benthic foraminifera yield similar εNd values for each of the cores investigated, we can hypothesise that foraminifera have recorded the εNd from bottom water. We can confirm that the Nd isotopic composition of foraminifera is mainly marked by εNd of authigenic phases due to incomplete oxidative and reductive cleaning procedures used as indicated with the Nd/Ca and Mn/Ca ratios and PAAS-normalized REE patterns. Such results support recent studies (Kraft et al., 2013; Tachikawa et al., 2013; Pomiès et al., 2002; Elmore et al., 2011) suggesting that foraminifera record the Nd isotopic seawater composition of the bottom water. It implies also that seawater εNd values from deep basins of the southern SCS are characterised by slightly more negative values than those of the northern SCS. Further investigations need to be carried in the future on seawater εNd of the southern SCS to explore this hypothesis.

4.5.4. Nd isotopic composition discrepancy in bulk sediment leachates for the last 25 kyr

In core MD05-2904, εNd values obtained from samples of foraminifera from the Holocene and the Last Glacial Maximum (LGM) exhibited a large range from -5.9±0.2 to -4.1±0.2 (Fig. 4.5 and Table 4.1). The LGM period is characterised on average by more unradiogenic εNd (-5 to -5.9±0.2) than the late Holocene (-4.1±0.2). In general, εNd values obtained from monospecific samples of planktonic foraminifera G.ruber, mixed planktonic foraminifera, mixed benthic foraminifera and reductive cleaning solution are similar and suggest that significant changes of seawater εNd have taken place over the past 25 kyr in the northern SCS.

εNd values obtained from acid-reductive HH leachates of bulk non-decarbonated sediments from the same samples, extracted by using different leaching procedures, range from

-4.4 to -4.7 and are also similar to modern seawater εNd in the Northern SCS at a depth of about 2100 m (between -4.0±0.3 and -4.5±0.4) (Wu et al., in prep.a). In addition, there is a high level of agreement when we compare values for each of the four downcore samples investigated in core MD05-2905, and the εNd values obtained from acid-reductive HH leachates of bulk non-decarbonated sediments and εNd obtained from cleaned and uncleaned foraminifera (Fig. 4.6). However, εNd values are slightly affected by sample weights and leaching times used in the leaching procedure. For all of the samples that we have investigated, an acid-reductive HH leaching of non-decarbonated sediments of 1 g, leached for 0.5 h, yields εNd values closer to those obtained from cleaned monospecific samples of planktonic foraminifera G.ruber (Fig. 4.6 and Table 4.2). Such results imply that seawater εNd could be extracted by using such a leaching procedure for bulk non-decarbonated sediments from our study site.

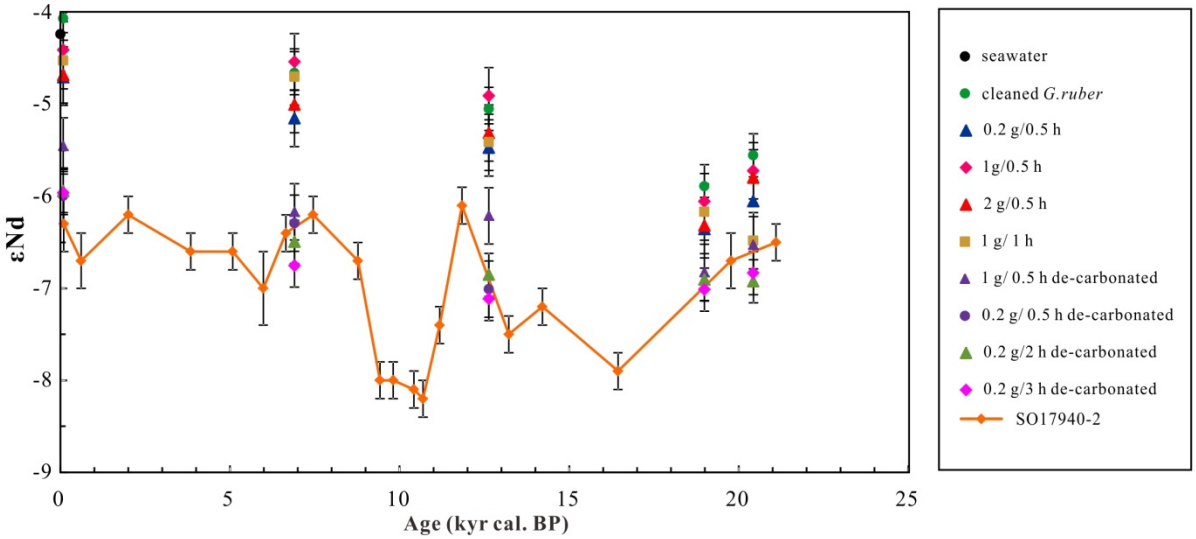

Figure 4.6. εNd of bulk sediment leachates. εNd from those samples without carbonate removal are similar to εNd obtained from cleaned G.ruber. εNd from de-carbonated samples are more negative than those from cleaned G.ruber. εNd values of sediment core SO 17940-2 are from Huang et al., 2013.

In contrast, εNd values obtained from acid-reductive HH leachates of bulk decarbonated sediments from the core-top samples (-5.2±0.3 to -5.9±0.2) differ from those of deep-water in the northern SCS (-4.0 to -4.5) (Wu et al., in prep.a) (Fig. 4.6 and Table 4.2). For each sample investigated in core MD05-2904, the εNd values obtained from acid-reductive HH leachates of bulk decarbonated sediments systematically display values which are 1.5 epsilon units lower than non-decarbonated sediments. Better, but still unsatisfactory, εNd values, have been obtained by using acid-reductive HH leaching of 1g samples of decarbonated sediments

leached for 0.5 h. The reduction of the leaching time (from 3 h to 0.5 h) and the increasing of sample weight (from 0.2 g to 1 g) resulted in a significant decrease of the εNd for each of the decarbonated samples (Fig. 4.6 and Table 4.2).

For the purposes of comparison, the results of pioneering work by Huang et al. (2013), who extracted εNd from acid-reductive HH leachates of bulk decarbonated sediments of the core SO17940-2, are reported in the Figure 4.6. The εNd record of this core is systematically more unradiogenic than the εNd of deep-water masses in the northern SCS derived from the core-top sample and from results that have been obtained on foraminifera. However, results are similar to those obtained from core MD05-2904 using a similar leaching procedure on the carbonate-free sediment fraction.

Considering that surface sediments around the study sites MD05-2904 and SO17940-2 are characterised by an εNd of about -11 (Wei et al., 2012), the negative offset observed in εNd from acid-reductive HH leachates of bulk decarbonated sediments may be caused by Nd deriving from the lithogenic fraction during the leaching procedure. The contamination of εNd from lithogenic fraction, volcanic ash and/or pre-formed Fe-Mn oxides has already been discussed in several studies (Bayon et al., 2002; Elmore et al., 2011; Wilson et al., 2012; Kraft et al., 2013). All of these results support the hypothesis that without removing carbonate from sediment, acid-reductive HH sediment leachates of sediment can reliably extract seawater εNd under certain sample size/solution ratios and leaching times, in agreement with results recently obtained in the Indian Ocean (Wilson et al., 2013).

4.5.5. Hydrological implications for the Pacific since the LGM

Taking into consideration that εNd values extracted from the foraminifera of core-top samples are similar to modern PDW εNd that enters the northern SCS, it is reasonable to hypothesise that the past seawater εNd record obtained from core MD05-2904 enables us to reconstruct past seawater εNd of deep-water masses in the western subtropical Pacific. Consequently, the large variations of εNd values between the LGM- (-5.9±0.2) and the Holocene (-4.1±0.2) sediments could be interpreted as indicating a major reorganization of the hydrology of the Pacific during the last deglaciation (Fig. 4.5). With the exception of localised εNd values obtained in the Northwest Pacific close to the East China Sea, that have been interpreted as being the result of lithogenic input, εNd values of the NPDW, obtained from

several water stations in the North Pacific, are generally characterised by radiogenic values of -4 (Amakawa et al., 2004 and 2009; Piepgras and Wasserburg, 1980). In contrast, the UCDW in the South Pacific is characterised by values of -6 to -8. Consequently, the seawater εNd record obtained from cleaned foraminifera appears to reflect a modification of the proportions of the NPDW and the UCDW in the Philippine Sea. The LGM, characterised by unradiogenic εNd values compared to those of the Holocene, would have seen a retreat of the NPDW to the north and/or a higher propagation of the UCDW to the north compared to the modern situation, which is characteristic of the late Holocene period (last 6 kyr) (Fig. 4.5).

Numerous studies have shown that, during the last glacial period, a slowdown of the NADW formation occurred which is associated with a reduction in its propagation to the south Atlantic (Oppo and Fairbank, 1987; Duplessy et al., 1988; Curry and Oppo, 2005; Labeyrie et al., 1996). Benthic - planktonic formaminifera ^{14}C age difference in the North Atlantic increased greatly in the last glacial period compared to the present suggesting a decreased ventilation rate or changes in the proportions of northern-sourced water (NSW) and southern-sourced water (SSW) (Kegwin, 2004; Kegwin and Schlegel, 2002; Robinson et al., 2005). Furthermore, deep-water εNd values obtained from the Atlantic Ocean and the Southern Ocean for the last glacial period are characterised by more radiogenic values than the Holocene implying a higher proportion of Southern Source Water (SSW) relative to Northern Source Water (NSW) (Ruterg et al., 2000; Piotrowski et al., 2004, 2005, 2012; Robert et al., 2010; Robinson and van de Flierdt, 2009; Skinner et al., 2013). Despite the poor level of documentation regarding past seawater changes in the Indian and Pacific Oceans, available studies indicate an enhanced northward propagation of the SSW during glacial periods. Studies undertaken on sediment cores from the equatorial Indian Ocean show positive excursions of past seawater εNd values, associated with lower $\delta^{13}C$, during glacial periods (Piotrowski et al, 2009; Wilson et al., 2012) suggesting more pronounced northward intrusion of SSW. The seawater εNd record obtained from core MD05-2904 also confirms the presence of a higher proportion of SSW in the western subtropical Pacific during the last glacial period than during the Holocene.

4.6. Conclusion

Neodymium isotopic compositions (εNd) extracted from cleaned- and uncleaned benthic and planktonic foraminifera, and Fe-Mn coatings precipitated on sediments, have been

investigated for the first time in the SCS. The results are compared to modern seawater εNd i) to assess the reliability of extraction of past seawater εNd from such an archive; ii) to establish past hydrological changes in deep water masses in the western subtropical Pacific over the past 25 kyr.

Mn/Ca and Nd/Ca ratios, and PAAS-normalized REE patterns, obtained from reductively/non reductively cleaned foraminifera and reductive cleaning solutions, used for extracting Nd from associated authigenic phases in foraminifera shells, reveal that the reductive cleaning process cannot remove the authigenic contaminants completely. Comparison of Nd isotopic compositions analysed for various species and authigenic phases are quite similar and indicate that εNd obtained from cleaned and uncleaned foraminifera are overprinted by Nd deriving from authigenic Fe-Mn coatings precipitated on foraminifera. Therefore, the Nd isotopic composition of both reductively cleaned and non-reductively cleaned foraminifea reflect the bottom and/or pore water εNd and can be used as a useful tracer to reconstruct past seawater changes.

In contrast, the interpretation of Nd isotopic composition in bulk sediment leachates is more complicated than that in foraminifera. Although Nd isotopic composition obtained from acid-reductive HH leachates of bulk non-decarbonated sediment exhibits similar εNd values to those of foraminifera and bottom seawater (for core-top-samples), partial dissolution of lithogenic fractions has been observed when acid-reductive HH leaching is carried out on decarbonated sediments.

The seawater εNd record obtained from core MD05-904 displays large variations in εNd values between the LGM (-5.9±0.2) and the Holocene (-4.1±0.2), implying a significant reorganization of the hydrology of the western subtropical Pacific during the last deglaciation. These variations reflect a modification of the relative proportions of the NSW (NPDW, εNd around -4) and the SSW (UCDW, εNd around -8) due to vertical mixing in the Philippine Sea. The unradiogenic glacial seawater εNd values obtained in core MD05-904 imply a slowdown of NPDW (and NPIW) formation and/or a higher propagation of the UCDW to the north compared to the late Holocene (last 6 kyr) (Fig. 4.3). Taking into account the high sedimentation rate in the northern SCS, further investigations, based on a high time resolution εNd record, need to be carried out in future in order to reconstruct, for the first time, past seawater εNd of the bottom water of the western subtropical Pacific.

Acknowledgements:

We would like to thank the captain, officers and crew of R/V Marion-Dufresne for their co-operation in collecting sediment cores during the MARCO POLO cruise of the International Marine Past Global Change Study (IMAGES) program in 2005. Louise Bordier is acknowledged for her assistance with elemental ratio measurements. This work was supported by the French-Chinese International Associated Laboratories (LIA) project MONOCL, the ‘‘Agence Nationale de la Recherche’’ through the project MONOPOL and the ANR-10-LABX-18-01.

Chapter 5

Introduction

In the previous chapters, we have established the εNd profiles for the western Pacific, the Luzon straits and the northern SCS. Results indicate a homogenous εNd value for the deep-water of the SCS and the Philippine Sea indicating that it is possible to reconstruct the εNd record of the western North Pacific from sediments in the northern SCS. In addition, we have also assessed the reliability of εNd extraction from northern SCS sediments. Planktonic foraminifera have been proposed as a reliable archive for reconstructing past seawater εNd changes in the northern SCS. A first seawater εNd record, obtained at low time resolution, and using different seawater εNd extraction procedures, indicates a stronger northward propagation of southern sourced water (SSW) into the western subtropical North Pacific during the last glacial maximum. In this chapter, based on the preliminary results obtained from the cleaned planktonic foraminifera in the chapter 4, we attempt to establish, for the first time, a high-resolution seawater εNd record for the western North Pacific based on planktonic foraminifera from core MD05-2904 collected in the northern SCS.

News insights into the hydrology of the north-western subtropical Pacific Ocean based on εNd investigations of South China Sea sediments

Wu Qiong[1,2], Christophe Colin[1], Zhifei Liu[2], Francois Thil[3], Eric Douville[3], Quentin Dubois-Dauphin[1], Norbert Frank[4], Giuseppe Siani[1]

1 Laboratoire de Geosciences Paris-Sud (GEOPS), UMR 8148, CNRS-Université de Paris-Sud, Bâtiment 504, 91405 Orsay Cedex, France.

2 State Key Laboratory of Marine Geology, Tongji University, Shanghai 200092, China.

3 Laboratoire des Sciences du Climat et de l'Environnement (LSCE/IPSL), UMR 8212 CNRS-CEA-UVSQ, Avenue de la Terrasse, 91198 Gif-sur-Yvette Cedex, France.

4 Universität Heidelberg, Im Neuenheimer Feld 229, 69120 Heidelberg, Germany.

* Corresponding author: E-mail: wuqiong06@gmail.com (Wu Qiong)

Abstract

Seawater Nd isotopic composition (εNd) extracted from cleaned planktonic foraminifera *Globigerinoides ruber* (*G.ruber*) has been investigated on core MD05-2904, collected at a depth of 2000 m on the north-western margin of the South China Sea (SCS). This study was undertaken in order to reconstruct hydrological variations since the Last Glacial Maximum (LGM) in the western subtropical North Pacific: up to now these variations have remained poorly documented. The εNd records obtained from foraminifera spanning the past 25 kyr, display a wide range of values, ranging from -4±0.2 to -6.7±0.3, suggesting important changes in the contribution of the NPDW (εNd = -4) and the UCDW (εNd -6 to -8) in the subtropical western Pacific. Interestingly, the glacial εNd values (~ -6.5) are similar to those obtained in the South Atlantic and in the Indian Ocean during the LGM, and indicate a strong northward propagation of the Southern Sourced Water (SSW) in the subtropical western North Pacific. During the period of deglaciation, εNd records indicate a relative decrease in the proportion of the SSW in the deep-water component of the western subtropical Pacific, interrupted by two negative excursions of the εNd implying a higher proportion of SSW during the time intervals 17 - 15 cal kyr BP and 10 - 8 cal kyr BP; these intervals are coeval with the Heinrich Stadial 1 (HS1) and the early Holocene. The seawater εNd record is also well correlated with the $\delta^{13}C$

record obtained from benthic foraminifera *Cibicides wuellerstorfi* in the SCS and Southern Ocean, confirming that the εNd record reflects global circulation changes. The negative shifts centered on the Heinrich Stadial 1 (HS1) coincide with an enhanced upwelling in the Southern Ocean, associated with a polewards shift of the southern westerlies, inducing an enhanced formation of the SSW that propagates to the subtropical western Pacific. The negative excursion of the εNd during the Early Holocene (~10 - 8 cal kyr BP) indicates a higher relative proportion of SSW that could be associated with higher production of the SSW, as has been recently observed in the South Atlantic, and/or with a possible reduction of the NPIW in the North Pacific induced by an intensification of the summer East Asian monsoon rainfall. Our data suggest that the present modern circulation pattern in the western subtropical Pacific Ocean was fully established after 4.6 cal kyr BP. There was a small event around 3.5 cal kyr BP associated with a northward propagation of the deep and intermediate-water of the SSW, which merits further investigation.

Keywords: Neodymium isotopic composition; foraminifera; paleohydrology; subtropical Pacific Ocean; South China Sea; Last glacial period; Holocene.

5.1 Introduction

Changes in global thermohaline circulation affect climate through heat redistribution by surface current flows from tropical to sub-polar latitudes and changes in the carbon storage capacity of the ocean resulting from deep-water ventilation or stratification (Stocker and Wright, 1996; Rahmstorf, 1995, 2003; Toggweiler and Russell, 2008; Marchitto et al., 2007; Bryan et al., 2010). The Pacific Ocean plays a key role in global climate due to its large volume and its role as a potential carbon reservoir (Matsumoto et al., 2002; Yu et al., 2013). Compared to the Atlantic Ocean, past hydrographical studies of the Pacific Ocean have been limited, particularly for deep and intermediate water masses. This is mainly due to the low sedimentation rate which characterises the deep-sea sediments of the Pacific Ocean, as well as poor preservation of bio-carbonate due to shallow CCD. There is also the difficulty of using classical paleoceanograhical proxies (e.g. $\delta^{13}C$ of dissolved inorganic carbon and Cd/Ca ratios as recorded by benthic foraminifers) for identifying the main water masses of the Pacific Ocean which undergo a high degree of mixing in the North Pacific. Despite the fact that the Pacific has received increasing attention over the last few decades (Talley et al., 1992; Reid., 1997; Zenk et al., 2005; Siedler et al., 2004; Kawabe and Fujio., 2010; McCave et al., 2008;

Insua et al., 2014), the evolution over time of NPDW formation, as well as the penetration of Southern Sources Water (SSW) into the North Pacific Ocean, are as yet not well constrained.

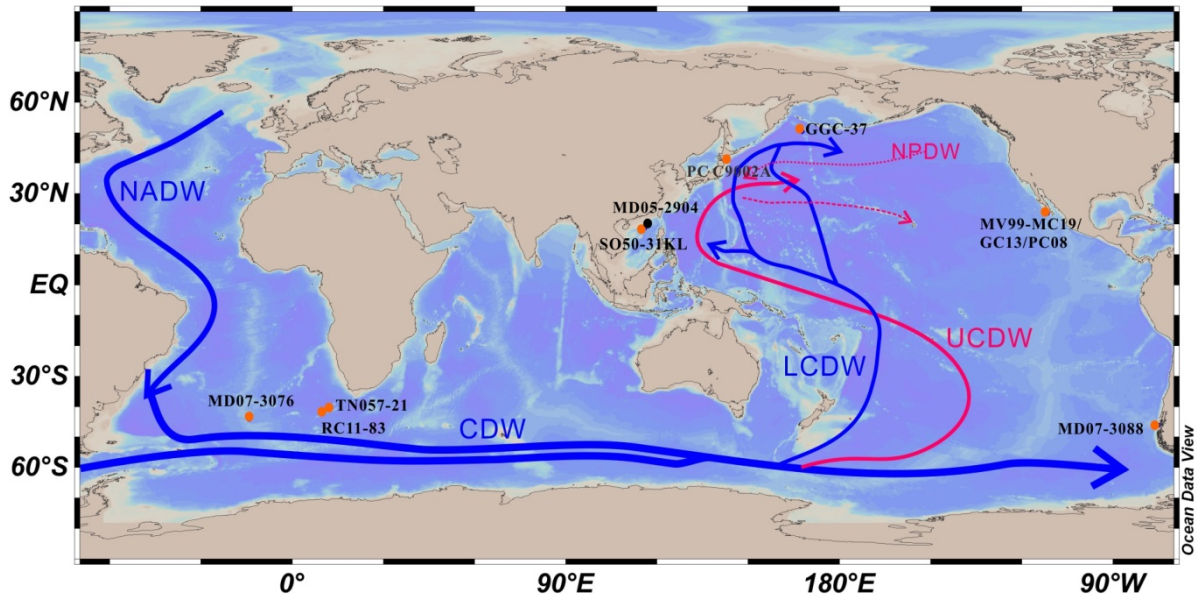

Figure 5.1. Map shows main deep water components in the Pacific Ocean. NADW: North Atlantic Deep Water; CDW: Circumpolar Deep Water; LCDW: Lower circumpolar Deep Water; UCDW: Upper Circumpolar Deep Water; NPDW: North Pacific Deep Water. Black dot represents core MD05-2904 investigated in this study. Orange dots show cores discussed in this study. Map was produced using Ocean Data View (Schlitzer, 2000).

For the last glacial maximum (LGM), stratification has been observed at high latitudes of the Northern and Southern Pacific Ocean (e.g. Shackleton e tal., 1988; Sikes et al., 2000; Keigwin et al., 1998; Matsumoto et al., 2002; Galbraith et al., 2007; Siani et al., 2013). On the basis of $\delta^{13}C$ records obtained on benthic foraminifera, it has been widely accepted that the LGM is also associated with a northward penetration of the SSW in the North Pacific (Ninnemann and Charles, 2002; Bostock et al., 2010) which coincided with a slowdown in the formation of NADW in the North Atlantic (Oppo and Fairbank, 1987; Duplessy et al., 1988; Curry and Oppo, 2005; Labeyrie et al., 1996) and an intrusion of SSW in both the Atlantic and Indian Oceans (Kegwin, 2004; Kegwin and Schlegel, 2002 ; Rutberg et al., 2000; Piotrowski et al., 2004, 2005, 2012; Robert et al., 2010; Skinner et al., 2013; Piotrowski et al, 2009; Wilson et al., 2012).

During the deglaciation, the occurrence of extremely depleted ^{14}C and low $\delta^{13}C$ values

obtained from benthic foraminifera of mid-depth sediments from the north-eastern Pacific Ocean (Baja California, Fig. 5.1) provide further evidence that glacial deep water was isolated and that it released old carbon to the atmosphere when well ventilated ocean conditions were restored during the Heinrich Stadial 1 (HS1) and the Younger Dryas (YD) (Spero and Lea., 2002; Marchitto et al., 2007; Stott et al., 2009).

More recently, Siani et al. (2013) have published records of ^{14}C age and $\Delta\delta^{13}C$ difference between benthic foraminifera - planktonic which provide evidence for an enhanced upwelling in the southern ocean during the last deglaciation at times intervals 17.5 – 14.5 and 12.5 and 11.5 cal kyr BP. This supports the hypothesis that Southern Ocean upwelling contributed to the deglacial rise in atmospheric CO_2. These intervals of strong ventilation are associated with poleward shifts of the southern westerlies observed in biogenic carbonate input in southern Chile (Lamy et al., 2010). Such a configuration is also favourable for enhanced formation of mid- and deep-water masses in the Southern Ocean (Skinner et al., 2010).

An ongoing puzzle regarding the Pacific is whether or not there was North Pacific Intermediate/Deep Water (NPIW, NPDW) formation during deglacial Northern Hemisphere cold events (Heinrich Stadial l, Younger Dryas) when NADW formation had collapsed (Mix et al., 1999; Ohkushi et al., 2003; Okazaki et al., 2010; Rella et al., 2012; Rae et al., 2014). An increase in the formation of the NPIW has been observed in the subarctic Pacific Ocean for the last glacial periods and the HS1 event (Rella et al., 2012; Max et al., 2014). A compilation of foraminifera benthic - planktonic ^{14}C age differences from several cores in the North Pacific have demonstrated that North Pacific ventilation decreased drastically during the HS1 (Okazaki et al., 2010). The data suggest significant formation of NPDW during the LGM that intensified during the HS1. However, available data also argue against such hydrological changes in the North Pacific. A sharp tracer gradient (i.e. benthic foraminifera $\delta^{13}C$) between deep and intermediate water masses was observed in the North Pacific suggesting that deep ocean water of the North Pacific was more stratified below a depth of around 2000 m during the last glacial period (Kegwin, 1998; Matsumoto et al., 2002). In addition, redox sensitive elements do not support the hypothesis of deep-water formation in the North Pacific during HS1, but rather, they indicate that NPIW formation was largely restricted to the upper layer, above a depth of 1300 m (Jaccard and Galbraith, 2013). Consequently, variability of the deep and intermediate water during the LGM, and its relationship with rapid climatic changes in high latitudes of the northern and southern hemisphere, is still a matter of debate.

The neodymium isotopic composition ($^{143}Nd/^{144}Nd$) of seawater has been shown to be a useful proxy for tracing water mass provenance (e.g. Von-Blanckenburg, 1999; Lacan and Jeandel, 2004 a,b, 2005, Ruteger et al., 2000; Piotrowski et al., 2008, 2009, 2012; Roberts et al., 2010; Basak et al., 2010). The residence time of Nd, recently re-assessed to about 600-1000 yrs (Tachikawa et al., 1999 and 2003), is shorter than the global turnover time of the ocean (about 1000 yrs; Broecker,1982). Consequently, through lithogenic inputs of material of various ages, and boundary-exchange processes that occur at the continental margin (Lacan and Jeandel, 2005), intermediate- and deep-water masses acquire Nd from downwelling surface water (Goldstein and Hemming, 2003). In the ocean, the only way that the initial isotopic composition of a water mass can be altered is through the addition of Nd with a different isotopic composition through riverine or eolian inputs, or by mixing with other water masses. Nd isotopic composition ($^{143}Nd/^{144}Nd$) is expressed as εNd, which is the deviation of the $^{143}Nd/^{144}Nd$ ratio from its average value in the ‘‘bulk Earth’’ $^{143}Nd/^{144}Nd$ ratio of 0.512638 in parts per 10^4 (Jacobsen and Wasserburg, 1980), expressed as:

$$\varepsilon Nd=[(^{143}Nd/^{144}Nd)sample/0.512638)-1]\times 10000$$

Unlike nutrient proxies, such as $\delta^{13}C$ or Cd/Ca, Nd isotopes are not known to be affected by biological processes, and thus they can serve as a quasi-conservative water mass tracer (Frank, 2002; Goldstein and Hemming, 2003; Vance et al., 2004; Martin and Scher, 2004). Today, the Nd isotopic composition of seawater is recognized as a powerful tracer of water mass provenance and mixing (e.g. Jeandel, 1993; Piepgras and Wasserburg, 1987; Jeandel et al., 1998; Lacan and Jeandel, 2004; Copard et al., 2011; Amakawa et al., 2004, 2013; Stichel et al., 2012). Moreover, it has been shown that sedimentary archives, such as foraminifera, fossil fish teeth, dispersed authigenic Fe-Mn sediment coatings, ferromanganese crusts and deep sea corals, allow tracing of past ocean circulation changes at various times scales (Burton and Vance, 2000; Colin et al., 2010; Copard et al., 2010; Elmore et al., 2011, Ling et al., 1997; Martin and Haley, 2000; Martin and Scher, 2004; Martin et al., 2006; O’Nions et al., 1998; Piotrowski et al., 2004, 2008, 2012; Roberts et al., 2010; Scher and Martin, 2004; van de Flierdt et al., 2006; Vance and Burton, 1999).

The South China Sea (SCS) is a key area for reconstructing past hydrological change in the western Pacific. The SCS is a semi-enclosed, marginal sea connected to the Philippine Sea

through the Luzon Straits. Consequently, the northern SCS has great potential for studies to establish past variability in the hydrology of the western subtropical Pacific Ocean that receives deep-water sourced from northern and southern high latitudes of the Pacific Ocean (Johnson and Toole, 1993; Kawabe et al., 2003, Talley, 2008). The spatial distribution of seawater εNd has recently been established for the Philippine Sea and the northern SCS permitting the identification of the εNd of the main water masses of the SCS and the Philippine Sea and the investigation of past seawater εNd records from deep-sea sediments. εNd in the Philippine Sea results from the vertical mixing of the SSW, corresponding to the Upper and Lower Circumpolar Deep Water (UCDW and LCDW) and characterised by εNd around -8 (Jeandel et al., 1993; Carter et al., 2012; Piepgras and Wasserburg, 1982; Jeandel et al., 2013; Amakawa et al., 2013), and the Northern Sourced Water (NSW), corresponding to the North Pacific Deep-Water (NPDW) characterised by an εNd of -4 (Piepgras and Wasserburg, 1988; Amakawa et al., 2004 and 2009). This contrasting seawater εNd between SSW and NSW allows us to track these water masses in the western subtropical Pacific in the past. In addition, it has been demonstrated recently that εNd values of deep-water masses in the northern SCS are homogenous and consistent with those of the Philippine Sea, indicating a Pacific origin for the SCS deep-water without any possible modification of the seawater εNd values by exchange of Nd with sediment from the oceanic margin of the SCS. Consequently, εNd values obtained from foraminifera in deep-sea sediments from the north-western margin of the SCS constitute an interesting means for reconstructing past changes of the deep-water masses of the western subtropical Pacific Ocean.

In the current study, seawater εNd extracted from planktonic foraminifera in core MD05-2904, collected at a location on the north-western margin of the South China Sea (SCS) at a depth of 2000 m, has been investigated in order to reconstruct the hydrology of the western subtropical North Pacific over the past 25 kyr: until now this past hydrology has been poorly documented.

5.2. Seawater εNd and the hydrological settings of the Philippine Sea and the SCS

Previous observations indicate that deep water masses of the Pacific Ocean are mainly derived from internal mixing of Circumpolar Deep Water (CDW) from the Southern Ocean (Talley, 2008; Kawabe and Fujo, 2010) (Fig. 5.1). The boundary between the Lower Circumpolar Deep Water (LCDW) and the Upper Circumpolar Deep Water (UCDW),

characterised by an εNd value of around -8, is located at approximately 3000 m (Talley, 2007; Kawabe and Fujio, 2010). Phosphate concentrations, along a north-south cross section of the Philippine Sea, allow different water masses to be clearly distinguished (Fig. 5.2) (Talley and Joyce, 1992; World Ocean Atlas, 2009). In general, the deep water in the Philippine Sea is composed of the Pacific Deep Water (PDW) which results from the mixing of water masses originating from the Southern Ocean and older North Pacific Deep Water (NPDW) (Johnson et al., 2006; Kawabe et al., 2003). The NPDW results from the internal vertical mixing of the North Pacific (Talley and Joyce, 1992).

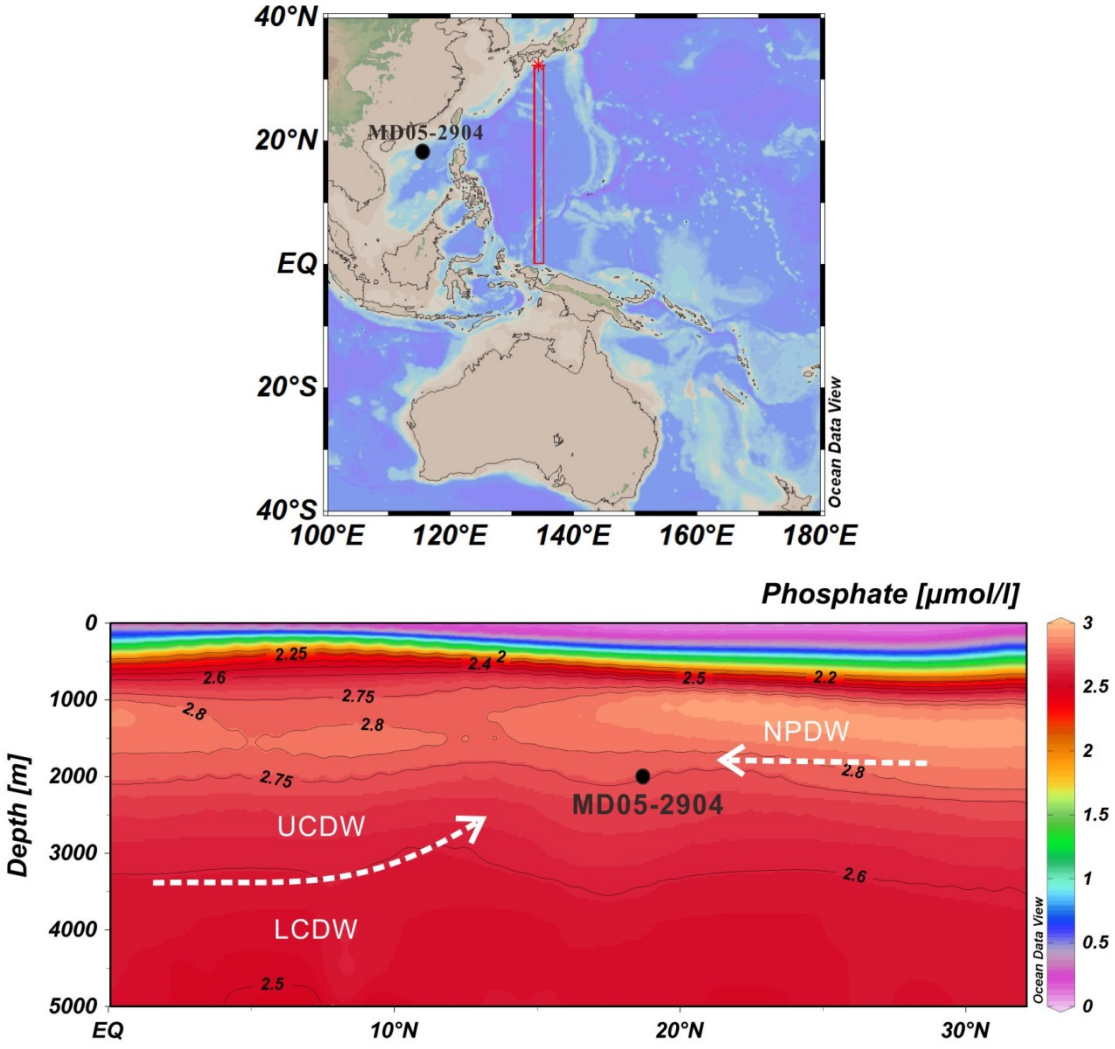

Figure 5.2. Core location and depth profile of annual mean phosphate concentration along the WOCE Pacific transect (World Ocean Atlas 2009) near core MD05-2904.

The SCS is connected in the south with the Sulu and Java Seas through the shallow Mindoro (~200 m) and Karimata Straits (<50 m) and in the north with the East China Sea and

Pacific Ocean through the Taiwan Straits (<100 m) and the deep channel of the Luzon Straits (>2400 m), respectively (Qu et al., 2009). The sea surface circulation of the SCS is mainly forced by the seasonal reversals in wind direction during the summer and winter monsoons: the winds induce a cyclonic surface circulation during the winter and an anti-cyclonic one during the summer (Shaw and Chao, 1994; Fang et al., 1998). North Pacific Tropical Water (NPTW), characterised by high salinity as it enters the SCS, is diluted by freshwater discharge from large Asian rivers. This induces relatively fresher South China Sea Tropical Water (SCSTW) (Xie et al., 2011). Consequently, εNd of surface water in the north-western SCS (-3.3 ~ 7.0) is less radiogenic than the NPTW (-3.5) and there is a marked north - south gradient of the sea surface water εNd, with higher unradioganic values in the southern SCS (εNd ~ -9; Wu et al., in prep.a). Due to vertical mixing with deep water, the intermediate water in the SCS (SCSIW) displays higher relative salinity (~ -34.4) and slightly unradiogenic εNd values (from -3.0±0.3 to -3.9±0.3) when compared with values for the North Pacific Intermediate Water (NPIW) (salinity of ~-34.0 and εNd of -2.7±0.4) (Tian et al., 2009; Xie et al., 2011; Wu et al., in prep.a).

Compared with the large number studies devoted to the hydrology of the surface and intermediate water masses, investigations of deep-water circulation of the SCS are rare and, to date, little is known of the circulation patterns. The presence of a water mass, characterised by homogenous physical properties similar to those of the subtropical western Pacific and corresponding to the Pacific Deep Water (PDW), has been established in the deep basins of the SCS, below a depth of 2000 m (Qu et al., 2006; Tian et al., 2006). Recently, Wu et al. (in prep.a) have shown that εNd values of deep-water masses of the Philippine Sea, and the north-western margin of the SCS, display a narrow range of between -4.1±0.3 and -4.4±0.3, indicating the presence of the PDW.

5.3. Material and methods

The Calypso core MD05-2904 (19º27.32´ N, 116º15.15´ E, 2066 m; 44.98 m long) was retrieved on the north-western margin of the SCS during the R/V Marion Dufresne MARCO POLO IMAGES XII Cruise in 2005 (Fig. 5.1, Table 5.1). Core MD05-2904 is currently bathed by PDW and is located at a comparable water depth as the Luzon strait, where the deepest sill is located at a depth about 2400 m in the Bashi Channel. It constitutes an ideal site for reconstructing past hydrological variations of the NSW (NPDW) and the SSW in the subtropical western Pacific.

Table 5.1. Nd isotopic composition of cleaned foraminiferas together with corresponding Mn/Ca ratios and Nd/Ca ratios

Core depth (cm)	Age (Cal. Kyr BP)	Nd/Ca (nmol/mol)	Mn/Ca (μmol/mol)	εNd	2σ
1-2	0.05	1155.39	215.91	-4.1	0.2
15-16	0.82	770.54	127.86	-4.6	0.3
35-36	1.63	792.36	139.02	-4.48	0.3
59-60	2.57	805.68	153.12	-4.42	0.3
83-84	3.52	735.41	148.02	-5.08	0.3
91-92	3.83	--	--	-4.52	0.3
111-112	4.62	911.76	187.38	-4.08	0.3
158-159	6.50	1365.16	298.20	-4.66	0.2
171-172	6.97	922.14	225.74	-4.98	0.3
191-192	7.55	1078.00	245.18	-5.71	0.3
227-228	8.56	1069.98	222.41	-5.48	0.3
259-260	9.45	1011.04	239.61	-6.16	0.3
295-296	10.45	960.41	221.87	-5.04	0.3
327-328	11.24	1156.46	421.38	-5.05	0.2
383-384	12.57	745.40	276.30	-5.27	0.3
423-424	13.52	974.12	323.38	-5.76	0.3
475-476	14.76	898.67	278.37	-6.30	0.3
535-536	15.73	1251.64	190.57	-6.75	0.3
600-601	16.73	740.02	183.32	-5.86	0.3
675-767	17.85	764.50	181.65	-6.45	0.3
727-728	18.57	1490.41	301.00	-5.89	0.2
771-772	19.27	1192.32	273.75	-5.76	0.3
800-801	20.04	1723.47	375.19	-5.55	0.2
835-836	21.02	1314.63	229.52	-6.01	0.3
880-881	22.22	1322.13	246.05	-5.67	0.3
915-916	23.20	1046.55	290.33	-6.08	0.3

The age model of core MD05-2904 was established on the basis of the oxygen isotope curve and 8 accelerator mass spectrometry (AMS) C-14 dating analysed by Ge et al. (2010) (Fig. 5.3a). Radiocarbon dates were performed on well preserved calcareous samples from planktonic foraminifera *G. ruber*. After subtracting 450 yr to account for the average surface regional reservoir effect (Butzin et al., 2005), the conventional radiocarbon ages were converted into calendar ages using the Calib 7 program (Stuiver et al., 2014). The age model was established by linear interpolation between 8 calibrated dates for the first 10 m of the core. The MD05- 2904 core thus provides a continuous record spanning the last 25 cal kyr BP, with higher accumulation rates for the last glacial stages (around 70 cm/kyr) than for the Holocene (around 25 cm/kyr).

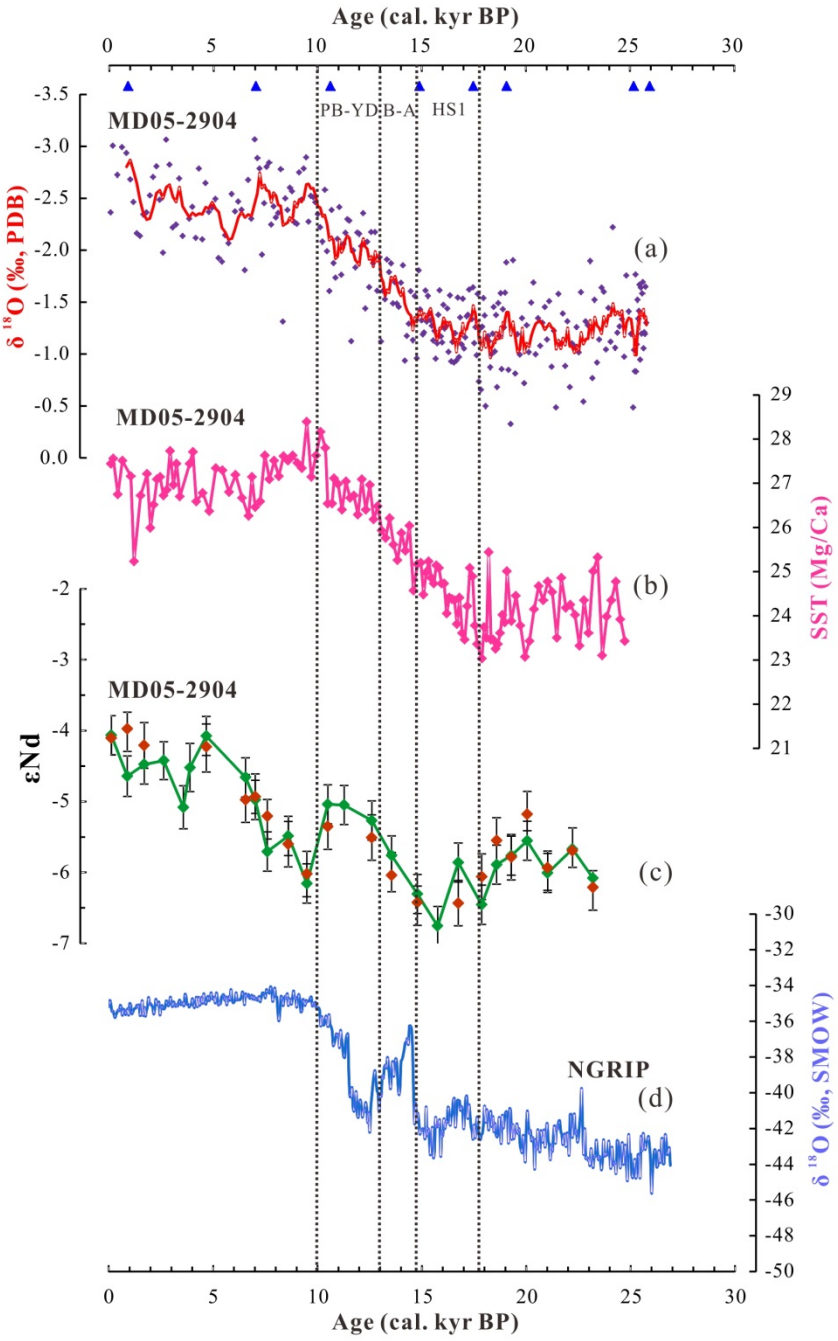

Figure 5.3. Comparison of proxy records from core MD05-2904 with ice core $\delta^{18}O$ record for the last 25 kyr BP. (a) $\delta^{18}O$ records obtained from Globigerinoides ruber (Ge et al., 2010); smooth curve is derived from a three-point average result (red line); blue dots show AMS ^{14}C age control points. (b) Sea surface temperature based on G. ruber shell Mg/Ca ratios (Steinke et al., 2011). (c) εNd record obtained from cleaned planktonic foraminifera and reductive cleaning solution (this study). (d) NGRIP $\delta^{18}O$ record (North Greenland Ice Core Project Members, 2004).

For Nd isotopic composition analyses, around 30 mg of well-preserved, mixed planktonic

foraminifera were handpicked from the >150 µm fraction. The cleaning procedure has been described in detail by Wu et al. (in prep.b). In brief, all of the foraminifera were gently crushed between two glass plates to open all chambers. The calcite fragments were then sonicated in an ultrasonic bath for approximately 1 min before pipetting the suspended particles with water to separate the waste. This step was repeated until the water became clear and free of clay. All samples were checked under a binocular microscope to ensure that all particles were removed. Physically cleaned samples were transferred to centrifuge tubes for the oxidative – reductive cleaning step (samples subjected to this process are hereafter referred to as "cleaned foraminifera"). The oxidative – reductive foraminiferal cleaning procedure used in this study followed Vance and Burton (1999), using 10 ml reductive solution (1 M hydrous hydrazine, 16 M NH_4OH, 0.25 M citric acid + 16 M NH_4OH in a ratio of 1:6:3) and 5 ml oxidative solution (0.2 M NaOH and 30% H_2O_2 in a 1:1 ratio) per sample to remove the authigenic Fe-Mn coating. For the reductive step, samples were heated in a water bath at 80ºC for 30 min and were ultrasonicated every 2.5 min for 10 s. After transferring the reductive cleaning solution to a centrifuge tube, the cleaned foraminifera were thoroughly rinsed with deionized water. The analytical procedure for the oxidative step was similar except that samples were ultrasonicated every 10 min for 30 s. All samples underwent a weak acid leach for 5 min in 1ml 0.001 M HNO_3 with an ultrasonicating bath. After the cleaning step, samples were then transferred to a 1.5 ml tube. Then, 0.5 ml deionized water was added to the tube and the foraminifera were dissolved by using stepwise 100 µl weak nitric acid (0.5 N HNO_3) until the dissolution reaction stopped. The dissolved samples were centrifuged and the supernatant was immediately transferred to Teflon beakers to prevent leaching of any possible remaining phases. All of the dissolved foraminifera shell fraction and authigenic fraction contained in the reductive cleaning solution were dried on a hotplate for Nd purification. Mn, Nd and Ca concentrations and REE pattern analysis were performed on a 10% cut of both the dissolved foraminifera shells and the corresponding "reductive cleaning solutions".

Nd was purified from all samples following the analytical procedure described in detail by Copard et al. (2010). In summary, samples were loaded using 2 mL of 1N HNO_3 on preconditioned TRU-Spec columns (83 mg portion of TRU-spec). The unwanted cations were eluted using 5 portions of 0.5 mL of 1N HNO_3. TRU-Spec columns were then placed over Ln-Spec columns. The LREEs were then eluted from the upper (TRU-Spec) column using seven portions of 0.1 mL of 0.05N HNO_3. After decoupling from the TRU-Spec columns, La, Ce and most of the Pr were rinsed from the Ln-Spec columns using 3.25 mL of 0.25N HCl. Nd

was then eluted with an additional 2.5 mL of 0.25N HCl.

Concentrations of Ca, Mn and REE were analysed on the Inductively Coupled Plasma-Quadrupole Mass Spectrometer (ICP-QMS X Series$^{II\ Thermo\ Fisher}$) at the LSCE, by measuring their isotopes- ^{46}Ca, ^{55}Mn and ^{146}Nd- and by using appropriate carbonate standards (JCp-1 coral). Samples and standard solutions were systematically adjusted to 100 ppm Ca through dilution, without further chemistry. This is because (1) dominant Ca signals need to be avoided as high concentrations can increase salt deposition on cones affecting ICP-MS stability and (2) adjusted Ca concentration levels introduced into ICP-QMS at 100 µL/min provide a means of controlling matrix effects due to the presence of Ca. Instrumental calibration, based on the standard addition method, was achieved using a mono-elementary standard solution for each element (Harding et al., 2006) and by routinely measuring carbonate standards (JCp-1, Okai et al., 2004). To compensate for a signal deviation of a few percentage values per day, a standard (JCp-1) was run every nine samples. When analysing the REE of the reductive cleaning solution from foraminifera and leachates from bulk sediments, a high purity REE solution was measured every 9 samples and additional internal standards (^{115}In and ^{103}Rh) were added to samples in order to monitor instrument stability. Our measurements were characterised by analytical uncertainties ranging from 5% for the lightest REE to 15 % for the heaviest, as published previously (Bourdin et al., 2011). The reproducibility of measurements for two repeated samples varied according to the different element to calcium ratios (2σ: 10% for Mn/Ca, 5% for Nd/Ca). The concentrations of Nd in blanks are less than 100 ppt, which is negligible compared to the average concentration of 15 ppb ± 5 % measured in samples.

The purified Nd fraction was analyzed using a ThermoFisher Neptune-Plus Multi-collector Inductively Coupled Plasma Mass Spectrometer (MC-ICP-MS) at the Laboratoire des Sciences du Climat et de l'Environnement (LSCE) in Gif-sur-Yvette. The mass-fractionation correction was made by normalizing ^{146}Nd/^{144}Nd to 0.7219 and applying an exponential-fractionation correction. During the analysis sessions, every two samples were bracketed with analyses of the JNdi-1 and La Jolla standards at a concentration similar to those of samples, and corrected to certified values of 0.512115 ± 0.000006 and 0.511858 ± 0.000007 (Tanaka et al., 2000), respectively. The external reproducibility (2σ) for time resolved measurement, deduced from repeated measurement of the La Jolla standard and JNdi-1 at similar concentrations to the samples, ranged from 0.2 to 0.3 ε units for different analytical sessions. The analytical error of each sample analysis is taken as the external reproducibility of the La Jolla standard for each session. Blank values were <150 pg, and can be ignored as they

represent less than 10% of the Nd from foraminifera samples.

5.4. Results

Mn/Ca and Nd/Ca ratios of cleaned foraminifera varied between around 130 - 400 nmol/mol and 740 – 1720 µmol/mol, respectively. REE concentrations obtained from cleaned planktonic foraminifera and reductive cleaning solutions were normalized to Post-Archean Average Australian Sedimentary rock (PAAS, Nance and Taylor, 1976). All of the PAAS-normalized REE patterns were quite similar and presented negative Ce-anomalies and MREE enrichment (Fig. 5.4).

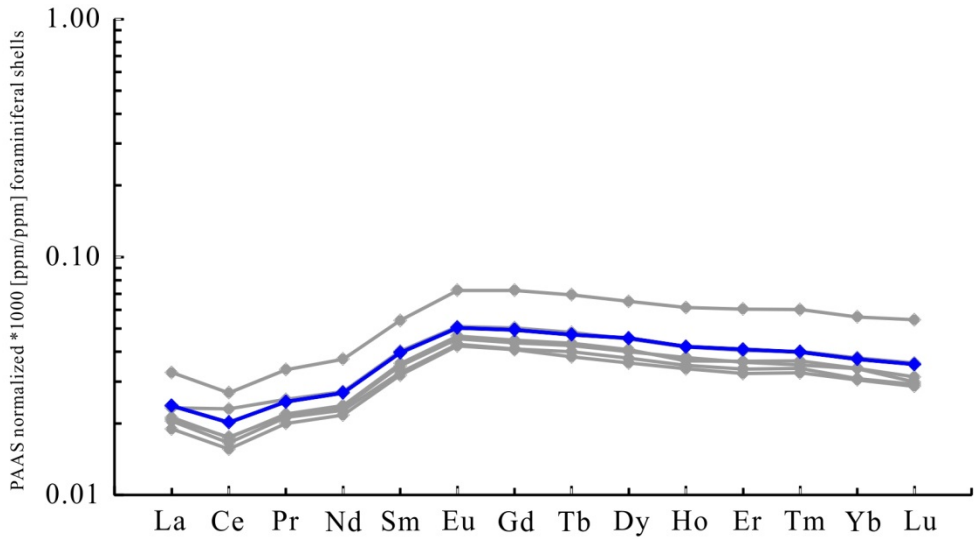

Figure 5.4. PAAS-normalized REE patterns of cleaned planktonic foraminifera

εNd records obtained from cleaned foraminifera in core MD05-2904 are illustrated in Figure 5.3c. εNd values obtained from foraminifera range from -6.8±0.3 to -4.1±0.2. In addition, Figure 5.3 also indicates the εNd of the leaching solution. In general, there is a good correlation (r^2 =0.88) between the εNd values obtained from cleaned foraminifera and those from the cleaning solution.

In general, the LGM period is characterised by a higher unradiogenic εNd value (around -6.8) than the late Holocene (-4.1) (Fig. 5.3c). In detail, the εNd values range from -5.6 to -6.0 between 24 and 19 kyr BP. At the beginning of the last deglaciation, a large negative excursion, to approximately -6.8, occurred around 15.8 cal kyr BP corresponding to the mid-HS1 cold

interval. This negative shift of the εNd was followed by a subsequent increase to -5 spanning the interval between15 and 10 cal kyr BP, coeval with the Bølling-Allerød (B-A) warm period and the YD. A second negative shift of the εNd, from -5.1 to -6.2, occurred around 9.5 cal kyr BP. The εNd values remained relatively low (between -6.2 to -5.7) in the early Holocene. Following the early Holocene, the εNd values displayed an increasing trend between 7.5 and 5 cal kyr BP, and reached approximately -4.1 at 4.6 cal kyr BP. Since then, the late Holocene is characterised by near constant εNd values of around -4.5, with one marked negative shift at 3.5 cal kyr BP (-5.0).

5.5. Discussion

5.5.1. Significance of the εNd obtained from foraminifera

Nd value obtained from cleaned planktonic foraminifera collected from the top of core MD05-2904 is -4.07±0.23, is identical to values obtained by Wu et al. (in prep.a) from cleaned benthic foraminifera (-4.08±0.23) and cleaning solutions (-4.10±0.28) (Table 5.1). Such values are also similar to those of the bottom water (εNd ~ -4.2) but are significantly different from surface seawater samples (~ -7 to -5.4) collected from several water stations close to the study site in the northern SCS (Wu et al., in prep.a). In addition, ranges in Nd/Ca and Mn/Ca ratios obtained from cleaned foraminifera in core MD05-2904 are much wider than Nd/Ca and Mn/Ca ratios obtained from living and non-fossil planktonic foraminifera collected in sediment traps (Nd/Ca from 8 to 700 nmol/mol and Mn/Ca from 0.25 to 15 μmol/mol) (Martínez-Botí et al., 2009; Pomiès et al., 2002; Robert et al., 2012). Reductively cleaned planktonic foraminifera and leaching solutions exhibit similar PAAS-normalized REE patterns despite the large range of concentrations obtained. PAAS-normalized REE patterns present negative Ce-anomalies and MREE enrichment, typically indicative of the presence of Fe-Mn hydroxide phases (Fig. 5.4). In addition, εNd obtained from leaching solutions is similar to that from the cleaned planktonic foraminifera. All of these results imply that εNd obtained from cleaned foraminifera is mainly overprinted by εNd from residual Fe-Mn hydroxide phases, due to the incomplete oxidative and reductive cleaning procedure applied. Such results support recent studies that have proposed that planktonic foraminifera reflect the Nd isotopic composition of bottom waters (Kraft et al., 2013; Tachikawa et al., 2013).

5.5.2. Origin of seawater εNd variation in the northern SCS

The εNd values obtained from cleaned foraminifera in core MD05-2904, exhibited a large range, from -6.8 to -4.1, implying major changes in the seawater εNd during the last 25 kyr (Fig. 5.3c). To understand such εNd variations, it is necessary to determine the εNd of the water masses circulating in the Northern SCS or, at least, to identify the main potential isotopic mixing end-members involved in the water mass balance. One must also assume that the Nd isotopic composition of these end-members has remained unchanged since the LGM.

In different regions of the ocean, distributions of seawater εNd are strongly influenced by a process termed “boundary exchange” which involves localised Nd exchange between seawater and sediments at the oceanic margins (Lacan and Jeandel, 2001, 2004, 2005). This process has been frequently identified along volcanic margins (Lacan et al., 2001; Grenier et al., 2013). However, the scale, timing and mechanisms involved in this process are still poorly understood. We can reasonably assume that εNd values of sediments from the north-western margin of the SCS have not changed drastically over the past 25 kyr because the sedimentary sources along this oceanic margin are characterised by quite similar εNd values (Liu et al., 2007; Wei et al., 2012). This north-western margin of the SCS is mainly supplied with sediments derived from the Pearl River and Taiwanese rivers, which are characterised by similar ranges of εNd (from -10.5 to -13.5 and -11.5 to -12.7, respectively). A small contribution of lithogenic material deriving from the volcanic arc of Luzon (mainly smectite), transported by surface and intermediate currents, has been also identified in sediments on the north-western margin of the SCS (Boulay et al., 2005; Liu et al., 2010). However, the εNd distribution of sediment along the north-western margin of the SCS presents a narrow value range (from -11 to -12) and does not display radiogenic values. This implies a strong dilution of the volcanic material by sediments deriving from Taiwanese and Chinese rivers (Wei et al., 2012). In addition, the clay mineral assemblage of core MD05-2904 shows that the smectite content varies between 10 and 40 % over the last 22 kyr, with a significantly higher proportion of smectite during the LGM (Liu et al., 2010). Considering that most of the smectite deposit from the north-western margin derives from the volcanic Luzon arc (Boulay et al., 2005; Liu et al., 2010), such results imply a significantly higher contribution of volcanic material to the north-western margin of the SCS during the LGM. However, εNd of the detrital fraction of the north-western margin of the SCS has varied negligibly (between -9.9 and -11.1) over the last 25 kyr BP for the ODP Sites 1145 and 1144, which are located close to core MD05-2904 (Boulay et al., 2005; Hu et al., 2012) (Fig. 5.5a). Such variations are small and insufficient to explain the 2 Epsilon Nd unit variations

observed in the foraminifera. In addition, no relation can be shown between variations in smectite contents and the seawater εNd record. This implies that seawater εNd is not affected by changes in the Nd isotopic composition of sediments from the northwest margin of the SCS. Such results are in agreement with a recent study that indicates an homogenous Nd isotopic composition for the PDW throughout the Northern SCS, similar to the Nd isotopic composition of the PDW in the Philippine Sea (-4) (Wu et al., in prep.a). This last study suggests no modification of the Nd isotopic signature of the PDW after it enters the SCS (Wu et al., in prep.a). Consequently, the large and rapid variations observed in seawater εNd obtained from foraminifera cannot be explained by a modification of the Nd isotopic composition of sediments from the northwest margin of the SCS through time, suggesting a negligible role for the "boundary exchange" process in our foraminifera εNd record.

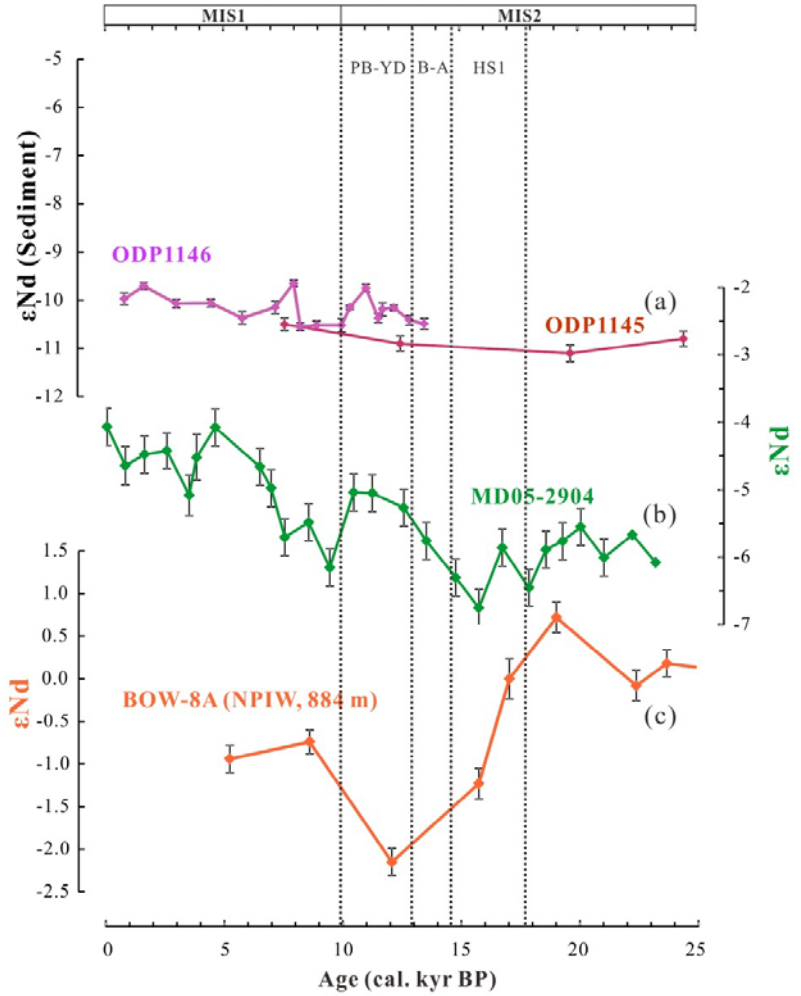

Figure 5.5. Comparison of εNd records in this study (b) with sediment εNd records in the SCS (a) (Boulay et al., 2005; Hu et al., 2012) and past intermediate water εNd records obtained from North Pacific (c) (Horikawa et al., 2010).

Core MD05-2904, collected at a depth of 2066 m, is bathed by deep-water masses originating from the Philippine Sea that result from the mixing of the NPDW from the north and the upwardly-diffused UCDW from the south (Fig. 5.2). With the exception of local εNd values obtained in the Northwest Pacific (near the East China Sea), which have been interpreted on the basis of lithogenic input, εNd values of the NPDW obtained from several water stations of the North Pacific are characterised by radiogenic values of -4 (Amakawa et al., 2004 and 2009; Piepergras and Wasserburg, 1980). In contrast, the UCDW in the South Pacific is characterised by εNd values ranging from -6 to -8. Consequently, the εNd record obtained from cleaned foraminifera may reflect a modification of the proportion of the NPDW and the UCDW in the Philippine Sea. The fact that the LGM is characterised by unradiogenic εNd values, compared to those of the Holocene, implies a slowdown in the formation of the NPDW to the north and/or a greater propagation of the UCDW to the north compared to the modern situation which characterises the late Holocene (last 6 kyr).

5.5.3. Implications for the formation of glacial North Pacific Deep Waters

Previous studies have suggested that NPIW formation was more intense during the last glacial period and the HS1 cold event in the northern hemisphere (Okazaki et al., 2010; Chikamoto et al., 2012; Max et al., 2014). The strong ventilation observed in the subarctic Pacific Ocean during the HS1 event induced vertical mixing with sea surface water, formation of relatively fresh mid- and deep-water masses, and a modification of the structure of deep-water masses in the North Pacific (Okazaki et al., 2010). In the Bering Sea, Horikawa et al. (2010) have shown that εNd obtained from the authigenic fraction of sediments from core BOW-8A displays more radiogenic values (+1) during the LGM than the Holocene (-3) (Fig. 5.5c). This has been interpreted as being the result of enhanced vertical mixing of the NPIW with surface water displaying a high radiogenic Nd isotopic composition strongly influenced by sediment from the volcanic margin of the Bering Sea (Horikawa et al., 2010). Such variations in the εNd of the NPIW observed in the subarctic region would have had a definite influence, through vertical mixing, on the Nd isotopic signature of the NPDW and would have produced a more radiogenic glacial NPDW in the North Pacific. The southward propagation of such radiogenic glacial NPDW to the western tropical Pacific would inevitably have resulted in a more radiogenic seawater Nd isotopic composition at our study site during the glacial period.

However, such a scenario is not supported by the seawater εNd record from core MD05-2904 that, in contrast, displays more unradiogenic values during the LGM (-6) than the late Holocene (-4) (Fig. 5.5b). Such conclusions are in agreement with the redox sensitive trace element records obtained from North Pacific sediments: these records do not display evidence for oxygen-enriched water masses in deep layers (Galbraith et al., 2007; Jaccard and Galbraith, 2013). In contrast, the strong ventilation in the North Pacific is restricted to water above a depth of 1300 m as a result of ocean stratification (Jaccard and Galbraith, 2013). This excludes any significant production of NPDW in the high latitudes of the North Pacific during the LGM. In addition, on the basis of the $\delta^{13}C$ record obtained from benthic foraminifera in cores from the subarctic region, there is no evidence for enhanced NPDW formation during the glacial period (Max et al., 2014). In agreement with the seawater εNd record of core MD05-2904, all of these observations suggest that deep-water formation in the North Pacific (NPDW) during the LGM was probably no greater than it is today.

5.5.4. Implications for the hydrology of the last glacial period and the Termination 1

The εNd record obtained from core MD05-2904 constitutes the first seawater εNd record for the North-western Pacific, permitting new comparisons with other seawater εNd records obtained in the South Atlantic and the Pacific Ocean (Fig. 5.6). Interestingly, glacial seawater εNd values (-6.5±0.3) obtained from core MD05-2904 are similar to other glacial εNd values obtained from sediments bathed by deep-water masses in the South Atlantic and in the Indian Ocean (around -6 to -7) (Piotrowski et al., 2004, 2008, 2009; Skinner et al., 2013). The glacial εNd values (more radiogenic) from the South Atlantic (core TN057-21 and MD07-3076) have been explained by weak NADW formation and a northward propagation of the Southern Source Water (SSW) in the Atlantic (Piotrowski et al., 2008; Skinner et al., 2013) (Fig. 5.6c, 5.6d). This would inevitably have triggered a modification of the εNd of the glacial SSW that would have become significantly more radiogenic as a result of a lower contribution of NADW (Piotrowski et al., 2004, 2008, 2009; Skinner et al., 2013). Such results suggest a homogenous glacial seawater εNd in the South Atlantic, Indian Ocean and North-western Pacific Ocean. In addition, εNd values for the last glacial period, obtained from corals and Fe-Mn crusts sampled in the Drake Passage (Southern Ocean), are -6.4 and -7 respectively (Robinson and van de Flierdt, 2009). It seems that, during the last glacial period, values for the southern end-member shifted to around -6.5 due to a marked reduction in the formation of NADW. This value is more radiogenic than the present-day SSW value, but remains more unradiogenic than NPDW and

NPIW εNd values (Piepgras and Wasserburg, 1982; Amakawa et al., 2009; Wu et al., in prep.a). Consequently, the εNd record of core MD05-2904 results from an equilibrium between contributions from the NSW (NPDW, εNd around -4) and the SSW (-8 at present and possibly -6.5 during the glacial period). The last glacial period is characterised by a dominant contribution of SSW, whereas the late Holocene is characterised by a higher relative proportion of NSW. Further investigations are necessary to improve our understanding of the potential modifications of the Nd isotopic composition of the SSW and NSW during glacial periods.

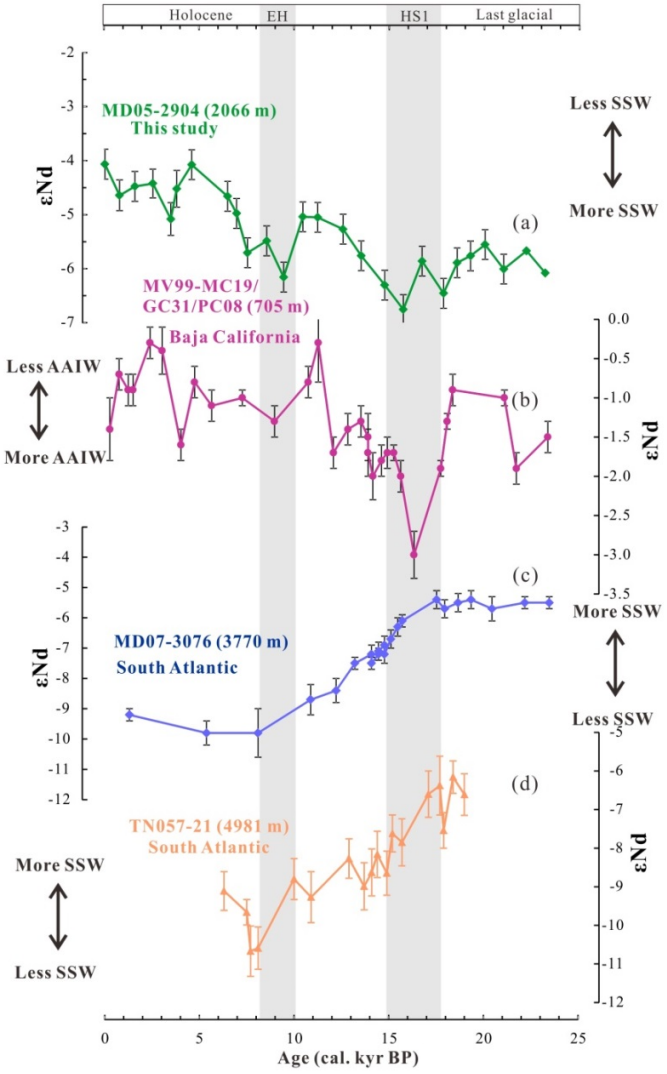

Figure 5.6. Comparison of εNd record in this study (a) with εNd records in the Pacific Ocean and the South Atlantic. (b) εNd records from the Baja California obtained from fish debris (Basak et al., 2010). (c) εNd records from the South Atlantic MD07-3076 obtained from uncleaned planktonic foraminifera (Skinner et al., 2013). (d) εNd records from the South Atlantic core TN057-21 obtained from uncleaned planktonic foraminifera (Piotrowski et al., 2012). EH and HS 1represent "early Holocene" and "Henrich Stadial 1", respectively.

Nevertheless, the global deep ocean circulation changed during the last glaciation and numerous records of $\delta^{13}C$, obtained on benthic foraminifera in different oceanic basins, provide evidence for altered Southern Ocean deep water (Ninnemann and Charles, 2002; Keigwin, 1998). In figure 5.7, we outline, for the purpose of comparison, the $\delta^{13}C$ records obtained from the benthic foraminifera *cibicides wuellerstorfi* from the northern SCS (core SO50-31KL, located close to the study site) together with results from the South Atlantic (RC11-83) and the North Pacific (core GGC-37) (Fig. 5.7c, 5.7d). Despite a spatial heterogeneity in the $\delta^{13}C$ records observed in the Atlantic sector of the Southern Ocean and in the North Pacific, in general the last glacial period is characterised in all ocean basins by lower $\delta^{13}C$ than is the case for the Holocene. This implies a reduced North Atlantic Deep Water input to the south and an increase in the northward propagation of the SSW during the last glacial period, in agreement with the lower εNd values observed in core MD05-2904. More specifically, the εNd record of core MD05-2904 exhibits an evolution which is similar to the $\delta^{13}C$ record obtained from core SO50-31KL, located close to the study site (Fig. 5.7b). The large negative excursions of εNd (-6.7), coeval with the HS1 cold interval (around 15.7 cal kyr BP), correspond to a negative shift in the $\delta^{13}C$, centred around 16 cal kyr BP, observed in core SO50-31KL. The increases in εNd values between 15 and 10.5 cal kyr BP, which coincide with the B-A and the YD, are also associated with an increase in the $\delta^{13}C$ obtained from benthic foraminifera cibicides wuellerstorfi. A second negative shift in εNd values, between 10 and 7.5 cal kyr BP, is also associated with negative shifts in the $\delta^{13}C$ of *cibicides wuellerstorfi*. This correlation supports the hypothesis of a major re-organization of deep water masses in the Philippine Sea over the past 25 kyr, with a higher relative proportion of SSW during the last glacial period, as well as during the intervals 18-16 cal kyr BP (coeval with the HS1) and 10-7.5 cal kyr BP (coeval with the early Holocene warm interval). The two negative shifts in εNd values are also mirrored in several $\delta^{13}C$ records obtained from benthic foraminifera *cibicides wuellerstorfi* from the high latitudes of the North Pacific (Keigwin, 1998; Wei et al., 2006) (Fig. 5.7b, 5.7d).

In addition, the timing of the major fluctuations in the deep-water εNd observed in core MD05-2904 is broadly in agreement with the published εNd record from the eastern Pacific Ocean, which was obtained at mid-depth (MV99-MC19/GC31/PC08, Baja California, 705 m water depth 23.5°N, 111.6°W, Fig. 5.1 and Fig. 5.6b) and which spans the Termination I and the Holocene. The mid-depth water near Baja California revealed relatively more negative εNd values (Fig. 5.6b) associated with extremely depleted-^{14}C during the HS1 cold event (Basak et al., 2010; Marchitto et al., 2007). This has been explained by an increasing flux of the Antarctic

Intermediate Water (AAIW) (Basak et al., 2010) (Fig. 5.6b). The three intervals of decreasing seawater εNd observed in core MD05-2904 (18-16 cal kyr BP; 10-7.5 cal kyr BP and around 3.5 cal kyr BP) are associated with a decrease in the mid-depth seawater εNd in core MV99-MC19/GC31/PC08, suggesting that the northward penetration of the AAIW in the high latitudes of the North Pacific is also associated, at greater water depths, with a northward penetration of the SSW in the north-western subtropical Pacific. This is particularly evident for the time interval corresponding to the HS1 (between 17 and 15 cal kyr BP). In contrast, the small decrease of the εNd observed in core MV99-MC19/GC31/PC08 between 12.8 and 11.5 cal kyr BP (coeval with the YD event) is not associated with any changes in the seawater εNd record of the northern SCS.

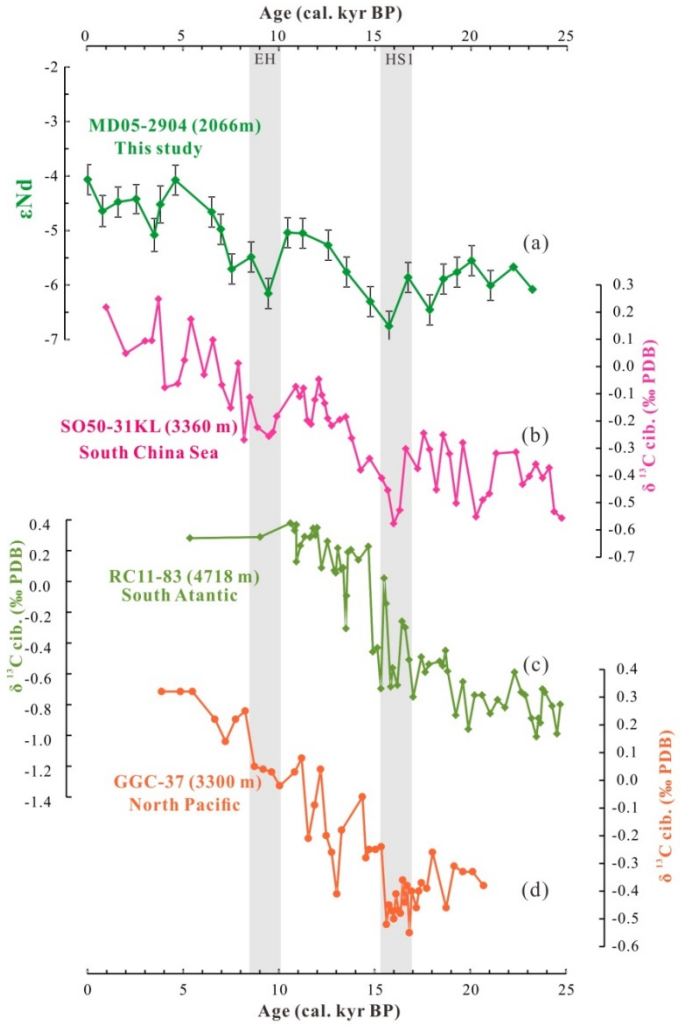

Figure 5.7. Comparison of εNd records in this study (a) with benthic $\delta^{13}C$ records. (b) Benthic $\delta^{13}C$ record from core RC11-83 in the South Atlantic (Charles et al., 1996). (c) Benthic $\delta^{13}C$ record from core SO50-31KL in the SCS (Wei et al., 2006). (d) Benthic $\delta^{13}C$ record from core GGC-37 in the North Pacific (Keigwin, 1998).

For the last deglaciation, Antarctic ice core records indicate a significant increase in atmospheric CO_2 concentrations during the Northern Hemisphere cold events HS1 (Shemesh et al., 2002; Monnin et al., 2001, Fig. 5.8e). This has been attributed to a restart of ocean ventilation in the Southern Ocean that released trapped old carbon from the deep ocean into the atmosphere during the HS1 event (Marchitto et al., 2007; Siani et al., 2013; Galbraith et al., 2007; Broecker and Barker, 2007; Burke and Robinson, 2012). This is well illustrated in previously published records of foraminifera benthic-planktonic ^{14}C age and $\delta^{13}C$ differences that provide evidence for an enhanced upwelling in the Southern Ocean (Siani et al., 2013, Fig. 5.8c, 5.8d) coeval with the negative shift in εNd values observed in core MD05-2904 between 17 and 15 cal kyr BP. This more intense upwelling is also observed in biogenic opal flux (Fig. 5.8b; Anderson et al., 2009) and is attributed to a polar-ward shift of the westerlies. This would have induced increased formation of SSW (Anderson et al., 2009). Consequently, the MD05-2904 εNd record is the first to provide evidence that restored ocean ventilation in the Southern Ocean during the HS1 is associated with an increase in UCDW formation: the UCDW subsequently propagated northwards and changed the water structure further north. We suggest that during the HS1, the northward propagation of the AAIW observed near Baja California is also associated with a major re-organization of the deeper-water masses and a northward propagation of the UCDW to the western subtropical Pacific.

5.5.6. Implications for Holocene hydrology

The early Holocene (from 10 to 7.5 cal kyr BP) is associated with a negative shift in □Nd values for the northern SCS, which is also observed at mid-depth in the north-east of the North Pacific (core MV99-MC19/GC31/PC08). This shift suggests the presence of a higher relative proportion of SSW. This εNd shift differs from the South Atlantic εNd records that indicate a relatively continuous diminishment in the proportion of SSW at the beginning of the Holocene (Skinner et al., 2013) (Fig. 5.6). In addition, the negative shift of the εNd values is not associated with any changes in the upwelling record along the southern Chile Margin (Core MD07-3088) (Siani et al., 2013) (Fig. 5.8c, 5.d). Taking into consideration the dating uncertainty, this event is coeval with a period of increased vertical ventilation (between 10-9 cal kyr BP) indicated by differences between the ^{14}C ages of benthic and planktonic foraminifera from core MD07-3076, which is located in the South Atlantic (Skinner et al., 2010, Fig. 5.9a). Such results might suggest a reduction in the NADW contribution and a higher relative

proportion of the CDW (AABW) in the South Atlantic. Consequently, the negative shift in the εNd values observed at the beginning of the Holocene in the Northern SCS sediments might also indicate increased formation of SSW that propagated northwards to the north-western subtropical Pacific Ocean.

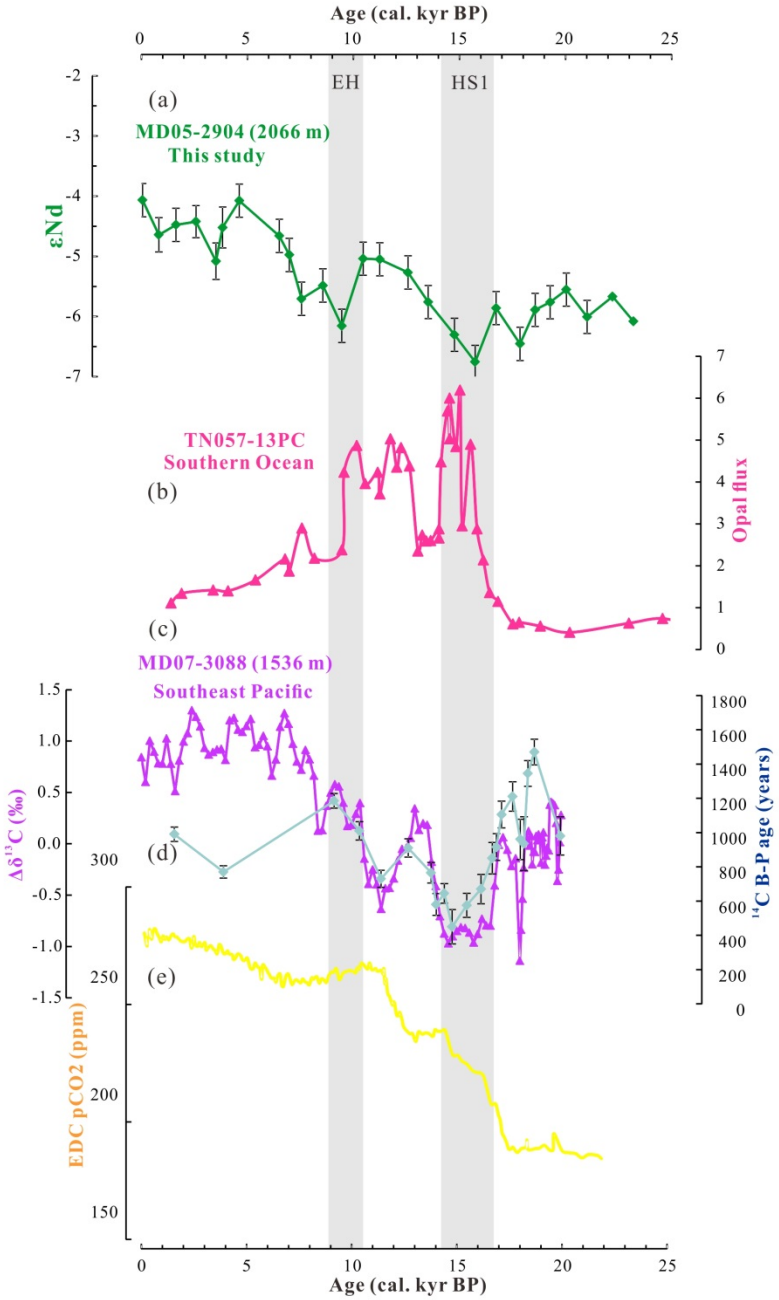

Figure 5.8. Comparison of εNd record from core MD05-2904 (a) with paleoclimatic records. (b) Opal flux variations in the Southern Ocean (Anderson et al., 2009). (c) $\Delta\delta^{13}C$ in core MD07-3088 (Siani et al., 2013) (d) Benthic-planktonic ^{14}C age difference from core MD07-3088 (Siani et al., 2013). (e) Atmospheric CO_2 from Antarctic ice-core EDC (Monnin et al., 2001). EDC represents ice core (EPICA Dome C).

However, we cannot exclude the possibility that this negative shift in the εNd observed in the northern SCS is also associated with weak ventilation in the North Pacific at the beginning of the Holocene. Past ventilation states of water masses, obtained from core PC C90002A (located off Shimokita peninsula) (Fig. 5.1), indicate a stratification of water masses, a reduction in the production of the NPIW and a greater influence of SSW between 11 and 8 can kyr BP (Rella and Uchida, 2014, Fig. 5.9b). Rella and Uchida (2014) suggest that the mid-depth NW Pacific ventilation state responded to changes in overturning in the Southern Ocean forced by latitudinal displacement of the southern westerly winds. However, the beginning of the Holocene is also associated with an intensification of East Asian monsoon rainfall with a northward displacement of the ITCZ. We suggest that this could have induced fresher sea surface water in the NW Pacific and a reduction in the NPIW. A decrease in the formation of NPIW would have resulted in the less radiogenic NPIW εNd values as observed in core BOW-8A, which displays less radiogenic εNd at the beginning of the Holocene (-1) than during the LGM (+1). This, ultimately, could have resulted in a significant decrease in the εNd of the NPDW. This hypothesis needs to be further investigated in the future.

From 7.5 cal kyr BP onwards, εNd values are similar to the present day εNd values for the PDW of the Philippine Sea (Amkawa et al., 2009; Wu et al., in prep.a), suggesting that the present day circulation in the western subtropical Pacific Ocean was already fully established at that time, with similar relative proportions of northern versus southern-sourced water masses. We cannot ignore a negative shift in εNd values between 3 and 4 cal kyr BP, also observed in the mid-depth core of Baja California (Basak et al., 2010, Fig. 5.4c), that suggests a significant increase in the proportion of SSW in the North Pacific. This implies a major re-organization of the North Pacific intermediate- and deep-water masses around 3.5 cal kyr BP. However, this interesting oceanic re-organization cannot be easily correlated with variations in deep-water masses in the southern Ocean and the Atlantic Ocean.

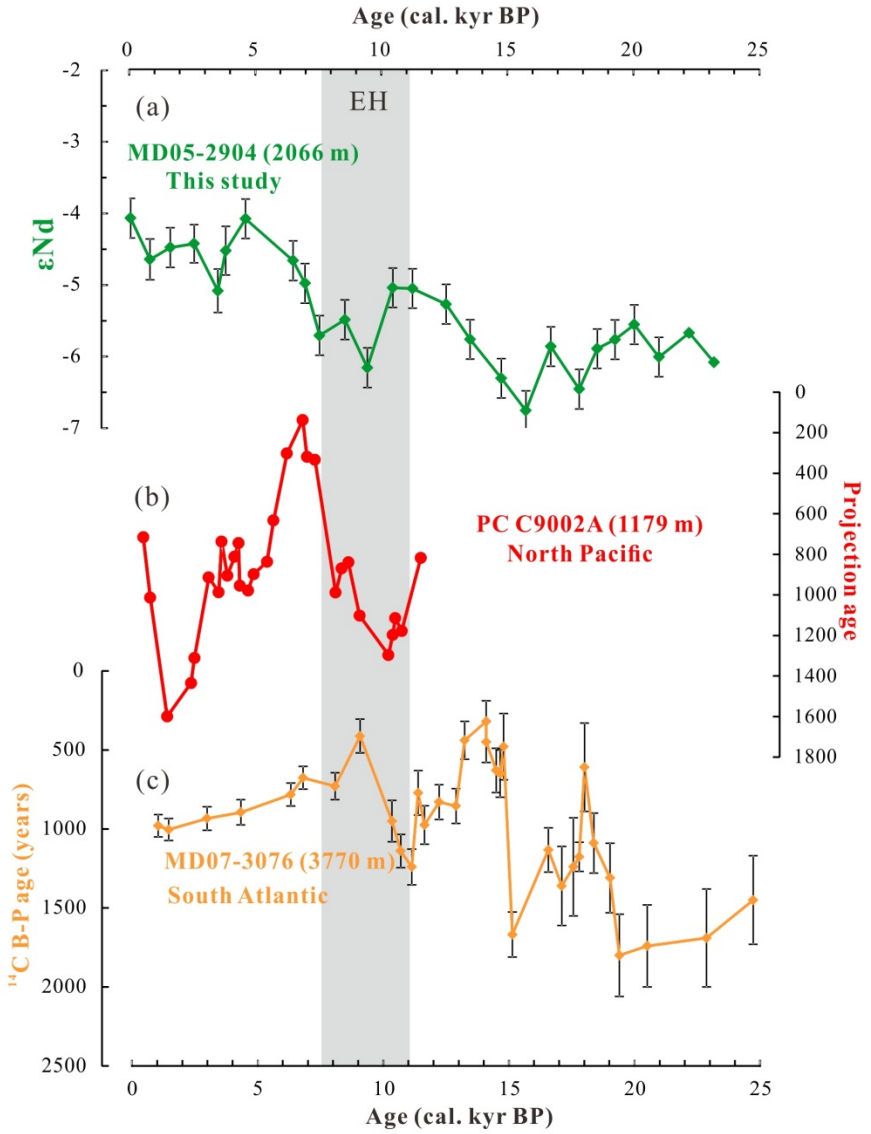

Figure 5.9. Comparisons of εNd record from core MD05-2904 (a) with ventilation changes in the North Pacific (b) (Rella and Uchida, 2014) and the Southern Ocean (c) (Skinner et al., 2010).

5.6. Conclusions

Mn, Ca and REE concentrations, and Nd isotopic composition (εNd), have been analysed on cleaned planktonic foraminifera *G. ruber* from core MD05-2904 (collected on the north-western margin of the South China Sea) in order to reconstruct hydrological variations in the western subtropical North Pacific over the past 25 cal kyr BP. Mn/Ca, Nd/Ca and PAAS-normalized REE patterns obtained from oxidatively- and reductively cleaned foraminifera and cleaning solutions indicate clearly that common cleaning procedures applied to foraminifera do not efficiently remove the Fe-Mn coating. This means that εNd values

obtained from cleaned planktonic foraminifera record the εNd of the bottom water.

εNd obtained from foraminifera displays a wide range of values, from -4.1±0.2 to -6.8±0.3, suggesting major changes in the contributions of the NPDW (εNd = -4) and the UCDW (εNd -6 to -8) in the subtropical western Pacific. The seawater εNd record obtained from core MD05-2904 correlates well with the $\delta^{13}C$ record obtained from benthic foraminifera *Cibicides wuellerstorfi* in the northern SCS and Southern Ocean, thereby confirming that the εNd record reflects global circulation changes. The deep-water εNd record of core MD05-2904 is also in agreement with published εNd records from the eastern Pacific Ocean obtained at mid-depth near Baja California. These records span the last deglaciation and the Holocene and suggest that the northward penetration of the AAIW in the high latitudes of the North Pacific is also associated, at greater water depths, with a northward penetration of the SSW in the north-western subtropical Pacific.

The LGM is characterised by an εNd value (-6.5) that is relatively unradiogenic compared to those of the Holocene, implying a slowdown of the NPDW formation to the north and/or a higher propagation of the UCDW. A higher proportion of the SSW can be clearly observed during the Northern Hemisphere HS1 interval, indicating that the greatest northward propagation of SSW was coeval with an increase in AAIW formation in the southern Ocean. This major event was followed by a gradual decrease in the proportion of the SSW in the western Pacific until 10 to 8 cal kyr BP when a negative shift in the εNd occurred. This event may have been associated with increased SSW production as has been recently observed in the South Atlantic. However, we cannot exclude a possible reduction in the NPIW in the North Pacific induced by an intensification of summer East Asian monsoon rainfall. After 7.5 cal kyr BP, the εNd record suggests that the present day circulation in the western subtropical Pacific Ocean was already fully established with similar relative proportions of northern- versus southern-sourced water masses.

Acknowledgements

We thank the captain, officers and crews of the R/V Marion-Dufresne for their co-operation in the collection of sediment cores during the MARCO POLO cruise of the International Marine Past Global Change Study (IMAGES) program in 2005. Louise Bordier is acknowledged for her assistance with analytical and laboratory work. This project was

supported by the French-Chinese International Associated Laboratories (LIA) project MONOCL, the ‘’Agence Nationale de la Recherche’’ through the MONOPOL project and the ANR-10-LABX-18-01.

Chapter 6

Conclusions

The main objective of this study is to reconstruct the hydrological evolution of the western subtropical North Pacific Ocean by using εNd proxy analysed on foraminifera and dispersed authigenic ferromanganese oxide precipitates in sediments from deep-sea cores collected in the northern SCS. As the distribution of the Nd isotopic compositions of seawater from the Philippine Sea and the SCS were not available prior to this study, it was necessary firstly i) to determine the present day distribution of seawater εNd in the SCS and the Philippine Sea and ii) to establish water masse exchanges between the SCS and the Philippine Sea through the deep channel of Luzon Straits. Although Nd isotopes extracted from sediment archives have been widely used over the past decade to reconstruct past seawater εNd changes at various time scales, the analytical procedure used to extract the Nd isotopic signal from foraminifera, and the leaching of the Fe-Mn oxide of the sediments, need to be evaluated for each site rather than being used as a simple method that can be uniformly applied. On the one hand, it was demonstrated that εNd extracted from the leaching of the Fe-Mn oxide of the sediments is strongly dependent of the lithology of the sediment and marine environments. On the other hand, while the Nd isotopic composition obtained from benthic foraminifera can undoubtedly be used to reconstruct bottom εNd seawater records, the significance of εNd values obtained from reductively and non-reductively cleaned planktonic foraminifera is still under debate. Some results indicate that εNd analyzed on reductively cleaned planktonic foraminifera represents sea surface εNd, whereas other studies indicate that the cleaning procedures currently used on foraminifera were not able to remove all of the Fe-Mn coating acquired at the sediment-seawater interface. Therefore, the second step of this study was to assess the reliability of chemical procedures used to extract Nd from foraminifera and Fe-Mn coatings precipitated on bulk sediment of the northern SCS.

For the first time, investigations have been carried on 16 vertical seawater profiles collected from the Philippine Sea, the Luzon straits and the northern SCS in order to establish the εNd of the main water masses of the SCS and the Philippine Sea and to establish water mass exchange between the SCS and the Philippine Sea. Nd concentrations are comparable to reported values obtained from the Philippine Sea and the SCS (Alibo and Nozaki, 2000) and

display a gradual increase with water depths. PAAS-normalized REE patterns display a pronounced Ce anomaly together with enrichment of heavy REEs due to poor solubility of Ce, compared to the other REEs, and the relatively higher solubility of the heavy REEs in the ocean (Bertram and Elderfield, 1993). εNd of intermediate/deep-water masses of the Philippine Sea and the SCS range from -2.3 to -4.4. In general, εNd values decrease with water depth suggesting the occurrence of different water masses.

In the Philippine Sea, North Pacific Intermediate Water (NPIW) εNd values reach -2.7±0.4 at mid-depths (500 to 1400 m). The Pacific Deep Water (PDW) is characterized by a less radiogenic Nd value of -4.1±0.5. This result indicates the intrusion of water masses of southern water origin, which are characterised by unradiogenic Nd isotopic compositions, into the deep water in the Philippine Sea.

For the SCS, εNd values of deep water (below 1500 m) are homogenous (~ -4.1) and are similar to those of PDW in the Philippine Sea. These results suggest that deep waters in the SCS are fed up by the PDW. εNd values for the South China Sea Intermediate Water (SCSIW - 500-1500 m) vary from -3.0 to -3.9 and are slightly lower than the εNd of NPIW. This difference in the εNd values is due to the vertical mixing of the NPIW with the PDW in the SCS. Nd isotopic compositions of deep water obtained above or near a series of huge sediment drifts are characterized by negative εNd values ranging from -5 to -8.5. However, seawater samples investigated in several nepheloid layers from the same area do not display any impact of the Nd isotopic composition of sediment on the Nd isotopic composition of the PDW. This suggests that exchange between seawater and re-suspended sediments above drift deposit systems might take place localised and temporarily and does not significantly modify the Nd isotopic composition of the PDW that flows along the northern and western margins of the SCS after its entrance through the Luzon straits. Consequently, the spatial distribution of dissolved Nd isotopic compositions of the main water masses of the northern SCS indicate that εNd values of the intermediate and deep-water masses of the SCS are not strongly modified by Nd exchange with sediments from the margin of the northern SCS.

Finally, a compilation of the surface seawater εNd values indicates that εNd gradually decreased from the northern to the southern SCS (-3.3 to -9.5). This may be induced by riverine input and/or penetration of surface water masses from the Indian Ocean characterized by unradiogenic εNd (~ -10).

In a second step, the εNd of benthic and planktonic foraminifera and Fe-Mn coatings precipitated on sediments have been analysed for the first time for the SCS. These are compared to modern seawater εNd presented in the chapter 3 in order to assess the reliability of the extraction of past seawater εNd from SCS sediments. First of all, Ca, Mn and REE concentration measurements were performed on cleaned foraminifera and reductive cleaning solutions from downcore samples. PAAS-normalized REE patterns of foraminifera and reductive cleaning solutions are similar and are characterized by Ce-anomalies and middle REE enrichment. Such results suggest that extracted REE represents seawater-derived REE incorporated into authigenic phases. When compared with values for living foraminifera (~ 8 nmol/mol) (Pomiès et al., 2002), the higher relative Nd/Ca ratios (617.7 ~ 1981.4 nmol/mol) obtained from reductively cleaned foraminifera confirmed that authigenic phases (i.e. Fe-Mn coatings), rather than foraminifera calcite, are the main phases carrying the Nd (Palmer, 1985; Tachikawa et al., 2013; Robert et al., 2012). Mn/Ca and Nd/Ca ratios obtained on reductively/non reductively cleaned foraminifera show no clear correlation indicating that the cleaning process could not completely remove the Nd associated with authigenic phases. Consequently, such result indicates that Nd extracted from both of the cleaned foraminifera and non-cleaned foraminifera reflect pore water and/or bottom water Nd signature in agreement with other recent studies (Pomiès et al., 2002; Kraft et al., 2013). In addition, εNd obtained from both core-top and downcore samples shows no difference between cleaned planktonic foraminifera, cleaned benthic foraminifera and reductive cleaning solutions. The εNd of the core-top foraminifera from the northern core presents values of around -4.1 that are similar to modern deep-water εNd in the northern SCS. This further confirmed that Nd isotopic compositions of uncleaned foraminifera are overprinted by Nd deriving from authigenic Fe-Mn coatings precipitated on foraminifera. Consequently, εNd values obtained on cleaned foraminifera, as well as on benthic foraminifera and associated authigenic phases, record bottom and/or pore-water εNd.

In contrast, Nd isotopic compositions of bulk sediment leachates are more complicated than that of foraminifera. Nd isotopic compositions obtained from acid-reductive HH leachates of bulk non-decarbonated sediment exhibit similar εNd values to those of foraminifera and bottom seawater (for core top-samples). However, εNd of acid-reductive leachates of de-carbonated sediments are more negative than those obtained for foraminifera implying that they are contaminated by partial dissolution of lithogenic particles. Consequently, it is not

recommended that εNd, extracted from acid-reductive HH leachates of de-carbonated sediments from the northern SCS, be used for paleohydrological reconstruction. Instead, Nd incorporated in the foraminifera is proposed as a reliable tool to reconstruct past seawater εNd records.

Based on the reliable proxy of εNd from the planktonic foraminifera, high resolution seawater εNd records were obtained from core MD05-2904 (19º27.32´ N, 116º15.15´ E, 2066 m water depth) in order to track water mass provenances in the western subtropical North Pacific over the last 25 cal kyr BP. Large variations in εNd values between the LGM (-5.9±0.2) and the late Holocene (-4.1±0.2) are observed. The possibility of significant modification of the seawater εNd through the process of "boundary exchange" has been discounted due to the nearly constant Nd isotopic composition characterizing the sediment of the northern SCS margin since the LGM (Boulay et al., 2005; Hu et al., 2012). Such variations mainly reflect a change, through time, of the relative proportions of the northern sourced water (North Pacific Deep Water, NPDW, εNd = ~ -4) and the southern sourced water (Upper Circumpolar Deep Water, UCDW, εNd= ~ -8) in the Philippine Sea. It has been suggested that the formation of North Pacific Intermediate Water (NPIW) intensified when NADW formation slowed down during the last glacial period. This glacial NPIW was characterized by more radiogenic εNd due to the downward intrusion of more radiogenic surface seawater (Horikawa et al., 2010). However, a more negative shift of seawater εNd values in the SCS during the last glacial period excludes such a hypothesis and implies an intensified northward propagation of southern sourced water to the western subtropical North Pacific (glacial εNd =~ -6).

Furthermore, the timing of the major fluctuations in the deep-water εNd observed in core MD05-2904 is broadly in agreement with the published εNd record from the eastern Pacific Ocean: this eastern Pacific record (core MV99-MC19/GC31/PC08) was obtained at mid-depth near Baja California. The three intervals of decreasing seawater εNd observed in core MD05-2904 (18-16 cal kyr BP; 10-7.5 cal kyr BP and around 3.5 cal kyr BP) are also associated with a decrease in the mid-depth seawater εNd in core MV99-MC19/GC31/PC08, suggesting that the northward penetration of the AAIW in the high latitudes of the North Pacific is also linked, at greater water depths, with a northward penetration of the SSW in the north-western subtropical Pacific. This is particularly evident for the time interval corresponding to the HS1 (between 18 and 16 cal kyr BP) when stronger ventilation in the Southern Ocean, and decreased formation of the NADW, have been observed (Basak et al., 2010; Siani et al., 2013). The second

negative excursion of εNd between 10 and 7.5 cal kyr BP could be associated with more pronounced ventilation in the Southern Ocean, as has been recently observed in the South Atlantic, and/or with a possible reduction in the formation of NPIW in the North Pacific induced by an intensification of the summer East Asian monsoon rainfall. After 7.5 cal kyr BP, the εNd record suggests that the present day circulation in the western subtropical Pacific Ocean was already fully established, with similar relative proportions of northern- versus southern-sourced water masses. Finally, a negative shift in εNd values between 3 and 4 cal kyr BP, also observed in the mid-depth core of Baja California, suggests a significant increase in the proportion of SSW in the North Pacific. This implies a major re-organization of the North Pacific intermediate- and deep-water masses around 3.5 cal kyr BP that needs to be further investigated in the future.

Perspectives

(1) Previous studies indicate that “boundary exchange” plays an important role in the Nd budget of the ocean, particularly in the marginal area (Lacan and Jeandel, 2005). This process of “boundary exchange” has been observed along several ocean margins whereas other regions of the ocean seem not to be affected. The mechanism responsible for this process of Nd exchange between marginal sediment and seawater is still not understood but could potentially allow us to constrain the sources of other REE and metal elements (potential pollution) in the Ocean. In this study, while the modification of εNd was restricted to the seawater collected from sites near large drift sediment deposits, Nd isotopic composition analysed on seawater collected from nepheloid layers does not indicate Nd exchange between the suspended particles and the seawater. Therefore, in order to better understand how “boundary exchange” influences the seawater εNd, the mass balance calculation of Nd concentration particle flux and seawater needs to be further investigated on nepheloid layers above these large sediment drift deposits. It is also important to determine which processes are responsible for such local modifications of the seawater εNd above these drift sediment deposits and which mineralogical phases and/or diagenetic processes are involved in such Nd exchanges between sediments and bottom waters.

(2) Previous observation indicated a seasonal variation in water exchange at mid-depths between the SCS and the Philippine Sea (Tian et al., 2006; Yang et al., 2010). As the SCSIW and the NPIW are characterized by different Nd isotopic compositions, εNd can be used to

identify the water masses in order to track water mass exchange in the SCSIW and the NPIW between the Philippine Sea and the SCS. In addition, εNd values of foraminifera from core-top samples retrieved from the southern SCS exhibit a more negative bottom water εNd compared to that of the northern SCS. More studies of the deep water in the southern SCS need to be carried out in order to better constrain the spatial distribution of deep-water εNd in the southern SCS.

(3) Nd records extracted from planktonic foraminifera and bulk sediment leachates are still a controversial issue. It is now well established that Nd enriched into planktonic foraminifera at the sediment-seawater interface overwrites Nd incorporated into living planktonic foraminifera in the water column. However, the mechanism of incorporation and the exact source of the Nd (seawater or pore-water) are still not well established. In the future, planktonic foraminifera retrieved from sediment traps and/or plankton tows at different depths, together with planktonic foraminifera separated from surface sediment, could be tested to better understand the exchange of Nd incorporated into foraminifera calcite and Nd carried by authigenic phases accumulated in the water column and sediment-seawater interface.

In addition, it is important to establish a means of reliably extracting seawater-derived Nd from bulk sediment and of avoiding contamination from the detrital fraction during the leaching process. Nd extracted from bulk sediment needs to be tested step by step to obtain Nd concentration and εNd in solution collected from each step and those in the detrital fraction for comparison. The influence of the reagent also needs to be evaluated for each leaching process.

(4) Reconstructed past hydrological changes in the western Pacific indicated that, in general, water mass changes are a response to northward propagation of southern sourced water from the Southern Ocean during the last deglaciation. Nevertheless, two events observed in the SCS during the Holocene are not associated with the hydrological changes in the Southern Ocean. The cause of these changes is not yet well constrained and could imply a modification of NPIW formation. Further investigations using εNd proxy in the western North and South Pacific are necessary in order to better understand such hydrological changes.

References

Abouchami W., Goldstein S. L., Galer S. J. G., Eisenhauer A., Mangini A. (1997). Secular changes of lead and neodymium in central Pacific seawater recorded by a Fe-Mn crust. Geochimica and Cosmochimica Acta 61, 3957–3974.

Ahagon N., Ohkushi K., Uchida M., Mishima T. (2003). Mid-depth circulation in the northwest Pacific during the last deglaciation: Evidence from foraminiferal radiocarbon ages, Geophysical Research Letters 30, doi:10.1029/2003GL018287.

Alibo D. S., Nozaki Y. (1999). Rare earth elements in seawater: Particle association, shale-normalization and Ce oxidation. Geochimica and Cosmochimica Acta 63, 363–372.

Alibo D. S., Nozaki Y. (2000). Dissolved rare earth elements in the South China Sea: Geochemical characterization of the water masses. Journal of Geophysical Research 105, 28,771-28,783.

Amakawa H., Alibo D. S., Nozaki Y. (2000). Nd isotopic composition and REE pattern in the surface waters of the eastern Indian Ocean and its adjacent seas. Geochimica and Cosmochimica Acta 64, 1715–1727.

Amakawa H., Nozaki Y., Alibo D. S., Zhang J., Fukugawa K., Nagai H. (2004). Neodymium isotopic variations in Northwest Pacific water. Geochimica et Cosmochimica Acta 68, 715–727.

Amakawa H., Sasaki K., Ebihara M. (2009). Nd isotopic composition in the central North Pacific. Geochimica et Cosmochimica Acta 73, 4705–4719.

Amakawa H., Tazoe H., Obata H., Gamo T., Sano Y., Shen C. C. (2013). Neodymium isotopic composition and concentration in the Southwest Pacific Ocean. Geochemical Journal 47, 409-422.

An Z. S., Porter S. C., Kutzbach J. E., Wu X. H., Wang S. M., Liu X. D., Li X. Q., Zhou W. J. (2000). Asynchronous Holocene optimum of the East Asian monsoon. Quaternary Science Reviews 19, 743-762.

Anderson R.F., Lao Y., Broecker W. S., Trumbore S. E., Hofmann H. J., Wolfli W. (1990). Boundary scavenging in the Pacific Ocean: acomparison of 10Be and 231Pa. Earth and Planetary Science Letters 96, 287–304.

Anderson R.F., Ali S., Bradtmiller L.I., Nielsen S.H.H., Fleisher M.Q., Anderson B.E., Burckle L.H. (2009). Wind-Driven Upwelling in the Southern Ocean and the Deglacial Rise in Atmospheric CO_2. Science, 323, 1443–1448.

Arsouze T., Dutay J.-C., Lacan F., Jeandel C. (2007). Modeling the neodymium isotopic composition with a global ocean circulation model. Chemical Geology 239, 165-177.

Arsouze T., Dutay J.-C., Lacan F., Jeandel C. (2009). Reconstructing the Nd oceanic cycle using a coupled dynamical-biogeochemical model. Biogeosciences 6, 2829-2846.

Arsouze T., TreguierA. M., Peronne S., Dutay J.-C., Lacan F., Jeandel C. (2010). Modeling the Nd isotopic composition in the North Atlantic basin using an eddy-permitting model. Ocean Science 6, 789-797.

Barker S., Knorr G., Vautravers M., Diz P., Skinner L.C. (2010). Extreme deepening of the Atlantic overturning circulation during deglaciation. Nature Geoscience 3, 567–571.

Basak C., Martin E. E., Horikawa K. Marchitto T. M. (2010). Southern Ocean source of ^{14}C-depleted carbon in the North PacificOcean during the last deglaciation. Nature Geoscience 3, 770-773.

Bau M., Koschinsky A. (2009). Oxidative scavenging of cerium on hydrous Fe oxide: Evidence from the distribution of rare earth elements and yttrium between Fe oxides and Mn oxides in hydrogenetic ferromanganese crusts. Geochemical Journal 43, 37–47.

Bayon G., German C.R., Burton K.W., Nesbitt R.W., Rogers N. (2004). Sedimentary Fe–Mn oxyhydroxides as paleoceanographic archives and the role of aeolian flux in regulating oceanic dissolved REE. Earth and Planetary Science Letters 224, 477–492.

Bayon G., Birot D., Ruffine L., Caprais J. C., Ponzevera E., Bollinger C., Donval J. P., Charlou J. L., Voisset M., Grimaud S. (2011) Evidence for intense REE scavenging at cold seeps from the Niger Delta Margin. Earth and Planetary Science Letters 312, 443–452.

Beaufort L., de Garidel-Thoron T., Linsley B., Oppo D., Buchet N. (2003). Biomass burning and oceanic primary production estimates in the Sulu Sea area over the last 380 kyr and the East Asian monsoon dynamics. Marine Geology 201, 53-65.

Bellon H., Yumul G.P. Jr. (2001). Miocene to Quaternary adakites and related rocks in western Philippine arc sequences. Comptes Rendus de l'Académie des Sciences 333, 343-350.

Bostock H. C., Opdyke B. N., Williams M. J. M., (2010). Characterising the intermediate depth waters of the Pacific Ocean using δ^{13}C and other geochemical tracers. Deep-Sea Research I 57, 847-859.

Bourdin C., Douville E., Genty D. (2011). Alkaline-earth metal and rare-earth element incorporation control by ionic radius and growth rate on a stalagmite from the Chauvet Cave, Southeastern France. Chemical Geology 290, 1-11.

Boulay S., Colin C., Trentesaux A., Frank N., Liu Z. (2005). Sediment sources and East Asian monsoon intensity over the last 450 ky: Mineralogical and geochemical investigations on South China Sea sediments. Palaeogeography, Palaeoclimatology, Palaeoecology 228, 260-277.

Boyle E. A. (1983). Manganese carbonate overgrowths on foraminifera tests. Geochimica and Cosmochimica Acta 47, 1815–1819. http://dx.doi.org/10.1016/0016-7037(83)90029-7.

Boyle, E. A. (1988). Cadmium: chemical tracer of deepwater paleoceanography. Paleoceanography 3, 471–489.

Broecker W. S., Peng. T. H. (1982). Tracers in the Sea. Lamont-Doherty Geological

Observatory, Palisades, N.Y.

Broecker W. S., Denton G. H. (1990). The role of ocean–atmosphere reorganizations in glacial cycles. Quaternary Science Reviews 9, 305–341.

Broecker W. S., Peng T. H. (1987). The role of $CaCO_3$ compensation in the glacial to interglacial CO2 change, Global Biogeochemical Cycles 1, 15–30.

Broecker W. S (1998). Paleocean circulation during the last deglaciation: A bipolar seesaw?. Paleoceanography 13, 119-121.

Broecker W.S., Barker S. (2007). A 190% drop in atmosphere's $\Delta^{14}C$ during the "Mystery Interval" (17.5 to 14.5 kyr). Earth and Planetary Science Letters 256, 90–99.

Bryan, S. P., Marchitto, T. M., and Lehman, S. J. (2010). The release of 14C-depleted carbon from the deep ocean during the last deglaciation: Evidence from the Arabian Sea. Earth and Planetary Science Letters 298, 244–254.

Bühring C., Sarnthein M., Erlenkeuser H. (2004). Toward a high resolution stable isotope stratigraphy of the last 1.1 m.y.: Site 1144, South China Sea. In: Prell W.L., Wang P., Blum P., Rea D.K. and Clemens S.C. (eds), Proc. ODP, Sci. Results 184: 1-29 [Online].

Burke A., Robinson L.F. (2012). The Southern Ocean's role in carbon exchange during the last deglaciation. Science 335, 557-561.

Butzin M., Prange M., Lohmann G. (2005). Radiocarbon simulations for the glacial ocean: the effect of wind stress, Southern Ocean sea ice and Heinrich events, Quaternary Science Reciews 24, 1781-1796;

Burton K. W., Vance D. (2000). Glacial–interglacial variations in the neodymium isotope composition of seawater in the Bengal Fan recorded by planktonic foraminifera. Earth and Planetary Science Letters 176, 425–441.

Byrne R. H., Sholkovitz E. R. (1996). Marine chemistry and geochemistry of the lanthanides, in Handbook on the Physics and Chemistry of Rare Earths, Elsevier Sci., New York, pp. 527–537.

Carter P., Vance D., Hillenbrand C. D., Smith J. A, Shoosmith D. R. (2012). The neodymium isotopic composition of waters masses in the eastern Pacific sector of the Southern Ocean. Geochimica and Cosmochimica Acta 79, 41–59.

Caruso M.J., Gawarkiewicz G.G., Beardsley R. (2006). Interannual variability of the Kuroshio intrusion in the South China Sea. Journal of Oceanography 62, 559–575.

Chao S.V., Shaw P.T., Wu S.Y. (1996). Deep water ventilation in the South China Sea. Deep-Sea Research II 43, 445-466.

Charles C. D., Wright J. D., Fairbanks R.G. (1993). Thermodynamic influences on the marine carbon-isotope record. Paleoceanography 8, 691– 697.

Charles C. D., Lynch-Stieglitz J., Ninnemann U. S., Fairbanks R. G. (1996). Climate connections between the hemisphere revealed by deep sea sediment core/ice core correlations. Earth and Planetary Science Letters 142, 19–27.

Chen C-T., Huang M. (1996). A mid-depth front separating the South China Sea water and the Philippine Sea water. Journal of Oceanography 52: 17-52.

Chen C.-T., Wang S. L., Wang B. J., Pai S. C. (2001). Nutrient budgets for the South China Sea basin. Marine Chemistry 75, 281–300.

Chester R., Hughes M. J. (1967). A chemical technique for the separation of ferro-manganese minerals, carbonate minerals and adsorbed trace elements from pelagic sediments. Chemical Geology 2, 249–262.

Chikamoto M. O., Menviel L., Abe-Ouchi A., Ohgaito R., Timmermann A., Okazaki Y., Harada a, AkiraOka N., Mouchet A. (2012). Variability in North Pacific intermediate and deep water ventilation during Heinrich events in two coupled climate models. Deep-Sea Research II 61-64, 114–126.

Clark P. U., Pisias N. G., Stocker T. F., Weaver A. J. (2002). The role of the thermohaline circulation in abrupt climate change. Nature 415, 863–869.

Clemens S. C., Murray D. W., Prell W. L. (1996). Nonstationary phase of the Plio-Pleistocene Asian monsoon. Science 274, 943-948.

Clement A. C., Peterson L. C. (2008). Mechanisms of abrupt climate change of the last glacial period. Reviews of Geophysics 46, doi:10.1029/2006RG000204.

Clemens S. C., Prell W., Murray D., Shimmield G., Weedon G. (1991). Forcing mechanisms of the Indian Ocean monsoon. Nature 353, 720-725.

Clemens S. C., Prell W. (2003). A 350,000 year summer-monsoon multi-proxy stack from the Owen Ridge, Northern Arabian Sea. Marine Geology 201, 35-51.

Colin, C., Frank N., Copard K., Douville E. (2010). Neodymium isotopic composition of deep - sea corals from the NE Atlantic: Implications for past hydrological changes during the Holocene, Quaternary Science Reviews 29, 2509–2517.

Colin C., Kissel C., Blamart D., Turpin L. (1998). Magnetic properties of sediments in the Bay of Bengal and the Andaman Sea: impact of rapid North Atlantic Ocean climatic events on the strength of the Indian monsoon. Earth and Planetary Science Letters 160, 623-635.

Colin C., Turpin L., Bertaux J., Desprairies A., Kissel C. (1999). Erosional history of the Himalayan and Burman ranges during the last two glacial-interglacial cycles. Earth and Planetary Science Letters 171, 647-660.

Copard, K., Colin C., Douville E., Freiwald A., Gudmundsson G., de Mol B., Frank N. (2010), Nd isotopes in deepsea corals in the North - eastern Atlantic. Quaternary Science Reviews 29, 2499–2508.

Copard K., Colin C., Frank N., Jeandel C., Montero-Serrano J. C., Reverdin G., Ferron B. (2011). Nd isotopic composition of water masses and dilution of the Mediterranean outflow along the southwest European margin. Geochemistry Geophysics Geosystems 12, doi: 10.1029/2011GC003529

Copard, K., Colin, C., Henderson, G. M., Scholten, J., Douville, E., Sicre, M. A., Frank, N. (2012). Late Holocene intermediate water variability in the northeastern Atlantic as recorded by deep-sea corals. Earth and Planetary Science Letters 313-314, 34–44.

Curry W. B., Oppo, D.W. (2005). Glacial water mass geometry and the distribution of 13C of ΣCO2 in the western Atlantic Ocean. Paleoceanography, 20, PA1017, doi:10.1029/2004PA001021.

de Garidel-Thoron T., Beaufort L., Linsley B.K., Dannenmann S. (2001). Millennial-scale dynamics of the East-Asian winter monsoon during the last 200,000 years. Paleoceanography 16, 491-502.

Ding Z. L., Liu T., Rutter N.W. (1995). Ice-volume forcing of East Asian winter monsoon variations in the past 800,000 years. Quaternary Research 44, 149-159.

Duplessy, J. C., Shackleton N. J., Fairbanks R. G., Labeyrie L., Oppo D., Kallel N. (1988). Deep water source variations during the last climatic cycle and their impact on the global deep water circulation. Paleoceanography 3, 343–360.

Duplessy J.-C., Arnold M., Bard E., Juillet-Leclerc A., Kallel N., Labeyrie L. (1989). AMS 14C study of transient events and of the ventilation rate of the Pacific intermediate water during the last deglaciation. Radiocarbon 31, 493–502.

Elderfield H., Upstill-Goddard R., Sholkovitz E. R. (1990). The rare earth elements in rivers, estuaries, and coastal seas and their significance to the composition of ocean waters. Geochimica and Cosmochimica Acta 54, 971–991.

Elderfield, H., Greaves M. J. (1982). The rare earth elements in seawater. Nature 296, 214–219.

Elmore A. C., Piotrowski A. M., Wright J. D., Scrivner A. E. (2011). Testing the extraction of past seawater Nd isotopic composition from North Atlantic deep sea sediments and foraminifera. Geochemistry Geophysics Geosystems 12, doi.org/10.1029/2011gc003741.

Emile-Geay J., Cane M. A., Naik N., Seager R., Clement A. C., van Geen A. (2003). Warren revisited: Atmospheric freshwater fluxes and “Why is no deep water formed in the North Pacific”. Journal of Geophysics Research-Oceans 108, 3178, doi:10.1029/2001JC0010583.

Fang G. H., Fang W. D., Fang Y., Wang K. (1998). A survey of studies on the South China Sea upper ocean circulation. Acta Oceanographica Taiwanica 37, 1-16.

Farris A., Wimbush M. (1996). Wind-induced intrusion into the South China Sea. Journal of Oceanography 52, 771–784

Francois R. F., Altabet M. A., Yu E. F., Sigman D.M., Bacon M. P., Frank M., Bohrmann G.,

Bareille G., Labeyrie L.D. (1997). Water column stratification in the Southern Ocean contributed to the lowering of glacial atmospheric CO2. Nature 389, 929-935.

Frank M. (2002). Radiogenic isotopes: tracers of past ocean circulation and erosional input. Reviews of Geophysics 40, doi: 10.1029/2000RG000094.

Frank M., Whiteley N., van de Flierdt T., Reynolds B. C., O'Nions K. (2006). Nd and Pb isotope evolution of deep water masses in the eastern Indian Ocean during the past 33 Myr. Chemical Geology 226, 264– 279.

Fujii Y., Nakano T., Usui N., Matsumoto S., Tsujino H., Kamachi M. (2013). Pathways of the North Pacific Intermediate Water identified through the tangent linear and adjoint models of an ocean general circulation model, Journal of Geophysical Research: Oceans 118, 2035–2051, doi:10.1002/jgrc.20094.

Fujio S., Yanagimoto D., Taira K. (2000). Deep current structure above the Izu-Ogasawara Trench. Journal of Geophysical Research 105, 6377–6386.

Galbraith E. D., Jaccard S. L., Pedersen T. F., Sigman D., Haug G. H., Cook M., Southon J., Francois R. (2007). Carbon dioxide release from the North Pacific abyss during the last deglaciation. Nature 449, 890–893.

Gan J., Li, H., Curchitser E.N., Haidvogel D.B., (2006). Modeling South China Sea circulation: response to seasonal forcing regimes. Journal of Geophysical Research 111, doi:10.1029/2005JC003298.

Ge H., Li Q., Cheng X., Zheng H., He J. (2010). Late Quaternary high resolution monsoon records in planktonic stable isotopes from northern South China Sea. Earth Science-Journal of China University of Geosciences 35, 515–525. doi:10.3799/dqkx.2010.067.(In Chinese).

German C. R., Klinkhammer G. P., Edmond J. M., Mura A., Elderfield H. (1990). Hydrothermal scavenging of rare-earth elements in the ocean. Nature 345, 516 – 518.

Gordon A. L., Visbeck M., Huber B. (2001). Export of Weddell Sea Deep and Bottom Water. Journal of Geophysical Research 106, 9005–9017, doi:10.1029/2000JC000281.

Goldstein S.L., O'Nions R.K., Hamilton P.J. (1984). A Sm–Nd isotopic study of atmospheric dusts and particulates from river systems. Earth and Planetary Science Letters 70, 221–236.

Goldstein S.J., Jacobsen S.B., (1988). Nd and Sr isotopic systematics of River water suspended material — implications for crustal evolution. Earth and Planetary Science Letters 87, 249–265.

Goldstein S. L., Hemming S. R. (2003). Long-lived Isotopic Tracers in Oceanography, Paleoceanography and Ice Sheet Dynamics. Treatise on Geochemstry, Volume Editor: H. Elderfield; Series Editors: H.D. Holland and K.K. Turekian; Vol. 6, 453-489.

Gong G. C., Liu K. K., Liu C. T., Pai S.C. (1992). The chemical hydrography of the South China Sea west of Luzon and a comparison with the West Philippine Sea. Terr Atmos Oceanic Sci 3, 587–602

Gourlan A.T., Meynadier L., Allegre C.J. (2008). Tectonically driven changes in the Indian Ocean circulation over the last 25 Ma: neodymium isotope evidence. Earth and Planetary Science Letters 26, 353-364.

Grasse P., Stichel T., Stumpf R., Stramma L., Frank M. (2012). The distribution of neodymium isotopes and concentrations in the Eastern Equatorial Pacific: water mass advection versus particle exchange. Earth and Planetary Science Letters 353–354, 198–207.

Grenier M., Jeandel C., Lacan F., Vance D., Venchiarutti C., Cros A., Cravatte S. (2013). From the subtropics to the central equatorial Pacific Ocean: neodymium isotopic composition and rare earth element concentration variations. Journal of Geophysical Research: Oceans 118, 1–27.

Grenier M., Cravatte S., Blanke B., Menkes C., Koch-Larrouy A., Durand F., Melet A., Jeandel C. (2011). From the western boundary currents to the Pacific Equatorial Undercurrent: Modeled pathways and water mass evolutions. Journal of Geophysical Research 116, doi:10.1029/2011JC007477.

Greaves M. J., Elderfield H., Sholkovitz E. R.. (1999). Aeolian sources of rare earth elements to the Western Pacific Ocean, Marine Chemistry 68, 31–38.

Guo Z., (1985). Wintertime South China Seawarm current and thewestward current on its right. Tropical Oceanol. 4, 1–9 (in Chinese with English abstract).

Gutjahr M., Frank M., Stirling C. H., Klemm V., van de Flierdt T., Halliday A. N. (2007). Reliable extraction of a deep water trace metal isotope signal from Fe–Mn oxyhydroxide coatings of marine sediments. Chemical Geology 242, 351–370.

Gutjahr M., Frank M., Stirling C. H., Keigwin L. D., Halliday A. N. (2008). Tracing the Nd isotope evolution of North Atlantic Deep and Intermediate Waters in the western North Atlantic since the Last Glacial Maximum from Blake Ridge sediments. Earth and Planetary Science Letters 266, 61–77.

Haley B. A., Klinkhammer G. P., McManus J. (2004). Rare earth elements in pore waters of marine sediments. Geochimica and Cosmochimica Acta 68, 1265–1279.

Haley B. A., Frank M., Hathorne E., Pisias N. (2014). Biogeochemical implications from dissolved rare earth element and Nd isotope distributions in the Gulf of Alaska. Geochimica and Cosmochimica Acta 126, 455-474.

Haley B. A., Klinkhammer G. P., Mix A. C. (2005). Revisiting the rare earth elements in foraminiferal tests. Earth and Planetary Science Letters 239, 79–97.

Halliday A. N., Davidson J. P., Holden P., Owen R. M., Olivarez A. M. (1992). Metalliferous sediments and the scavenging residence time of Nd near hydrothermal vents. Geophysical Research Letter 19, 761-764.

Hannigan R. E., Sholkovitz E. R. (2001). The development of middle rare earth element enrichments in freshwaters: Weathering of phosphate minerals. Chemical Geology 175, 495–

508.

Harding D. J., Arden J. W., Rickaby R. E. M. (2006). A method for precise analysis of trace element/calcium ratios in carbonate samples using quadrupole inductively coupled plasma mass spectrometry. Geochemistry Geophysics Geosystems 7, doi:10.1029/2005GC001093.

Herguera, J. C., Herbert T., Kashgarian M., Charles C. (2010). Intermediate and deep water mass distribution in the Pacific during the Last Glacial Maximum inferred from oxygen and carbon stable isotopes. Quaternary Science Reviews 29, 1228–1245.

Higginson M., Maxwell J.R., Altabet M. A. (2003). Nitrogen isotope and chlorin paleoproductivity records from the Northern South China Sea: remote vs. local forcing of millennial- and orbital-scale variability. Marine Geology 201, 223-250.

Horikawa K., Asahara Y., Yamamoto K., Okazaki, Y. (2010). Intermediate water formation in the Bering Sea during glacial periods: Evidence from neodymium isotope ratios. Geology 38, 435–438.

Hu D., Böning P., Köhler C. M., Hillier S, Pressling N., Wan S, Brumsack H. J., Clift P. D. (2012). Deep sea records of the continental weathering and erosion response to East Asian monsoon intensification since 14 ka in the South China Sea. Chemical Geology 326–327, 1–18.

Huang W. (2004). Sediment distributional patterns and evolution in the South China Sea since the Oligocene. PhD thesis, Tongji Univ., Shanghai. pp.114.

Huang K.-F., Oppo D. W., Curry W. B. (2014). Decreased influence of Antarctic intermediate water in the tropical Atlantic during North Atlantic cold events. Earth and Planetary Science Letters 389, 200-208.

Huang K.-F., You C.-F., Chung C.-H, Lin Y.-H., Liu Z. F. (2013). Tracing the Nd isotope evolution of North Pacific Intermediate and Deep Waters through the last deglaciation from South China Sea sediments. Journal of Asian Earth Sciences 79, 564-573.

Hutchison C.S. 1989. Geological Evolution of South-East Asia. Oxford Monogr. Geol. Geophys. No. 13, Clarendon Press, Oxford, pp. 368.

Hutchison C.S. (2004). Marginal basin evolution: the southern South China Sea. Marine and Petroleum Geology 21, 1129-1148.

Ingri J., Widerlund A., Land M., Gustafsson Ö., Andersson P., Öhlander B. (2000). Temporal variations in the fraction of the rare earth elements in a boreal river: The role of colloidal particles, Chemical Geology 166, 23–45, 2000.

Insua T. L., Spivack A. J., Graham D., D'Hondt S., Moran K. (2014). Reconstruction of Pacific Ocean bottom water salinity during the Last Glacial Maximum, Geophysical Research Letters 41, 2914–2920, doi:10.1002/2014GL059575.

Jaccard S. L., Galbraith E. D. (2013). Direct ventilation of the North Pacific did not reach the deep ocean during the last deglaciation. Geophysical Research Letters 40, 199–203.

Jacobsen S. B., Wasserburg G. J. (1980). Sm-Nd isotopic evolution of chondrites. Earth and Planetary Science Letters 50, 139-155.

Jeandel C. (1993). Concentration and isotopic composition of Nd in the South Atlantic Ocean. Earth and Planetary Science Letters 117, 581-591.

Jeandel C., Bichop J. K., Zindler A. (1995). Exchange of neodymium and its isotopes between seawater and small and large particles in Sargasso Sea. Geochimica and Cosmochimica Acta 59, 535-547.

Jeandel C., Thouron D., Fieux M. (1998). Concentrations and isotopic compositions of Nd in the eastern Indian ocean and Indonesian straits. Geochimica and Cosmochimica Acta 62, 2597–2607.

Jeandel C., Arsouze T., Lacan F., Téchiné P., Dutay J.-C. (2007). Isotopic Nd compositions and concentrations of the lithogenic inputs into the ocean : A compilation, with an emphasis on the margins. Chemical Geology 239, 156-164.

Jeandel C., Delattre H., Grenier M., Pradoux C., Lacan F. (2013). Rare earth element concentrations and Nd isotopes in the Southeast Pacific Ocean. Geochemistry Geophysics Geosystems 14, 328–341.

Jian Z., Huang B., Lin H., Kuhnt W. (2001). Late Quaternary upwelling intensity and East Asian monsoon forcing in the South China Sea. Quaternary Research 55, 363-370.

Johnson H. P., Hautala S. L., Bjorklund T. A., Zarnetske M. R. (2006). Quantifying the North Pacific silica plume. Geochemistry Geophysics Geosystems 7, doi:10.1029/2005GC001065.

Johnson G. C., Toole J. M. (1993). Flow of deep and bottom waters in the Pacific at 10°N. Deep-Sea Research I 40, 371–394.

Jones C. E., Halliday A. N., Rea D. K., Owen R. M. (1994). Neodymium isotopic variations in North Pacific modern silicate sediment and the insignificance of detrital REE contributions to seawater. Earth and Planetary Science Letters127, 55–66.

Joyce T. M., Warren B. A., Talley L. D. (1986). The geothermal heating of the abyssal subarctic Pacific Ocean. Deep-Sea Research 33, 1003-1015.

Jung S. J. A., Kroon D., Ganssen G., Peeters F., Ganeshram R. (2009). Enhanced Arabian Sea intermediate water flow during glacial North Atlantic cold phases, Earth Planet. Sci. Lett., 280, 220–228.

Kaneko I., Takatsuki Y., Kamiya H. (2001). Circulation of Intermediate and Deep Waters in the Philippine Sea. Journal of Oceanography 57, 397-420.

Kashino Y., Watanabe H., Herunadi B., Aoyama M., Hartoyo D. (1999). Current variability at the Pacific entrance of the Indonesian Throughflow. Journal of Geophysical Research 104, 11021 -11035.

Kawabe M., Fujio S. (2010). Pacific Ocean Circulation Based on Observation. Journal of Oceanography 66, 389 – 403.

Kawabe M., Fujio S., Yanagimoto D. (2003). Deep-water circulation at low latitudes in the western North Pacific. Deep-Sea Res I 50, 631–656.

Kawabe M., Yanagimoto D., Kitagawa S., Kuroda Y. (2005). Variations of the deep western boundary current in Wake Island Passage. Deep-Sea Res I 52, 1121–1137.

Kawabe M., Yanagimoto D., Kitagawa S. (2006). Variations of deep western boundary currents in the Melanesian Basin in the western North Pacific. Deep-Sea Research. I 53, 942–959.

Kawabe M., Fujio S., Yanagimoto D., Tanaka K. (2009). Water masses and currents of deep circulation southwest of the Shatsky Rise in the western North Pacific. Deep-Sea Res I 56, 1675–1687.

Keigwin, L. D. (1998). Glacial-age hydrography of the far northwest Pacific Ocean. Paleoceanography 13, 323-339.

Keigwin L. (2004). Radiocarbon and stable isotope constraints on Last Glacial Maximum and Younger Dryas ventilation in the Western North Atlantic. Paleoceanography 19, PA4012, doi:10.1029/2004PA001029.

Keigwin L., Schlegel M. (2002). Ocean ventilation and sedimentation since the glacial maximum at 3 km in the western North Atlantic. Geochemistry Geophysics Geosystems 3, doi:10.1029/2001GC000283.

Klevenz V., Vance D., Schmidt D. N., Mezger K. (2008). Neodymium isotopes in benthic foraminifera: core-top systematics and a down-core record from the Neogene south Atlantic. Earth and Planetary Science Letters 265, 571–587.

Knauss J. A. (1962). On some aspects of the deep circulation of the Pacific. Journal of Geophysical Research 67, 3943–3954.

Kraft S., Frank M., Hathorne E. C., Weldeab S. (2013). Assessment of seawater Nd isotope signatures extracted from foraminiferal shells and authigenic phases of Gulf of Guinea sediments. Geochimica Cosmochimica Acta 121, 414-435.

Lacan F., Jeandel C. (2001). Tracing Papua New Guinea imprint on the central Equatorial Pacific Ocean using neodymium isotopic compositions and Rare Earth Element patterns. Earth and Planetary Science Letters 186, 497-512.

Lacan F., Jeandel C. (2004a). Denmark Strait water circulation traced by heterogeneity in neodymium isotopic compositions. Deep-sea Research I 51, 71-82.

Lacan F., Jeandel C. (2004b). Neodymium isotopic composition and rare earth element concentrations in the deep and intermediate Nordic Seas: Constraints on the Iceland Scotland Overflow Water signature. Geochemistry Geophysics Geosystems 5, n° 11.

Lacan F., Jeandel C. (2004c). Subpolar Mode Water formation traced by neodymium isotopic composition. Geophysical Research Letters 31, L14306.

Lacan F., Jeandel C. (2005). Neodymium isotopes as a new tool for quantifying exchange fluxes at the continent-ocean interface. Earth and Planetary Science Letters 232, 245-257.

Lacan F., Tachikawa K., Jeandel C. (2012) Neodymium isotopic composition of the oceans: a compilation of seawater data. Chemical Geology 300–301, 177–184.

Labeyrie, L. D., Labracherie M., Gorfti N., Pichon J.-J., Vautravers M. J., Arnold M., Duplessy, J.-C., Paterne M., Michel E., Duprat J., Caralp M., Turon, J.-L. (1996). Hydrographic changes of the Southern Ocean (southeast Indian sector) over the last 230 kyr. Paleoceanography 11, 57-76.

Lamy F., Kilian R., Arz H. W., Francois, J. P. Kaiser J., Prange M., Steinke T. (2010). Holocene changes in the position and intensity of the southern westerly wind belt. Nature Geoscience 3, 695–699.

Li X. H., Wei G. J., Shao L., Liu Y., Liang X. R., Jian Z. M., Sun M., Wang P. X. (2003). Geochemical and Nd isotopic variations in sediments of the South China Sea: a response to Cenozoic tectonism in SE Asia. Earth and Planetary Science Letters 211, 207–220.

Liu C.-T., Liu R. J. (1988). The deep current in the Bashi Channel. Acta Oceanographica Taiwanica 20, 107–116.

Li L., Qu T. (2006). Thermohaline circulation in the Deep South China Sea basin as inferred fromoxygen distributions. Journal of Geophysical Research 111.

Liu Z., Colin C., Trentesaux A., Blamart D., Bassinot F., Siani G., Sicre M.-A. (2004). Erosional history of the eastern Tibetan Plateau since 190 kyr ago: clay mineralogical and geochemical investigations from the southwestern South China Sea. Marine Geology 209, 1-18.

Liu Z., Colin C., Trentesaux A., Siani G., Frank N., Blamart D., Farid S. (2005). Late Quaternary climatic control on erosion and weathering in the eastern Tibetan Plateau and the Mekong Basin. Quaternary Research 63, 316-328.

Liu Z., Colin C., Huang W., Le K.P., Tong S., Chen Z., Trentesaux A. (2007). Climatic and tectoniccontrols on weathering in South China and the Indochina Peninsula: clay mineralogical and geochemical investigations from the Pearl, Red, and Mekong drainage basins. Geochemistry Geophysics Geosystems 8, doi:10.1029/2006GC001490.

Liu Z., Li X., Colin C., Ge H. (2010). A high-resolution clay mineralogical record in the northern South China Sea since the Last Glacial Maximum, and its time series provenance analysis. Chinese Science Bulletin 55, 4058-4068.

Li Y., Wang F. (2012). Spreading and salinity change of North Pacific tropical water in the Philippine Sea. Journal of Oceanography 68, 439–452.

Liang W. D., Yang Y. J., Tang T. Y., Chuang W. S. (2008). Kuroshio in the Luzon Strait.

Journal of Geophysical Research 113, doi:10.1029/2007JC004609.

Lindstrom E., Butt J., Lukas R., Godfrey S. (1990). The flow through Vitiaz Strait and St. George's Channel. In L. J. Pratt (Ed.), The physical oceanography of sea straits. 171–189. Dordtrecht: Kluwer Academic.

Ling H. F., Burton K. W., O'Nions R. K., Kamber B. S., von Blanckenburg F., Gibb A. J., Hein J. R. (1997). Evolution of Nd and Pb isotopes in Central Pacific seawater from ferromanganese crusts. Earth and Planetary Science Letters 146, 1– 12.

Lippold J., Luo Y. M., Francois R., Allen S. E., Gherardi J., Pichat J., Hickey B., Schulz H. (2012). Strength and geometry of the glacial Atlantic Meridional Overturning Circulation. Nature Geoscience 5, 813-816.

Lu, H. Y., Huissteden, K. V., Zhou, J., Vandenberghe, J., Liu, X. D., An, Z.S. (2000). Variability of East Asian winter monsoon in Quaternary climatic extremes in North China. Quaternary Research 54, 321– 327.

Lu, H. Y., Huissteden, K. V., An, Z. S., Nugteren, G., Vandenberghe, J., (1999). East Asian winter monsoon changes on millennial time scale before the last glacial–interglacial cycle. Journal of Quaternary Science 14, 101– 110.

Lüdmann T., Wong H.K., Berglar K. (2005). Upward flow of North Pacific Deep Water in the northern South China Sea as deduced from the occurrence of drift sediments. Geophysical Research Letters 32, doi:10.1029/2004GL021967.

Lukas, R., Yamagata, T., McCreary, J.P., (1996). Pacific low-latitude western boundary currents and the Indonesian Throughflow. Journal of Geophysical Research 101, 12209–12216.

Lund D. C., Mix A. C., Southon J. (2011). Increased ventilation age of the deep northeast Pacific Ocean during the last deglaciation. Nature Geoscience 4, 771–774.

Lynch-Stieglitz J., Stocker T. F., Broecker W. S., Fairbanks R.G. (1995). The influence of air-sea exchange on the isotopic composition of oceanic carbon—observations and modeling. Global Biogeochemical Cycles 9, 653– 665.

Mackensen A., Hubberten H. W., Bickert T., Fischer G., Futterer D. K. (1993). The Delta-C-13 in benthic foraminiferal tests of Fontbotia–Wuellerstorfi (Schwager) relative to the Delta- C-13 of dissolved inorganic carbon in southern-ocean deep-water—implications for glacial ocean circulation models. Paleoceanography 8, 587–610.

McCorkle D. C., Martin P. A., Lea D. W., Klinkhammer G. P. (1995). Evidence of a dissolution effect on benthic foraminiferal shell chemistry—$\delta^{13}C$, Cd/Ca, Ba/Ca, and Sr/Ca results from the Ontong Java Plateau. Paleoceanography 10, 699–714.

Marchitto T. M., Curry W. B., Oppo D.W. (2000). Zinc concentrations in benthic foraminifera reflect seawater chemistry. Paleoceanography 15, 299– 306.

Marchal O., Francois R., Stocker T. F., Joos F. (2000). Ocean thermohaline circulation and

sedimentary Pa-231/Th-230 ratio. Paleoceanography 15, 625– 641.

McManus J. F., Francois R., Gherardi J. M., Keigwin L. D., Brown-Leger S. (2004). Collapse and rapid resumption of Atlantic meridional circulation linked to deglacial climate changes. Nature 428, 834–837.

McCave I Nick., Carter Larry S., Hall Ian R. (2008). Glacial-interglacial changes in water mass structure and flow in the SW Pacific Ocean. Quaternary Science Reviews 27, 1886-1908, doi:10.1016/j.quascirev.2008.07.010.

Martin, E.E., Scher, H.D. (2004). Preservation of seawater Sr and Nd isotopes in fossil fish teeth: bad news and good news. Earth and Planetary Science Letters 220, 25–39.

Martin E. E., Haley B. A. (2000). Fossil fish teeth as proxies for seawater Sr and Nd isotopes. Geochimica Cosmochimica Acta 64, 835-847.

Marchitto, T. M., Lehman, S. J., Ortiz, J. D., Flückiger, J., and van Geen, A. (2007). Marine radiocarbon evidence for the mechanism of deglacial atmospheric CO2 rise. Science 316, 1456–1459.

Martínez-Botí M.A., Vance D., Mortyn P.G. (2009). Nd/Ca ratios in plankton-towed and core top foraminifera: confirmation of the water column acquisition of Nd. Geochemistry Geophysics Geosystems 10, Q08018.

Masujima, M., Yasuda I., Hiroe Y., Watanabe T. (2003). Transport of Oyashio water across the Subarctic Front into the mixed water region and formation of NPIW, Journal of Oceanography 59, 855–869.

Matsumoto, K., Oba T., Lynch-Stieglitz J., Yamamoto H. (2002). Interior hydrography and circulation of the glacial Pacific Ocean. Quaternary Science Reviews 21, 1693–1704.

Max L., Lembke-Jene L., Riethdorf J.-R., Tiedemann R., Nürnberg D., Kühn H., Mackensen A. (2014). Pulses of enhanced North Pacific IntermediateWater ventilation from the Okhotsk Sea and Bering Sea during the last deglaciation. Climate of the Past 10, 591–605.

Meynadier L., Allègre C.J., O'Nions R.K. (2008). Plate tectonics, radiogenic isotopic tracers and paleoceanography: the case of the manganese crusts in the Pacific. Earth and Planetary Science Letters 272 (3-4), 513-522.

Miao Q., Thunell R. C. Andersen D. M. (1994). Glacial-Holocene carbonate dissolution and sea surface temperatures in the South China and Sulu seas. Paleoceanography 9, 269-290.

Michard A., Albarède F., Michard G., Minster J. F., Charlou J. L., (1983). Rare-earth elements and uranium in high-temperature solutions from East Pacific Rise hydrothermal vent field (13°N. Nature 303, 795-797.

Mix A.C., and Fairbanks R.G. (1985). North Atlantic surface-ocean control of late Pleistocene deep-ocean circulation. Earth and Planetary Science Letters 73, 231-243.

Mix, A. C., Lund D. C., Pisias N. G., Bodén P., Bornmalm L., Lyle M., Pike J. (1999). Rapid

climate oscillations in the Northeast Pacific during the last deglaciation reflect Northern and Southern Hemisphere sources, in Mechanisms of Global Climate Change at Millennial Time Scales, Geophys. Monogr. Ser., vol. 112, edited by Clark P. U., Webb S., and Keigwin D. 127–148, doi:10.1029/GM112p0127, AGU, Washington, D. C.

Miyao T., Ishikawa K. (2003) Formation, distribution and volume transport of the north pacific intermediate water studied by repeat hydrographic observations. Journal of Oceanography 59, 905–919.

Molina-Kescher M., Frank M., Hathorne E. (2014). South Pacific dissolved Nd isotope compositions and rare earth element distributions: Water mass mixing versus biogeochemical cycling. Geochimica et Cosmochimica Acta 127, 171-189.

Monnin E., Indermühle A., Dällenbach A., Flückiger J., Stauffer B., Stocker T. F., Raynaud D., Barnola J.-M. (2001). Atmospheric CO_2 concentrations over the last glacial termination. Science 291, 112–114.

Montero-Serrano J.-C., Bout-Roumazeilles V., Carlson A. E., Tribovillard N., Bory A., Meunier G., Sionneau T., Flower B. P., Martinez P., Billy I., Riboulleau A. (2011). Contrasting rainfall patterns over North America during the Holocene and Last Interglacial as recorded by sediments of the northern Gulf of Mexico. Geophysical Research Letters 38, doi: 10.1029/2011gl048194.

Morley, J. J.,. Heusser L. E. (1997). Role of orbital forcing in east Asian monsoon climates during the last 350 kyr: Evidence from terrestrial and marine climate proxies from core RC14-99. Paleoceanography, 12, 483–493, doi:10.1029/97PA00213.

Nan F., Xue H., Chai F., Shi L., Shi M., Guo P., (2011). Identification of different types of Kuroshio intrusion into the South China Sea. Ocean Dynamics, doi: 10.1007/s10236-011-0426-3.

Nance W. B., Taylor S. R. (1976). Rare-earth element patterns and crustal evolution.1. Australian post-archean sedimentaryrocks. Geochimica and Cosmochimica Acta 40, 1539–1551.

Nakano, T., Kaneko I., Soga T., Tsujino H., Yasuda T., Ishizaki H., Kamachi M. (2007). Mid-depth freshening in the North Pacific subtropical gyre observed along the JMA repeat and WOCE hydrographic sections. Geophysical Research Letters 34, doi:10.1029/2007GL031433.

Noble T. L., Piotrowski A. M., McCave I. N. (2013). Neodymium isotopic composition of intermediate and deep waters in the glacial southwest Pacific. Earth and Planetary Science Letters 384, 27–36.

North Greenland Ice Core Project Members, (2004). High resolution record of Northern Hemisphere climate extending into the last interglacial period. Nature 431, 147-151.

Ninnemann U. S., Charles C. D. (1997). Regional differences in Quaternary Subantarctic nutrient cycling: Link to intermediate and deep water ventilation. Paleoceanography 12, 560-567.

Ohkushi K., Itaki T., Nemoto N. (2003). Last Glacial- Holocene change in intermediate-water ventilation in the northwestern Pacific. Quaternary Science Reviews 22, 1477–84.

Ohta A., Kawabe I. (2001). REE (ш) adsorption onto Mn dioxide (δ-MnO_2) and Fe oxyhydroxide: Ce (ш) oxidation by δ-Mno2. Geochimica and Cosmochimica Acta 65, 695–703.

Okazaki Y., Timmermann A., Menviel L., Harada N., Abe-Ouchi A., Chikamoto M. O., Mouchet A., Asahi H. (2010). Deepwater Formation in the North Pacific During the Last Glacial Termination. Science 329, 200–204.

Okai T., Suzuki A., Terashima S., Inoue M., Nohara M., Kawahata H., Imai N. (2004). Collaborative analysis of GSJ/AIST geochemical reference materials JCp-1 (Coral) and JCt-1 (Giant Clam). Chikyu Kagaku 38, 281-286.

O'Nions R. K., Frank M., von Blanckenburg F., Ling. H.-F. (1998). Secular variation of Nd and Pb isotopes in ferromanganese crusts from the Atlantic, Indian and Pacific Oceans, Earth and Planetary Science Letters 155, 15–28.

Oppo, D. W., Fairbanks, R. G. (1987). Variability in the deep and intermediate water circulation of the Atlantic Ocean during the past 25,000 years — Northern Hemispere modulation of the Southern Ocean. Earth and Planetary Science Letters 86, 1–15.

Oppo D. W., Lehman S. J. (1993). Mid-depthc irculationo f the subpolar North Atlanticd uringt he Last Glacial M aximum. Science 259, 1148-1152.

Oppo D.W., Linsley B.K., Dannemann S., Beaufort L. (2001). A 400-kyr long planktic δ18O record from the Sulu Sea: constraints on ice volume and the tropical hydrologic cycle. EOS Trans. AGU 82, F737.

Orsi A. H., Johnson G. C., Bullister J. L. (1999). Circulation, mixing, and production of Antarctic Bottom Water. Progress in Oceanography 43, 55–109.

Pahnke, K., Goldstein S. L., Hemming S. R. (2008), Abrupt changes in Antarctic Intermediate Water circulation over the past 25,000 years, Nature Geoscience, 1, 870–874.

Palmer M. R. (1985). Rare earth elements in foraminifera tests. Earth and Planetary Science Letters 73, 285–298.

Palmer M.R., Elderfield H. (1985). Variations in the Nd isotopic composition of foraminifera from Atlantic Ocean sediments. Earth and Planetary Science Letters 73, 299-305.

Pedro, J. B., van Ommen T. D., Rasmussen S. O., Morgan V. I., Chappellaz J., Moy A. D., Masson-Delmotte V., Delmotte, M. (2011). The last deglaciation: timing the bipolar seesaw, Climate of the Past 7, 671–683.

Pena L. D., Calvo E., Cacho I., Eggins S., Pelejero C. (2005). Identification and removal of Mn–Mg-Rich contaminant phases on foraminiferal tests: Implications for Mg/Ca past temperature reconstructions. Geochem. Geophys. Geosyst. 6, Q09P02.

Pena L.D., Goldstein S.L., Hemming S.R., Jones K.M., Calvo E., Pelejero C., Cacho I. (2013). Rapid changes in meridional advection of Southern Ocean intermediate waters to the tropical Pacific during the last 30 kyr. Earth and Planetary Science Letters 368, 20-32.

Peterson L. C., Haug G. H., Hughen A. K., Röhl U. (2000). Rapid changes in the hydrologic cycle of the tropical Atlantic during the last glacial. Science 290, 1947-1951.

Pflaumann U., Jian Z. 1999. Modern distribution patterns of planktonic foraminifera in the SouthChina Sea and western Pacific: A new transfer technique to estimate regional sea-surface temperatures. Marine Geology 156, 41-83.

Piepgras D. J., Wasserburg G. J., Dasch E. J. (1979). The isotopic composition of Nd in different ocean masses. Earth and Planetary Science Letters 45, 223-236.

Piepgras D. J., Wasserburg G. J. (1980). Neodymium isotopicvariations in seawater. Earth and Planetary Science Letters 50, 128–138.

Piepgras D. J., Wasserburg G. J. (1982). Isotopic composition of neodymium in waters from Drake Passage. Science 217, 207–217.

Piepgras D. J., Jacobsen S. B. (1988). The isotopic composition of neodymium in the North Pacific. Geochimica et Cosmochimica Acta 52, 1373-1381.

Piepgras D. J., Jacobsen S. B. (1992). The behavior of rare earth elements in seawater: Precise determination of variation in the North Pacific water column. Geochemistry Geophysics Geosystems 56, 1851–1862.

Pin C., Santos Zalduegui J. F. (1997). Sequential separation of light rare-earth elements, thorium and uranium by miniaturized extraction chromatography: Application to isotopic analyses of silicate rocks. Analytica Chimica Acta 339, 79-89.

Piotrowski A. M., Goldstein S. L., Hemming S. R., Fairbanks R. G. (2004). Intensification and variability of ocean thermohaline circulation through the last deglaciation. Earth and Planetary Science Letters 225,205–220.

Piotrowski A. M., Goldstein S. L., Hemming S. R., Fairbanks R. G. (2005). Temporal relationships of carbon cycling and ocean circulation at glacial boundaries. Science 307, 1933–1938.

Piotrowski A. M., Goldstein S. L., Hemming S. R., Fairbanks R. G., Zylberberg D. R. (2008). Oscillating glacial northern and southern deep water formation from combined neodymium and carbon isotopes. Earth and Planetary Science Letters 272, 394–405.

Piotrowski A. M., Banakar V. K., Scrivner A. E., Elderfield H., Galy A., Dennis A. (2009). Indian Ocean circulation and productivity during the last glacial cycle. Earth and Planetary Science Letters 285, 179-189.

Piotrowski A. M., Galy A., Nicholl J. A. L., Roberts N., Wilson D. J., Clegg J. A. and Yu J. (2012). Reconstructing deglacial North and South Atlantic deep water sourcing using

foraminiferal Nd isotopes. Earth and Planetary Science Letters 357–358, 289–297.

Placzek, C., Patchett, P. J., Quade, J., Wagner, J.D.M. (2006). Strategies for successful U-Th dating of paleolake carbonates: An example from the Bolivian Altiplano. Geochemistry Geophysics Geosystems 7, doi: 10.1029/2005GC001157.

Pomiès C., Davies G. R., Conan S. M.-H. (2002). Neodymium in modern foraminifera from the Indian Ocean: implications for the use of foraminiferal Nd isotope compositions in paleooceanography. Earth and Planetary Science Letters 203, 1031–1045.

Porter S.C., An Z. S. (1995). Correlation between climate events in the North Atlantic and China during the last glaciation. Nature 375, 305-308.

Prell W. L. (1984). Covariance pattern of foraminiferal $\delta^{18}O$: An evaluation of Pliocene ice volume change near 3.2 million years ago. Science 226, 692-693.

Qiu B., Lukas R. (1996). Seasonal and interannual variability of the North Equatorial Current, the Mindanao Current, and the Kuroshio along the Pacific western boundary. Journal of Geophysical Research 101: doi: 10.1029/95JC03204.

Qiu D., Yang T., Guo Z. (1984). A westward current in the northeastern part of the South China Sea. Tropical Oceanol 33, 65–73 (in Chinese with English abstract).

Qu T., Song Y T., Yamagata T. (2009). An introduction to the South China Sea throughflow: Its dynamics, variability, and application for climate. Dynamics of Atmospheres and Oceans 47, 3-14.

Qu T., Kagimoto T., Yamagata T. (1997). A subsurface countercurrent along the east coast of Luzon. Deep-Sea Research I 44, 413–423.

Qu T., Mitsudera H., Yamagata T. (1998). On the western boundary currents in the Philippine Sea. Journal of Geophysical Research 103, 7537–7548.

Qu T., Mitsudera H., Yamagata T. (1999). A climatology of the circulation and water mass distribution near the Philippine coast. Journal of Physical Oceanography 29, 1488–1505.

Qu T., Mitsudera H., Yamagata T. (2000). Intrusion of the North Pacific waters into the South China Sea. Journal of Geophysical Research 105: 6415-6424.

Qu T., Lindstrom E. (2004). Northward intrusion of Antarctic Intermediate Water in the western North Pacific. Journal of Geophysical Research 34, 2104–2118.

Qu T., Du Y., Meyers G., Ishida A.,Wang D. (2005). Connecting the tropical Pacific with Indian Ocean through South China Sea. Geophysical Research Letter 32, doi:10.1029/2005GL024698.

Qu T., Du Y., Sasaki H. (2006). South China Sea throughflow: a heat and freshwater conveyor. Geophysical Research Letter 33, doi:10.1029/2006GL028350.

Rae J. W. B., Sarnthein M., Foster G. L., Ridgwell A., Grootes P. M., Elliott T. (2014). Deep

water formation in the North Pacific and deglacial CO2 rise. Paleoceanography doi: 10.1002/2013PA002570.

Rahmstorf, S. (1994). Rapid climate transitions in a coupled ocean-atmosphere model. Nature, 372, 82-85.

Rahmstorf, S. (1995). Bifurcations of the Atlantic thermohaline circulation in response to changes in the hydrological cycle. Nature 378, 145–149.

Rahmstorf, S. (2002). Ocean circulation and climate during the past 120,000 years. Nature 419, 207-214.

Rahmstorf, S. (2003). Thermohaline circulation: The current climate. Nature 421, 699.

Reid J. L. (1997). On the total geostrophic circulation of the Pacific Ocean: Flow patterns, traces and transports. Progress in Oceanography 39, 263–325.

Reid J. L. (1965). Intermediate waters of the Pacific Ocean. Johns Hopkins Oceanographic Studies 2, 85.

Rella S. F., Tada R., Nagashima K., Ikehara M., Itaki T., Ohkushi K., Sakamot, T., Harada N., Uchida M. (2012). Abrupt changes of intermediate water properties on the northeastern slope of the Bering Sea during the last glacial and deglacial period. Paleoceanography 27, doi:10.1029/2011PA002205.

Rella S. F., Uchida M. (2014). A Southern Ocean trigger for Northwest Pacific ventilation during the Holocene?. Scientific Reports 4, doi:10.1038/srep04046.

Rempfer J., Stocker T. F., Joos F., Dutay J.-C., Siddall M. (2011). Modelling Nd-isotopes with a coarse resolution ocean circulation model: Sensitivities to model parameters and source/sink distributions. Geochimica and Cosmochimica Acta 75, 5927–5950.

Rempfer J., Stocker T. F., Joos F., Dutay J.-C. (2012). Sensitivity of Nd isotopic composition in seawater to changes in Nd sources and paleoceanographic implications. Journal of Geophysical Research 117, doi:10.1029/2012JC008161.

Reynolds B. C., Frank M., O'Nions R. K. (1999). Nd- and Pbisotope time series from Atlantic ferromanganese crusts: Implications for changes in provenance and paleocirculation over the last 8 Myr. Earth and Planetary Science Letters 173, 381–396.

Rintoul S.R., Hughes C.W., Olbers D. (2001). The Antarctic Circumpolar Current System. In: Siedler G., Church J. (Eds.), Ocean Circulation and Climate, International Geophysics Series. Academic Press, San Diego, CA, 271-302.

Rodman, M. R., Gordon A. L. (1982). Southern ocean bottom water of the Australian-New Zealand sector, Journal of Geophysical Research 87, 5771–5778.

Rodehacke C.B., Hellmer H. H., Beckmann A., Roether W. (2007). Formation and spreading of Antarctic deep and bottom waters inferred from a chlorofluorocarbon (CFC) simulation. Journal of Geophysical Research 112, doi: 10.1029/2006JC003884.

Roberts N. L., Piotrowski A. M., McManus J. F., Keigwin L. D. (2010). Synchronous deglacial overturning and water mass source changes. Science 327, 75–78.

Roberts N. L., Piotrowski A. M., Elderfield H., Eglinton T. I., Lomas M. W. (2012). Rare earth element association with foraminifera. Geochimica and Cosmochimica Acta 94, 57-71.

Robinson L., Adkins J. F., Keigwin L. D., Southon J., Fernandez D. P., Wang S.-L., Scheirer D. S. (2005). Radiocarbon variability in the Western North Atlantic during the last deglaciation. Science, 310, 1469–1473.

Robinson, L. F., van de Flierdt T. (2009). Southern Ocean evidence for reduced export of North Atlantic Deep Water during Heinrich event 1. Geology 37, 195–198.

Robinson L. R., Adkins J. F., Frank N., Gagnon A. C., Prouty N. G., Roark E. B., van de Flierdt T. (2014). The geochemistry of deep-sea coral skeletons: A review of vital effects and applications for palaeoceanography. Deep-Sea Research II 99, 184-198.

Romahn S., Mackensen A., Groeneveld J., Pätzold J. (2014). Deglacial intermediate water reorganization: new evidence from the Indian Ocean. Climate of the Past 10, 293–303.

Rutberg R. L., Hemming S. R., Goldstein S. L. (2000). Reduced North Atlantic Deep Water flux to the glacial Southern Ocean inferred from neodymium isotope ratios. Nature 405, 935–938.

Sagawa, T., Ikehara K. (2008). Intermediate water ventilation change in the subarctic northwest Pacific during the last deglaciation, Geophysical Research Letters 35, L24702, doi:10.1029/2008GL035133.

Scher, H. D., Martin E. E. (2004). Circulation in theSouthern Ocean during the Paleogene inferred from Nd isotopes. Earth and Planetary Science Letters 228, 391–405.

Schimel D. S., Braswell B.H., Parton W. J. (1997). Equilibration of the terrestrial water, nitrogen, and carbon cycles. Proceedings of the National Academy of Sciences 94, 8280-8283.

Schlitzer R. (2000). Electronic atlas of WOCE hydrographic and tracer data now available. EosTrans. AGU 81,45.

Shackleton N. J., Duplessy J.-C. Arnold M., Maurice P., Hall M. A., Cartlidge J. (1988) Radiocarbon age of the last glacial Pacific deepw ater. Nature 335, 708-711, 1988.

Shakun J. D., Carlson A. E. (2010). A global perspective on Last Glacial Maximum to Holocene climate change. Quaternary Science Reviews 29, 1801-1816.

Shao C., Chen J., Li L (2013). Grazing alters the biophysical regulation of carbon fluxes in a desert steppe. Environmental Research Letter 8, 025012.

Shaw P. T., Chao S. Y. (1994). Surface circulation in the South China Sea. Deep-Sea Res I 41, 1663-1683

Shemesh A., Hodell D., Crosta X., Kanfoush S., Charles C., Guilderson T. (2002). Sequence of events during the last deglaciation in Southern Ocean sediments and Antarctic ice cores. Paleoceanography 17, doi: 10.1029/2000PA000599.

Siani G., Michel E., De Pol-Holz R., DeVries T., Lamy T., Carel M., Isguder G., Dewilde F., Lourantou A. (2013). Carbon isotope records reveal precise timing of enhanced Southern Ocean upwelling during the last deglaciation. Nature Communications 4, doi:10.1038/ncomms3758.

Siedler G., Holfort J., Zenk W., Müller T. J., Csernok T. (2004). Deep-water flow in the mariana and caroline basins. Journal of Physical Oceanography 34, 566-581.

Sigman, D., Boyle E. A. (2000). Glacial/Interglacial variations in atmospheric carbon dioxide. Nature 407, 859–869.

Sikes, E., Samson C., Guilderson T., Howard W. (2000). Old radiocarbon ages in the southwest Pacific Ocean during the last glacial period and deglaciation. Nature 405, 555–559.

Singh S. P., Singh S. K., Goswami V., Bhushan R. and Rai V. K. (2012) Spatial distribution of dissolved neodymium and eNd in the Bay of Bengal: role of particulate matter and mixing of water masses. Geochimica and Cosmochimica Acta 94, 38–56.

Skinner L.C., Fallon S., Waelbroeck C., Michel E., Barker S. (2010). Ventilation of the deep Southern Ocean and deglacial CO2 rise. Science 328, 1147–1151.

Skinner L. C., Scrivner A. E., Vance D., Barker S., Fallon S., Waelbroeck C. (2013). North Atlantic versus Southern Ocean contributions to a deglacial surge in deep ocean ventilation. Geology 4, 667-670.

Spencer D.W., Bacon M. P., Brewer P. G. (1981).Models of the distribution of 210Pb in a section across the North Equatorial Atlantic Ocean. Journal of Marine Research 39, 119–138.

Spero, H. J. and Lea, D. W. (2002). The cause of carbon isotope minimum events on glacial terminations. Science 296, 522–525.

Spivack A. J., Wasserburg G. J. (1988). Neodymium isotopic composition of the Mediterranean outflow and the eastern North Atlantic, Geochimica and Cosmochimica Acta 52, 2767–2773.

Staudigel H., Doyle P., Zindler A. (1985). Sr and Nd isotope systematics in fish teeth. Earth and Planetary Science Letters 76, 45–56.

Steinke S., Glatz C., Mohtadi M., Groeneveld J., Li Q., Jian Z. (2011). Past dynamics of the East Asian monsoon: No inverse behaviour between the summer and winter monsoon during the Holocene. Global and Planetary Change 78, 170–177.

Stichel T., Frank M., Rickli J., Haley B. A. (2012). The hafnium and neodymium isotope composition of seawater in the Atlantic sector of the Southern Ocean. Earth and Planetary Science Letters 317–318, 282–294.

Stocker T. F., Wright D. G. (1996). Rapid changes in ocean circulation and atmospheric radiocarbon. Paleoceanography 11, 773-796.

Stott L., Southon J., Timmermann A., Koutavas A. (2009). Radiocarbon age anomaly at intermediate water depth in the Pacific Ocean during the last deglaciation, Paleoceanography 24, doi:10.1029/2008PA001690.

Stuiver M., Reimer, P.J. (1993). Extended ^{14}C database and revised CALIB radiocarbon calibration program. Radiocarbon 35, 215–230.

Suga T., Kato A., Hanawa K., (2000) North Pacific Tropical Water: its climatology and temporal changes associated with the climate regime shift in the 1970s. Progress in Oceanography 47, 223-256. doi:10.1016/S0079-6611(00)00037-9

Surya Prakash L., Ray D., Paropkari A. L., Mudholkar A. V., Satyanarayanan M., Sreenivas B., Chandrasekharam D., Kota D., Kamesh Raju K. A., Kaisary S., Balaram V., Gurav T. (2012). Distribution of REES and yttrium among major geochemical phases of marine Fe–Mn-oxides: Comparative study between hydrogenous and hydrothermal deposits. Chem. Geol. 312–313, 127–137.

Tachikawa K., Jeandel C., Dupré B. (1997). Distribution of rare earth elements and neodymium isotopes in settling particulate material of the tropical Atlantic ocean (eumeli site). Deep-Sea Res. 44, 1769-1792.

Tachikawa K., Jeandel C., Roy-Barman M. (1999). A new approach to the Nd residence time in the ocean : the role of atmospheric inputs. Earth and Planetary Science Letters 170, 433-446.

Tachikawa K., Athias V., Jeandel C. (2003). Neodymium budget in the modern ocean and paleo-oceanographic implications. Journal of Geophysical Research 108, 1-13.

Tachikawa K., Toyofuku T., Basile-Doelsch I., Delhaye T. (2013). Microscale neodymium distribution in sedimentary planktonic foraminiferal tests and associated mineral phases. Geochimica Cosmochimica Acta 100, 11-23.

Tachikawa K., Piotrowski A.M., Bayon G. (2014). Neodymium associated with foraminiferal carbonate as a recorder of seawater isotopic signatures. Quaternary Science Reviews 88, 1-13.

Tada R., Irino T., Koizumi I. (1999). Land-ocean linkages over orbital and millennial timescales recorded in late Quaternary sediments of the Japan Sea. Paleoceanography 14, 236-247.

Talley L.D. (2007). Hydrographic Atlas of the World Ocean Circulation Experiment (WOCE). Volume 2: Pacific Ocean. In: Sparrow, M., Chapman, P., Gould, J. (Eds.). International WOCE Project Office, Southampton, UK.

Talley L. D. (2008). Freshwater transport estimates and the global overturning circulation: shallow, deep and throughflow components. Progress in Oceanography 78, 257-303.

Talley L. D., Pickard G. L., Emery W. J., Swift J. H. (Eds, 2011). Descriptive physical oceanography: an introduction. Elsevier, UK.

Talley L.D. (1993). Distribution and formation of North Pacific IntermediateWater. Journal of Physical Oceanography 23, 517-537.

Talley L. D., Joyce T. M. (1992). The double silica maximum in the North Pacific. Journal of Geophysical Research 97, 5465–5480.

Talley . D. Yun J.-Y. (2001). The role of cabbeling and double diffusion in setting the density of the North Pacific Intermediate Water salinity minimum. Journal of Physical Oceanography 31, 1538-1549.

Talley L.D. (1999). Some aspects of ocean heat transport by the shallow, intermediate and deep overturning circulation. Mechanisms of Global Climate Change at Millenial Time Scales, Geophys. Monogr., No. 112, Amer. Geophys. Union, 1–22.

Talley L.D., Nagata Y., Fujimura M., Iwao T., Tokihiro K., Inagake D., Hirai M., Okuda K. (1995). North Pacific Intermediate Water in the Kuroshio/Oyashio mixed water region in Spring, 1989. Journal of Physical Oceanography 25, 475-501.

Tanaka T., Togashi S., Kamioka H., Amakawa H., Kagami H., Hamamoto T., Yuhara M., Orihashi Y., Yoneda S., Shimizu H., Kunimaru T., Takahashi K., Yanagi T., Nakano T., Fujimaki H., Shinjo R., Asahara Y., Tanimizu M., Dragusanu C. (2000). JNdi-1:a neodymium isotopic reference in consistency with La Jolla neodymium. Chemical Geology168, 279–281.

Tian J., Yang Q., Liang, X., Hu D., Wang F., Qu T. (2006). The observation of Luzon strait transport. Geophysical Research Letters 33, L19607, doi:10.1029/2006GL026272.

Tian J., Yang Q., Zhao W. (2009). Observation of enhanced diapycnal mixing in the South China Sea. Journal of Physical Oceanography 39, 3191–3203.

Toggweiler J.R., Russell J.L. (2008). Ocean circulation in a warming climate. Nature 451, 286-288.

Thomas D. J., Bralower T. J., Jones C. E. (2003). Neodymium isotopic reconstruction of late Paleocene-early Eocene thermohaline circulation. Earth and Planetary Science Letters 209, 309–322.

Thomas D. J. (2004). Evidence for deep-water production in the North Pacific Ocean during the early Cenozoic warm interval. Nature 430, 65–68.

Tozuka T., Qu T., Yamagata T., (2007). Effect of South China Sea throughflow on the Makassar strait throughflow. Geophysical Research Letters 34, doi:10.1029/2007GL030420.

Tozuka T., Qu T., Masumotoa. Y., Yamagata, T. (2009). Impacts of the South China Sea Throughflow on seasonal and interannual variations of the Indonesian Throughflow. Dynamics of Atmospheres and Oceans 47, 73-85.

Trenberth K. E., Branstator G. W., Karoly D., Kumar A., Lau N., Ropelewski C. (1998).

Progress during TOGA in understanding and modeling global teleconnections associated with tropical sea surface temperatures. Journal of Geophysical Research 103, doi: 10.1029/97JC01444.

Tsuchiya M. (1991). Flow path of the Antarctic Intermediate Water in the western equatorial South Pacific Ocean. Deep-Sea Res 38 (Suppl.), S273–S279.

Vance D., Burton K. (1999). Neodymium isotopes in planktonic foraminifera: a record of the response of continental weathering and ocean circulation rates to climate change. Earth and Planetary Science Letters 173, 365–379.

Vance D., Scrivner A. E., Beney P., Staubwasser M., Henderson G. M., Slowey N. C. (2004). The use of foraminifera as a record of the past neodymium isotope composition of seawater. Paleoceanography 19, http://dx.doi.org/10.1029/ 2003pa000957.

van de Flierdt T., Frank M., Lee D. C., Halliday A. N., Reynolds B. C., Hein J. R. (2004). New constraints on the sources and behaviour of neodymium and hafnium in seawater from Pacific ocean ferromanganese crusts. Geochimica and Cosmochimica Acta 68, 3827 – 3843.

van de Flierdt T., Robinson L. F., Adkins J. F., Hemming S. R., Goldstein S. L. (2006). Temporal stability of the neodymium isotope signature of the Holocene to glacial North Atlantic. Paleoceanography 21, doi:10.1029/2006PA001294.

van de Flierdt T., Robinson L. F., Adkins J. F. (2010). Deep-sea corals aragonite as a recorder for the neodymium isotopic composition of seawater. Geochimica and Cosmochimica Acta 74, 6014-6032.

Von Blanckenburg F., O'Nions R. K. (1999). Response of beryllium and radiogenic isotopes ratios in Northern Atlantic Deep Water to the onset of northern hemisphere glaciation. Earth and Planetary Science Letters 167, 175-1782.

Wang B., Wu R. G., Lau K.-M. (2001). Interannual Variability of the Asian Summer Monsoon: Contrasts between the Indian and the Western North Pacific–East Asian Monsoons. Journal of Climate 14, 4073-4090.

Wang B., LinHo, Zhang Y. S., Lu M.-M., (2004). Definition of South China Sea Monsoon Onset and Commencement of the East Asia Summer Monsoon. Journal of Climate, 17, 699–710.

Wang G., Xie S.-P., Qu T., Huang R. X. (2011). Deep South China Sea circulation, Geophysical Research Letter 38, doi:10.1029/2010GL046626.

Wang L., Wang P. (1990). Late Quaternary paleoceanography of the South China Sea: glacial-interglacial contrasts in an enclosed basin. Paleoceanography 5, 77-90.

Wang L., Sarenthein M., Erlenkeuser H., Grimalt J., Grootes P., Heilig S., Ivanova E., Kienast M., Pelejero C. and Pflaumann U. 1999a. East Asian monsoon Climate during the late Pleistocene: high- resolution sediment records from the South China Sea. Marine Geology 156, 245-284.

Wang P. (1999). Response of Western Pacific marginal seas to glacial cycles: Paleoceanographic and sedimentological features. Marine Geology 156, 5-39.

Wang P., Clemens S., Beaufort L., Braconnot P., Ganssen G., Jian Z., Kershaw P., Sarnthein M. (2005). Evolution and variability of the Asian monsoon system: state of the art and outstanding issues. Quaternary Science Reviews 24, 595-629.

Wang Y. J., Cheng H., Edwards R. L., An Z. S., Wu J. Y., Shen C. C., Dorale J. A. (2001). A high-resolution absolute-dated late Pleistocene monsoon record from Hulu Cave, China. Science 294, 2345-2348.

Wang Y. J., Cheng H., Edwards R. L., He Y. Q., Kong X. G., An Z. S., Wu J. Y., Kelly M. J., Dykoski C.A., Li X. D. (2005). The Holocene Asian monsoon: Links to solar changes and North Atlantic climate. Science 308, 854-857.

Webster P. J. (1987). The elementary monsoon. In Monsoons, ed. Fein J. S., Stephens P. L. 3–32. New York: Wiley.

Wehausen R., Brumsack H. J. (2002). Astronomical forcing of the East Asian monsoon mirrored by the composition of Pliocene South China Sea sediments. Earth and Planetary Science Letters 201, 621–636.

Wei G. J., Huang C.-H., Wang C.-C., Lee M.-Y., Wei K.-Y. (2006). High-resolution benthic foraminifer δ13C records in the South China Sea during the last 150 ka. Marine Geology 232, 227–235.

Wei G. J., Liu Y., Ma J. L., Xie L. H., Chen J. F., Deng W. F., Tang S. (2012). Nd, Sr isotopes and elemental geochemistry of surface sediments from the South China Sea: Implications for Provenance Tracing. Marine Geology 319–322, 21–34.

White W. M. (Ed, 2005). Geochemistry. AGU, Washington, D. C.

Whitworth T., Warren B. A., Nowlin Jr. W. D., Rutz S. B., Pillsbury R.D., Moore M.I. (1999). On the deep western boundary current in the Southwest Pacific Basin. Progress in Oceanography 43, 1-54.

Wilson D. J., Piotrowski A. M., Galy A., McCave I. N. (2012). A boundary exchange influence on deglacial neodymium isotope records from the deep western Indian Ocean. Earth and Planetary Science Letters 341–344, 35–47.

Wilson D. J., Piotrowski A. M., Galy A., Clegg J. A. (2013). Reactivity of neodymium carriers in deep sea sediments: Implications for boundary exchange and paleoceanography. Geochim. Cosmochim. Acta 109, 197-221.

Wu Q., Colin C., Liu Z., Thil F., Douville E., Dubois-Dauphin Q., Frank N. (in prep. a). New insights into hydrological exchange between the South China Sea and the western Pacific Ocean based on the Nd isotopic composition of seawater.

Wu Q., Colin C., Liu Z., Thil F., Dubois-Dauphin Q., Frank N., Douville E. (in prep. b). Neodymium isotopic composition in foraminifera and authigenic phases of South China Sea

sediments: implications for the hydrology of the North Pacific Ocean over the past 25 kyr.

Wyndham T., McCulloch M., Fallon S., Alibert C. (2004). High resolution coral records of rare earth elements in coastal seawater: biogeochemical cycling and a new environmental proxy. Geochimica and Cosmochimica Acta 68, 2067–2080.

Wyrtki K. (1961). Physical oceanography of the Southeast Asian waters. Naga Report 2, Scripps Institution of Oceanography, La Jolla, CA, 195pp.

Xiao J., Porter S. C., An Z., Kumai H., Yoshikawa S. (1995). Grain size of quartz as an indicator of winter monsoon strength on the loess plateau of central China during the last 130,000 yr. Quaternary Research 43, 22-29.

Xie L., Tian J., Zhang S., Zhang Y., Yang Q. (2011). An anticyclonic eddy in the intermediate layer of the Luzon Strait in Autumn 2005. Journal of Oceanography 67, 37-46.

Xie R. C., Marcantonio F., Schmidt M.W. (2012). Deglacial variability of Antarctic intermediate water penetration into the North Atlantic from authigenic neodymium isotope ratios. Paleoceanography 27, doi.org/10.1029/2012PA002337.

Yang Q., Tian J., Zhao W. (2010). Observation of Luzon Strait transport in Summer 2007. Deep Sea Research I 57, 670–676.

Yasuda, I. (1997). The origin of the North Pacific Intermediate Water, Journal of Geophysical Research 102, 893-909, doi:10.1029/96JC02938.

Yasuda, I., Okuda K., Shimizu Y. (1996). Distribution and modification of North Pacific Intermediate Water in the Kuroshio-Oyashio interfrontal zone. Journal of Physical Oceanography 26, 448– 465.

You Y., Suginohara N., Fukasawa M., Yasuda I., Kaneko I., Yoritaka H., Kawamiya M. (2000). Roles of the Okhotsk Sea and Gulf of Alaska in forming the North Pacific Intermediate Water. Journal of Geophysical Research 105, 3253– 3280.

You Y. (2003). The pathway and circulation of North Pacific Intermediate Water. Geophysical Research Letters 30, doi:10.1029/ 2003GL018561.

You Y. (2010). A scenario of North Pacific Intermediate Water formation Deep-Sea Research II, 57, 1171–1176, doi:10.1016/j.dsr2.2009.12.006.

Yu J. M, Broecker, W. S, Elderfield, H., Jin, Z. D., McManus, J., Zhang, F. (2010). Loss of carbon from the deep sea since the Last Glacial Maximum. Science 330, 1084-1087.

Yu J. M., Anderson R. F., Jin Z. D., Rae J. W. B., Opdyke B. N., Eggins S. M. (2013). Responses of the deep ocean carbonate system to carbon reorganization during the Last Glacialeinterglacial cycle. Quaternary Science Reviews 76, 39-52.

Yuan Y., Liao G., Guan W., Wang H., Lou R., Chen H. (2008). The circulation in the upper and middle layers of the Luzon Strait during spring 2002. Journal of Geophysical Research 113, doi:10.1029/2007JC004546

Yuan Y., Liao G., Yang C. (2009). A diagnostic calculation of the circulation in the upper and middle layers of the Luzon Strait and the northern South China Sea during March 1992. Dynamics of Atmospheres and Oceans 47, 86–113.

Zenk W., Siedler G., Ishida A., Holfort J., Kashino Y., Kuroda Y., Miyama T., Müller T. J. (2005). Pathways and variability of the Antarctic Intermediate Water in the western equatorial Pacific Ocean. Progress in Oceanography 67, 245–281.

Zhang Y., Liu Z., Zhao Y., Wang W, Li J., Xu J. (2014). Mesoscale eddies transport deep-sea sediments. Scientific Reports 4, doi: 10.1038/srep05937.

Zhao W., Zhou C., Tian J., Yang Q., Wang B., Xie L., Qu T. (2014). Deep water circulation in the Luzon Strait. Journal of Geophysical Research 119, doi:10.1002/ 2013JC009587.

Appendix

Table A1. Seawater REE concentrations (pmol/kg) obtained from this study

Station	depth	La	Ce	Pr	Nd	Sm	Eu	Gd	Tb	Dy	Ho	Er	Tm	Yb	Lu
P1	5	3.08	5.56	0.64	2.26	0.38	0.05	0.78	0.09	0.60	0.19	0.65	0.06	0.50	0.08
P1	500	20.91	8.48	2.96	13.02	2.42	0.39	3.48	0.53	4.29	1.15	3.85	0.53	3.53	0.61
P2	5	5.32	8.19	0.95	3.92	0.69	0.02	1.09	0.15	1.12	0.31	1.11	0.12	0.79	0.12
P2	500	20.72	3.81	2.87	12.68	2.55	0.68	3.64	0.59	4.39	1.23	4.28	0.60	3.99	0.69
P2	1000	28.82	8.15	3.85	17.19	3.39	0.90	4.91	0.81	5.94	1.73	5.98	0.90	6.28	1.12
P2	1600	51.39	23.84	8.59	33.48	6.21	1.19	7.86	1.33	10.15	2.75	9.44	1.13	10.12	1.80
P2	1800	42.97	16.03	6.39	28.62	5.37	1.18	6.70	1.18	8.57	2.27	8.00	1.22	8.63	1.51
P2	2000	44.15	6.72	6.31	26.85	5.13	1.55	6.97	1.19	8.96	2.51	8.98	1.31	9.50	1.79
P2	2200	46.38	8.04	6.57	29.17	5.48	1.43	7.72	1.29	9.58	2.56	9.09	1.39	10.02	1.68
P2	2400	48.42	9.15	7.03	31.14	5.88	1.31	7.63	1.35	9.61	2.70	9.22	1.40	10.09	1.75
P2	2600	50.01	21.57	7.35	32.53	5.96	1.10	7.79	1.26	9.50	2.58	9.13	1.37	9.78	1.76
P2	3000	49.40	9.69	7.17	32.39	6.60	1.67	8.21	1.38	10.11	2.67	9.24	1.41	9.89	1.66
P2	3500	53.72	9.53	8.16	36.33	7.19	1.77	8.62	1.48	10.80	2.89	9.82	1.49	10.68	1.77
N18-05	5	7.87	11.58	1.55	5.92	1.31	0.17	1.67	0.23	1.63	0.49	1.54	0.16	1.25	0.19
N18-05	1000	22.57	23.16	3.16	13.47	2.68	0.56	3.42	0.58	4.43	1.20	3.94	0.53	3.71	0.62
N18-05	1400	37.70	8.01	5.27	23.86	4.67	1.21	6.60	1.03	8.14	2.14	7.68	1.19	8.33	1.44
N18-05	1600	38.89	5.08	5.23	24.08	4.42	1.03	6.82	1.14	8.33	2.34	8.11	1.27	8.83	1.58
N18-05	1800	43.03	9.97	5.83	26.46	5.22	1.51	7.15	1.16	8.93	2.43	8.46	1.30	9.07	1.64
N18-05	2000	45.88	11.47	6.68	30.20	5.54	1.33	7.58	1.25	9.55	2.58	9.01	1.35	9.34	1.73
N18-05	2400	44.76	7.39	6.66	27.96	5.55	1.26	7.43	1.21	9.18	2.43	8.25	1.21	9.16	1.63
N18-05	2600	49.64	7.65	7.49	32.98	6.13	1.66	8.43	1.36	10.11	2.82	9.65	1.44	10.31	1.82
N18-05	2800	56.31	47.31	11.17	48.39	9.80	2.02	9.54	1.59	10.96	2.78	9.40	1.33	9.73	1.62
N18-05	3000	23.41	8.60	3.41	15.00	2.91	0.47	4.00	0.65	4.61	1.26	4.25	0.60	4.09	0.71
N18-05	3500	53.30	15.16	8.07	34.61	6.60	1.44	8.47	1.42	10.14	2.75	9.08	1.31	9.65	1.59
A3	10	10.68	7.17	2.29	10.47	2.28	0.70	3.23	0.62	4.28	1.05	3.50	0.47	2.30	0.46
A3	300	13.46	3.56	2.06	9.65	1.90	0.48	2.74	0.49	3.72	0.96	3.25	0.47	2.34	0.48
A3	600	25.99	4.61	3.84	17.06	3.63	0.92	4.46	0.78	5.80	1.61	5.30	0.78	4.29	0.93
A3	900	29.43	4.88	4.18	19.04	3.94	0.80	5.24	0.88	6.59	1.73	6.08	0.92	5.29	1.09
A3	1171	34.24	6.85	5.03	22.73	4.79	1.15	6.09	1.06	7.56	1.99	6.82	1.01	5.61	1.24

A3	1200	37.33	5.84	5.41	24.90	4.88	1.43	6.85	1.18	8.55	2.22	7.62	1.12	6.57	1.31
A3	1400	38.70	5.78	5.70	25.64	5.21	1.19	6.65	1.12	8.27	2.27	7.60	1.10	6.56	1.39
A3	1550	40.66	7.18	6.00	27.42	5.53	1.60	7.22	1.23	8.64	2.37	7.98	1.16	6.52	1.46
A3	1600	41.69	6.56	6.00	27.57	5.80	1.35	7.11	1.23	9.18	2.36	8.00	1.20	6.73	1.46
A3	1650	41.18	6.55	6.07	27.39	5.70	1.64	6.89	1.25	9.14	2.31	7.99	1.20	6.68	1.47
A3	1700	44.97	7.34	6.54	29.81	6.32	1.66	7.74	1.38	9.48	2.55	8.69	1.32	7.32	1.65
A3	1750	41.52	6.53	5.87	27.38	5.50	1.40	7.10	1.23	8.96	2.35	8.16	1.19	6.84	1.47
A6	5	11.45	7.16	2.55	12.25	3.01	0.94	3.87	0.72	5.32	1.27	4.15	0.59	2.96	0.56
A6	600	23.97	5.45	3.70	16.67	3.48	0.94	4.44	0.79	5.67	1.55	5.05	0.74	4.25	0.86
A6	900	28.22	5.14	4.17	19.13	3.87	0.90	4.93	0.86	6.30	1.72	5.85	0.85	4.87	1.08
A6	1300	39.15	6.52	5.68	26.29	5.30	1.52	6.72	1.19	8.24	2.28	7.79	1.19	6.40	1.39
A6	1600	41.82	7.14	6.11	27.70	5.55	1.58	7.37	1.22	8.83	2.41	8.11	1.23	7.18	1.45
A6	1800	39.42	8.11	5.80	26.95	5.50	1.46	6.74	1.14	8.45	2.22	7.64	1.10	6.19	1.39
A6	2000	40.91	6.98	6.12	27.28	5.68	1.45	7.02	1.22	8.56	2.23	7.62	1.16	6.66	1.43
A6	2200	46.77	7.89	7.19	31.64	6.44	1.77	8.00	1.36	10.06	2.66	9.09	1.38	7.90	1.66
A6	2400	44.24	7.61	6.58	29.84	6.20	1.62	7.64	1.35	9.50	2.55	8.68	1.24	7.22	1.60
A6	2700	40.02	6.09	5.85	26.29	5.32	1.34	6.74	1.12	8.54	2.30	8.05	1.23	6.70	1.46
A6	300	14.91	4.07	2.56	11.34	2.35	0.63	3.03	0.54	4.03	1.03	3.44	0.50	2.49	0.51
A6	3012	41.54	6.73	5.92	27.75	5.40	1.49	6.88	1.29	9.17	2.42	8.34	1.26	7.30	1.56
C3a	5	3.33	4.37	0.60	2.79	0.57	0.22	1.14	0.16	1.38	0.39	1.44	0.19	1.14	0.18
C3a	500	24.74	8.46	3.60	15.92	3.29	0.88	4.66	0.73	5.24	1.44	4.75	0.68	4.63	0.80
C3a	1000	38.79	12.95	5.95	25.88	5.25	1.13	6.86	1.16	8.03	2.14	7.34	1.06	7.49	1.33
C3a	1400	45.74	11.12	6.84	29.81	6.18	1.36	7.75	1.33	9.41	2.54	8.64	1.26	9.05	1.57
C3a	1600	61.98	40.73	8.29	34.64	6.65	1.50	8.26	1.43	9.83	2.52	8.32	1.13	8.57	1.48
C3a	1800	45.81	10.20	6.78	30.85	5.77	1.40	8.12	1.37	9.73	2.51	8.50	1.29	8.99	1.57
C3a	2000	59.62	38.15	10.00	43.05	7.97	2.05	9.84	1.63	10.85	2.85	9.54	1.36	9.95	1.83
C3a	2400	46.05	13.05	6.73	30.38	5.65	1.58	7.78	1.27	9.37	2.50	8.47	1.30	9.22	1.58
C3a	2500	45.34	12.53	6.32	29.13	5.65	1.59	7.74	1.25	9.36	2.57	8.50	1.32	9.11	1.62
C3a	2600	45.16	8.65	6.42	29.74	5.94	1.78	7.96	1.33	9.62	2.59	8.88	1.38	9.45	1.65
C3a	2800	47.83	10.01	6.96	30.70	6.25	1.60	8.24	1.37	9.80	2.73	9.17	1.38	9.86	1.73
C3a	3000	48.77	12.48	7.43	32.60	5.98	1.47	8.06	1.37	10.18	2.62	9.25	1.36	9.65	1.73
C5	5	11.20	9.26	2.38	10.84	2.61	0.45	3.40	0.62	4.33	1.05	3.26	0.49	2.32	0.47
C5	300	14.47	5.79	2.44	11.06	2.27	0.60	3.06	0.58	3.91	1.05	3.45	0.51	2.44	0.52
C5	600	24.69	6.52	3.66	16.94	3.48	1.92	4.77	0.82	5.87	1.51	5.12	0.75	4.02	0.91
C5	1000	39.05	9.84	6.10	27.98	5.90	1.49	7.14	1.26	8.83	2.25	7.91	1.19	6.35	1.41

C5	1250	38.26	9.93	5.90	27.54	5.89	1.50	7.61	1.25	8.86	2.28	7.71	1.15	6.89	1.37
C5	1400	41.37	9.28	6.38	29.05	5.81	1.76	7.72	1.30	9.32	2.46	8.14	1.21	6.84	1.45
C5	1600	44.47	10.19	6.82	31.56	6.91	1.82	8.66	1.40	9.99	2.55	8.76	1.29	7.32	1.57
C5	1800	43.20	9.24	6.46	30.23	6.35	1.59	7.78	1.33	9.48	2.43	8.36	1.27	6.94	1.45
C5	2000	40.24	9.27	6.26	28.83	5.81	1.66	7.58	1.30	9.17	2.35	7.90	1.18	7.58	1.43
C5	2200	45.51	10.41	7.14	32.67	6.82	1.73	8.71	1.50	10.06	2.63	8.77	1.30	7.59	1.56
C5	2500	43.94	9.87	6.82	31.22	6.68	1.57	8.10	1.41	9.62	2.46	8.30	1.23	7.18	1.51
C5	2800	47.45	10.18	7.28	33.30	7.22	2.05	8.31	1.43	10.51	2.62	8.88	1.38	7.80	1.55
D3	5	10.34	8.18	2.32	10.32	2.52	0.79	3.37	0.60	4.21	1.06	3.27	0.47	2.29	0.43
D3	200	10.96	4.85	1.97	8.80	2.18	0.51	2.61	0.48	3.67	0.87	3.02	0.41	2.31	0.41
D3	400	18.59	3.04	2.94	13.24	2.64	0.85	3.57	0.64	4.57	1.21	4.11	0.58	3.25	0.71
D3	700	23.95	3.50	3.56	15.96	3.47	0.82	4.47	0.80	5.71	1.49	5.02	0.77	4.54	0.90
D3	900	28.91	3.86	4.29	19.44	4.04	1.11	5.38	0.90	6.69	1.77	6.09	0.90	5.25	1.04
D3	1000	28.99	4.67	4.15	19.47	3.87	1.08	5.23	0.86	6.24	1.75	5.81	0.85	4.81	1.06
D3	1200	35.11	5.82	5.06	23.07	4.72	1.16	6.13	1.05	7.73	2.05	6.99	1.04	6.51	1.28
D3	1400	36.29	6.16	5.29	24.11	4.45	1.20	6.15	1.10	7.70	2.10	7.13	1.06	6.28	1.33
D3	1600	40.52	7.06	5.98	27.94	5.20	1.53	7.14	1.24	8.81	2.32	7.70	1.13	6.45	1.43
D3	1800	41.87	7.25	6.41	28.98	5.99	1.47	7.51	1.33	9.39	2.45	8.28	1.22	7.73	1.55
D3	2000	35.12	5.69	5.23	24.13	5.17	1.20	6.50	1.05	7.46	1.94	6.66	0.97	8.53	1.23
D3	2107	45.27	9.95	7.05	31.66	6.40	1.78	8.09	1.42	9.94	2.52	8.50	1.28	7.62	1.56
E405	1500	53.95	26.75	7.45	33.07	6.90	1.38	8.59	1.48	10.15	2.64	8.83	1.29	9.08	1.53
E405	2500	141.02	170.52	29.38	123.50	34.11	7.50	35.14	5.60	32.60	6.26	19.36	2.29	17.25	2.70
10JJW-07	5	13.62	11.85	2.80	12.71	2.75	1.01	4.01	0.65	4.77	1.16	3.70	0.51	3.19	0.48
10JJW-07	500	24.92	6.74	3.91	17.22	3.56	1.00	4.83	0.84	5.71	1.48	4.89	0.70	4.79	0.81
10JJW-07	1000	34.32	6.25	5.00	21.71	4.30	1.17	6.20	0.98	7.30	1.97	6.80	0.98	6.89	1.22
10JJW-07	1500	43.77	9.23	6.13	28.18	5.84	1.58	7.65	1.26	9.08	2.44	8.39	1.28	8.77	1.54
10JJW-07	1750	50.39	14.19	7.74	35.50	7.53	2.30	10.03	1.63	10.89	2.75	9.21	1.39	9.37	1.68
10JJW-07	2000	52.38	11.32	8.38	37.78	8.55	2.35	10.90	1.75	11.99	2.97	9.86	1.47	10.12	1.79
10JJW-07	2250	62.46	18.82	11.99	55.33	13.67	3.93	17.23	2.88	17.39	3.95	12.09	1.77	11.61	1.99
10JJW-07	2500	50.78	11.87	7.80	35.18	7.20	1.80	9.27	1.56	10.44	2.76	9.55	1.43	9.97	1.70
10JJW-82	5	14.96	11.23	3.08	14.40	3.59	0.78	4.54	0.73	5.39	1.34	4.21	0.59	3.63	0.56
10JJW-82	1000	36.23	5.43	5.44	24.09	4.33	1.30	6.20	1.02	7.84	2.11	6.91	1.04	7.46	1.24
10JJW-82	1500	44.12	7.15	6.39	28.10	5.59	1.16	7.49	1.25	9.12	2.44	8.29	1.23	8.76	1.56
10JJW-82	2000	47.18	8.07	6.99	31.46	5.91	1.42	7.81	1.35	9.48	2.54	8.33	1.27	8.96	1.61
10JJW-82	2500	81.57	23.82	13.07	56.06	10.70	2.11	12.84	2.29	15.74	4.23	14.10	2.00	14.58	2.61

E418	1500	52.17	21.66	7.41	32.77	6.44	1.54	8.12	1.44	9.62	2.58	8.64	1.29	9.28	1.59
E418	2000	49.05	11.06	7.38	31.57	6.36	1.76	7.97	1.32	9.57	2.45	8.61	1.24	9.10	1.58
E418	2500	49.52	11.69	7.56	32.92	6.32	1.40	8.43	1.42	10.22	2.58	8.95	1.30	9.28	1.56
SEATS	5	15.18	12.94	2.66	11.21	2.82	0.58	4.01	0.63	4.83	1.28	3.96	0.53	3.62	0.55
SEATS	200	18.04	7.37	3.04	13.05	2.98	0.89	4.01	0.65	4.52	1.10	3.64	0.48	3.26	0.53
SEATS	400	34.62	16.88	3.24	14.67	3.00	0.79	4.28	0.73	4.90	1.31	4.52	0.63	4.04	0.72
SEATS	600	28.02	7.05	3.96	18.23	3.87	0.84	5.27	0.85	6.41	1.68	5.63	0.85	5.67	0.95
SEATS	800	39.38	23.51	5.19	22.68	4.69	1.21	5.90	0.98	7.11	1.85	6.22	0.89	6.29	1.10
SEATS	1000	34.64	6.18	4.80	22.23	4.50	1.29	6.40	1.05	7.78	2.01	7.04	1.08	7.29	1.24
SEATS	1200	36.90	8.82	5.09	23.04	4.81	0.88	6.43	1.01	7.52	2.03	6.93	1.04	7.20	1.28
SEATS	1400	42.96	9.44	5.81	26.42	5.49	1.20	7.17	1.19	8.40	2.22	7.83	1.18	8.08	1.43
SEATS	1600	47.10	14.62	6.67	29.97	6.02	1.30	7.76	1.26	9.28	2.47	8.10	1.22	8.58	1.53
SEATS	1800	46.62	9.52	6.77	30.00	5.90	1.42	7.78	1.32	9.50	2.52	8.46	1.25	8.83	1.54
SEATS	1900	49.60	13.44	7.27	32.20	6.19	1.60	8.11	1.31	9.55	2.52	8.72	1.28	8.95	1.56
SEATS	2000	53.21	13.45	7.64	33.92	6.55	1.59	9.22	1.44	10.28	2.70	9.28	1.37	9.58	1.69
SEATS	2100	48.17	9.58	6.99	31.24	6.00	1.50	7.96	1.28	9.37	2.48	8.22	1.25	8.91	1.54
SEATS	2200	48.19	10.18	6.96	31.51	6.30	1.72	7.82	1.34	9.48	2.49	8.66	1.29	8.87	1.55
SEATS	2300	52.30	10.76	7.80	34.87	6.84	1.71	8.77	1.47	10.55	2.74	9.48	1.40	9.71	1.71
SEATS	2400	39.94	10.36	5.85	25.92	5.19	1.18	7.01	1.15	8.24	2.14	7.49	1.09	7.53	1.30
SEATS	2500	53.17	15.64	7.49	33.48	6.99	1.58	8.84	1.39	9.88	2.59	8.74	1.30	9.14	1.61
SEATS	2600	51.97	8.54	7.81	34.93	7.11	2.01	8.67	1.46	10.61	2.77	9.33	1.40	9.87	1.81
SEATS	2700	50.60	10.53	7.49	33.79	6.74	1.81	8.43	1.42	10.53	2.66	8.83	1.35	9.59	1.65
SEATS	2800	65.97	27.68	8.14	36.53	7.21	1.72	9.01	1.54	10.61	2.73	9.29	1.38	9.63	1.69
SEATS	2900	51.10	12.12	7.82	34.53	7.12	1.69	8.43	1.44	10.48	2.60	8.86	1.30	9.22	1.62
SEATS	3100	51.25	13.09	8.00	35.89	6.92	1.60	8.67	1.49	10.25	2.62	8.86	1.32	9.25	1.61
SEATS	3300	56.81	11.51	8.47	37.57	7.68	2.27	9.77	1.58	11.47	2.95	9.89	1.47	10.48	1.79
SEATS	3500	50.91	11.47	7.70	34.15	6.95	1.81	9.21	1.46	10.38	2.71	9.19	1.36	9.61	1.68
10JJW-46	5	17.18	11.24	3.71	15.41	3.79	0.90	5.34	0.92	6.45	1.57	4.86	0.62	4.29	0.65
10JJW-55	5	28.03	19.70	5.42	24.08	5.52	1.57	7.05	1.28	8.75	2.06	6.30	0.84	5.37	0.86
E202	5	36.98	39.77	5.70	25.12	5.15	1.24	6.04	1.07	7.33	1.64	5.23	0.69	4.51	0.71

*Table A2. PAAS-normalized REE *10^6(ppm/ppm) of foraminifera collected from core MD05-2904*

Species	Age (Kyr)	La	Ce	Pr	Nd	Sm	Eu	Gd	Tb	Dy	Ho	Er	169Tm	174Yb	175Lu
uncleaned PF	0.05	3.356	2.468	3.569	4.147	6.176	8.452	8.562	8.075	7.908	7.754	7.549	7.611	7.258	7.030
uncleaned PF	6.50	3.986	3.647	4.290	4.850	7.411	9.818	10.100	9.637	9.429	9.058	8.848	8.654	8.394	8.103
uncleaned PF	11.24	3.246	3.388	3.611	4.076	6.312	8.140	8.458	7.667	7.453	7.111	6.792	6.716	6.301	6.101
Mixed PF	0.05	2.487	1.344	2.583	2.914	4.490	6.076	6.167	5.812	5.819	5.515	5.332	5.575	5.122	4.980
Mixed PF	18.57	4.302	3.663	4.691	4.984	7.191	8.804	9.268	8.476	7.879	7.055	6.664	6.430	5.951	5.476
BF	0.05	1.969	1.155	2.020	2.310	3.456	4.814	4.795	4.438	4.270	4.095	4.018	3.908	3.691	3.551
BF	6.50	1.794	1.115	1.687	1.844	2.738	3.559	3.586	3.483	3.274	2.974	2.965	2.908	2.816	2.712
PF	0.05	3.251	2.162	3.443	3.870	5.982	7.810	7.953	7.544	7.330	7.000	6.853	6.890	6.483	6.219
PF	0.82	1.346	1.112	1.425	1.563	2.352	3.124	3.084	3.036	2.910	2.758	2.691	2.706	2.547	2.434
PF	1.63	1.470	1.262	1.560	1.724	2.676	3.527	3.503	3.459	3.326	3.192	3.085	3.011	2.939	2.667
PF	2.57	1.504	1.258	1.585	1.762	2.758	3.607	3.616	3.550	3.414	3.105	3.113	3.146	2.974	2.817
PF	3.52	1.168	0.980	1.258	1.397	2.139	2.856	2.862	2.704	2.605	2.499	2.449	2.431	2.361	2.235
PF	4.62	1.717	1.489	1.819	2.031	3.125	4.001	4.074	3.935	3.882	3.631	3.593	3.493	3.372	3.244
PF	6.50	3.265	2.802	3.490	3.868	5.931	7.676	7.870	7.473	7.318	6.673	6.465	6.399	6.068	5.682
PF	6.97	1.727	1.742	1.913	2.112	3.258	4.198	4.270	4.131	3.962	3.716	3.618	3.617	3.456	3.375
PF	7.55	2.039	2.182	2.241	2.452	3.748	4.870	5.021	4.685	4.536	4.179	4.037	4.012	3.696	3.546
PF	8.56	2.110	2.251	2.331	2.559	3.873	4.948	5.180	4.820	4.573	4.236	4.033	3.939	3.700	3.479
PF	9.45	1.873	2.213	2.072	2.247	3.420	4.459	4.483	4.262	4.020	3.596	3.432	3.267	3.174	2.882
PF	10.45	1.287	1.392	1.448	1.550	2.491	3.167	3.095	2.899	2.728	2.510	2.441	2.320	2.259	2.084
PF	11.24	4.002	3.947	4.286	4.774	7.219	9.254	9.676	8.978	8.598	8.009	7.604	7.514	7.120	6.944
PF	12.57	1.695	1.794	1.834	1.972	2.983	3.747	4.033	3.644	3.427	3.285	3.134	3.054	2.896	2.705
PF	13.52	2.360	2.627	2.592	2.740	4.184	5.081	5.290	4.824	4.639	4.231	4.036	3.919	3.726	3.465
PF	14.76	2.274	2.716	2.408	2.616	3.834	4.650	5.002	4.414	4.244	3.785	3.531	3.401	3.202	2.964
PF	15.73	2.344	2.681	2.528	2.642	3.808	4.638	4.785	4.310	3.928	3.495	3.271	3.147	2.873	2.595
PF	16.73	1.793	1.940	1.921	2.033	2.934	3.579	3.659	3.320	3.099	2.795	2.640	2.481	2.302	2.029
PF	17.85	1.944	1.967	2.067	2.162	3.263	3.903	3.974	3.683	3.373	3.115	2.948	2.833	2.607	2.397
PF	18.57	3.173	2.908	3.431	3.633	5.215	6.514	6.812	6.153	5.726	5.038	4.801	4.782	4.348	3.901
PF	19.27	2.723	2.810	2.933	3.111	4.477	5.565	5.839	5.339	4.926	4.509	4.234	4.088	3.780	3.486
PF	20.04	3.338	3.097	3.604	3.856	5.582	6.948	7.254	6.582	6.101	5.582	5.268	5.075	4.736	4.372
PF	21.02	3.112	3.185	3.367	3.660	5.247	6.441	6.683	6.203	5.762	5.056	4.835	4.634	4.271	3.882
PF	22.22	2.945	2.941	3.205	3.369	4.956	6.051	6.288	5.780	5.310	4.819	4.510	4.461	4.050	3.584
PF	23.20	2.348	2.589	2.517	2.678	3.968	4.829	5.042	4.508	4.260	3.908	3.717	3.565	3.247	3.029

*Table A3. PAAS-normalized REE *10^6 (ppm/ppm) of bulk sediment leachates collected from core MD05-2904.*

Age (kyr)	Weight (g)	Leaching time (h)	Decarbonate	139La	140Ce	141Pr	145Nd	147Sm	151Eu	157Gd	159Tb	163Dy	165Ho	166Er	169Tm	174Yb	175Lu
0.05	0.2	0.5	No	1.28	1.04	1.46	1.85	2.64	3.77	3.57	3.15	3.05	2.63	2.35	2.47	2.10	2.23
6.50	0.2	0.5	No	1.49	1.46	1.77	2.28	3.24	4.33	4.34	3.84	3.70	3.08	2.74	2.87	2.47	2.55
11.24	0.2	0.5	No	1.25	1.36	1.52	1.90	2.74	3.64	3.69	3.20	3.08	2.52	2.22	2.23	1.94	2.02
18.57	0.2	0.5	No	1.19	1.40	1.46	1.82	2.56	3.15	3.34	2.81	2.56	2.11	1.79	1.82	1.64	1.68
20.04	0.2	0.5	No	1.28	1.44	1.58	2.00	2.78	3.42	3.61	3.03	2.80	2.29	2.02	2.03	1.80	1.85
0.05	1	0.5	No	4.39	3.49	4.95	6.31	8.86	12.40	11.96	10.69	10.51	9.06	8.18	8.55	7.50	7.73
6.50	1	0.5	No	4.47	4.48	5.26	6.66	9.58	12.49	12.70	11.43	11.15	9.39	8.39	8.81	7.73	7.95
11.24	1	0.5	No	4.60	5.16	5.53	6.93	10.00	12.95	13.37	11.88	11.44	9.53	8.42	8.81	7.69	7.86
18.57	1	0.5	No	3.29	3.92	4.09	5.08	7.11	8.90	9.58	8.04	7.55	6.14	5.46	5.44	4.81	4.94
20.04	1	0.5	No	3.51	3.89	4.24	5.31	7.49	9.25	9.94	8.55	8.03	6.64	5.79	5.94	5.18	5.38
0.05	2	0.5	No	4.46	3.53	4.93	6.22	8.74	12.05	11.67	10.60	10.39	8.97	8.06	8.51	7.49	7.62
6.50	2	0.5	No	5.41	5.39	6.31	7.88	10.99	14.57	14.86	13.48	13.24	11.12	9.97	10.63	9.27	9.45
11.24	2	0.5	No	5.13	5.87	6.23	7.71	11.08	14.35	14.69	13.14	12.73	10.45	9.24	9.67	8.48	8.62
18.57	2	0.5	No	5.18	6.31	6.22	7.77	10.98	13.35	14.45	12.43	11.68	9.55	8.44	8.55	7.46	7.56
20.04	2	0.5	No	5.35	6.05	6.36	7.98	11.28	13.70	14.79	12.84	12.18	10.11	8.89	9.06	7.90	8.05
0.05	1	1	No	3.35	2.67	3.79	4.81	6.70	9.25	9.17	8.27	8.06	6.98	6.23	6.59	5.73	5.90
6.50	1	1	No	5.76	5.76	6.67	8.41	12.16	16.01	16.16	14.55	14.23	11.98	10.81	11.27	9.96	10.17
11.24	1	1	No	5.60	6.20	6.61	8.39	12.03	15.66	16.05	14.18	13.64	11.54	10.12	10.49	9.13	9.34
18.57	1	1	No	5.66	7.04	6.82	8.52	12.16	14.80	16.03	13.65	12.83	10.56	9.17	9.28	8.19	8.29
20.04	1	1	No	6.30	7.63	7.50	9.42	13.51	16.65	17.83	15.25	14.39	11.97	10.43	10.61	9.25	9.62
0.05	1	0.5	Yes	0.54	0.63	0.75	0.98	1.51	1.97	2.05	1.68	1.55	1.29	1.13	1.21	1.08	1.18
6.50	1	0.5	Yes	0.51	0.61	0.79	1.07	1.64	2.11	2.20	1.81	1.63	1.31	1.14	1.18	1.05	1.13
11.24	1	0.5	Yes	0.48	0.61	0.72	0.96	1.44	1.97	1.97	1.61	1.47	1.18	1.02	1.07	0.95	0.99
18.57	1	0.5	Yes	0.71	0.97	0.99	1.28	1.80	2.20	2.31	1.85	1.66	1.33	1.17	1.23	1.10	1.12
20.04	1	0.5	Yes	0.70	0.93	1.02	1.30	1.92	2.33	2.43	1.99	1.79	1.42	1.23	1.31	1.18	1.19
0.05	1	0.5	Yes	0.22	0.29	0.33	0.44	0.71	0.91	0.91	0.73	0.63	0.49	0.40	0.42	0.36	0.37
6.50	1	0.5	Yes	0.20	0.26	0.33	0.44	0.68	0.94	0.89	0.72	0.61	0.45	0.37	0.35	0.32	0.31
11.24	1	0.5	Yes	0.25	0.33	0.40	0.52	0.83	1.08	1.09	0.83	0.73	0.53	0.45	0.44	0.40	0.40
18.57	1	0.5	Yes	0.29	0.40	0.40	0.51	0.76	0.83	0.94	0.73	0.64	0.50	0.42	0.44	0.39	0.39
20.04	1	0.5	Yes	0.25	0.34	0.37	0.46	0.70	0.86	0.83	0.68	0.60	0.45	0.39	0.40	0.36	0.36
0.05	0.2	0.5	Yes	0.16	0.21	0.23	0.31	0.48	0.66	0.65	0.51	0.45	0.35	0.29	0.31	0.26	0.27
6.50	0.2	0.5	Yes	0.18	0.22	0.28	0.37	0.61	0.80	0.76	0.62	0.53	0.39	0.32	0.31	0.28	0.29

11.24	0.2	0.5	Yes	0.19	0.24	0.29	0.39	0.62	0.80	0.80	0.62	0.52	0.40	0.33	0.32	0.28	0.27
18.57	0.2	0.5	Yes	0.30	0.41	0.42	0.51	0.75	0.93	0.90	0.72	0.65	0.49	0.42	0.45	0.38	0.38
20.04	0.2	0.5	Yes	0.32	0.42	0.47	0.60	0.88	1.09	1.10	0.88	0.76	0.56	0.49	0.50	0.45	0.42
0.05	0.2	2	Yes	0.32	0.42	0.49	0.61	1.10	1.54	1.38	1.06	0.88	0.66	0.60	0.52	0.48	0.43
6.50	0.2	2	Yes	0.27	0.35	0.45	0.56	1.04	1.41	1.33	0.99	0.78	0.59	0.50	0.43	0.39	0.35
11.24	0.2	2	Yes	0.31	0.40	0.49	0.62	1.10	1.45	1.36	1.01	0.81	0.62	0.54	0.47	0.42	0.37
18.57	0.2	2	Yes	0.45	0.60	0.64	0.73	1.15	1.52	1.46	1.09	0.91	0.72	0.65	0.60	0.54	0.51
20.04	0.2	2	Yes	0.42	0.54	0.60	0.72	1.23	1.43	1.48	1.12	0.92	0.75	0.59	0.61	0.53	0.49
0.05	0.2	3	Yes	0.34	0.46	0.53	0.68	1.16	1.68	1.48	1.16	0.94	0.72	0.63	0.56	0.52	0.44
6.50	0.2	3	Yes	0.28	0.36	0.45	0.60	1.05	1.49	1.31	1.01	0.81	0.58	0.50	0.44	0.41	0.34
11.24	0.2	3	Yes	0.33	0.43	0.51	0.63	1.17	1.55	1.54	1.10	0.87	0.65	0.59	0.45	0.44	0.39
18.57	0.2	3	Yes	0.46	0.62	0.64	0.76	1.24	1.56	1.52	1.14	0.96	0.79	0.67	0.61	0.58	0.51
20.04	0.2	3	Yes	0.44	0.57	0.63	0.75	1.24	1.59	1.54	1.20	0.98	0.76	0.68	0.57	0.55	0.50

Table A4. PAAS-normalized REE *106 (ppm/ppm) of reductive cleaning solution of foraminifera retrieved from core MD05-2904

Species	Age (Kyr)	139La	140Ce	141Pr	146Nd	147Sm	151Eu	157Gd	159Tb	163Dy	165Ho	166Er	169Tm	172Yb	175Lu
BF	0.05	0.008	0.005	0.007	0.009	0.016	0.031	0.019	0.021	0.019	0.019	0.017	0.017	0.018	0.016
BF	6.50	0.007	0.006	0.007	0.008	0.014	0.022	0.017	0.014	0.016	0.016	0.015	0.011	0.015	0.012
Mixed PF	0.05	0.026	0.019	0.026	0.035	0.055	0.070	0.067	0.061	0.067	0.061	0.063	0.061	0.058	0.059
Mixed PF	18.57	0.046	0.047	0.052	0.068	0.090	0.118	0.121	0.115	0.111	0.100	0.097	0.095	0.098	0.085
PF	0.05	0.041	0.032	0.042	0.054	0.077	0.111	0.110	0.101	0.106	0.100	0.099	0.105	0.104	0.104
PF	0.82	0.029	0.025	0.029	0.038	0.051	0.077	0.075	0.069	0.073	0.069	0.068	0.065	0.069	0.064
PF	1.63	0.030	0.025	0.029	0.037	0.054	0.085	0.076	0.066	0.077	0.064	0.070	0.074	0.065	0.062
PF	2.57	0.027	0.022	0.028	0.036	0.047	0.081	0.075	0.066	0.069	0.066	0.063	0.062	0.062	0.063
PF	2.57	0.027	0.022	0.027	0.039	0.046	0.063	0.066	0.064	0.074	0.058	0.065	0.068	0.068	0.060
PF	3.52	0.025	0.020	0.023	0.033	0.043	0.069	0.063	0.059	0.061	0.055	0.054	0.060	0.057	0.052
PF	6.50	0.031	0.029	0.033	0.043	0.062	0.099	0.099	0.078	0.086	0.078	0.083	0.078	0.085	0.084
PF	4.62	0.024	0.020	0.025	0.032	0.045	0.063	0.067	0.057	0.060	0.059	0.057	0.058	0.055	0.059
PF	6.97	0.030	0.028	0.030	0.040	0.059	0.085	0.077	0.069	0.082	0.066	0.071	0.074	0.064	0.062
PF	7.55	0.038	0.039	0.043	0.055	0.100	0.125	0.144	0.122	0.123	0.108	0.112	0.164	0.134	0.149
PF	8.56	0.042	0.042	0.069	0.082	0.250	0.309	0.293	0.274	0.235	0.227	0.213	0.475	0.336	0.573
PF	9.45	0.041	0.046	0.046	0.057	0.087	0.111	0.112	0.108	0.110	0.095	0.090	0.089	0.095	0.085
PF	10.45	0.026	0.026	0.028	0.036	0.050	0.070	0.074	0.065	0.064	0.058	0.056	0.061	0.057	0.049

PF	11.24	0.041	0.044	0.046	0.059	0.085	0.126	0.115	0.102	0.115	0.104	0.104	0.093	0.098	0.096
PF	12.57	0.043	0.046	0.044	0.056	0.083	0.105	0.112	0.094	0.100	0.087	0.087	0.088	0.081	0.081
PF	13.52	0.051	0.055	0.056	0.070	0.101	0.135	0.129	0.111	0.118	0.100	0.097	0.096	0.091	0.088
PF	14.76	0.053	0.063	0.058	0.070	0.090	0.121	0.128	0.114	0.116	0.100	0.101	0.092	0.096	0.084
PF	15.73	0.060	0.071	0.070	0.084	0.118	0.135	0.152	0.135	0.134	0.116	0.112	0.106	0.103	0.105
PF	16.73	0.069	0.078	0.080	0.095	0.128	0.165	0.176	0.151	0.153	0.128	0.125	0.124	0.122	0.107
PF	17.85	0.061	0.064	0.067	0.084	0.120	0.130	0.147	0.131	0.130	0.109	0.110	0.108	0.107	0.093
PF	18.57	0.036	0.038	0.042	0.053	0.069	0.096	0.095	0.086	0.085	0.074	0.073	0.075	0.070	0.059
PF	19.27	0.074	0.078	0.084	0.106	0.142	0.172	0.190	0.164	0.168	0.149	0.143	0.135	0.140	0.129
PF	20.04	0.054	0.055	0.061	0.078	0.115	0.136	0.132	0.128	0.126	0.107	0.108	0.108	0.105	0.097
PF	21.02	0.073	0.075	0.081	0.101	0.134	0.177	0.185	0.167	0.169	0.149	0.140	0.147	0.133	0.125
PF	22.22	0.061	0.059	0.068	0.085	0.117	0.145	0.156	0.140	0.143	0.121	0.124	0.124	0.112	0.114
PF	23.2	0.076	0.081	0.087	0.103	0.141	0.180	0.184	0.168	0.174	0.148	0.144	0.142	0.138	0.121